UNIVERSIDADE ESTADUAL PAULISTA "JÚLIO DE MESQUITA FILHO"
FACULDADE DE MEDICINA

KEVIN SILVA MULLER

Implicações da reconstrução nervosa experimental associada ao biopolímero heterólogo de fibrina no sistema nervoso central e periférico

Dissertação apresentada à Faculdade de Medicina, Universidade Estadual Paulista "Júlio de Mesquita Filho", Câmpus de Botucatu, para obtenção do título de Mestre em Cirurgia e Medicina Translacional, Área de Biologia Geral.

Orientador(a): Profa. Dra. Selma Maria Michelin Matheus
Coorientador(a): Prof. Dr. José de Anchieta de Castro e Horta-Júnior

Botucatu, São Paulo
2024

Kevin Silva Muller

Implicações da reconstrução nervosa experimental associada ao biopolímero heterólogo de fibrina no sistema nervoso central e periférico

Dissertação apresentada à Faculdade de Medicina, Universidade Estadual Paulista "Júlio de Mesquita Filho", Câmpus de Botucatu, para obtenção do título de Mestre em Cirurgia e Medicina Translacional, Área de Biologia Geral.

Área de Concentração: Reparação, Regeneração e Transplante de Órgãos e Tecidos.

Área de Conhecimento: Biologia Geral.

Orientadora: Profa. Dra. Selma Maria Michelin Matheus
Coorientador: Prof. Dr. José de Anchieta de Castro e Horta-Júnior

Botucatu, São Paulo
2024

M958i

Muller, Kevin Silva
Implicações da reconstrução nervosa experimental associada ao biopolímero heterólogo de fibrina no sistema nervoso central e periférico / Kevin Silva Muller. -- Botucatu, 2024
150 p. : il., tabs., fotos

Dissertação (mestrado) - Universidade Estadual Paulista (UNESP), Faculdade de Medicina, Botucatu
Orientadora: Selma Maria Michelin Matheus
Coorientadora: Jose de Anchieta de Castro e Horta Júnior

1. neurorrafia. 2. medicina regenerativa. 3. rato. I. Título

Sistema de geração automática de fichas catalográficas da Unesp. Biblioteca da Universidade Estadual Paulista (UNESP), Faculdade de Medicina, Botucatu. Dados fornecidos pelo autor(a).

Essa ficha não pode ser modificada.

Impactos sociais

A lesão nervosa é uma condição devastadora que afeta a qualidade de vida dos pacientes, limitando a mobilidade e a autonomia (ODS 3: Saúde e Bem-estar). O biopolimero heterólogo de fibrina associado ao reparo representa um avanço na medicina regenerativa ao criar um ambiente mais favorável à regeneração, mitigando a degeneração e a atrofia muscular. Isso pode levar a uma melhora significativa nas capacidades motoras dos pacientes.

Social impacts

Nerve injury is a devastating condition that affects patients' quality of life, limiting mobility and autonomy (SDG 3: Good Health and Well-being). The heterologous fibrin biopolymer associated with repair represents an advance in regenerative medicine by creating a more favorable environment for regeneration, mitigating degeneration and muscle atrophy. This can lead to a significant improvement in patients' motor abilities.

UNIVERSIDADE ESTADUAL PAULISTA

Câmpus de Botucatu

ATA DA DEFESA PÚBLICA DA DISSERTAÇÃO DE MESTRADO DE KEVIN SILVA MULLER, DISCENTE DO PROGRAMA DE PÓS-GRADUAÇÃO EM CIRURGIA E MEDICINA TRANSLACIONAL, DA FACULDADE DE MEDICINA.

Aos 24 dias do mês de julho do ano de 2024, às 08:30 horas, por meio de Videoconferência, realizou-se a defesa de DISSERTAÇÃO DE MESTRADO de KEVIN SILVA MULLER, intitulada **Implicações da reconstrução nervosa experimental associada ao biopolímero heterólogo de fibrina no sistema nervoso central e periférico**. A Comissão Examinadora foi constituida pelos seguintes membros: Profa. Dra. SELMA MARIA MICHELIN MATHEUS (Orientador(a) - Participação Virtual) do(a) Depto de Biologia Estrutural e Funcional / IB/Botucatu - Unesp, Profa. Dra. CRISTINA GUATIMOSIM FONSECA (Participação Virtual) do(a) Depto. de Morfologia / ICB/Belo Horizonte - UFMG, Profa. Dra. LUCIANA POLITTI CARTAROZZI (Participação Virtual) do(a) Depto. de Biologia Estrutural E Funcional / IB/Campinas - Unicamp. Após a exposição pelo mestrando e arguição pelos membros da Comissão Examinadora que participaram do ato, de forma presencial e/ou virtual, o discente recebeu o conceito final: APROVADO . Nada mais havendo, foi lavrada a presente ata, que após lida e aprovada, foi assinada pelo(a) Presidente(a) da Comissão Examinadora.

gov.br Documento assinado digitalmente
SELMA MARIA MICHELIN MATHEUS
Data: 31/07/2024 15:16:14-0300
Verifique em https://validar.iti.gov.br

Profa. Dra. SELMA MARIA MICHELIN MATHEUS

Aos indivíduos que enfrentam as dificuldades e desafios das lesões traumáticas de nervo.

Que este trabalho contribua para a ciência e para o desenvolvimento de tratamentos que garantam a recuperação e a qualidade de vida desses pacientes.

AGRADECIMENTOS

Aos meus pais, Jurg e Creusa, e meu irmão, Lívio, que sempre deram todo o apoio, suporte e estrutura para que eu pudesse ter chegado tão longe hoje. Embora distantes fisicamente, vocês sempre estiveram por perto.

A professora Dra. Selma Maria Michelin Matheus, por mais uma vez acreditar no meu trabalho e me capacitar, e por contribuir e compartilhar suas experiências, além da confiança e disposição para abraçar a realização dessa dissertação, enquanto também me permitiu seguir explorando por outros rumos que não só a pesquisa, me incentivando a desenvolver ainda mais minha paixão pela extensão e divulgação científica.

Ao professor Dr. José de Anchieta por ter aceitado me co-orientar e participar desta empreitada, contribuindo grandemente para sua execução, sempre servindo como um exemplo exepcional não só de professor e cientista, mas também de pessoa.

Aos meus companheiros de casa da república Caverna do Dragão e em especial as “Jullies” que proporcionaram experiências e momentos fabulosos que ficaram marcados pra sempre. Até o impossível ficou mais possível e alcançável com o apoio de vocês.

Aos meus colegas dos laboratórios Fefo, Youssef, Higor, Stephane, Ygor, Verônica e Gabrielly, que contribuíram enormemente para que os dias no laboratório fossem muito mais do que trabalho. Vocês transformaram o ambiente em um espaço de diversão e companheirismo, repleto de ótimos momentos e boas histórias. Tornaram todos os bons pratos, congressos e passeios muito mais significativos.

A professora Dra. Carla de Moraes e professora Dra. Cíntia Matsumura pelo apoio e revisões ao longo das bancas de acompanhamento. Suas contribuições foram muito importantes para a construção do trabalho, seu desenvolvimento e resultado final.

Aos membros da minha banca de qualificação, professora Dra. Elaine Minatel e professor Dr. Rogério Buchaim pelas muitas contribuições que ajudaram a tornar esse trabalho mais completo e coeso, além de me incentivar a continuar trabalhando e desenvolvendo novas abordagens de investigação.

A professora Dra. Luciana Cartarozzi e professora Dra. Cristina Guatimosim que além de diversas contribuições também tornaram a concretização destes anos de trabalho um momento ainda mais memorável através de uma bela arguição.

Ao Instituto de Biociências de Botucatu (IBB), Faculdade de Medicina de Botucatu (FMB) e a Unidade de Pesquisa Experimental (Unipex) por toda a infraestrutura e apoio técnico e físico, que foram indispensáveis para a realização deste trabalho. Em especial, aos servidores Luciene de Almeida, Rinaldo Ortiz, Ricardo Teixeira, Leandro Alves e a Vanda Tofoli.

Ao Programa de Pós-Graduação em Cirurgia e Medicina Translacional pelos diversos apoios técnicos e financeiros para o meu próprio desenvolvimento e também do projeto. Em especial, a Márcia Fonseca, secretária do programa, pela enorme ajuda com burocrácias, cordialidade e disponibilidade.

Agradeço ao Centro de Microscopia Eletrônica do IBB, a professora Dra. Daniela Carvalho e a Claudete Tardivo, Thiago Tardivo, Marilena e Shelly Favorito pela enorme disponibilidade, ajuda técnica e capacitação para preparo de amostras e visualização para microscopia eletrônica.

Também agradeço a todos os amigos que já passaram e que foram feitos ao longo desta grandiosa jornada por Botucatu.

Aos animais que tiveram suas vidas cedidas involuntariamente para a realização deste trabalho.

E a Gabriela Larissa, obrigado por tudo. Você me ajudou a mer tornar uma pessoa melhor. Independente de onde e como estivermos, sempre haverá uma parte de você em mim. Eu sou grato por isso.

O presente trabalho foi realizado com o apoio da Fundação de Amparo à Pesquisa do Estado de São Paulo (Fapesp) com a concessão de bolsa de pesquisa nível Mestrado (processo 2022/07551-1).

“O correr da vida embrulha tudo, a vida é assim:

esquenta e esfria, aperta e daí afrouxa,

sossega e depois desinquieta.

***O que ela quer da gente é coragem**.”*

- João Guimarães Rosa. Grande Sertão: Veredas.

LISTA DE ILUSTRAÇÕES

Figura 1. Esquema ilustrativo da unidade motora – página 16.

Figura 2. Organização da junção neuromuscular – página 18.

Figura 3. Classificação das lesões nervosas – página 22.

Figura 4. Mudanças desencadeadas pela lesão nervosa – página 24.

Figura 5. Eventos celulares e moleculares associados à desnervação e reparo muscular ao nível da junção neuromuscular – página 28.

Figura 6. Diagrama demonstrativo dos estudos para revisão de escopo – página 38.

Figura 7. Fotografias do procedimento de cirurgia experimental – página 40.

Figura 8. Procedimento de injeção do neurotraçador Fluorogold – página 41.

Figura 9. Imagem representativa de medida automatizada utilizando o software AxonDeepSeg – página 45.

Figura 10. Representações para análise de densitometria óptica e contagem de células marcadas por IBA-1 – página 49.

Figura 11. Representações do procedimento utilizado para realização da reconstrução 3D – página 50.

LISTA DE ABREVIATURAS

ACh – Acetilcolina

AChE – Acetilcolinesterase

ANOVA – Análise de variância paramétrica

BHF – Biopolímero Heterólogo de Fibrina

BDNF – Fator Neurotrófico Derivado do Encéfalo

BSA – Albumina sérica bovina

C – Grupo Controle

CEVAP – Centro de Estudos de Venenos e Animais Peçonhentos

D – Grupo Desnervado

DAMPS – padrões moleculares associados a danos

DBEF – Departamento de Biologia Estrutural e Funcional

DAB-Ni – 3,3’ diaminobenzidina-tetrahidrocloreto intensificado com níquel amônio sulfato

Dok7 – Proteína Docking 7

GAPDH – Gliceraldeído-3-fosfato desidrogenase

HE – Hematoxilina e Eosina

HRP – Horseradish Peroxidase

FG - Fluorogold

FMB – Faculdade de Medicina de Botucatu

IL – Interleucina

JNM – Junção neuromuscular

LRP4 – Receptor lipoproteico relacionado a proteína 4

MMP3 – Metaloproteinase de matriz 3

MRFs – Fatores de regulação miogênica

MuSK – Receptor tirosina quinase músculo-específico

MyoD – Myoblast Determination Protein 1

N – Grupo Neurorrafia

NF200 – Proteína Neurofilamento 200

nAChRs – Receptores nicotínicos de acetilcolina

NB – Grupo Neurorrafia + BHF

PBS – Tampão fosfato salino

PCL – Policaprolactona

RIPA – Tampão de ensaio de radioimunoprecipitação

SEM – Erro padrão da média

S100 – Proteína S100

TBS-T – Tampão tris salino com Tween 20

TNF- – Fator de Necrose Tumoral

tSCs – células de Schwann terminais

UNESP – Universidade Estadual Paulista

UNIPEX – Unidade de Pesquisa Experimental

v – Versão

VAChT – Transportador vesicular de acetilcolilna

VGLUT-1 – Transportador Vesicular Glutamatérgico 1

(w/v) – peso/volume

(v/v) – volume/volume

% – Porcentagem

® – Marca registrada

h – Horas

HCl – Ácido clorídrico

kg – Kilogramas

m – Metro

M – Molar / mol por litro

mg – Miligramas

min – Minutos

mL – Mililitros

mm – Milímetros

ºC – Graus Celsius

p – Probabilidade de significância

pH – Potencial hidrogeniônico

SP – São Paulo

x – Vezes

α – Alfa

γ – Gama

µL – Microlitros

µm – Micrômetros

SUMÁRIO

Lista de ilustrações **10**
Lista de abreviaturas **11**
Resumo **13**
Abstract **14**
Introdução **15**
Estrutura e função do sistema nervoso **15**
Junção Neuromuscular **19**
Lesões nervosas **22**
Patofisiologia da lesão nervosa **25**
Abordagens de reparo após lesão **31**
Biopolímero Heterólogo de Fibrina **32**
Justificativa **35**
Objetivos **36**
Material e métodos **37**
Revisão bibliográfica **37**
Animais **38**
Procedimento cirúrgico **39**
Coleta do material biológico **42**
Estudos do SNP **43**
Estudos do SNC **47**
Referências Bibliográficas **52**
Capítulo 1 ..... **57**
Capítulo 2 ..... **87**
Capítulo 3 ..... **113**
Conclusão **147**
Anexo 1 (Certificados CEUA) **148**
Anexo 2 (Tabela de Anticorpos utilizados) **150**

RESUMO

Lesões nervosas representam desafios significativos para a clínica médica devido à sua ocorrência frequente e impacto substancial na qualidade de vida. A secção completa do nervo resulta no bloqueio da condução nervosa, levando a mudanças no sistema nervoso à medida que uma série de respostas patofisiológicas e metabólicas ocorrem para estabilizar e reparar os tecidos lesionados. O primeiro grande desafio é manter os neurônios lesionados vivos e posteriormente gerenciar o crescimento dos axônios. Outra preocupação crítica surge da interrupção das conexões nervo-músculo e degeneração das junções neuromusculares (JNMs), levando à atrofia e perda substancial da função muscular. A técnica padrão ouro, neurorrafia, é insuficiente para alcançar uma recuperação motora significativa e, portanto, novas técnicas estão sendo estudadas. Um candidato adjunto promissor é o biopolímero de fibrina heterólogo (BHF), que é livre de componentes humanos e vêm exibindo potencial notável para regeneração de lesões periféricas e da medula espinhal. No entanto, perguntas sobre seus efeitos regenerativos tardios para a interação nervo-músculo e na medula espinhal após lesão nervosa permanecem inexploradas. Portanto, investigamos os efeitos da reconstrução nervosa via neurorrafia associada ao BHF 120 dias após a lesão e reparo do nervo isquiático em ratos Wistar, abordando aspectos do sistema nervoso periférico - nervo, JNM e músculo associado - e do sistema nervoso central - neurônios motores inferiores e microglia da medula espinhal. Para isso, quarenta e quatro ratos Wistar machos adultos foram distribuídos aleatoriamente em quatro grupos experimentais: Controle (C), em que o nervo isquiático direito foi visualizado; Denervado (D), em que a neurotmese foi realizada com remoção de um fragmento de 6 mm do nervo isquiático; Neurorrafia (N), em que após neurotmese os cotos do nervo isquiático foram reconectados por neurorrafia; e Neurorrafia + BHF (NB), no qual o BHF foi adicionado após a mesma neurorrafia. Aos 105 dias pós-lesão, o neurotraçador Fluorogold (FG) foi aplicado no músculo tibial cranial direito para marcação retrógrada dos neurônios motores na coluna anterior da porção lombar (L2-L5) da medula espinhal. Aos 120 dias, foi realizado coleta a fresco ou perfusão transcardíaca para obtenção das medulas espinhais, dos nervos isquiáticos e fibulares e dos músculos tibiais craniais. Em relação ao eixo nervo-músculo, para o nervo fibular, foi observado aumento no número de axônios intactos no grupo NB, resultando em aumento na frequência de axônios, referentes à razão G/diâmetro do axônio. Com relação às JNMs, o grupo NB apresentou aproximação morfológica ao grupo C, e também aumento na expressão da subunidade alfa-1 do nAChR e da proteína Rapsina. Tomados em conjunto, esses resultados contribuíram para a recuperação muscular, em que os grupos NB e C exibiram resultados morfométricos de fibras musculares saudáveis. Em relação a medula espinal, ultraestruturalmente, os grupos NB e N apresentaram neurônios com sinais de preservação de suas organelas, embora alguns indicadores de lesão também tenham sido observados. A reinervação e o fluxo de FG do músculo para a medula espinhal foi observada nos grupos C, N e NB, onde no grupo NB foi observado maior número de neurônios marcados quando comparado ao grupo N. Destaca-se ainda que no grupo NB houve menor dispersão dos neurônios motores estando mais próximo ao grupo C. O mesmo ocorreu em relação às células da microglia e à topografia do nervo isquiático. Os resultados observados neste estudo indicam que o BHF promoveu maior sobrevivência dos neurônios motores e consequentemente melhor reinervação, levando a um aumento no número de axônios regenerados e retorno morfológico da JNMs, desse modo, prevenindo a degeneração muscular. Esses resultados destacam os efeitos benéficos do BHF no reparo do nervo, superando aqueles alcançados apenas pela neurorrafia. Como um todo, destacamos os efeitos benéficos tardios do BHF na reparação da lesão e asseguram seu potencial para superar os efeitos de regeneração alcançados pela neurorrafia sozinha, endossando o BHF como um bioproduto promissor para ensaios clínicos.

ABSTRACT

Nerve injuries represent significant challenges for medical practice due to their frequent occurrence and substantial impact on quality of life. Complete nerve transection results in the blockade of nerve conduction, leading to changes in the nervous system as a series of pathophysiological and metabolic responses occur to stabilize and repair the injured tissues. The first major challenge is to keep the injured neurons alive and subsequently manage axonal growth. Another critical concern arises from the disruption of nerve-muscle connections and degeneration of neuromuscular junctions (NMJs), leading to atrophy and substantial loss of muscle function. The gold standard technique, neurorrhaphy, is insufficient to achieve significant motor recovery, and therefore, new techniques are being studied. A promising adjunct candidate is the heterologous fibrin biopolymer (HFB), which is free of human components and has shown remarkable potential for the regeneration of peripheral and spinal cord injuries. However, questions about its late regenerative effects on nerve-muscle interaction and the spinal cord after nerve injury remain unexplored. Therefore, we investigated the effects of nerve reconstruction via neurorrhaphy associated with HFB 120 days after injury and repair of the sciatic nerve in Wistar rats, addressing aspects of the peripheral nervous system - nerve, NMJ, and associated muscle - and the central nervous system - lower motor neurons and spinal cord microglia. For this, forty-four adult male Wistar rats were randomly distributed into four experimental groups: Control ©, where the right sciatic nerve was visualized; Denervated (D), where neurotmesis was performed with removal of a 6 mm fragment of the sciatic nerve; Neurorrhaphy (N), where after neurotmesis the stumps of the sciatic nerve were reconnected by neurorrhaphy; and Neurorrhaphy + HFB (NB), where HFB was added after the same neurorrhaphy. At 105 days post-injury, the neurotracer Fluorogold (FG) was applied to the right cranial tibial muscle for retrograde labeling of motor neurons in the anterior column of the lumbar portion (L2-L5) of the spinal cord. At 120 days, fresh collection or transcardiac perfusion was performed to obtain the spinal cords, sciatic and fibular nerves, and cranial tibial muscles. Regarding the nerve-muscle axis, for the fibular nerve, an increase in the number of intact axons was observed in the NB group, resulting in an increase in axon frequency, referring to the G-ratio/axon diameter. Regarding the NMJs, the NB group showed morphological approximation to the C group, and also an increase in the expression of the alpha-1 subunit of the nAChR and the protein Rapsyn. Taken together, these results contributed to muscle recovery, where the NB and C groups exhibited morphometric results of healthy muscle fibers. Regarding the spinal cord, ultrastructurally, the NB and N groups presented neurons with signs of preservation of their organelles, although some injury indicators were also observed. Reinnervation and FG flow from the muscle to the spinal cord were observed in the C, N, and NB groups, where the NB group showed a higher number of labeled neurons compared to the N group. It is also noteworthy that in the NB group there was less dispersion of motor neurons, being closer to the C group. The same occurred in relation to microglial cells and the topography of the sciatic nerve. The results observed in this study indicate that HFB promoted greater survival of motor neurons and consequently better reinnervation, leading to an increase in the number of regenerated axons and morphological return of the NMJs, thus preventing muscle degeneration. These results highlight the beneficial effects of BHF on nerve repair, surpassing those achieved by neurorrhaphy alone. Overall, we emphasize the late beneficial effects of BHF in injury repair and affirm its potential to exceed the regenerative effects achieved by neurorrhaphy alone, endorsing BHF as a promising bioproduct for clinical trials.

1. Introdução

1.1. Estrutura e função do sistema nervoso

Os nervos periféricos são estruturas frágeis e delicadas, propensos a serem facilmente danificados por lesões como compressões, esmagamentos e traumas (1). As lesões nervosas constituem um caso clínico comum, com alta prevalência e incidência mundial, afetando cerca de 18 indivíduos por 100.000 a cada ano (2), superando, por exemplo, a incidência de cânceres de ovário e estômago (3). Embora essas lesões estejam frequentemente associadas a traumas como acidentes de veículos ou com armas perfurocortantes, também é grande o número de lesões iatrogênicas, isto é, erro médico, durante cirurgias emergenciais ou eletivas (4). Estudos epidemiológicos realizados ao redor do mundo (3-6) apontam uma maior propensão de jovens do sexo masculino, sendo as lesões de nervos no carpo ou membros inferiores as mais prevalentes, seguidas por lesões no braço. Muitos indivíduos acometidos por lesões nervosas, tanto em casos graves quanto moderados, apresentam recuperação incompleta, resultando em perdas transitórias ou permanentes das funções motoras e sensoriais, além de apresentarem dor crônica, atrofia muscular e fraqueza. Aproximadamente um terço de todas as lesões nervosas demonstram recuperação incompleta com má restauração da função (7).

Os nervos são estruturas formadas por feixes de fibras nervosas que fazem parte do sistema nervoso periférico e podem ser classificados de acordo com sua origem em cranianos ou espinais. Os nervos espinhais são aqueles conectados à medula espinal, tendo sua origem real no gânglio da raiz dorsal e na coluna anterior de substância cinzenta da medula espinal. Os nervos consistem em feixes de axônios, que são prolongamentos longos e delgados de neurônios que alcançam uma estrutura alvo, que determina o tipo de inervação como sensitiva ou motora. Os nervos sensitivos são formados por fibras aferentes, responsáveis por levar informações do meio ambiente e do interior do corpo para os centros nervosos. Os nervos motores apresentam fibras eferentes, que conduzem informações dos centros nervosos para os órgãos efetores. Já os nervos mistos, sendo estes a grande maioria dos nervos presentes no corpo humano, já que todo nervo espinal é misto, possuem tanto fibras eferentes quanto aferentes. Assim, estabelece-se uma via de comunicação mútua entre o sistema nervoso central e as áreas periféricas do corpo (1), como por exemplo no nervo isquiático, o maior nervo do corpo, que tem origem na porção lombar da

medula espinal e se ramifica nos nervos tibial, fibular e sural, sendo responsável pela maior parte da inervação sensitiva e motora do membro pélvico.

A conexão entre o neurônio motor e as fibras musculares, se dá através dos axônios. O conjunto de axônios formam o nervo. Cada nervo é composto por uma camada externa de tecido conjuntivo denso, conhecida como epineuro, que reveste o nervo e preenche os espaços entre os feixes de fibras nervosas, proporcionando resistência e rigidez à estrutura. Cada feixe contém vários fascículos nervosos e é revestido por uma bainha externa de tecido conjuntivo e uma camada interna de células achatadas e justapostas, o perineuro. As células da bainha perineural se unem por meio de junções oclusivas, formando uma barreira à passagem de muitas macromoléculas, o que representa um importante mecanismo de defesa contra agentes agressivos. Essas células são permeadas por pequenos vasos sanguíneos, conhecidos como *vasa nervorum*, que irrigam o interior do tecido nervoso. Dentro de cada fascículo, encontram-se axônios, cada um envolvido pela bainha de células de Schwann (bainha de mielina), com sua lâmina basal e um envoltório conjuntivo composto principalmente por fibras reticulares sintetizadas pelas células de Schwann, chamado endoneuro (8-10).

Os neurônios motores somáticos são células nervosas especializadas, com arborização dendrítica altamente desenvolvida, que conduzem impulsos nervosos para fora do sistema nervoso central, com a principal função de controlar os órgãos efetores, entre eles os músculos estriados esqueléticos. O neurônio, é composto por três partes: soma, o corpo celular; projeções a partir do soma, axônios e dendritos.

Os neurônios motores são multipolares, ou seja, possuem um único axônio e múltiplos dendritos. Seu corpo celular está localizado na coluna anterior da substância cinzenta da medula espinal, principalmente na lâmina 9 de Rexed, podendo ser classificados em neurônios motores alfa, beta e gama. No caso dos neurônios motores alfa, seus axônios se estendem por todo o corpo através de nervos periféricos até atingirem os órgãos-alvo (11, 12), o músculo estriado esquelético, onde forma uma região morfológica, molecular e funcionalmente especializada chamada junção neuromuscular (JNM) (Figura 1). Um neurônio motor e as fibras musculares por ele inervadas constituem uma unidade motora.

Na JNM, ocorre a transdução de um sinal elétrico (impulso nervoso) para um sinal físico-químico (neurotransmissores) do neurônio motor para a fibra muscular, promovendo a contração muscular. Esta junção apresenta uma subclasse importante de sinapse no sistema nervoso de mamíferos, crítica para realização de um movimento coordenado (11).

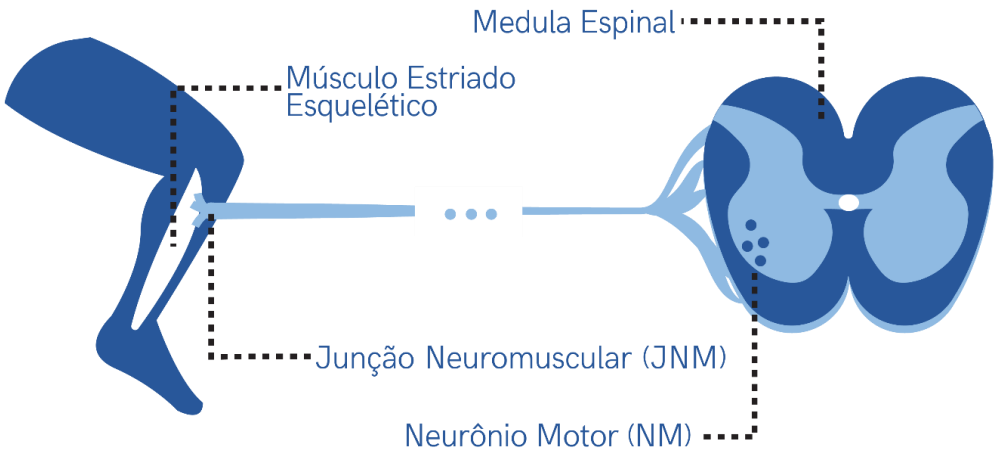

Figura 1. Esquema ilustrativo da unidade motora, sendo exemplificado estruturas relevantes para a realização de um movimento, desde o neurônio motor situado na coluna anterior da medula espinal até a junção neuromuscular no músculo estriado esquelético (8).

Além dos neurônios, o meio celular da medula espinhal também contém outra classe importante de células conhecidas como glia (13). Essas células gliais podem ser categorizadas em micróglias e macróglias, e ambas desempenham um papel central no sistema nervoso, proporcionando um ambiente otimizado para o desenvolvimento saudável e a função neuronal (13, 14).

As macróglias compreendem astrócitos e oligodendrócitos no SNC, e células de Schwann no SNP (13). Os astrócitos são células heterogêneas que desempenham um papel crítico na otimização do ambiente extracelular para a função neuronal (15, 16). Suas funções incluem regular os níveis de neurotransmissores e íons, para garantir um meio ideal para a sinalização neuronal. Além disso, os astrócitos contribuem para mudanças coordenadas no diâmetro dos vasos sanguíneos do SNC e no fluxo sanguíneo. Eles expressam altos níveis de transportadores para

neurotransmissores (como glutamato, GABA e glicina), removendo essas moléculas da fenda sináptica. Os astrócitos também são fundamentais para a formação da barreira hematoencefálica (BBB), que controla seletivamente a entrada de certas moléculas no parênquima cerebral com base na polaridade e no tamanho (13, 14, 17).

Em tecido saudável, os astrócitos exibem elevações transitórias de cálcio intracelular, representando uma forma de excitabilidade. Essas flutuações de cálcio estão envolvidas em funções astrocíticas dinâmicas críticas, incluindo interações com sinapses e regulação do fluxo sanguíneo. Além disso, os astrócitos respondem a todas as formas de injúria ao SNC através de um processo denominado astrogliosis reativa, que se tornou uma característica patológica de lesões estruturais no SNC (15, 16) na qual a dinâmica do Ca2+ dos astrócitos e as respostas da rede tornam-se aberrantes, alterando assim as funções sinápticas e o comportamento, resultando na perda de suporte trófico ou antioxidante dos astrócitos (18).

Por outro lado, como células inflamatórias residentes no sistema nervoso central, as micróglias exibem um fenótipo de vigilância, no qual detectam diversos sinais extracelulares, e também os integram e respondem a eles para manter a homeostase do SNC (13, 14, 19). As micróglias residentes também desempenham um papel central na regulação da homeostase vascular e na angiogênese, sugerindo que podem representar uma fonte alternativa de fatores de crescimento pró-angiogênicos e citocinas (20). Em condições normais, elas fornecem efeitos protetores e moduladores liberando fatores tróficos de sobrevivência e removendo células mortas e removendo sinapses em excesso. No entanto, quando ativadas em condições patológicas, elas sofrem mudanças morfológicas e funcionais complexas, tendo um papel central na lesão do SNC e na progressão da doença ao liberar mediadores inflamatórios e citotóxicos (14). Em condições não inflamatórias, as micróglias têm uma morfologia altamente ramificada com longos ramos sinuosos que surgem de um pequeno corpo celular. Após a detecção de um estímulo patológico, as micróglias mudam rapidamente sua morfologia encurtando seus processos e aumentando seu corpo celular (21, 22). Essa mudança morfológica ocorre continuamente e o grau de desramificação está relacionado à gravidade do estímulo patológico (22). Assim, a interação entre motoneurônios e o microambiente circundante desempenha um papel crítico em sua sobrevivência, regulação do estado funcional e conectividade sináptica.

1.2. Junção Neuromuscular

As JNMs são estruturas pequenas (30-60 µm) quando comparadas ao comprimento das fibras musculares inervadas, e a maior parte das fibras musculares esqueléticas são recrutadas por uma única JNM (Figura 2-A)(23). A morfologia clássica da JNM, descrita inicialmente em roedores, é caracterizada por uma estrutura em forma de “pretzel”, e mudanças nessa estrutura estão intimamente associadas a patologias motoras (24). Morfologicamente as JNMs são compostas por três compartimentos celulares intimamente associados (25), sendo eles o terminal nervoso (ou membrana pré-sináptica), a fenda sináptica e a membrana pós-sináptica.

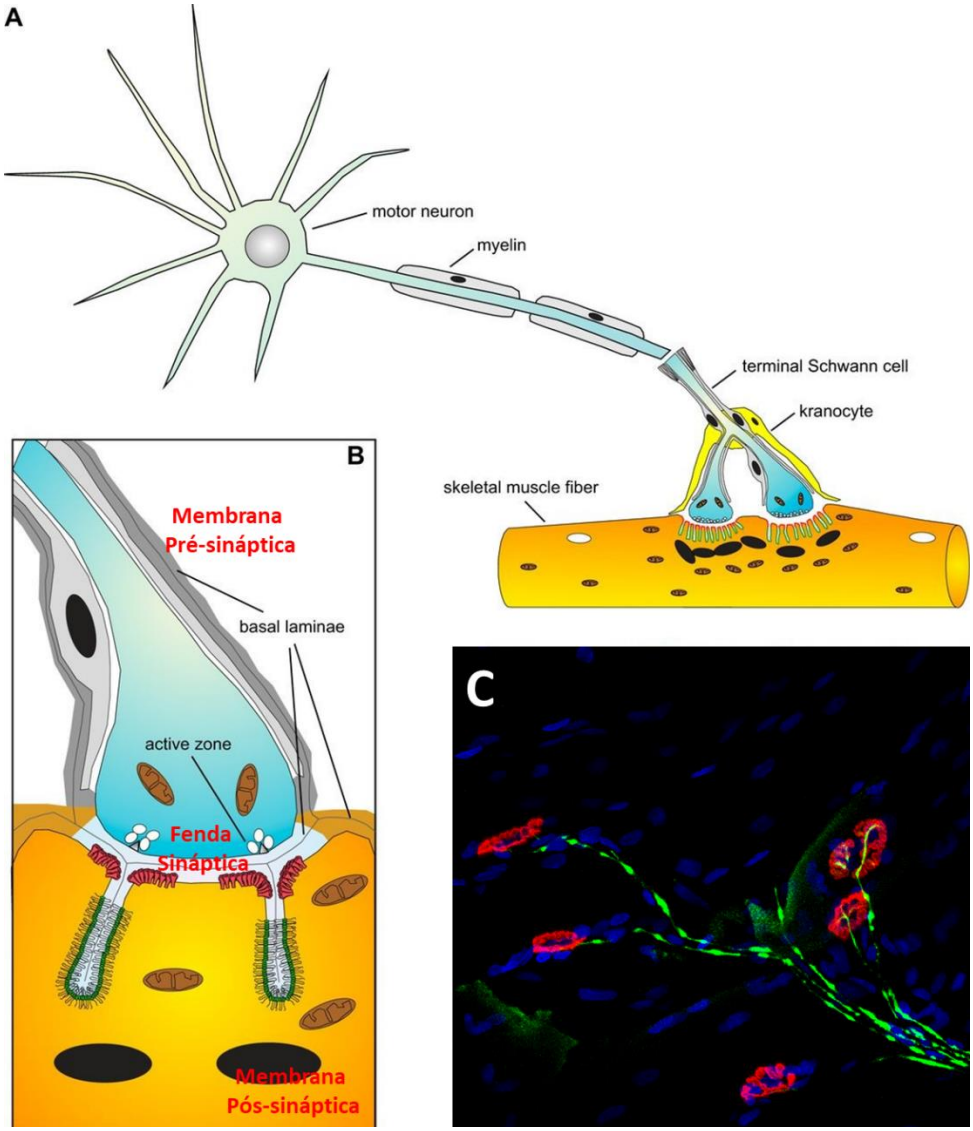

Figura 2: Organização da junção neuromuscular. A: Neurônios motores, cujos corpos celulares e dendritos estão localizados na medula espinhal, enviam seus axônios para a periferia e formam junções neuromusculares para inervar fibras musculares esqueléticas. B: Alta ampliação da junção

neuromuscular. C: Vista de montagem completa da faixa sináptica de um sóleo de rato, fotomicrografia cedida pela autora Selma Matheus. Axônios motores são rotulados com anticorpos para a proteína NF200 (Neurofilamento-200; verde), núcleos inespecíficos são vistos em azul pela marcação com DAPI, e nAChRs pós-sinápticos são visualizados por α-BTX (vermelho). Imagem adaptada de (24).

Na membrana pré-sináptica (Figura 2-B), os ramos terminais dos axônios dos neurônios motores inferiores formam botões sinápticos que, no caso de mamíferos, abrigam vesículas sinápticas contendo o neurotransmissor acetilcolina (ACh). Este terminal nervoso possui vários componentes celulares, incluindo mitocôndrias, retículo endoplasmático, endossomos de reciclagem, substâncias orgânicas e íons metálicos (26, 27). Uma grande quantidade de vesículas sinápticas e células de Schwann terminais ou peri-sinápticas (tSCs) também são encontradas nesta região (28-30); elas são células gliais não mielinizantes cujas extensões cobrem os terminais nervosos, protegendo-os de lesões químicas e mecânicas (31). Além disso, as tSCs são as principais responsáveis pela plasticidade estrutural das JNMs, detectando possíveis alterações na transmissão sináptica (32, 33). Uma a três tSCs cercam o terminal nervoso e participam ativamente do desenvolvimento, manutenção e reparo da função sináptica (23). Quando o potencial de ação do nervo motor chega ao terminal do neurônio pré-sináptico, ele abre canais de cálcio que dependem da voltagem. Isso permite que íons de Ca^{2+} entrem no citosol do neurônio pré-sináptico a partir do fluido extracelular. Esse aumento de Ca^{2+} provoca a fusão de várias centenas de vesículas cheias de neurotransmissores com a membrana celular do neurônio pré-sináptico, utilizando proteínas SNARE, liberando assim a ACh por meio da exocitose para a fenda sináptica.

A fenda sináptica separa o terminal nervoso pré-sináptico da membrana pós-sináptica, constituindo um estreito espaço de 50 a 80 nm de largura (Figura 2-B). Ela é preenchida com a lâmina basal sináptica, composta por moléculas secretadas tanto pelo terminal nervoso quanto pela fibra muscular associada (34). Esta região abriga proteínas cruciais para a estabilidade, função e manutenção da JNM, incluindo aquelas responsáveis pelo agrupamento de receptores nicotínicos de acetilcolina (nAChRs) no sarcolema, como agrina, lamininas-4, 9 e 11, metaloproteinase de matriz 3 (MMP3) e colágeno IV. A acetilcolinesterase (AChE), essencial para degradar a ACh após a contração muscular, também está concentrada aqui (35, 36).

A membrana pós-sináptica (Figura 2-B) compreende a membrana plasmática da fibra muscular, sendo constituída por pregas e o sarcoplasma da fibra muscular (citoplasma) (29, 30). Essas pregas exibem duas regiões distintas: o ápice, que contém os nAChRs e proteínas adicionais como rapsina, utrofina e α-distrobrevina-1; e o fundo, que abriga α-distrobrevina-2, distrofina e moléculas de adesão neurais. Além disso, canais de sódio dependentes de voltagem, responsáveis pela geração de potenciais de ação, também estão presentes nesse local (24, 37, 38). As dobras do sarcolema amplificam a área de superfície da membrana pós-sináptica e facilitam a justaposição dos nAChRs com as áreas pré-sinápticas, enquanto os canais de sódio se estendem dentro do sarcoplasma. A lâmina basal, que envolve componentes da matriz extracelular, envolve firmemente as fibras musculares, conectando-se com a lâmina basal da fenda sináptica produzida pelas tSCs na periferia da JNM (24).

Na JNM, os nAChRs (Figura 2-C) são os principais responsáveis pela comunicação motora neuromuscular (39), facilitando a transmissão sináptica. Estruturalmente, eles são compostos por cinco subunidades dispostas em um padrão de roseta, formando canais iônicos (40). Esses receptores existem em duas formas: extrajuncionais imaturos, presentes em fibras musculares embrionárias e desnervadas, sendo compostos pelas subunidades duas alfas [α], beta [β], delta [δ] e gama [γ]; e as formas juncionais maduras, onde as subunidades α [2], β e δ são mantidas, e a subunidade γ é substituída pela epsilon [ε] (27).

A ativação dos nAChRs é iniciada pela ligação simultânea de duas moléculas de ACh às subunidades αδ e αε, induzindo uma alteração conformacional que abre o poro iônico e ativa o receptor (41, 42). A duração desse estado ativo é modulada pela interação entre o receptor e as moléculas de ACh, que são rapidamente degradadas pela acetilcolinesterase (AChE), retornando os nAChRs à sua configuração inativa (42). Em casos de lesão ou patologia, os nAChRs frequentemente retornam a um padrão embrionário, apresentando a subunidade γ em vez de ε (43). Essa troca de subunidades contribui para várias mudanças nas propriedades de estabilidade, cinética e transmissão (11). Existem sinais positivos e negativos envolvidos na manutenção da JNM e nos agrupamentos de nAChRs (23). O principal sinal positivo é a ligação que ocorre na via Agrina/LRP4/Musk/Rapsina (44), que está diretamente relacionada com a formação, agregação e manutenção funcional dos nAChRs.

A Agrina, uma glicoproteína liberada pelos axônios motores, se liga ao receptor LRP4 na membrana muscular. Esta ligação ativa a quinase específica do músculo (MuSK), que inicia uma cascata de sinalização intracelular. A ativação de MuSK resulta na fosforilação de várias proteínas, promovendo o agrupamento dos nAChRs na membrana pós-sináptica. A Rapsina, uma proteína associada aos nAChRs, é fundamental para ancorar e estabilizar esses receptores na membrana, garantindo a formação de sinapses funcionais (23, 29, 45).

A importância desta via é evidenciada por estudos que mostram que mutações ou disfunções em qualquer um dos componentes levam a falhas na formação das JNMs, resultando em doenças neuromusculares como a miastenia gravis (23, 24). Além disso, a via Agrina/LRP4/MuSK/Rapsina é essencial não apenas para a formação inicial das JNMs, mas também para sua manutenção e reparo ao longo da vida, adaptando-se a mudanças e lesões, configurando uma estrutura extremamente plástica e adaptativa (31, 46).

1.3. Lesões nervosas

As lesões nervosas são categorizadas em vários graus, baseados na severidade da lesão do tecido nervoso (1). Essas categorizações auxiliam profissionais da saúde e pesquisadores a entenderem melhor a fisiopatologia das lesões nervosas e a estabelecerem o tratamento mais adequado. Isso ocorre porque essas classificações possibilitam uma correlação entre as mudanças microscópicas observadas no nervo e os sintomas apresentados pelo paciente.

A primeira classificação clássica foi proposta por Sir Herbert Seddon, que estabeleceu uma classificação para as lesões em três níveis (47). Essa classificação foi baseada na existência de desmielinização e no grau de dano aos axônios e aos envoltórios conjuntivos do nervo. Em seguida, Sir Sydney Sunderland expandiu a classificação de Seddon, adicionando uma subdivisão, que foi baseada na descontinuidade das diversas camadas dos envoltórios conjuntivos no nervo (48) (Figura 3).

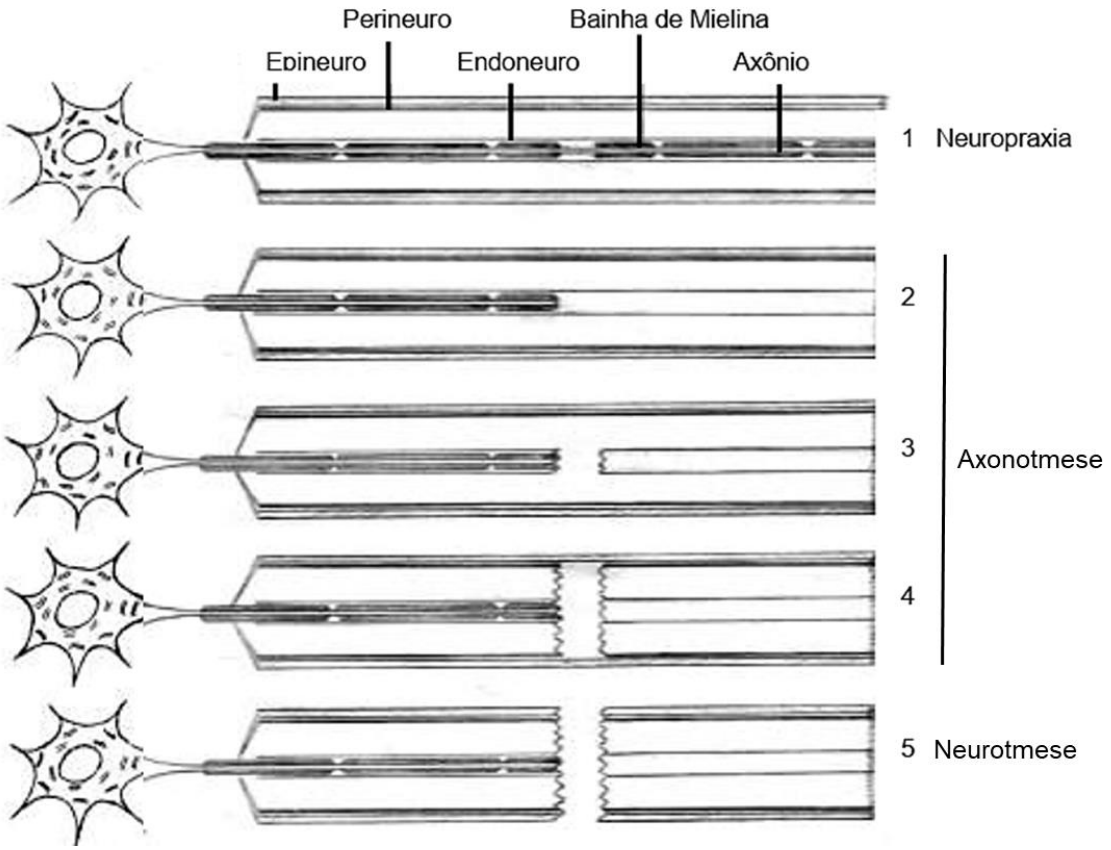

Figura 3. Classificação das lesões nervosas proposta por Sunderland. Adaptado de (49).

A classificação de Seddon categoriza as lesões nervosas em três graus distintos: neuropraxia (Figura 3-1), axonotmese (Figura 3-2) e neurotmese (Figura 3-5). A neuropraxia é considerada a forma mais branda, caracterizada pela perda da bainha de mielina, mas sem danos ou ruptura do tecido nervoso, de maneira que não há descontinuidade axonal, resultando apenas em uma interrupção temporária da transmissão do impulso nervoso (47). Neste caso, há uma perda funcional transitória e que normalmente apresenta recuperação rápida e completa sem necessidade de intervenção (1).

Já a axonotmese é considerada um tipo intermediário de lesão. Nela o tecido nervoso é danificado, embora haja preservação parcial dos envoltórios conectivos (epineuro, perineuro e endoneuro) que protegem o nervo e não há ruptura da continuidade axonal (47). Nestes casos a recuperação funcional depende do crescimento axonal, e ocorre mais comumente associada às lesões por esmagamento e fraturas ósseas. Dado que os envoltórios de tecido conjuntivo permanecem preservados, a perspectiva de recuperação é positiva, no entanto, a recuperação total é menos provável do que na neuropraxia (1).

O terceiro grau, ou neurotmese, é a forma mais grave, em que ocorre um dano generalizado com transecção completa de todas as camadas nervosas, dessa forma afetando a bainha de mielina, os envoltórios conectivos e os axônios (47). Neste último caso, uma intervenção cirúrgica é necessária para possibilitar regeneração e recuperação motora após a lesão (1).

Em seguida, a classificação proposta por Sunderland (48) expandiu a classificação de proposta por Seddon, a fim de distinguir a dimensão do dano nos envoltórios conjuntivos, ressaltando principalmente os diferentes graus possíveis em casos de axonotmese, assim descrevendo cinco possíveis estágios para a lesão nervosa (1). O primeiro estágio corresponde à neuropraxia de Seddon (Figura 3-1). Os estágios 2, 3 e 4 podem ser comparados à axonotmese, com variações no grau de lesão (Figura 3-2 a 4). No estágio 2, a lesão ocorre a nível de bainha de mielina e axônios, mas sem descontinuidade dos envoltórios conjuntivos, de maneira que há desnervação dos órgãos-alvo e distúrbio das funções sensoriais e motoras, mas sem necessidade de qualquer intervenção cirúrgica. A recuperação funcional acontece de maneira espontânea, embora possa levar de semanas a meses, dado que a regeneração axonal é essencial. No estágio 3, a lesão se estende à bainha, aos axônios e ao endoneuro, de maneira que a recuperação autônoma se torna mais desafiadora. No estágio 4, a lesão também atinge o perineuro, de maneira que há continuidade apenas do epineuro, configurando um dano bastante severo, comumente ocasionado por esmagamentos. O estágio 5, o mais grave, é equivalente à neurotmese de Seddon (Figura 3-5), em que há uma ruptura de todas as camadas nervosas (48).

Na transecção completa do nervo, ou neurotmese, todas as estruturas do aparato neuromuscular são prejudicadas, desde as JNMs e as fibras musculares até o corpo celular do neurônio motor na medula espinal, devido ao bloqueio da condução nervosa. Ao contrário do sistema nervoso central, o sistema nervoso periférico apresenta capacidade de regeneração e reinervação, sendo que os axônios lesionados se regeneram lentamente a uma taxa de 1 a 4 mm/dia (50). No entanto, diversos fatores dificultam essa regeneração após a lesão, incluindo a severidade, o mecanismo de lesão, a grande distância entre o corpo celular do neurônio e o tecido alvo e a perda do suporte das células de Schwann, de modo que a recuperação funcional total normalmente não é alcançada (51, 52).

1.4. Patofisiologia da lesão nervosa

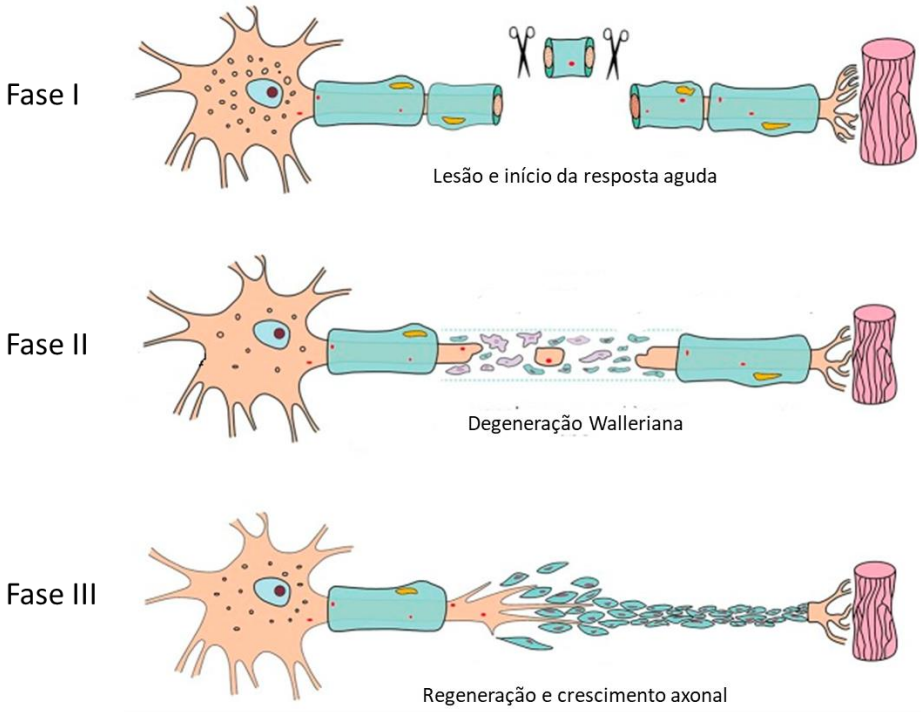

Figura 4. Representação esquemática das mudanças desencadeadas pela lesão de nervo. Adaptado de (53).

Após a lesão nervosa, uma cascata de respostas fisiológicas e metabólicas é desencadeada no nível celular no local da lesão e no corpo celular dos neurônios afetados, na tentativa de se restabelecer o dano resultante da lesão (23) (Figura 4 - Fase I). Na neurotmese, o nervo é segmentado em dois cotos, distal e proximal ao local da lesão, que estão sujeitos a processos relativamente distintos (54). O coto proximal se mantém ligado ao corpo celular na medula e adota um perfil regenerativo, enquanto que o órgão alvo e o coto distal são privados de sua fonte de estímulo elétrico e passam por alterações degenerativas seguidas por um processo de regeneração após inervação.

No coto distal, em que os axônios perdem contato com os corpos neuronais, rapidamente tem início o processo da degeneração Walleriana, manifestando-se como quebra da mielina e desintegração axonal (Figura 4 - Fase II). Esse processo inicia-se com um influxo de cálcio intracelular, desencadeando a ativação e

granulação de proteases dentro do axoplasma através da proteólise de microtúbulos e neurofilamentos. Essa sucessão de eventos compromete ainda mais a integridade organizacional da estrutura celular (54, 55). Nesse meio, padrões moleculares associados a danos (DAMPs) e agentes pró-inflamatórios, incluindo fator de necrose tumoral (TNF-)α, interleucina (IL-) 1β e CCL2, ativam a resposta imune inicial, principalmente atribuída a macrófagos (56). Uma das principais funções desses macrófagos é a depuração de resíduos teciduais, papel reforçado pelas células de Schwann através da autofagia da mielina (57). As células de Schwann, fibroblastos e macrófagos residentes também contribuem para o meio inflamatório, liberando mediadores pró-inflamatórios (58).

Dentro da depuração tecidual, a regeneração começa lentamente na extremidade proximal do local da lesão e prossegue em direção ao segmento distal (Figura 4 - Fase III). Nesse contexto, as células de Schwann próximas à região lesada se desdiferenciam, proliferam e migram para o local da lesão. Lá, elas se alinham dentro dos tubos endoneurais, formando colunas longitudinais conhecidas como bandas de Büngner, dentro das quais liberam fatores de crescimento e fatores tróficos para estimular o alongamento axonal até o órgão previamente inervado (52). É importante ressaltar que a orientação correta das bandas de Büngner é dependente de uma vasculatura polarizada, induzida pelo fator de crescimento endotelial vascular derivado de macrófagos ao estímulo da hipóxia. Esses vasos sanguíneos recém-formados são essenciais para a regeneração guiando a migração das células de Schwann através da ferida e subsequente alongamento axonal (59).

Dentre as proteínas constituintes do citoesqueleto axonal, as mais comumente estudadas são os neurofilamentos, cuja principal função é assegurar a integridade mecânica dos axônios (60). Em quadros de lesão no sistema nervoso, ocorre a interrupção da organização e/ou expressão dos neurofilamentos, desse modo o aumento dessas estruturas está relacionado a maturidade do tecido e melhora na recuperação pós lesão. Estudos utilizando como modelo a lesão nervosa em diferentes intervalos de tempo comprovaram que há associação do aumento de neurofilamentos à melhora do desempenho funcional (61-64). Durante o processo de regeneração, as células de Schwann expressam proteínas essenciais como a S100 (65, 66) e mielinizam os axônios de médio a grande calibre, assegurando a transmissão adequada do impulso nervoso.

No coto proximal, a neurotmese evoca uma resposta retrógrada nos corpos celulares neuronais (10), havendo mudanças estruturais e alterações em seu perfil de expressão gênica adotando uma função regenerativa ao invés de sináptica/de transmissão (52). Os neurônios sobreviventes sofrem uma série de alterações fisiológicas e morfológicas denominada cromatólise, caracterizada pelo inchaço e arredondamento do corpo celular, dissolução dos grânulos de Nissl, deslocamento excêntrico do núcleo e retículo endoplasmático e desorganização das organelas (1, 67). Essas modificações estruturais são paralelas a uma mudança no metabolismo celular fisiológico em direção à síntese de proteínas envolvidas na regeneração axonal (10), como aqueles relacionados ao citoesqueleto e fatores de crescimento (54). Com a eliminação dos resíduos de mielina, a regeneração começa lentamente na extremidade proximal do local da lesão e prossegue em direção ao segmento distal. Os axônios seccionados produzem um grande número de brotos, intimamente associados às células de Schwann, formando vários cones de crescimento com axônios de pequeno calibre que crescem gradativamente ao longo da deposição da bainha de mielina.

De maneira coordenada, as células gliais ativadas proliferam significativamente após a lesão, sendo um processo que persiste de dois dias a vários meses após a axotomia (68). A ativação astrogliar e microgliar após a axotomia parece desempenhar um papel crucial na retração sináptica dos corpos celulares dos motoneurônios em que realizam alterações sinápticas retrógradas conhecidas como “*synaptic stripping*”, um processo pelo qual a micróglia residente seletivamente remove sinapses de neurônios lesionados (69). Nesse processo há o extenso descolamento de terminais pré-sinápticos de perfis neuronais e dendritos de motoneurônios axotomizados (70), pela ação da glia residente. Esse estímulo rapidamente recruta maiores números de astrócitos e micróglia nas proximidades dos terminais sinápticos afetados que, em seu modo regenerativo, reagem através de mudanças conformacionais e estruturais de suas projeções citoplasmáticas se contactando com a membrana do motoneurônio lesionado e os terminais sinápticos degenerados (71), em especial, aqueles de origem glutamatérgicas (72), que podem ser identificados através de marcações dos transportadores vesiculares de glutamato 1 ou 2 (VGLUT-1/2).

Nesse cenário, a distância da lesão do corpo celular implica piora do quadro regenerativo, como observado em neurônios sensoriais, onde a maior proximidade

com os gânglios da raiz dorsal está diretamente relacionada ao número de células nervosas mortas (73) e uma maior distância efetiva para a regeneração. Outro desafio importante é o emparelhamento equivocado dos axônios em regeneração, que podem se conectar com outros fascículos nervosos, direcionando-os para outros músculos ou outros tecidos (72). Esses erros alteram a conectividade original dos motoneurônios, levando a deficiências funcionais motoras. Surpreendentemente, embora os axônios se regenerem, estudos têm demonstrado que a recuperação morfológica do nervo e do músculo não é suficiente para promover a recuperação funcional, pois ainda pode haver comprometimento da funcionalidade sináptica (74, 75).

As lesões nervosas também afetam diretamente o sistema muscular, causando prejuízo aos músculos inervados que perdem sua fonte de estímulo elétrico. São observadas diversas alterações morfológicas e moleculares, geralmente associadas à atrofia muscular, com redução da área das fibras, do número de mionúcleos e células satélites (76); desorganização extracelular dos sarcômeros e intracelular de suas organelas, com dano mitocondrial e vacuolização; e alteração na expressão de proteínas relacionadas à degeneração, inflamação e atrofia muscular (44, 77). Ainda que haja uma alta plasticidade neuromuscular após lesão e reinervação, o processo autônomo é insuficiente para recuperação dos movimentos finos, visto que atrasos na reinervação muscular ainda comprometem também a capacidade regenerativa dos motoneurônios afetados e há um desvio considerável da direção das fibras nervosas em regeneração (54).

Por fim, as terminações nervosas que formaram as JNMs também são perdidas e, mesmo com o brotamento axonal bem-sucedido, a falha da reinervação limita a recuperação da função muscular (78) (Figura 5A). Alguns fatores como o brotamento de um ramo irregular do nervo, poli-inervação (79) e, o mais comum, reinervação colateral das fibras musculares são obstáculos para uma recuperação funcional satisfatória. As JNMs desnervadas sofrem degeneração grave e subsequente desintegração (80) e desagregação dos nAChRs e das proteínas ancoradas, fundamentais para a manutenção de sua função (81). Os DAMPs dos axônios lesionados ativam as células de Schwann terminais (tSCs), as quais mantém contato íntimo com a porção do terminal nervoso das JNMs, e liberam quimiocinas, sinalizando como substratos de orientação para pontes de tSCs e reinervação da JNM (11, 82) .

A subunidade nAChR-ε é substituída pela nAChR-γ levando à falha na ativação sináptica, além de falência muscular e atrofia (83).

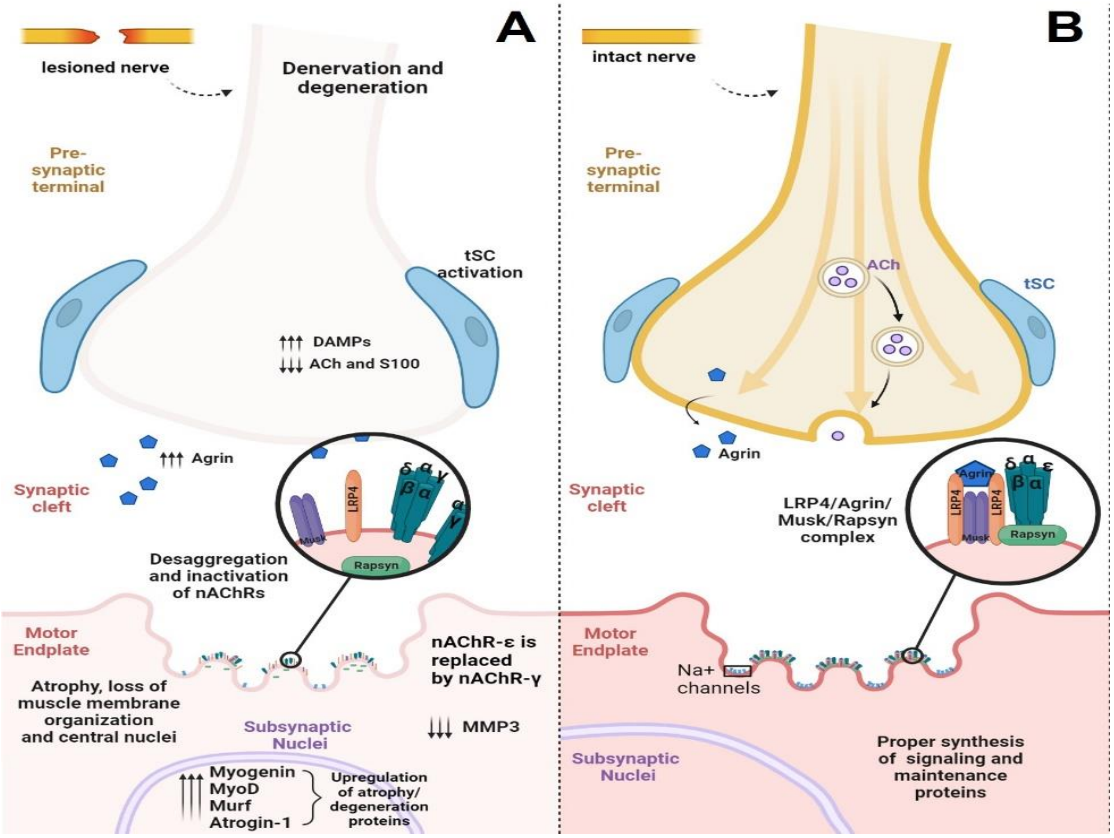

Figura 5. Eventos celulares e moleculares associados à desnervação e reparo muscular ao nível da junção neuromuscular. Esquema de junção neuromuscular desnervada (A) e saudável (B). Após a lesão nervosa, todos os componentes da JNM são prejudicados e a via de sinalização Agrina/LRP4/Musk/Rapsina desempenha um papel significativo para a formação dos novos cluster nAChRs e manutenção da JNM. Adaptado de (25).

Outro prejuízo decorrente da desnervação as JNMs é relacionado a mudanças significativas na expressão de proteínas da via da Agrina/Rapsina/Musk/LRP4, fundamental para a manutenção e estabilização dos clusters de nAChR (84), levando a alterações da área e conformação da JNM (77). Logo após a lesão, proteínas desta via têm síntese aumentada, mas sua complexa desorganização leva à falha no funcionamento adequado, inativação de MMP3 e acúmulo de Agrina na fenda sináptica (11). Devido a desorganização, o microambiente da JNM também é privado de outros sinais retrógrados e anterógrados que mantêm sua estabilidade (11), em que as tSC ativadas estendem seus processos de síntese de nAChR em regiões musculares não-sinápticas.

Para o processo regenerativo, a proteína Agrina tem um papel fundamental em iniciar a via de agrupamento de receptores, remodelando e retornando as JNMs à sua forma convencional (23). A proteína LRP4, dependente de Agrina para ativação (84), também tem papel fundamental no processo regenerativo, contribuindo para a ativação das tSCs após lesão, que são responsáveis por orientar a reinervação dos JNMs nas fibras desnervadas (77). Notavelmente, as tSCs ativas também mantêm a organização dos JNMs secretando substratos que regulam proteínas pós-sinápticas, como a MMP3, que está envolvida na integridade da lâmina basal e da placa terminal (80, 85). Outras proteínas sintetizadas pelo músculo também desempenham um papel fundamental na manutenção e regeneração pós-sináptica, já que são participantes de vias de regulação importantes, como as proteínas MusK e Dok7 da via da Agrina ou MURF-1 e atrogina-1 da via da ubiquitina-proteassoma, que previnem a desnervação (11, 77). Ademais, o retorno da subunidade épsilon substituindo a subunidade gama é um indicador de regeneração, pois ocorre somente após a reinervação e diferenciação dos miotubos (11).

Em conjunto, grandes eventos celulares e moleculares ocorrem e privam não só o nervo associado, as células de Schwann e as fibras musculares, mas também a JNM, provocando uma série de sinais que, mesmo com a regeneração morfológica dos axônios, podem não resultar em associação definitiva com a recuperação funcional. A compreensão do nicho terapêutico da JNM é essencial para proporcionar resultados positivos após a reinervação, o que inclui não apenas a reinervação através da chegada de axônios regenerados aos domínios musculares pós-sinápticos desnervados, mas também a capacidade de ativação sináptica (Figura 5B). Estudos indicam que somente a partir de 12 semanas após reconstrução nervosa com neurorrafia isolada, que as placas motoras estão completamente reinervadas, com retorno da morfologia das JNMs aos padrões normais (74, 86). Surpreendentemente, estudos em roedores (74, 75) demonstraram que existe um período crítico após o qual, mesmo com 4 meses após reparo, reinervação do músculo-alvo e formação das JNMs, não há resultado motor satisfatório, o que pode refletir em um possível defeito na transmissão sináptica. Isto sugere que o reparo por neurorrafia (sutura) isolada é insuficiente para restauração funcional das JNMs (75).

1.5. Abordagens de reparo após lesão

Nos últimos anos, várias abordagens têm sido testadas e utilizadas com o objetivo de aperfeiçoar a funcionalidade do nervo lesionado (87, 88). A maioria dos modelos experimentais utiliza roedores, em que são cirurgicamente realizadas lesões nos nervos facial, ulnar ou isquiático (89). Tratamentos que resultam em completa recuperação morfológica e funcional permanecem um desafio para a prática médico-cirúrgica. As principais dificuldades estão relacionadas à própria reconexão e regeneração nervosa, em que os axônios regenerados não conseguem atingir seus tubos endoneurais originais (54), além disso há dificuldade na revascularização local, perda progressiva do caráter regenerativo nas células de Schwann, atrofia dos órgãos inervados. Além disso o tempo prolongado entre a intervenção médica após a lesão são fatores cruciais que interferem na recuperação (9, 54, 60, 90).

Dentre as técnicas de correção para transecção nervosa, a neurorrafia término-terminal é o padrão-ouro (39). Esse tipo de neurorrafia só é possível quando os cotos nervosos estão preservados, visíveis e íntegros, sem perda tecidual, e não há tensão para reaproximação e reconexão dos cotos (91). Apesar dos avanços nas técnicas de reparo microcirúrgico, a recuperação funcional satisfatória das estruturas acometidas ainda não foi alcançada, pois mesmo com o sucesso da reconexão entre os cotos nervosos, as taxas de recuperação motora tardia atingem apenas 50% de sucesso (92). Desse modo, a investigação e desenvolvimento de novas estratégias e abordagens que visem uma melhor regeneração são necessários. Diversos estudos têm investigado a associação de terapias adjuntas à neurorrafia, como a utilização de enxertos nervosos, tubos conduítes, terapias celular, fotobiomodulação e aplicação de selantes de fibrina (1, 2, 7).

Os selantes de fibrina são substâncias adesivas que mimetizam os estágios finais da coagulação sanguínea, através da formação de um coágulo de fibrina estável e fisiológico no local de aplicação. Eles ainda fornecem um suporte físico para a matriz extracelular e podem ser associados a outros compostos de tratamento, já que possuem a capacidade de preservar os fatores bioquímicos e as propriedades originais dos implantes. (93-96). Dessa maneira, os selantes são muito úteis para proporcionar hemostase, permitir a redução no número de suturas e proteger o ambiente contra infecções por microrganismos (95, 97). Eles também permitem diminuição das reações inflamatórias e da incidência de trauma (1, 98),

proporcionando uma agilidade na cirurgia e na recuperação, devido à facilidade e rapidez de aplicação.

Em linhas gerais, os selantes de fibrina são produzidos de duas formas: a partir de derivados sanguíneos autólogos ou homólogos. Os selantes autólogos utilizam o sangue do próprio paciente, de maneira que são biocompatíveis e não apresentam risco de transmissão de doenças infecciosas, mas não são viáveis em cirurgias e aplicações de emergência. Como alternativa, selantes homólogos de fibrina produzidos por um pool de sangue humano têm sido utilizados. No entanto, nesses casos há riscos de transmissão de doenças infecciosas como hepatite, HIV e parvovirose humana (99). Além de ter um alto custo de matérias-primas, dado a necessidade de extração sanguínea de trombina bovina ou humana e fibrinogênio humano. Devido à sua composição com sangue humano, outro problema comum é a fibrinólise rápida, que se inicia em menos de 24 horas após a aplicação e desprende prematuramente os cotos nervosos (99).

Mesmo com sua introdução não tão recente na clínica humana, ainda não há consenso sobre o uso e a eficácia dos selantes de fibrina para reparo nervoso, com predomínio na literatura de estudos com modelos de roedores e poucas avaliações em humanos (98, 100). O uso de selantes ainda não é aprovado por agências reguladoras, como a Anvisa e Food and Drug Administration (americana) para reparo de nervos, mas o interesse nesta terapia, não só para reconstrução nervosa, é crescente. Até hoje, os selantes de fibrina disponíveis comercialmente são produzidos a partir de trombina bovina e humana e fibrinogênio (homólogo) e apresentam desvantagens e riscos, de modo que, além de transmissores de doenças infecciosas, podem gerar fibrose, toxicidade e necrose (1). Também podem levar ao desenvolvimento de anticorpos contra trombina bovina, reação anafilática a proteínas bovinas, entre outras reações adversas (101, 102).

1.6. Biopolímero Heterólogo de Fibrina

Considerando as desvantagens presentes nos selantes de fibrina comercialmente disponíveis, um grupo de pesquisadores do Centro de Estudos de Venenos e Animais Peçonhentos (CEVAP) da Universidade Estadual Paulista, Botucatu, São Paulo, Brasil, desenvolveu e padronizou um novo selante de fibrina na

década de 1990. O biopolímero heterólogo de fibrina (BHF) consiste em dois componentes principais, sendo eles uma enzima semelhante à trombina (serina protease) extraída do veneno da cascavel *Crotalus durissus terrificus* e um crioprecipitado rico em fibrinogênio e outros fatores coagulantes obtido do sangue do búfalo *Bubalus bubalis (95, 102)*. Quando ambos os componentes são misturados na presença do diluente de cloreto de cálcio, o produto polimeriza-se, formando uma robusta rede de fibrina. O BHF é um fármaco inteiramente brasileiro que tem atividade comparável aos selantes comerciais, ainda sendo biodegradável, absorvível e sem sinais de toxicidade ou reação adversa (103). Devido à sua composição única e ausência de sangue humano, é considerado o único biopolímero heterólogo de fibrina no mundo (100). Além disso, possui excelente capacidade adesiva e hemostática (95).

Comparado a outros selantes comerciais de fibrina utilizados clinicamente, apresenta outras vantagens devido ao seu baixo custo de produção, alta disponibilidade de matéria-prima para sua fabricação e possibilidade de adaptar sua formulação de acordo com o tipo de procedimento (102). Sua formulação permite sua utilização em pronta entrega na clínica médica e em diversos procedimentos cirúrgicos, como enxertos de pele e reconstruções cirúrgicas, auxiliando na hemostasia e reforço de sutura (91, 99). Além disso, sua capacidade regenerativa foi testada em 40 pacientes de um ensaio clínico de fase I/II para o tratamento de úlceras venosas crônicas, demonstrando ser um produto seguro, não imunogênico e com eficácia promissora, já que houve melhora significativa da qualidade do leito da úlcera, redução significativa da área da úlcera e cicatrização em vários pacientes (104, 105).

Nos últimos anos, o BHF tem sido utilizado em associação com sutura e outros fatores terapêuticos, a fim de potencializar ou minimizar as dificuldades do tratamento padrão-ouro atual para lesões nervosas. Em associação a neurorrafia para reparo de uma transecção nervosa, a aplicação do BHF demonstrou resultados positivos na redução do trauma mecânico do nervo (redução do número de pontos de sutura) (106), demonstrou resultados morfológicos e/ou moleculares semelhante a sutura tradicional (44, 101, 106, 107), apresentou fácil utilização com boa capacidade adesiva (108); ainda proporcionou biocompatibilidade com outros materiais, principalmente terapias celulares, em que garantiu melhor sobrevivência das células e efetividade de suas funções (65, 66, 109).

Nosso grupo de pesquisa tem realizado diversos estudos investigando os efeitos regenerativos do BHF na reparação de lesões nervosas em ratos em diferentes tempos de reparo e situações de tratamento. De fato, foram observados muitos efeitos positivos associados ao potencial do BHF desde períodos iniciais após lesão, durante o pico de efeito pró-inflamatório, até períodos intermediários com um microambiente mais estabilizado (44, 77, 106, 107). Ressalta-se que a associação do BHF à neurorrafia resultou em melhorias significativas na regeneração nervosa, incluindo aumento do crescimento axonal, melhora no recrutamento da resposta imune e da vascularização tecidual, mais similaridade morfológica entre os tipos celulares observados e restauração e ancoramento das JNMs. Em uma perspectiva funcional, embora ainda não satisfatório, a combinação de BHF com sutura também já promoveu uma restauração mais eficaz do impulso nervoso, marcha e função motora. Esses resultados são promissores para o avanço do conhecimento na área de regeneração nervosa.

2. Justificativa

A recuperação motora segue sendo um desafio devido às diversas dificuldades da reconexão e regeneração das estruturas lesionadas. Uma hipótese é a falta de tempo suficiente para restabelecimento dessa coordenação motora refinada. Diante do proposto, este estudo tem como objetivo ampliar uma série de estudos já realizados pelo nosso grupo de pesquisa, analisando os efeitos regenerativos da associação do BHF à neurorrafia após 120 dias de reconstrução, que já demonstraram a consolidação precoce de um ambiente pro-regenerativo com potencial angiogênico e imunogênico associado ao BHF.

Outra questão relevante para assegurar um bom crescimento axonal e reinervação dos órgãos alvos é assegurar uma maior sobrevivência neuronal, através de ações sobre os neurônios motores e o parênquima celular da medula espinhal. Assim, é fundamental mais estudos que envolvam o sistema nervoso central.

Acrescido a isso, estudos experimentais em ratos demonstraram que as JNMs atingem seu potencial de regeneração em torno de 120 dias após a reconstrução. Assim, considerando esses aspectos, nosso estudo pretende contribuir para entender o efeito do BHF frente a distribuição e atividade dos neurônios motores, sua eficiência de reinervação e os efeitos de consolidação da regeneração. Desse modo, comprovar os efeitos positivos da associação do BHF à lesão nervosa, oportunizando o uso desse potente e inovador biofármaco brasileiro para a clínica médica.

3. Objetivos

Objetivo geral: Investigar os efeitos na reconstrução nervosa via neurorrafia associada ao BHF aos 120 dias após lesão e reparo do nervo isquiático de ratos Wistar, com ênfase em aspectos do sistema nervoso periférico (nervo, JNMs e músculo) e central (neurônios motores inferiores da medula espinal).

Objetivos específicos:

- Estudo do Sistema Nervoso Periférico:
  - ✓ Avaliação do caráter regenerativo nervoso através da análise morfológica e morfométrica do nervo fibular;
  - ✓ Análise da topografia nervosa (regeneração axonal e reatividade das células de Schwann) do nervo isquiático pelas imunomarcações de NF-200 e S100;
  - ✓ Avaliação do grau de atrofia e degeneração das fibras musculares através da análise das colorações de H.E. e Picrossirius Red;
  - ✓ Avaliação da integridade morfológica e morfométrica das JNMs através da marcação por esterase inespecífica;
  - ✓ Análise do microambiente e organização ultraestrutural das fibras musculares e das Junções Neuromusculares por Microscopia Eletrônica de Transmissão;
  - ✓ Análise da recuperação molecular de proteínas essenciais para manutenção e estabilização da fibra muscular e suas junções neuromusculares associadas por Western Blotting.

- Estudo do Sistema Nervoso Central:
  - ✓ Quantificação da população dos motoneurônios marcados retrogradamente após injeção de fluorogold no músculo tibial cranial;
  - ✓ Avaliação da dispersão e reconexão neuronal através da reconstrução tridimensional da população neuronal retrogradamente marcada;
  - ✓ Análise ultraestrutural do microambiente regenerado do corpo celular dos neurônios motores por Microscopia Eletrônica de Transmissão;
  - ✓ Análise do parênquima medular por imunomarcação de IBA-1.

4. Materiais e Métodos

4.1. Revisão Bibliográfica

Foi elaborado uma revisão de escopo que segue as diretrizes delineadas nos Itens Preferidos para Relatórios de Revisões Sistemáticas e Meta-Análises (PRISMA). Para isso, realizamos buscas nas bases de dados PubMed/MEDLINE, Scopus (Elsevier), Web of Science e SciELO, abrangendo artigos publicados até agosto de 2023. A busca utilizou as palavras-chave: “selante de fibrina heterólogo”, “biopolímero de fibrina heterólogo”, “biopolímero de fibrina”, “neurorrafia” e “lesão nervosa”, restritas a publicações em inglês.

Para garantir precisão, analisamos cuidadosamente títulos e resumos para considerar possíveis sobreposições de palavras-chave. Os artigos foram subsequentemente incluídos ou excluídos com base em critérios de elegibilidade predeterminados. Dois autores independentes conduziram o processo de seleção utilizando procedimentos padronizados. Quando o título e o resumo não forneciam clareza suficiente, análises de artigos completos foram realizadas. Artigos de revisão foram examinados para identificar possíveis estudos experimentais, e artigos que não ofereciam novos insights foram excluídos após uma avaliação abrangente.

Entre os 103 artigos inicialmente identificados, 31 foram eliminados devido à duplicação, e outros 58 foram excluídos de acordo com os critérios de elegibilidade (não estudo com modelo animal; sem modelo de lesão nervosa ou envolvimento de degeneração/regeneração nervosa; sem uso de HFB; não artigo de pesquisa). Notavelmente, seis artigos de pesquisa alinhados com os critérios de elegibilidade estipulados foram identificados através de revisões de escopo e sistemáticas. Um total de 20 artigos sobre o uso de HFB para reparo de lesões nervosas foram então escolhidos para avaliação detalhada do texto, atendendo aos critérios de inclusão predefinidos, formando a base para o escopo desta revisão (Figura 6). Além disso, outros artigos foram consultados livremente para aprofundar aspectos da biologia da junção neuromuscular, a fisiopatologia da lesão nervosa e a exploração de selantes de fibrina para reparo de lesões nervosas.

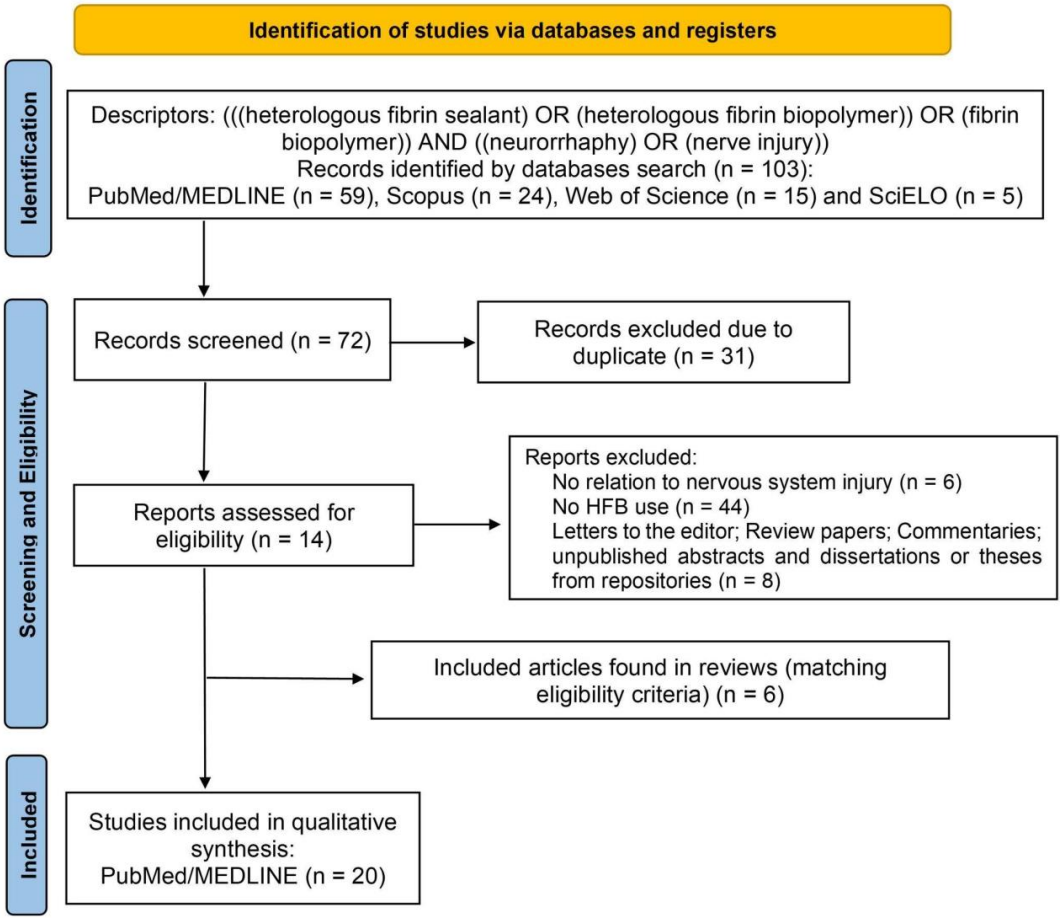

Figura 6. Diagrama demonstrativo dos critérios de seleção e inclusão de estudos para a construção da revisão de escopo. Retirado de (25).

4.2. Animais

Para realização da parte experimental, foram utilizados 44 ratos Wistar machos adultos, provenientes do Biotério Central da Unesp, Câmpus de Botucatu, entre 90 e 95 dias de idade e peso corporal médio de 300g. Durante todo o período experimental, os animais foram mantidos no Biotério de Roedores 5 da Unidade de Pesquisa Experimental (Unipex) da Faculdade de Medicina de Botucatu (FMB/Unesp), em caixas de polietileno (medindo 40 x 30 x 15 cm), com fundos sólidos forrados com substrato de maravalha, sob condições controladas de luminosidade (12h claro/12h escuro), temperatura (24 ± 2 ºC), sendo fornecida água filtrada e ração Presence® *ad libitum*.

Os animais foram distribuídos aleatoriamente em 4 grupos experimentais, sendo que cada grupo foi constituído de 9 animais: Controle (C); Desnervado (D), Neurorrafia (N) e Neurorrafia + BHF (NB). Todos os procedimentos mencionados

foram aprovados pelo Comitê de Ética local, inscrito sob o número CEUA-FMB:1402/2021 (anexo 1).

4.3. Procedimento cirúrgico

Os animais foram anestesiados através de injeção intraperitoneal de solução anestésica contendo Ketamina (Dopalen, 70 mg/kg) e Xilazina (Anasedan, 30 mg/kg). Após tricotomia do membro pélvico direito, os animais foram posicionados em decúbito ventral, mantendo-se as patas dianteiras e traseiras em abdução. Foi realizada a aplicação de Lidocaína (7 mg/kg) no local da incisão e antissepsia com álcool-iodado, seguida de incisão sobre a face lateral da coxa, desde a altura do trocânter maior até o joelho, com exposição dos nervos isquiáticos direitos.

Nos animais do grupo C foi realizada apenas a localização e visualização do nervo isquiático e em seguida os tecidos moles e a pele foram reposicionados e suturados (Mononylon 7-0 e 5-0, Polysuture) (Figura 7A). Nos animais dos grupos D, N e NB, de forma padronizada, a cerca de 3 milímetros acima de sua trifurcação, foi realizada uma lesão nervosa por transecção do nervo isquiático (neurotmese). Nos animais do grupo D, a fim de evitar regeneração espontânea, foi removido um fragmento de 6 mm do nervo, e os cotos proximais e distais foram invertidos a 180º e fixados na musculatura adjacente, com pontos simples com fio de nylon (Mononylon 10-0, Polysuture) (Figura 7B). Nos grupos N e NB, imediatamente após a neurotmese os cotos nervosos foram reconectados. No grupo N, os cotos foram religados por meio de neurorrafia término-terminal (anastomose epineural) com 2 pontos simples, com fio de nylon (Mononylon 10-0, Polysuture) (Figura 7C). No grupo NB a reconstrução nervosa foi realizada por neurorrafia com 2 pontos simples seguida da aplicação de 250µL do BHF (44, 77, 107) (Figura 3D), cedido pelo CEVAP, Unesp Botucatu, SP, Brasil, cujos componentes e fórmula de aplicação constam das suas patentes (Números de registro: BR1020140114327 e BR1020140114360). No momento do uso, os componentes foram previamente descongelados e reconstituídos. A aplicação foi feita através da colocação simultânea da fração 1 (125 µL) com a fração 2 (125 µL) – feito imediatamente antes da aplicação, através da homogeneização de mesmas quantidades do fibrinogênio e fator diluente - no local da lesão.

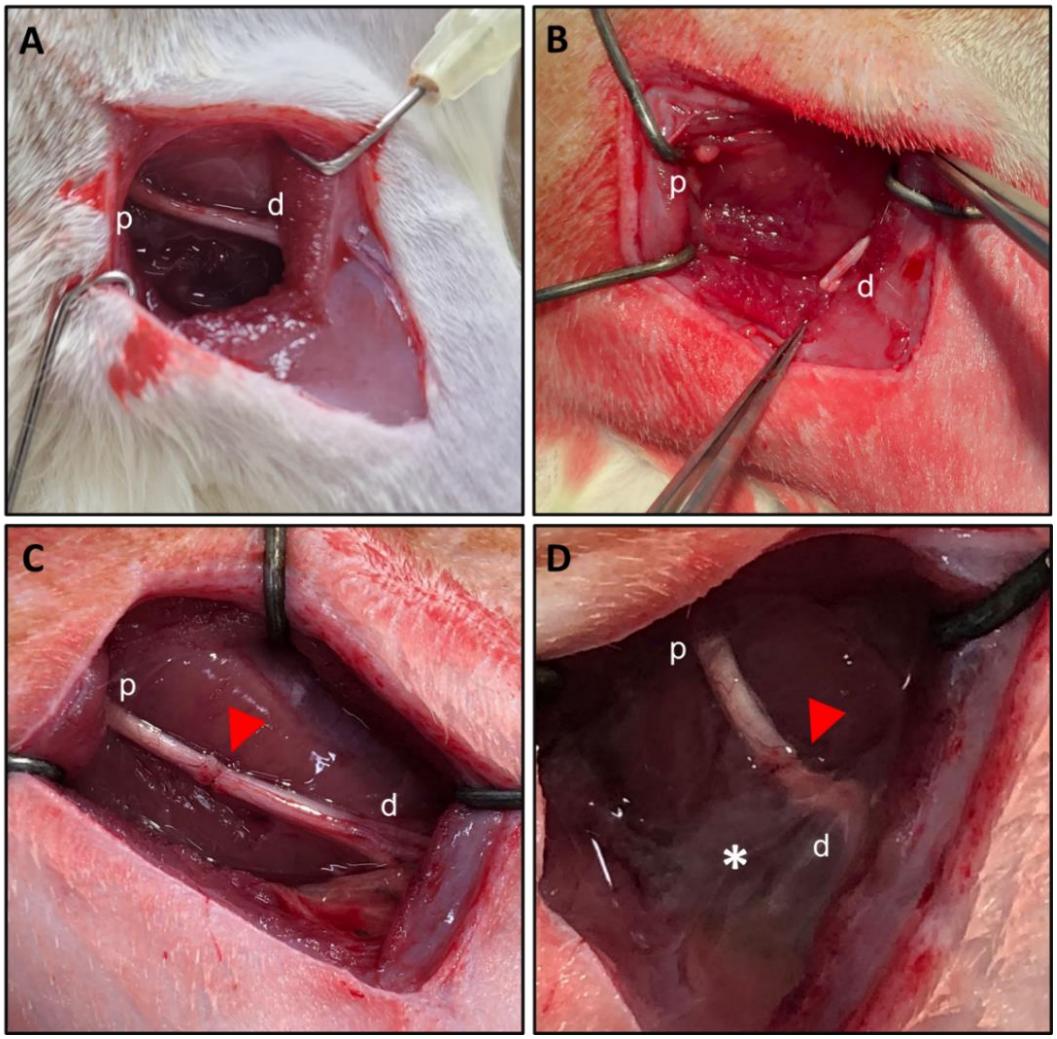

Figura 7. Fotografias do procedimento de cirurgia experimental, em que é possível observar as lesões de nervo para os grupos experimentais Controle (A), Desnervado (B), Neurorrafia (C) e Neurorrafia + BHF (D). (p): coto proximal; (d): coto distal; (cabeça de seta vermelha): local/ponto de neurorrafia; (*): BHF polimerizado.

Após a realização da reconstrução nervosa, os tecidos moles e pele foram suturados com pontos simples utilizando fio de nylon (Mononylon 7-0 e 5-0, Polysuture), os animais ficaram sob vigia e aquecimento até a recuperação. Em seguida foi administrado Tramadol (5 mg/kg) para analgesia da dor e Enrofloxacino (Baytril®, 10 mg/kg) para evitar infecções oportunistas via injeção subcutânea. Nos três dias consecutivos, o protocolo pós-cirúrgico contemplou a administração do analgésico por 3 dias a cada 24 horas, e se necessário até 5 dias, além da aplicação de Iodopovidona durante o período de cicatrização no local da incisão. Devido a dificuldade da cirurgia e seu caráter de alto grau invasivo, houve uma taxa de perda de cerca de 10% dos animais, devido majoritariamente a não recuperação da

anestesia, atingindo por volta de 1 a 2 animais por grupo (totalizando 44 cirurgias bem sucedidas).

Decorrido o período de 105 dias após a cirurgia, seis animais de cada grupo foram novamente anestesiados através de injeção intraperitoneal de solução anestésica de Ketamina (Dopalen, 70 mg/kg) e Xilazina (Anasedan, 30 mg/kg). Após efeito do anestésico, os animais foram posicionados em decúbito dorsal e foi realizada tricotomia do membro pélvico direito. Foram realizadas injeções do neurotraçador FluoroGold a 4% em NaCL 0,9%, de maneira padronizada, em 3 pontos ao longo do ventre do músculo tibial cranial direito (Figura 8).

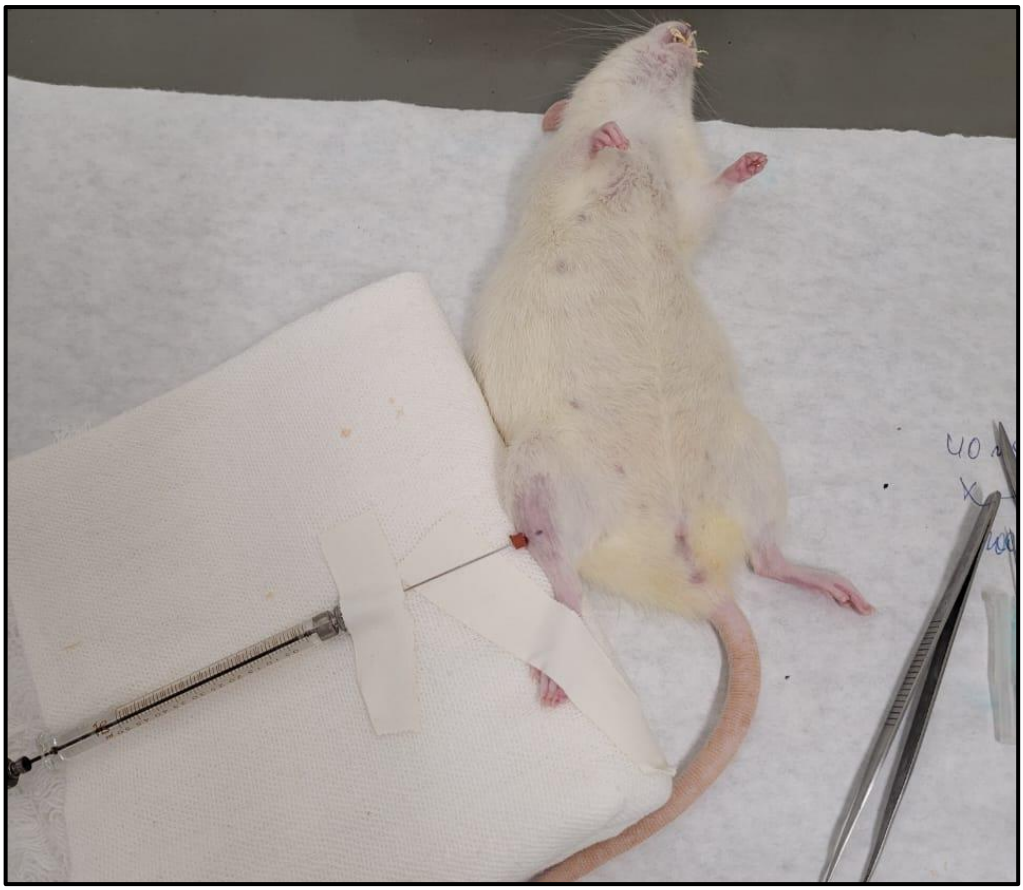

Figura 8. Fotografias do procedimento de injeção do neurotraçador Fluorogold no músculo tibial cranial direito de rata anestesiada usada para padronização da técnica.

Em cada ponto foram injetados 2µL de neurotraçador, lentamente durante 5 minutos, com 6mm de penetração da agulha a partir da pele. O primeiro ponto foi realizado a 4mm da porção anterior da crista tibial dos animais e a 26mm de distância do calcâneo. Os pontos seguintes foram realizados 5mm acima e abaixo do primeiro

ponto. Após a injeção, a agulha foi mantida em posição durante 5 minutos a fim de evitar refluxo do traçador e removida lentamente.

Neste estudo, foi escolhido para análise o músculo tibial cranial, devido a sua localização anatômica superficial, por ser volumoso e de fácil acesso para a injeção do neurotraçador, considerando ainda que as unidades motoras sofrem influência direta da lesão do nervo isquiático, já que o músculo é inervado pelo nervo fibular.

4.4. Coleta do material biológico

Decorrido o período experimental, aos 120 dias após a cirurgia, os animais foram anestesiados através de injeção intraperitoneal de solução anestésica de Ketamina (Dopalen, 70 mg/kg) e Xilazina (Anasedan, 30 mg/kg). Para a coleta da medula espinal e do nervo isquiático direito, foi realizada perfusão transcardíaca nos 6 animais de cada grupo em que foi realizada a injeção de neurotraçador. O protocolo de perfusão consistiu na passagem inicial de solução salina 0,9% com heparina (30ml/minuto) durante cerca de 1 minuto até esvaziamento do leito vascular, indicado pelo esbranquiçamento do fígado, seguida da passagem de uma solução fixadora de formaldeído a 4% recém preparada a partir de paraformaldeído e tampão fosfato de sódio (PBS) 0,1M pH 7,4, durante 30 minutos (30ml/minuto). Após pelo menos 30 minutos da finalização do procedimento, as medulas e os nervos isquiáticos foram coletadas e armazenadas em formaldeído 4% por um dia. No dia seguinte foram retiradas as meninges, raízes nervosas, as medulas foram reduzidas e armazenadas em solução de sacarose 30% feita em PBS 0,1M pH 7,4.

Para as análises do músculo tibial cranial, suas JNMs associadas e nervo fibular, os tecidos foram coletados a fresco, armazenados e imediatamente mantidos em solução fixadora apropriada (Karnovsky - paraformaldeído a 4%, glutaraldeído 2,5% - paraformaldeído 4%) ou foram congelados. Após a coleta do material biológico, os animais foram eutanasiados através de injeção de tiopental intracardíaco. É importante ressaltar que para as análises de microscopia eletrônica da medula, após coleta a fresco dos tecidos, foi realizado perfusão transcardíaca em 3 animais de cada grupo utilizando solução fixadora de Karnovsky.

4.5. Estudos do SNP

4.5.1. Análise do peso relativo dos músculos tibiais craniais (n=9)

Previamente à anestesia os animais foram pesados e, após coleta, os músculos tibiais craniais foram removidos, limpos em solução salina, dissecados e pesados para posterior cálculo do peso relativo do músculo (peso do músculo/peso do animal *100) para cada animal de cada grupo experimental.

4.5.2. Análise morfológica e morfométrica das JNMs (n=5)

Para caracterização das JNMs, secções longitudinais de 400µm do músculo tibial cranial direito foram realizadas através do uso de um vibrátomo (Hyrax V50 Vibratome/Carl Zeiss). Essas secções foram conservadas em solução de Karnovsky e então submetidas à reação de Esterase Inespecífica (Lehrer e Ornstein, 1959). Inicialmente foram lavadas em água corrente por 10 minutos e incubadas a 37ºC por 12 minutos em um meio com pH entre 6.8 a 7.2, composto por solução Tris HCl 0,05M (5 ml), alfa-naftil acetato a 1% (0,125 ml) e pararosanilina azotizada (0,4 ml) por animal. Após a incubação, as peças foram lavadas em água corrente por 10 minutos, desidratadas, diafanizadas e montadas em lâminas. As fotomicrografias das JNMs foram obtidas no microscópio Olympus Bx41 (câmera SC30) do setor de Anatomia do Departamento de Biologia Estrutural e Funcional, IBB-UNESP. Foram tomadas medidas da área, perímetro, diâmetro mínimo e máximo, diâmetro de Feret, Feret mínimo, angulação e ângulo de Feret para pelo menos 50 JNMs para cada animal. Essas medidas foram analisadas através do software ImageJ (v.1.53) (110).

4.5.3. Análise ultraestrutural das junções neuromusculares e fibras musculares (n=3)

Para a análise das junções neuromusculares e fibras musculares, porções mediais do músculo tibial cranial foram seccionadas em retângulos e armazenadas em solução de Karnovsky para posterior processamento e obtenção de secções longitudinais. O material foi processado seguindo a rotina do Centro de Microscopia Eletrônica do Instituto de Biociências (CME/IBB/UNESP) e foi fotodocumentado utilizando o Microscópio Eletrônico de Transmissão (TECNAI Spirit, Fei).

4.5.4. Análise morfológica e morfométrica das fibras musculares e tecido conjuntivo intramuscular (n=5)

Após a coleta, as extremidades distais do músculo tibial cranial foram seccionadas e fixadas em formol tamponado a 10% por 24 horas, lavados em água

corrente por 48 horas, incluídos em Paraplast® e seccionados em micrótomo com espessura de 4 µm. Foram confeccionadas 2 lâminas histológicas para cada animal de cada grupo experimental. Após a coloração mencionada abaixo as lâminas foram fotografadas em aumento de 200x no microscópio Olympus Bx41 (câmera SC30).

A primeira lâmina foi submetida à coloração de H.E. e foram selecionadas entre 300 a 400 fibras musculares de 3 a 4 campos aleatórios para análise morfométrica da área, perímetro, circularidade, diâmetro mínimo e máximo, diâmetro de Feret, Feret mínimo, angulação e ângulo de Feret das fibras musculares e contagem do número de núcleos centrais.

A segunda lâmina foi submetida à coloração de Picrosirius Red, em que o tecido conjuntivo é corado em vermelho e as fibras musculares em amarelo. A quantificação do tecido conjuntivo foi realizada por meio da análise de porcentagem na seção total do músculo, através da ferramenta de Threshold do software ImageJ.

4.5.5. Análise morfológica e morfométrica do nervo fibular (n=5)

Após a exposição dos nervos fibulares direitos, um fragmento de aproximadamente 1 cm foi removido e fixado em solução de Karnovsky por pelo menos 24 horas. Em seguida, os fragmentos foram colocados em solução de tetróxido de ósmio durante 24 horas, lavados em tampão fosfato, armazenados em álcool 70% e incluídos em historesina. Após essa rotina, os blocos contendo os nervos foram seccionados transversalmente (2 µm) em um ultramicrótomo Leica RM2265. As lâminas histológicas foram contracoradas com azul de toluidina 1% em água ultrapura e fotografadas em um microscópio Olympus Bx41 (câmera SC30) no Setor de Anatomia do Departamento de Biologia Estrutural e Funcional (DBEF) do IBB/Unesp. Foram obtidas imagens com aumento de 100x, 400x e 1000x, com utilização de óleo de imersão. É importante salientar que devido a atrofia e degeneração não foi possível coletar os nervos fibulares dos animais do grupo D. Os nervos foram analisados com auxílio do software “ImageJ” para obtenção da contagem do número total de axônios e área e perímetro do fascículo nervoso utilizando imagens em 100x e 400x. Através do programa livre “AxonDepSeeg” (111) que utiliza aprendizado de máquinas e redes neurais para realizar morfometria das fibras nervosas de maneira automatizada, fibras nervosas de 5 campos aleatoriamente escolhidos no aumento de 1000x (totalizando pelo menos 50% das fibras presentes no fascículo) foram utilizadas para obtenção das seguintes medidas (Figura 9): área e perímetro do axônio, diâmetro do axônio,

área e espessura da bainha de mielina, área e perímetro da fibra nervosa, e foi realizado o cálculo da razão G. Após cada análise, critérios de seleção e adequação padronizados foram utilizados para retirar eventuais erros de medidas e retiras medidas de fibras nervosas das extremidades.

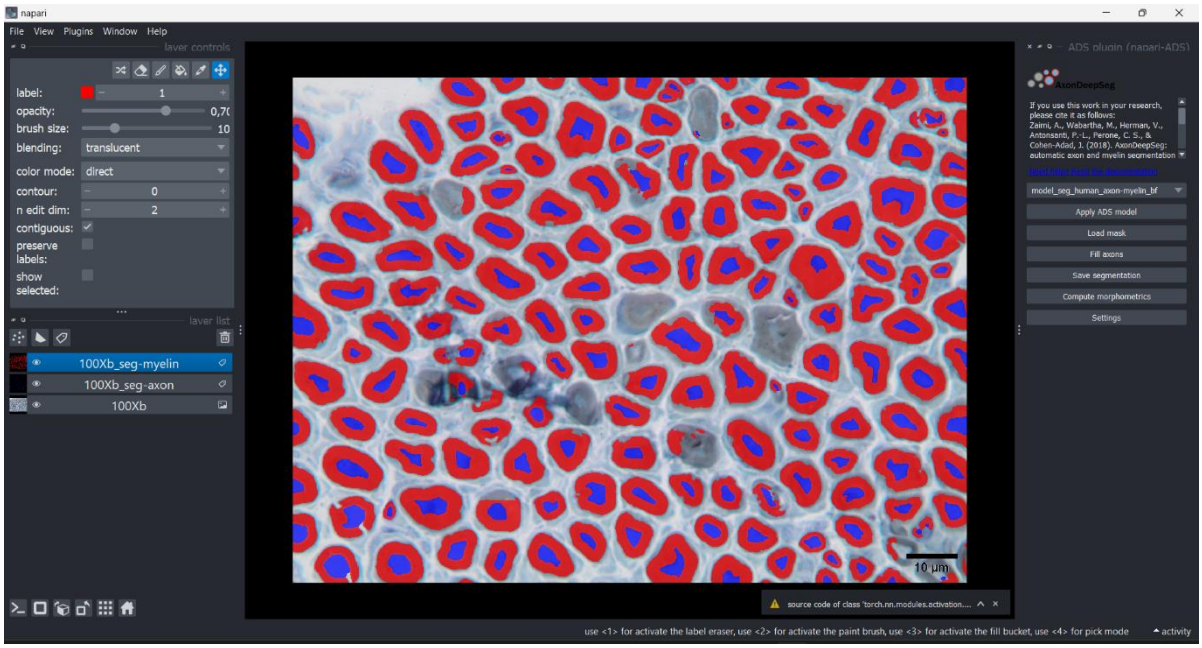

Figura 9. Imagem representativa de medida automatizada utilizando o software *AxonDeepSeg*, em que é possível observar a bainha de mielina dos axônios pintada em vermelho e o interior de cada fibra em azul. A fotomicrografia apresentada foi tirada com aumento de 100x e a análise do software não foi corrigida e ajustada, de maneira que podem ser visualizados alguns erros.

4.5.6. Imunomarcação de NF-200 e S100 no nervo isquiático (n=5)

Nos animais submetidos à perfusão transcardíaca com paraformaldeído 4%, os fragmentos do nervo isquiático referentes a área da reconstrução foram coletados e posteriormente armazenados em paraformaldeído a 4% por 24 h, crioprotegidos em sacarose (diluída em PBS 0,1 M) 10%, 20% e 30% por 24 h cada, embebidos em meio de congelamento (Tissue Plus® O.C.T. Compound, Fisher Healthcare), congelados em N-hexano resfriado em nitrogênio líquido e armazenados em biofreezer a -80 ºC, para posterior corte, montagem em lâminas e realização da imunomarcação. Em seguida, as lâminas foram descongeladas em temperatura ambiente durante 1h, lavadas em PBS, incubadas em solução bloqueadora (PBS 3% BSA (w/v)) por 1 hora,

seguido de incubação pelo anticorpo primário (NF200, feito em coelho, #N5389, Sigma, 1/1.000; S-100, feito em coelho, #ab4066, Abcam, 1/1.000 – diluídos em solução de PBS 1% BSA (w/v), 0,2% Triton-X (v/v)) por 18 horas em caixa escura úmida a 4º C. No dia seguinte, as lâminas foram lavadas novamente em tampão PB, incubadas por 1h em anticorpo secundário (IgG Mouse Alexa Fluor 488, feito em coelho, #ab15007, Abcam, 1/1.000 diluído em solução de PBS 1% BSA (w/v), 0,2% Triton-X (v/v)), em seguida foram novamente lavadas em PBS e montadas com lamínulas e meio de montagem (VectaShield).

As lâminas foram fotografadas pelo microscópio confocal Leica TCS SP5 em aumento de 200x, escolhendo aleatoriamente 2 campos por animal e, em seguida, analisadas usando o software ImageJ. Para excluir espaços vazios gerados por variações na largura da seção longitudinal do nervo, foi utilizado um quadro (500 × 500 unidades) cobrindo apenas as áreas de amostra. Os valores médios de intensidade de fluorescência foram obtidos através da quantificação da área fluorescente para cada animal, utilizando a ferramenta de “threshold” de maneira padronizada.

4.5.7. Análise da expressão proteica por Western Blotting (n=5)

As porções proximais do músculo tibial cranial foram descongelados, pesados e sonicados e homogeneizadas em tampão RIPA e inibidores de proteases (30mg de tecido/100µl de tampão de extração). Os extratos dos tecidos foram extraídos por centrifugação durante 20 minutos a 14000 rpm a 4ºC. Para cada animal, o conteúdo de proteína foi determinado utilizando o método de Bradford (Bio-Rad protein assay) e o correspondente a 50 microgramas de proteínas foi aplicado em gel de poliacrilamida. Após eletroforese, o material foi transferido para membranas de nitrocelulose e incubado com os anticorpos primários em overnight. Após a lavagem, as membranas foram incubadas por 1 hora em anticorpo secundário HRP e reveladas utilizando-se substrato quimioluminescente para Western Blotting (AMERSHAM ECLTM PRIME, GE Healthcare). A análise semiquantitativa de densitometria das bandas foi realizada pelo software ImageJ. Os dados foram normalizados com a GAPDH de mesma membrana e expressos em unidades arbitrárias (112).

4.6. Estudos do SNC

4.6.1. Estudo da imunorreatividade ao FluoroGold e IBA-1 (n=5)

Para cada animal, a intumescência lombar da medula espinhal foi seccionada longitudinalmente em fatias de 40µm de espessura, usando um micrótomo deslizante (Leica SM2010R) equipado com uma plataforma de congelamento (BFS-30MP, Physiotemp Inc.). As seções foram coletadas sequencialmente em uma série de 4 frascos preenchidos com solução anticongelante, de modo que o intervalo entre seções consecutivas em cada frasco fosse de 160µm. Cada série de seções foi armazenada a -20°C até o momento do processamento.

As seções histológicas foram inicialmente lavadas em PBS 0,1M pH 7,4, passando para a inibição da peroxidase endógena em uma solução de 3% de peróxido de hidrogênio em PBS por 20 minutos. Subsequentemente, as seções foram lavadas em PBS e tampão Tris 0,05M com Triton-X100 0,25% em solução salina pH 7,6 (TBS-TX) e incubadas em uma solução de soro de cabra a 2% para bloquear a marcação não específica. Após isso, a incubação dos anticorpos primários foi realizada em TBS-TX por 48h, a uma temperatura de 4ºC, e as seções foram mantidas sob agitação constante de acordo com cada protocolo: anti-FluoroGold (produzido em coelho, #AB138870, Abcam, 1/10.000), anti-IBA1 (produzido em coelho, WAKO, 1/5.000). Após a incubação, as seções foram lavadas em TBS-TX 0,05M pH 7,6 e incubadas em anticorpo secundário biotinilado para a espécie onde o anticorpo primário foi obtido, anti-IgG de coelho (#BA-1000, Vector Laboratories, 1/200), produzido em cabra, por 2 horas à temperatura ambiente. Em seguida, as seções foram lavadas em TBS-TX e incubadas em complexo peroxidase avidina-biotina (Vectastain ABC Kit, PK-4000, 1/200), diluído em TBS-TX, por 1 hora à temperatura ambiente. Depois, as seções foram lavadas em tampão Tris-HCl 0,05M pH 8,0. Por fim, a peroxidase ligada ao complexo ABC foi evidenciada pela reação com peróxido de hidrogênio, usando 3,3’ diaminobenzidina-tetrahidrocloreto intensificado com sulfato de níquel amoniacal (DAB-Ni) como cromógeno. Após o processo de imunohistoquímica, as seções foram transferidas para uma solução de gelatina a 0,4%, em tampão Tris-HCl 0,05M e montadas em lâminas.

Para analisar a microglia, foi utilizado o protocolo para densitometria óptica. O microscópio óptico (Axioplan2, Carl Zeiss), equipado com uma câmera digital (axioCam HRc, Zeiss), foi ajustado para obter a condição de iluminação ideal com a lente objetiva de 20X, usada para capturar todas as imagens. O feixe de luz foi

centrado no CCD da câmera digital, e a intensidade da iluminação foi fixada observando o histograma de brilho RGB da imagem, a fim de distribuí-lo ao longo da faixa dinâmica da câmera digital. Todos os parâmetros de iluminação de campo, aberturas de diafragma, conjuntos de filtros e tempo de exposição da câmera foram controlados manualmente para evitar variações nesses parâmetros durante a sessão de captura.

Todas as imagens foram capturadas na mesma sessão e 11 imagens de referência foram inicialmente adquiridas para calibração de densidade óptica (Figura 10B), representando densidades entre 0,04 e 1,0, usando um filtro de densidade neutra escalonado (Figura 10A) (Edmund Industrial Optics, #32-599). Em seguida, para cada animal, cerca de 2500 µm (8 imagens) de cada sessão de medula espinhal anterior (3~4) foi capturada, de acordo com os neurônios marcados com FG reconstruídos em 3D.

Em seguida, essas imagens foram combinadas em um mosaico, para criar imagens panorâmicas de toda a intumescência lombar. No ImageJ, para excluir espaços vazios gerados por variações na largura da seção de nossa análise, foi adotada uma moldura ROI (1900 × 600 unidades) e usada para realizar a quantificação comparativa da densidade óptica das seções de tecido entre os vários grupos experimentais, refletindo a quantidade de densidade de células IBA-1+ (Figura 10C).

Para a análise de cada conjunto de imagens capturadas na mesma sessão, a calibração da densidade óptica foi inicialmente realizada usando imagens de referência com uma escala crescente de níveis de cinza. Para garantir a uniformidade na imunomarcação IBA-1+, todas as seções dos casos experimentais foram processadas simultaneamente, usando soluções com composições idênticas e parâmetros imuno-histoquímicos como concentração de anticorpos, duração da coloração e tempo de desenvolvimento foram mantidos consistentes em todas as seções para alcançar intensidade de coloração uniforme. Além disso, um terço padronizado da mesma ROI e imagens foram usados para a contagem de células IBA-1+ entre os grupos (Figura 10D).

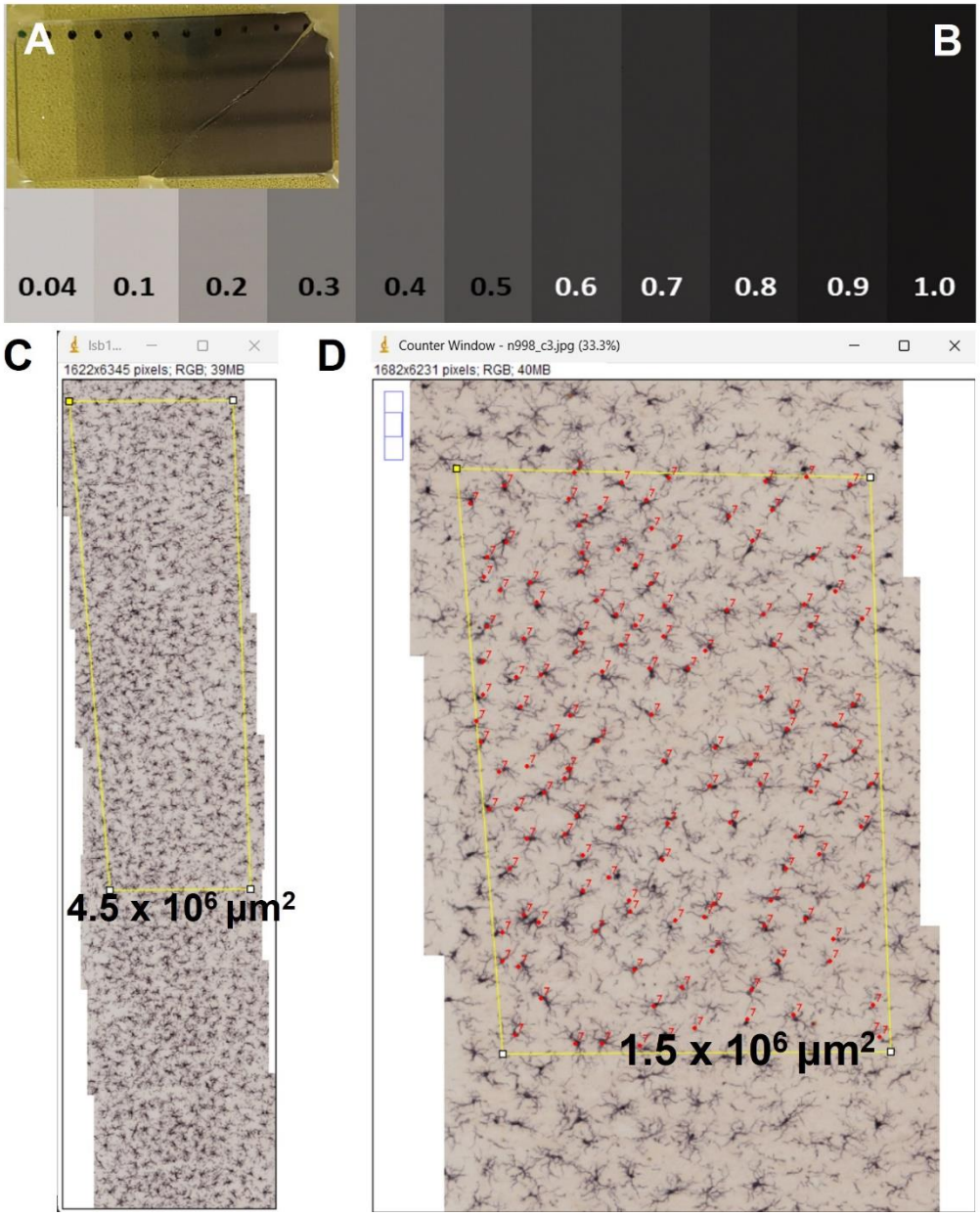

Figura 10. Imagem da lâmina microscópica utilizada para obter o filtro de densidade óptica (A) e representação do filtro de densidade óptica neutra, com seus respectivos valores de densidade óptica, utilizado para captura de imagens de referência e posterior calibração através do ImageJ (B). Representação de medida com imagem de marcação IBA-1 reconstruída em painel e região de interesse delimitando a área total analisada (C) e representação de contagem do número de células marcadas pelo IBA-1 em área região de interesse (D).

4.6.2. Reconstrução 3D da distribuição dos neurônios motores (n=1)

Para a reconstrução 3D, a medula espinhal de um animal de cada grupo foi seccionada longitudinalmente em fatias de 40µm de espessura e imediatamente montada em séries em uma lâmina com uma solução de gelatina a 0,1%. Em seguida, todas as seções foram inteiramente fotografadas em um microscópio de fluorescência

(Zeiss Scope.A1) e cada corte foi reconstruído em uma única imagem (Figura 11A e 11a).

Subsequentemente, a reconstrução tridimensional foi realizada atráves do software *Neurolucida* (versão 10.31, MBF Bioscience, MicroBrightfield, Inc). As reconstruções de cada corte da medula espinhal delimitaram toda a intumescência lombar. Os passos para criar os modelos 3D incluíram calibrar o programa, inserir informações sobre o intervalo de avaliação e o número de seções usadas na reconstrução, definir os contornos que limitam as estruturas de referência citoarquitetônicas, alinhar individualmente cada nova seção em relação à sua predecessora imediata. Em cada seção, o contorno externo da medula espinhal, as colunas de substância cinzenta da medula espinhal e os neurônios rotulados retrogradamente foram delineados (Figura 11B). A organização citoarquitetônica das regiões de interesse foi ilustrada em quadros com figuras esquemáticas que representam seções longitudinais em duas dimensões e imagens dos modelos tridimensionais (Figura 11C). A partir da reconstrução, também foram tiradas informações referentes à distribuição do pool de neurônios motores retrogradamente marcados para cada animal.

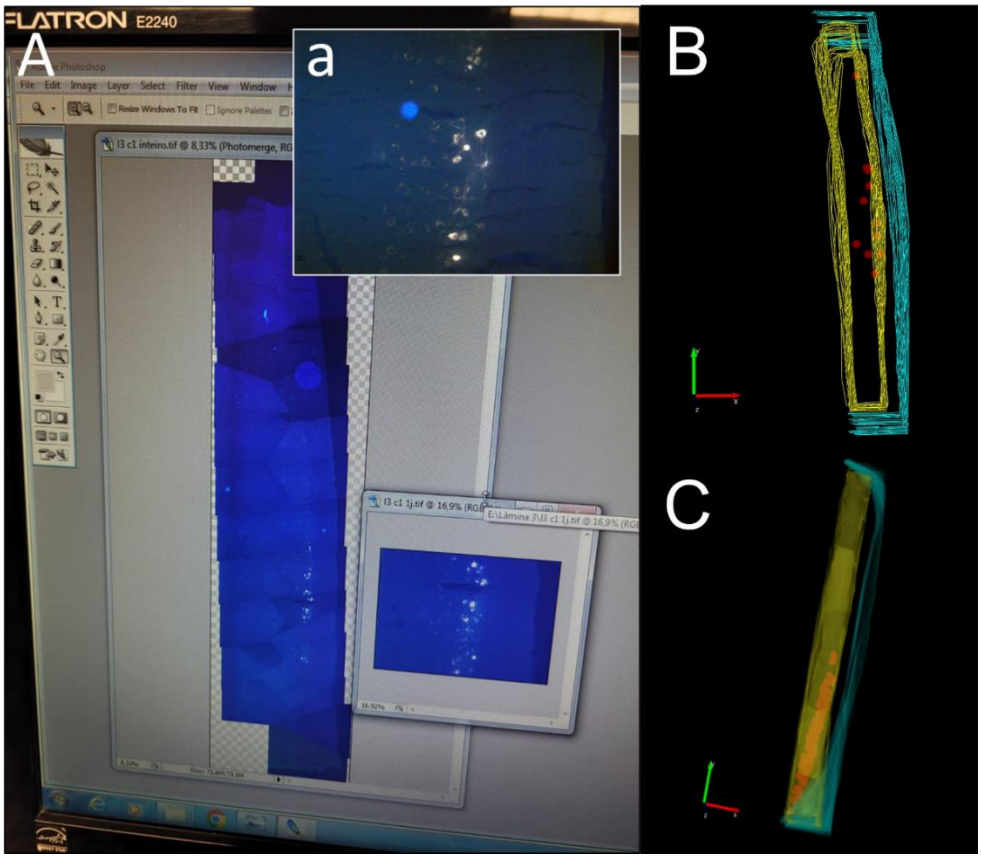

Figura 11. Representação da montagem finalizada (A) de uma série de fotografias de um animal do grupo controle, com os neurônios motores que inervam o músculo tibial cranial evidenciados em branco. No detalhe os neurônios podem ser visualizados em maior aumento (a). Delimitação e sobreposição de diversas seções de medula que evidenciam o contorno externo (azul), substância cinzenta (amarelo) e neurônios retrogradamente marcados (bola vermelha) (B). Reconstrução tridimensional para um animal (C).

4.6.3. Análise ultraestrutural dos neurônios motores (n=3)

Os animais foram perfundidos com solução Karnovsky, as medulas espinais foram coletadas e reduzidas em sua porção lombar. Posteriormente, foi feito a redução da medula para um segmento de 2 mm, o lado direito, referente a lesão nervosa, foi destacado e foram armazenados 2 segmentos da região da coluna anterior para processamento e análise ultraestrutural por microscopia eletrônica de transmissão no Centro de Microscopia Eletrônica do Instituto de Biociências de Botucatu. Ademais, para um animal de cada grupo, o restante da porção lombar imediatamente acima da porção reduzida foi seccionado transversalmente para visualização dos neurônios motores através de coloração de Nissl.

4.7. Análise estatística

Todos os dados referentes a quantificações morfológicas e morfométricas e as análises estatísticas foram realizadas às cegas pelo pesquisador principal. Os resultados de todas as variáveis quantitativas foram comparados entre os grupos e antes de qualquer análise a distribuição normal e a homocedasticidade dos dados foram verificadas através do teste de Shapiro-Wilk ou teste de normalidade apropriado. A comparação entre os grupos com aderência à distribuição normal de probabilidades foi realizada por meio da técnica de análise de variância paramétrica (ANOVA) para o modelo com um fator complementada com o teste de comparações múltiplas de Tukey ou pelo procedimento não-paramétrico (Kruskal-Wallis) complementado pelo teste de Dunn na ausência de aderência à distribuição normal. Outros testes e modelos foram adotados em caso de melhor adequação para a análise em questão. Todos os dados foram considerados utilizando o nível de 5% de significância ($p \leq 0,05$). Os dados foram analisados com auxílio do software “GraphPad Prism 9” e todos os gráficos foram confeccionados no mesmo software.

5. Referências bibliográficas

1. Hussain G, Wang J, Rasul A, Anwar H, Qasim M, Zafar S, et al. Current Status of Therapeutic Approaches against Peripheral Nerve Injuries: A Detailed Story from Injury to Recovery. Int J Biol Sci. 2020;16(1):116-34.
2. Jones S, Eisenberg HM, Jia X. Advances and Future Applications of Augmented Peripheral Nerve Regeneration. Int J Mol Sci. 2016;17(9).
3. Murphy RNA, de Schoulepnikoff C, Chen JHC, Columb MO, Bedford J, Wong JK, et al. The incidence and management of peripheral nerve injury in England (2005-2020). J Plast Reconstr Aesthet Surg. 2023;80:75-85.
4. Kouyoumdjian JA, Graça CR, Ferreira VFM. Peripheral nerve injuries: A retrospective survey of 1124 cases. Neurol India. 2017;65(3):551-5.
5. Asplund M, Nilsson M, Jacobsson A, von Holst H. Incidence of traumatic peripheral nerve injuries and amputations in Sweden between 1998 and 2006. Neuroepidemiology. 2009;32(3):217-28.
6. Kim SJ, Kwon YM, Ahn SM, Lee JH, Lee CH. Epidemiology of upper extremity peripheral nerve injury in South Korea, 2008 to 2018. Medicine (Baltimore). 2022;101(48):e31655.
7. Wang ML, Rivlin M, Graham JG, Beredjiklian PK. Peripheral nerve injury, scarring, and recovery. Connect Tissue Res. 2019;60(1):3-9.
8. Zelada D, Bermedo-García F, Collao N, Henríquez JP. Motor function recovery: deciphering a regenerative niche at the neuromuscular synapse. Biol Rev Camb Philos Soc. 2021;96(2):752-66.
9. Jones RA, Harrison C, Eaton SL, Llavero Hurtado M, Graham LC, Alkhammash L, et al. Cellular and Molecular Anatomy of the Human Neuromuscular Junction. Cell Rep. 2017;21(9):2348-56.
10. Jessen KR. Glial cells. Int J Biochem Cell Biol. 2004;36(10):1861-7.
11. Ceprian M, Fulton D. Glial Cell AMPA Receptors in Nervous System Health, Injury and Disease. Int J Mol Sci. 2019;20(10).
12. Pekny M, Pekna M, Messing A, Steinhäuser C, Lee JM, Parpura V, et al. Astrocytes: a central element in neurological diseases. Acta Neuropathol. 2016;131(3):323-45.
13. Sofroniew MV, Vinters HV. Astrocytes: biology and pathology. Acta Neuropathol. 2010;119(1):7-35.
14. Feng Z, Ko CP. The role of glial cells in the formation and maintenance of the neuromuscular junction. Ann N Y Acad Sci. 2008;1132:19-28.
15. Escartin C, Galea E, Lakatos A, O'Callaghan JP, Petzold GC, Serrano-Pozo A, et al. Reactive astrocyte nomenclature, definitions, and future directions. Nat Neurosci. 2021;24(3):312-25.
16. Salter MW, Stevens B. Microglia emerge as central players in brain disease. Nat Med. 2017;23(9):1018-27.
17. Brandenburg S, Müller A, Turkowski K, Radev YT, Rot S, Schmidt C, et al. Resident microglia rather than peripheral macrophages promote vascularization in brain tumors and are source of alternative pro-angiogenic factors. Acta Neuropathol. 2016;131(3):365-78.
18. Savage JC, Carrier M, Tremblay M. Morphology of Microglia Across Contexts of Health and Disease. Methods Mol Biol. 2019;2034:13-26.
19. Green TRF, Murphy SM, Rowe RK. Comparisons of quantitative approaches for assessing microglial morphology reveal inconsistencies, ecological fallacy, and a need for standardization. Sci Rep. 2022;12(1):18196.
20. Carlstedt T. An overture to basic science aspects of nerve injuries. J Hand Surg Eur Vol. 2011;36(9):726-9.
21. Faroni A, Mobasseri SA, Kingham PJ, Reid AJ. Peripheral nerve regeneration: experimental strategies and future perspectives. Adv Drug Deliv Rev. 2015;82-83:160-7.
22. Gordon T. Nerve Regeneration: Understanding Biology and Its Influence on Return of Function After Nerve Transfers. Hand Clin. 2016;32(2):103-17.
23. Rodríguez Cruz PM, Cossins J, Beeson D, Vincent A. The Neuromuscular Junction in Health and Disease: Molecular Mechanisms Governing Synaptic Formation and Homeostasis. Front Mol Neurosci. 2020;13:610964.
24. Tintignac LA, Brenner HR, Rüegg MA. Mechanisms Regulating Neuromuscular Junction Development and Function and Causes of Muscle Wasting. Physiol Rev. 2015;95(3):809-52.
25. Muller KS, Tibúrcio FC, Ferreira RS, Barraviera B, Matheus SMM. Heterologous fibrin biopolymer as an emerging approach to peripheral nerve repair: a scoping review. J Venom Anim Toxins Incl Trop Dis. 2024;30:e20230060.
26. Hughes BW, Kusner LL, Kaminski HJ. Molecular architecture of the neuromuscular junction. Muscle Nerve. 2006;33(4):445-61.
27. Sanes JR, Lichtman JW. Development of the vertebrate neuromuscular junction. Annu Rev Neurosci. 1999;22:389-442.

28. Nishimune H, Shigemoto K. Practical Anatomy of the Neuromuscular Junction in Health and Disease. Neurol Clin. 2018;36(2):231-40.
29. Lepore E, Casola I, Dobrowolny G, Musarò A. Neuromuscular Junction as an Entity of Nerve-Muscle Communication. Cells. 2019;8(8).
30. Iyer SR, Shah SB, Lovering RM. The Neuromuscular Junction: Roles in Aging and Neuromuscular Disease. Int J Mol Sci. 2021;22(15).
31. Bloch-Gallego E. Mechanisms controlling neuromuscular junction stability. Cell Mol Life Sci. 2015;72(6):1029-43.
32. Sugiura Y, Lin W. Neuron-glia interactions: the roles of Schwann cells in neuromuscular synapse formation and function. Biosci Rep. 2011;31(5):295-302.
33. Ko CP, Robitaille R. Perisynaptic Schwann Cells at the Neuromuscular Synapse: Adaptable, Multitasking Glial Cells. Cold Spring Harb Perspect Biol. 2015;7(10):a020503.
34. Patton BL, Miner JH, Chiu AY, Sanes JR. Distribution and function of laminins in the neuromuscular system of developing, adult, and mutant mice. J Cell Biol. 1997;139(6):1507-21.
35. Patton BL. Basal lamina and the organization of neuromuscular synapses. J Neurocytol. 2003;32(5-8):883-903.
36. Engel AG. The neuromuscular junction. Handb Clin Neurol. 2008;91:103-48.
37. Ruff RL. Neurophysiology of the neuromuscular junction: overview. Ann N Y Acad Sci. 2003;998:1-10.
38. Conti-Fine BM, Milani M, Kaminski HJ. Myasthenia gravis: past, present, and future. J Clin Invest. 2006;116(11):2843-54.
39. Wu P, Chawla A, Spinner RJ, Yu C, Yaszemski MJ, Windebank AJ, et al. Key changes in denervated muscles and their impact on regeneration and reinnervation. Neural Regen Res. 2014;9(20):1796-809.
40. Ma J, Shen J, Garrett JP, Lee CA, Li Z, Elsaidi GA, et al. Gene expression of myogenic regulatory factors, nicotinic acetylcholine receptor subunits, and GAP-43 in skeletal muscle following denervation in a rat model. J Orthop Res. 2007;25(11):1498-505.
41. Grosman C, Auerbach A. Kinetic, mechanistic, and structural aspects of unliganded gating of acetylcholine receptor channels: a single-channel study of second transmembrane segment 12' mutants. J Gen Physiol. 2000;115(5):621-35.
42. Naguib M, Flood P, McArdle JJ, Brenner HR. Advances in neurobiology of the neuromuscular junction: implications for the anesthesiologist. Anesthesiology. 2002;96(1):202-31.
43. Unwin N. Nicotinic acetylcholine receptor and the structural basis of neuromuscular transmission: insights from Torpedo postsynaptic membranes. Q Rev Biophys. 2013;46(4):283-322.
44. Pinto CG, Leite APS, Sartori AA, Tibúrcio FC, Barraviera B, Junior RSF, et al. Heterologous fibrin biopolymer associated to a single suture stitch enables the return of neuromuscular junction to its mature pattern after peripheral nerve injury. Injury. 2021;52(4):731-7.
45. Lacomis D. What's in the Neuromuscular Junction Literature? J Clin Neuromuscul Dis. 2020;21(4):195-204.
46. Krivoi II, Petrov AM. Cholesterol and the Safety Factor for Neuromuscular Transmission. Int J Mol Sci. 2019;20(5).
47. Seddon HJ. A Classification of Nerve Injuries. Br Med J. 1942;2(4260):237-9.
48. SUNDERLAND S. A classification of peripheral nerve injuries producing loss of function. Brain. 1951;74(4):491-516.
49. Modrak M, Talukder MAH, Gurgenashvili K, Noble M, Elfar JC. Peripheral nerve injury and myelination: Potential therapeutic strategies. J Neurosci Res. 2020;98(5):780-95.
50. Fu SY, Gordon T. Contributing factors to poor functional recovery after delayed nerve repair: prolonged axotomy. J Neurosci. 1995;15(5 Pt 2):3876-85.
51. Chan KM, Gordon T, Zochodne DW, Power HA. Improving peripheral nerve regeneration: from molecular mechanisms to potential therapeutic targets. Exp Neurol. 2014;261:826-35.
52. Gordon T. Peripheral Nerve Regeneration and Muscle Reinnervation. International Journal of Molecular Sciences. 2020;21(22):8652.
53. Lubińska L. Patterns of Wallerian degeneration of myelinated fibres in short and long peripheral stumps and in isolated segments of rat phrenic nerve. Interpretation of the role of axoplasmic flow of the trophic factor. Brain Res. 1982;233(2):227-40.
54. Lindborg JA, Mack M, Zigmond RE. Neutrophils Are Critical for Myelin Removal in a Peripheral Nerve Injury Model of Wallerian Degeneration. J Neurosci. 2017;37(43):10258-77.
55. Gomez-Sanchez JA, Carty L, Iruarrizaga-Lejarreta M, Palomo-Irigoyen M, Varela-Rey M, Griffith M, et al. Schwann cell autophagy, myelinophagy, initiates myelin clearance from injured nerves. J Cell Biol. 2015;210(1):153-68.

56. Gaudet AD, Popovich PG, Ramer MS. Wallerian degeneration: gaining perspective on inflammatory events after peripheral nerve injury. J Neuroinflammation. 2011;8:110.
57. Cattin AL, Burden JJ, Van Emmenis L, Mackenzie FE, Hoving JJ, Garcia Calavia N, et al. Macrophage-Induced Blood Vessels Guide Schwann Cell-Mediated Regeneration of Peripheral Nerves. Cell. 2015;162(5):1127-39.
58. Jiang BG, Han N, Rao F, Wang YL, Kou YH, Zhang PX. Advance of Peripheral Nerve Injury Repair and Reconstruction. Chin Med J (Engl). 2017;130(24):2996-8.
59. Bombeiro AL, Thomé R, Oliveira Nunes SL, Monteiro Moreira B, Verinaud L, Oliveira AL. MHC-I and PirB Upregulation in the Central and Peripheral Nervous System following Sciatic Nerve Injury. PLoS One. 2016;11(8):e0161463.
60. Bombeiro AL, Pereira BTN, de Oliveira ALR. Granulocyte-macrophage colony-stimulating factor improves mouse peripheral nerve regeneration following sciatic nerve crush. Eur J Neurosci. 2018;48(5):2152-64.
61. Bombeiro AL, Pereira BTN, Bonfanti AP, Oliveira ALR. Immunomodulation by dimethyl fumarate treatment improves mouse sciatic nerve regeneration. Brain Res Bull. 2020;160:24-32.
62. Bombeiro AL, Lima BHM, Bonfanti AP, Oliveira ALR. Improved mouse sciatic nerve regeneration following lymphocyte cell therapy. Mol Immunol. 2020;121:81-91.
63. Rodríguez-Sánchez DN, Pinto GBA, Cartarozzi LP, de Oliveira ALR, Bovolato ALC, de Carvalho M, et al. 3D-printed nerve guidance conduits multi-functionalized with canine multipotent mesenchymal stromal cells promote neuroregeneration after sciatic nerve injury in rats. Stem Cell Res Ther. 2021;12(1):303.
64. Cartarozzi LP, Spejo AB, Ferreira RS, Barraviera B, Duek E, Carvalho JL, et al. Mesenchymal stem cells engrafted in a fibrin scaffold stimulate Schwann cell reactivity and axonal regeneration following sciatic nerve tubulization. Brain Res Bull. 2015;112:14-24.
65. Rishal I, Fainzilber M. Axon-soma communication in neuronal injury. Nat Rev Neurosci. 2014;15(1):32-42.
66. Cullheim S, Thams S. The microglial networks of the brain and their role in neuronal network plasticity after lesion. Brain Res Rev. 2007;55(1):89-96.
67. Blinzinger K, Kreutzberg G. Displacement of synaptic terminals from regenerating motoneurons by microglial cells. Z Zellforsch Mikrosk Anat. 1968;85(2):145-57.
68. Alvarez FJ, Titus-Mitchell HE, Bullinger KL, Kraszpulski M, Nardelli P, Cope TC. Permanent central synaptic disconnection of proprioceptors after nerve injury and regeneration. I. Loss of VGLUT1/IA synapses on motoneurons. J Neurophysiol. 2011;106(5):2450-70.
69. Rotterman TM, Akhter ET, Lane AR, MacPherson KP, García VV, Tansey MG, et al. Spinal Motor Circuit Synaptic Plasticity after Peripheral Nerve Injury Depends on Microglia Activation and a CCR2 Mechanism. J Neurosci. 2019;39(18):3412-33.
70. Alvarez FJ, Rotterman TM, Akhter ET, Lane AR, English AW, Cope TC. Synaptic Plasticity on Motoneurons After Axotomy: A Necessary Change in Paradigm. Front Mol Neurosci. 2020;13:68.
71. Fu SY, Gordon T. The cellular and molecular basis of peripheral nerve regeneration. Mol Neurobiol. 1997;14(1-2):67-116.
72. Ma CH, Omura T, Cobos EJ, Latrémolière A, Ghasemlou N, Brenner GJ, et al. Accelerating axonal growth promotes motor recovery after peripheral nerve injury in mice. J Clin Invest. 2011;121(11):4332-47.
73. Sakuma M, Gorski G, Sheu SH, Lee S, Barrett LB, Singh B, et al. Lack of motor recovery after prolonged denervation of the neuromuscular junction is not due to regenerative failure. Eur J Neurosci. 2016;43(3):451-62.
74. Moimas S, Novati F, Ronchi G, Zacchigna S, Fregnan F, Zentilin L, et al. Effect of vascular endothelial growth factor gene therapy on post-traumatic peripheral nerve regeneration and denervation-related muscle atrophy. Gene Ther. 2013;20(10):1014-21.
75. Leite APS, Pinto CG, Tibúrcio FC, Muller KS, Padovani CR, Barraviera B, et al. Acetylcholine receptors of the neuromuscular junctions present normal distribution after peripheral nerve injury and repair through nerve guidance associated with fibrin biopolymer. Injury. 2023;54(2):345-61.
76. Rios R, Jablonka-Shariff A, Broberg C, Snyder-Warwick AK. Macrophage roles in peripheral nervous system injury and pathology: Allies in neuromuscular junction recovery. Mol Cell Neurosci. 2021;111:103590.
77. Su HL, Chiang CY, Lu ZH, Cheng FC, Chen CJ, Sheu ML, et al. Late administration of high-frequency electrical stimulation increases nerve regeneration without aggravating neuropathic pain in a nerve crush injury. BMC Neurosci. 2018;19(1):37.

78. Chao T, Frump D, Lin M, Caiozzo VJ, Mozaffar T, Steward O, et al. Matrix metalloproteinase 3 deletion preserves denervated motor endplates after traumatic nerve injury. Ann Neurol. 2013;73(2):210-23.
79. Palispis WA, Gupta R. Surgical repair in humans after traumatic nerve injury provides limited functional neural regeneration in adults. Exp Neurol. 2017;290:106-14.
80. Jablonka-Shariff A, Lu CY, Campbell K, Monk KR, Snyder-Warwick AK. Gpr126/Adgrg6 contributes to the terminal Schwann cell response at the neuromuscular junction following peripheral nerve injury. Glia. 2020;68(6):1182-200.
81. Cisterna BA, Cardozo C, Sáez JC. Neuronal involvement in muscular atrophy. Front Cell Neurosci. 2014;8:405.
82. Guarino SR, Canciani A, Forneris F. Dissecting the Extracellular Complexity of Neuromuscular Junction Organizers. Front Mol Biosci. 2019;6:156.
83. VanSaun M, Humburg BC, Arnett MG, Pence M, Werle MJ. Activation of Matrix Metalloproteinase-3 is altered at the frog neuromuscular junction following changes in synaptic activity. Dev Neurobiol. 2007;67(11):1488-97.
84. Campbell WW. Evaluation and management of peripheral nerve injury. Clin Neurophysiol. 2008;119(9):1951-65.
85. Martins RS, Siqueira MG, Da Silva CF, Plese JP. Overall assessment of regeneration in peripheral nerve lesion repair using fibrin glue, suture, or a combination of the 2 techniques in a rat model. Which is the ideal choice? Surg Neurol. 2005;64 Suppl 1:S1:10-6; discussion S1:6.
86. Ray WZ, Mackinnon SE. Management of nerve gaps: autografts, allografts, nerve transfers, and end-to-side neurorrhaphy. Exp Neurol. 2010;223(1):77-85.
87. Wanner R, Gey M, Abaei A, Warnecke D, de Roy L, Dürselen L, et al. Functional and Molecular Characterization of a Novel Traumatic Peripheral Nerve-Muscle Injury Model. Neuromolecular Med. 2017;19(2-3):357-74.
88. Sulaiman W, Gordon T. Neurobiology of peripheral nerve injury, regeneration, and functional recovery: from bench top research to bedside application. Ochsner J. 2013;13(1):100-8.
89. Biscola NP, Cartarozzi LP, Ulian-Benitez S, Barbizan R, Castro MV, Spejo AB, et al. Multiple uses of fibrin sealant for nervous system treatment following injury and disease. J Venom Anim Toxins Incl Trop Dis. 2017;23:13.
90. Robinson PP, Loescher AR, Smith KG. A prospective, quantitative study on the clinical outcome of lingual nerve repair. Br J Oral Maxillofac Surg. 2000;38(4):255-63.
91. Peretti GM, Randolph MA, Zaporojan V, Bonassar LJ, Xu JW, Fellers JC, et al. A biomechanical analysis of an engineered cell-scaffold implant for cartilage repair. Ann Plast Surg. 2001;46(5):533-7.
92. Ringe J, Kaps C, Burmester GR, Sittinger M. Stem cells for regenerative medicine: advances in the engineering of tissues and organs. Naturwissenschaften. 2002;89(8):338-51.
93. de Barros CN, Miluzzi Yamada AL, Junior RS, Barraviera B, Hussni CA, de Souza JB, et al. A new heterologous fibrin sealant as a scaffold to cartilage repair-Experimental study and preliminary results. Exp Biol Med (Maywood). 2016;241(13):1410-5.
94. Bayer IS. Advances in Fibrin-Based Materials in Wound Repair: A Review. Molecules. 2022;27(14).
95. Buchta C, Dettke M, Funovics PT, Höcker P, Knöbl P, Macher M, et al. Fibrin sealant produced by the CryoSeal FS System: product chemistry, material properties and possible preparation in the autologous preoperative setting. Vox Sang. 2004;86(4):257-62.
96. Sameem M, Wood TJ, Bain JR. A systematic review on the use of fibrin glue for peripheral nerve repair. Plast Reconstr Surg. 2011;127(6):2381-90.
97. Buchaim DV, Cassaro CV, Shindo JVTC, Coletta BBD, Pomini KT, Rosso MPO, et al. Unique heterologous fibrin biopolymer with hemostatic, adhesive, sealant, scaffold and drug delivery properties: a systematic review. J Venom Anim Toxins Incl Trop Dis. 2019;25:e20190038.
98. Koopman JE, Duraku LS, de Jong T, de Vries RBM, Michiel Zuidam J, Hundepool CA. A systematic review and meta-analysis on the use of fibrin glue in peripheral nerve repair: Can we just glue it? J Plast Reconstr Aesthet Surg. 2022;75(3):1018-33.
99. Barros LC, Ferreira RS, Barraviera SR, Stolf HO, Thomazini-Santos IA, Mendes-Giannini MJ, et al. A new fibrin sealant from Crotalus durissus terrificus venom: applications in medicine. J Toxicol Environ Health B Crit Rev. 2009;12(8):553-71.
100. Ferreira RS, de Barros LC, Abbade LPF, Barraviera SRCS, Silvares MRC, de Pontes LG, et al. Heterologous fibrin sealant derived from snake venom: from bench to bedside - an overview. J Venom Anim Toxins Incl Trop Dis. 2017;23:21.
101. Fattahi T, Mohan M, Caldwell GT. Clinical applications of fibrin sealants. J Oral Maxillofac Surg. 2004;62(2):218-24.

102. Abbade LPF, Ferreira RS, Dos Santos LD, Barraviera B. Chronic venous ulcers: a review on treatment with fibrin sealant and prognostic advances using proteomic strategies. J Venom Anim Toxins Incl Trop Dis. 2020;26:e20190101.
103. Abbade LPF, Barraviera SRCS, Silvares MRC, Lima ABBC, Haddad GR, Gatti MAN, et al. Treatment of Chronic Venous Ulcers With Heterologous Fibrin Sealant: A Phase I/II Clinical Trial. Front Immunol. 2021;12:627541.
104. Leite APS, Pinto CG, Tibúrcio FC, Sartori AA, de Castro Rodrigues A, Barraviera B, et al. Heterologous fibrin sealant potentiates axonal regeneration after peripheral nerve injury with reduction in the number of suture points. Injury. 2019;50(4):834-47.
105. Tibúrcio FC, Muller KS, Leite APS, de Oliveira IRA, Barraviera B, Ferreira RS, et al. Neuroregeneration and immune response after neurorrhaphy are improved with the use of heterologous fibrin biopolymer in addition to suture repair alone. Muscle Nerve. 2023;67(6):522-36.
106. Buchaim RL, Andreo JC, Barraviera B, Ferreira Junior RS, Buchaim DV, Rosa Junior GM, et al. Effect of low-level laser therapy (LLLT) on peripheral nerve regeneration using fibrin glue derived from snake venom. Injury. 2015;46(4):655-60.
107. Ortiz AC, Fideles SOM, Pomini KT, Bellini MZ, Pereira ESBM, Reis CHB, et al. Potential of Fibrin Glue and Mesenchymal Stem Cells (MSCs) to Regenerate Nerve Injuries: A Systematic Review. Cells. 2022;11(2).
108. Schneider CA, Rasband WS, Eliceiri KW. NIH Image to ImageJ: 25 years of image analysis. Nat Methods. 2012;9(7):671-5.
109. Zaimi A, Wabartha M, Herman V, Antonsanti PL, Perone CS, Cohen-Adad J. AxonDeepSeg: automatic axon and myelin segmentation from microscopy data using convolutional neural networks. Sci Rep. 2018;8(1):3816.
110. Muller KS, Tibúrcio FC, de Barros JWF, Matsumura CY, Matheus SMM. Statin exposure during pregnancy promotes neuromuscular junction alterations in postpartum Wistar rats. Muscle Nerve. 2023;67(6):537-47.

Capítulo 1

Heterologous fibrin biopolymer as an emerging approach to peripheral nerve repair: a scoping review

Published article in Journal of Venomous Animals and Tropical Diseases (JVATiTD). Disponível em: https://doi.org/10.1590/1678-9199-JVATITD-2023-0060

Kevin Silva Muller[1,2] (kevin.muller@unesp.br - orcid.org/0000-0001-9774-1435)
Felipe Cantore Tibúrcio[1,2] (felipe.cantore@unesp.br - orcid.org/0000-0003-2660-6089)
Rui Seabra Ferreira Junior[3,4] (rui.seabra@unesp.br - orcid.org/0000-0001-6952-0512)
Benedito Barraviera[2,3,4] (benedito.barraviera@unesp.br - orcid.org/0000-0002-9855-5594)
Selma Maria Michelin Matheus[1,2*] (selma.matheus@unesp.br - orcid.org/0000-0001-7870-5404)

[1]Department of Structural and Functional Biology, São Paulo State University - Unesp, Institute of Biosciences, Botucatu, SP, Brazil.
[2] Medical School, São Paulo State University - Unesp, Botucatu, SP, Brazil.
[3]Center for the Study of Venoms and Venomous Animals - Cevap, Sao Paulo State University - Unesp, Botucatu, SP, Brazil.
[4]Center for Translational Sciences and Biopharmaceuticals Development, Botucatu, SP, Brazil.

Abstract

Nerve injuries present a substantial challenge within the medical domain due to their prevalent occurrence and significant impact. In nerve injuries, a range of physiopathological and metabolic responses come into play to stabilize and repair the resulting damage. A critical concern arises from the disruption of connections at neuromuscular junctions, leading to profound degeneration and substantial loss of muscle function, thereby hampering motor tasks. While end-to-end neurorrhaphy serves as the established technique for treating peripheral nerve injuries, achieving comprehensive morphofunctional recovery remains a formidable challenge. In pursuit of enhancing the repair process, alternative and supportive methods are being explored. A promising candidate is the utilization of heterologous fibrin biopolymer, a sealant devoid of human blood components. Notably, this biopolymer has showcased its prowess in establishing a stable and protective microenvironment at the site of use in multiple scenarios of regenerative medicine. Hence, this scoping review is directed towards assessing the effects of associating heterologous fibrin biopolymer with neurorrhaphy to treat nerve injuries, drawing upon findings from prior studies disseminated through PubMed/MEDLINE, Scopus, and Web of Science databases. Further discourse delves into the intricacies of the biology of neuromuscular junctions,

nerve injury pathophysiology, and the broader utilization of fibrin sealants in conjunction with sutures for nerve reconstruction procedures. The association of HFB with neurorrhaphy emerges as a potential avenue for surmounting the limitations associated with traditional sealants while also mitigating degeneration in nerves, muscles, and NMJs post-injury, thereby fostering a more conducive environment for subsequent regeneration. Indeed, queries arise regarding the long-term regenerative potential of this approach and its applicability in reconstructive surgeries for human nerve injuries.

Keywords: *fibrin sealant; neurorrhaphy; nervous system; regenerative medicine.*

1. Background

Peripheral nerves are some of the most delicate structures in the human body, prone to easily being damaged by injuries such as compressions, crushes, and traumas [1]. Nerve injuries are a common clinical case with a high global incidence, affecting around 18 individuals per 100,000 each year [2]. Many individuals affected by nerve injuries, both in severe and moderate cases, have incomplete recovery, resulting in transient or permanent losses of motor and sensory functions, as well as chronic pain, muscle atrophy, and weakness. Approximately one-third of all nerve injuries demonstrate incomplete recovery with poor restoration of function [3]. Several factors hinder axonal regeneration, including severity, mechanism of injury, the large distance between the neuron cell body and target tissue, and the loss of regenerative support from Schwann cells (nerve glial cells) after injury, so that effective functional recovery is typically not achieved [4, 5]. The proper reinnervation of neuromuscular junctions (NMJs) by the nerve terminal plays an important role in obtaining a functional NMJ and, thus, a positive outcome.

Upon transection/neurotmesis, all structures of the neuromuscular apparatus are hindered, from the muscle fibers up to the motor neuron cell body in the spinal cord, undermining the quality of life of patients. Despite advances in microsurgical repair techniques, researchers have not yet achieved satisfactory functional recovery of the affected structures. Even with successful reconnection between the nerve stumps, the rates of motor recovery only reach a 50% success rate [6]. Then, the development of new strategies and approaches aimed at better regeneration is necessary. In this way, a new heterologous fibrin biopolymer (HFB) calls out attention as a promising candidate for adjunct therapy, as it has been showing positive results in a range of regenerative treatments, such as bone, tendon, spinal cord, and skin injuries, developing a more permissive environment for regeneration.

The current HFB consists of two major components, namely a thrombin like-enzyme (serine protease) extracted from the *Crotalus durissus terrificus* venom and a cryoprecipitate rich in fibrinogen, obtained from the blood of the buffalo *Bubalus bubalis* [7]. When both components are mixed with the calcium chloride diluent, the product polymerizes, forming a robust fibrin network. HFB has an activity comparable to commercial sealants, as it is biodegradable, bioabsorbable, and has no toxicity or

adverse reaction [8]. Because of its unique composition and absence of human blood, it is considered the only heterologous fibrin biopolymer in the world [9].

The use of HFB as an adjunct in peripheral and central nerve reconstruction has been showing promising results through the development of an immunomodulatory and neuroprotective environment at the injury site [10-13] and has also been applied in various other experimental models of reconstructive surgery [7, 14]. The use of HFB has already been experimentally shown to provide a microenvironment of stability and protection at the reconstruction site, leading to positive scenarios of nerve regeneration. Therefore, this scoping review shed light on the association of HFB with sutures for nerve reconstruction following injury, highlighting its immunomodulatory and neuroprotective properties. Notably, integrating HFB with neurorrhaphy presents a promising avenue for surpassing the constraints of conventional sealants, while concurrently curtailing the extent of initial degeneration subsequent to injury.

2. Methods

This scoping review follows the guidelines outlined in the Preferred Reporting Items for Systematic Reviews and Meta-Analyses (PRISMA) [15]. To achieve this, we conducted searches in PubMed/MEDLINE, Scopus (Elsevier), Web of Science, and SciELO databases, encompassing articles published until August 2023. The search used the keywords: “heterologous fibrin sealant,” “heterologous fibrin biopolymer,” “fibrin biopolymer,” “neurorrhaphy,” and “nerve injury” restricted to English-language publications.

To ensure precision, we carefully analyzed titles and abstracts to account for potential keyword overlaps. Articles were subsequently included or excluded based on predetermined eligibility criteria. Two independent authors conducted the selection process by using standardized procedures. When the title and abstract did not provide sufficient clarity, full-article analyses were undertaken. Review articles were scrutinized to identify potential experimental studies, and articles offering no novel insights were excluded following a comprehensive assessment.

Among the initially identified 103 articles, 31 were eliminated due to duplication, and an additional 58 were excluded in line with eligibility criteria (not animal model study; no nerve injury model or nerve degeneration/regeneration involvement; no HFB use; not a research article). Notably, six research articles aligning with the stipulated eligibility criteria were identified through scoping and systematic reviews. A total of 20 articles regarding the use of HFB for nerve injury repair were then chosen for detailed text evaluation, which meets the predefined inclusion criteria, forming the basis for this review's scope (Figure 1). Furthermore, other articles were freely consulted to delve into further aspects of the biology of the neuromuscular junction, the pathophysiology of nerve injury, and the exploration of fibrin sealants for nerve injury repair. Table 1 summarizes experimental articles, which used HFB for neuronal regeneration included in this review.

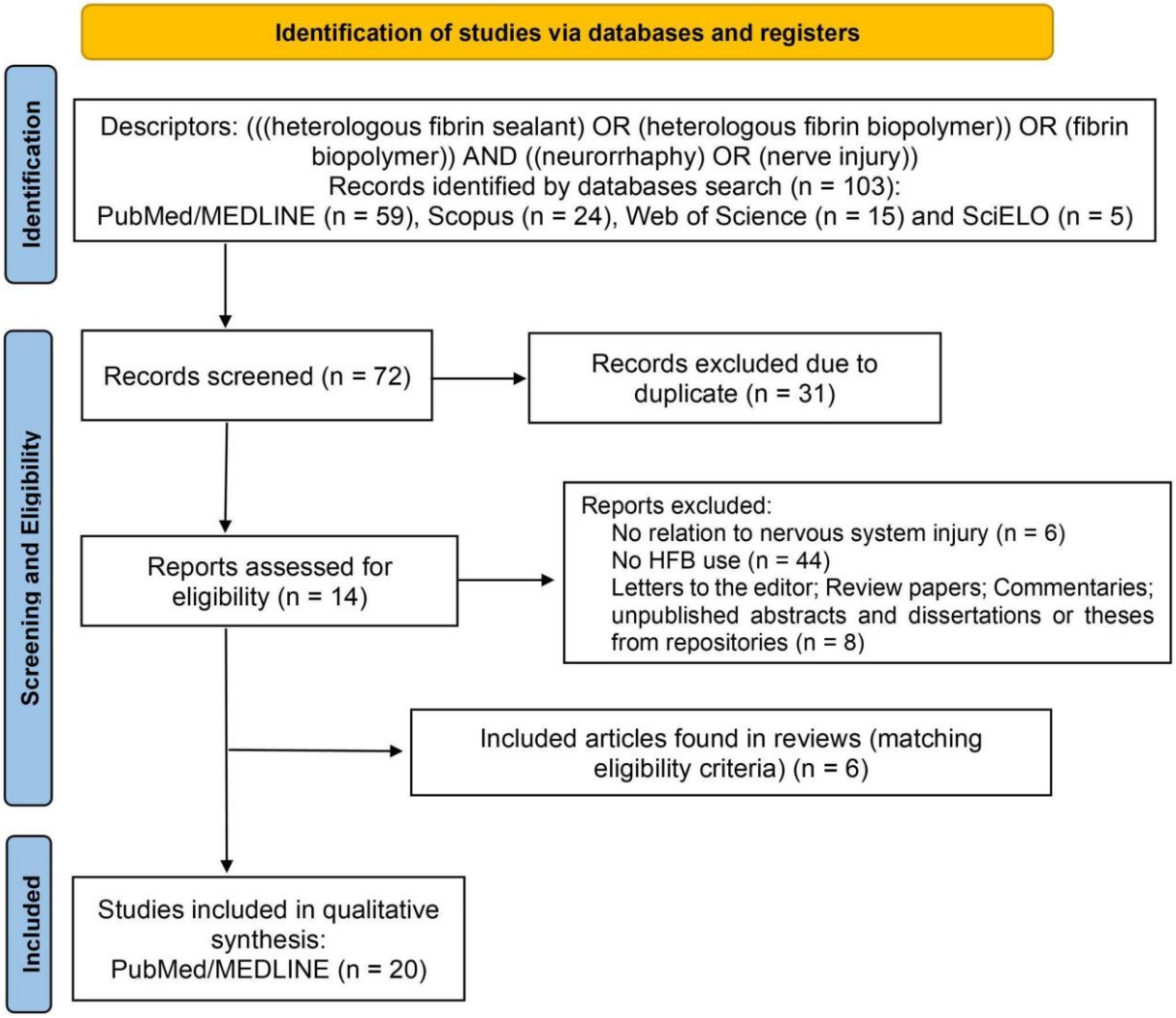

Figure 1. Flow diagram showing the study selection.

Table 1. Summary of experimental articles involving neuronal regeneration (CNS and PNS) included in this scoping review.

Author	Objective	Methods	Results	Conclusion
Barbizan et al. (2014) [16]	To investigate two delivery strategies of mononuclear cells (MC), comparing the local injection to the spinal cord with the possibility of mixing MC with HFB on the interface of the CNS/PNS.	Forty female adult Lewis rats divided into: G1: avulsion only; G2: reimplantation with HFB; G3: root repair with HFB and MC; G4: root repair with HFB and injected MCs.	HFB enhanced cell therapy effects resulting in greater survival of spinal motoneurons up to four weeks post-surgery. MC added to the HFB increased neurotrophic factor gene transcript levels in the spinal cord ventral horn. The motor recovery was	The use of HFB as a scaffold for the MC delivery approach gave the best and most long-lasting results. MC therapy was neuroprotective by increasing levels of brain-derived neurotrophic factor (BDNF) and glial-

			similar to cell-treated groups.	derived neurotrophic factor (GDNF).
Buchaim et al. (2015) [17]	To assess whether HFB permits the collateral repair of axons originating from a vagus nerve to the interior of a sural nerve graft and whether low-level laser therapy (LLLT) assists in the regeneration process.	Thirty-two adult male Wistar rats divided into: G1: intact sural nerve; G2: the ends of the sural nerve graft were coapted to the vagus nerve using HFB; G3: same procedures as G2 + LLLT.	The vagus nerve demonstrated collateral regeneration of axons to the interior of the autologous graft in all groups. G3 was similar to G1 concerning the area and thickness of the myelin sheath.	HFB + LLLT makes axonal regeneration feasible and is an efficient method to recover injured peripheral nerves, as well as improve myelination.
Cartarozzi et al. (2015) [18]	To investigate the effectiveness of mesenchymal stem cells (MSCs) associated with HFB for the peripheral regenerative process after nerve tubulization.	One hundred adult Lewis rats divided into G1: empty tube; G2: tube filled with HFB; G3: tube filled with HFB and grafted with MSCs.	G3 had a greater value for myelinated axon counting, more compact fibers, and a tendency to increase the thickness of the myelin sheath; with better motor function.	MSCs + HFB treatment was effective in improving nerve regeneration, as it positively modulated Schwann Cells reactivity.
Buchaim et al. (2016) [19]	To assess the impact of LLLT on the repair of the buccal branch of the facial nerve using two surgical methods: end-to-end epineural suturing and coaptation with HFB.	Forty adults male Wistar rats divided into: G1: suture; G2: HFB; G3: suture + HFB; G4: suture + LLLT; G5: suture + HFB + LLLT.	Axonal sprouting and morphology were similar among the experimental groups. G5 showed the closest results to the G1, in all measured variables, except in the axon area.	HFB allowed the coaptation of the stumps without trauma to the nerve fibers.
Rosso et al. (2017) [20]	To assess the impact of LLLT on facial nerve injuries repaired with the end-to-side method or coaptation with HFB.	Thirty-two adults male Wistar rats divided into G1: control; G2: suture; G3: HFB; G4: suture + LLLT; G5: suture + HFB + LLLT.	G4 and G5 groups showed higher mean values for histomorphometry and functional recovery variables.	The functional recovery of whisker movement occurred more rapidly in G4 and G5, with results closer to G1. LLLT expedited morphological and functional nerve repair in both techniques.

Spejo et al. (2018) [21]	To evaluate whether the combination of MSCs and HFB enhances the regeneration of the spinal cord following intramedullary axotomy (IA)	Eighty-eight adult female Lewis rats underwent a unilateral ventral funiculus incision at the L4, L5, and L6 spinal levels. The animals were divided into: G1: IA, G2; IA + vehicle; G3: IA + HFB; G4: IA + MSC; G5: IA + HFB + MSC.	MSC therapy: increased neuronal survival and functional recovery, reduced astrogliosis, and preserved spinal circuits. HFB promoted: early macrophage recruitment and expression of proinflammatory cytokines.	MSC therapy provides neuroprotection and, when combined with HFB, shifts the immune response towards the proinflammatory profile.
Mozafari et al. (2018) [22]	To determine whether human embryonic stem cells (hESC), either independently or in conjunction with HFBs, could aid in regeneration in a mouse model of sciatic nerve damage.	Forty-eight C57BL/6 J mice were divided into: G1: suture; G2: suture + HFB; G3: suture + HFB + doxycycline; G4: suture + HFB + wild type hESC; G5: suture + HFB + hESC off; G6: suture + HFB + hESC + doxycycline.	Sensory function was enhanced in G5, resulting in heightened reflexes, upon paw stimulation ipsilateral to the lesion, as evidenced by von-Frey evaluation, which was corroborated by immunohistochemistry.	Transgenic hESC could be used to support regeneration. HFB has the potential to aid nerve repair and is thought to promote superior functional recovery and improved motor neuron reinnervation when combined with this therapy.
Leite et al. (2019) [23]	To assess the effectiveness of HFB in association with suture, with 1 or 3 stitches after ischiatic nerve injury.	Thirty-six Wistar rats were divided into: G1: control; G2: denervated (6 mm gap); G3: 3 stitches suture; G4: 1 stitch suture + HFB.	G3 and G4 muscle analysis indicated an increase in muscle weight, frequency of fast fibers, and a decrease in collagen infiltration, while G4 had better nerve morphometric values compared to G3.	The findings imply a protective effect at the site of the lesion due to the use of HFB. The reduction in sutures lessens the trauma inflicted by the needle and expedites the surgical procedure.
Kempe et al. (2020) [24]	To determine whether the combination of pharmacological treatment with dimethyl fumarate (DF) and root reimplantation using HFB could promote neuroprotection, preservation, and	Seventy-nine adult female Lewis rats underwent ventral root avulsion of L4-L6 roots, followed by reimplantation and daily DF treatment for four weeks. HFB was utilized as an adjunct to ventral root reimplantation.	The association between HFB and DF preserved motoneurons and synapses, reduced astrogliosis and microglial reactions, and downregulated the expression of pro-inflammatory gene transcripts.	The association with HFB and DF demonstrated neuroprotective and immunomodulatory properties and 50% of motor function recovery following spinal cord root injury.

	recovery of motor function.			
Pinto et al. (2021) [25]	To determine whether the combination of HFB with a single stitch has the potential to restore the function of the neuromuscular apparatus following sciatic nerve injury.	Forty Wistar rats divided into G1: Control; G2: Denervated (6 mm gap); G3: 3 stitches suture; G4: 1 stitch suture + HFB.	G1 exhibited normal morphology. In G2 flattening of the NMJ (fragmentation of nAChRs and tangled nerve terminals). G3 and G4: most parameter values were similar to G1 and G2. G3 and G4: planar area.	G3 and G4 showed less fragmentation of nAChRs, and protein expression values suggested a return of nAChRs to a mat The use of HFB in conjunction with a single suture stitch reduced surgical time, minimized suture injuries, did not affect nerve regeneration, and showed potential for restoring the NMJ apparatus.
Rodríguez-Sánchez et al. (2021) [26]	To determine if Polycaprolactone Nerve Guidance Conduits (PCL-NGCs) produced by 3D printing with canine Adipose-derived Mesenchymal Stem Cells (AdMSCs) embedded in HFB could enhance nerve regeneration after sciatic nerve injury.	Twenty-nine adult Wistar rats submitted to sciatic nerve injury were divided into G1: Sham; G2: autograft; G3: PCL (empty NGC); G4: PCL + HFB+ MSCs (NGC multi-functionalized with 10^6 canine AdMSCs embedded in HFB).	G4 showed improved functional motor and electrophysiological recovery compared to the G3 after 12 weeks. G4 also increased the expression of neurotrophins and tended to higher reactivity of Schwann cells and axonal branching.	PCL + HFB+ MSCs promoted neuroregenerative effects and amplified the trophic microenvironment, resulting in a pro-regenerative state. These findings were associated with a shift in the regeneration process towards the formation of myelinated fibers.
Leite et al. (2023) [10]	To assess the impact of combining tubulization and HFB following peripheral nerve injury on the NMJ.	Fifty-two adult male Wistar rats divided into G1: control; G2: denervated; G3: tubulization; and G4: tubulization + HFB.	In G4 the NMJs presented morphological and morphometric similarities to G1 with an increase in S100 and AChRε protein expression and a decrease in MyoD.	The HFB association with tubulization resulted in nAChRs stabilization highlighting the beneficial effect of HFB when used in conjunction with the tubulization technique.

Tibúrcio et al. (2023) [13]	To assess neuroregeneration and the immune response in the context of neuromuscular recovery, using HFB in conjunction with suturing for rat sciatic nerve repair.	Forty male Wistar rats divided into groups of 7 or 30 days after nerve repair: G1: control; G2: denervated; G3: suture; G4: suture + HFB.	G4 had the highest M2 macrophage area in both periods. After seven days, the G4 showed an increase in nerve area, number, and area of blood vessels. In this period, G4 was the only one similar to G1 in terms of the number of axons. After 30 days, the G4 was closer to the G1 concerning blood vessels and central myonuclear numbers, NMJ angle, and connective tissue volume.	HFB enhances the immune response, increases axonal regeneration, induces angiogenesis, prevents severe muscle degeneration, and aids NMJ recovery.
Kempe et al. (2023) [27]	To examine the effects of combining surgical repair of lesioned roots with HFB and pharmacological treatment with dimethyl fumarate (DF).	Forty adult females divided into G1: reimplantation + vehicle; G2: VRA without reimplantation + DF; G3: reimplantation + vehicle + HFB; G4: reimplantation + HFB + DF.	HFB + DF association demonstrated: nerve sprouting, restoration of the 'G' ratio, and that most of the alpha motoneuron synapses were preserved in clusters. These parameters were associated with up to 50% of gait recovery, as the walking track test observed.	Combining root restoration with HFB and DF administration proved to be neuroprotective and can enhance motoneuron survival and regeneration after proximal lesions.
Bueno et al. (2023) [24]	To investigate the application of HFB in the repair of the buccal branch of the facial nerve (BBFN) in conjunction with photobiomodulation (PBM), using a low-level laser (LLLT).	Twenty-one rats divided into: G1: control; G2: LLLT; G3: denervated; G4: denervated + LLLT; G5: suture + HFB; G6: suture + HFB + LLLT.	G5 and G6 presented normal parameters related to functional analysis. G6 showed an increase in nerve fiber diameter and axon diameter compared to G6. In terms of muscle fiber area, G6 was similar to G1.	HFB+LLLT had positive effects on the morphological and functional stimulation of the BBFN, presenting a favorable alternative for the regeneration of severe injuries.

3. Neuromuscular interaction

Nerves are formed by bundles of axons or nerve fibers, which are long and slender projections of a neuron that typically conduct electrical impulses, connecting different parts of the body to the central nervous system (CNS). Sensory signals are transmitted to the CNS through sensory nerve fibers (afferents), and the resulting response is carried by motor nerve fibers (efferents) to the target organs. Thus, a mutual communication pathway is established between the CNS and the peripheral areas of the body [1].

Among the motor nerve fibers, there is the lower motor neuron, a specialized cell with a highly developed dendritic arborization. Its cell body is located in the ventral column of the gray matter of the spinal cord, and its axons extend throughout the body via peripheral nerves until they reach the target organs [28, 29], the skeletal striated muscle, where it forms a morphologically, molecularly, and functionally specialized region called NMJ. At this site, there is transmission and transduction of an electrical signal (nerve impulse) and a chemical signal (neurotransmitters) from the motor neuron to the muscle fiber, promoting muscle contraction. This junction presents a major subclass of synapses in the mammalian nervous system, critical for the transfer of information between the lower motor neuron and the skeletal muscle. It also represents a conveniently accessible "model" synapse within the peripheral nervous system [29].

3.1. Neuromuscular junction organization

The NMJs are small structures (30-60 um) when compared to the length of innervated muscle fibers, and each skeletal muscle fiber is recruited by a single NMJ [30]. The classic morphology of the NMJ, first described in rodents, is characterized as a "pretzel" shaped structure, and changes in this structure are closely associated with motor pathologies [28, 30]. The most common classification of NMJs divides them into three closely associated cellular compartments (Figure 2):

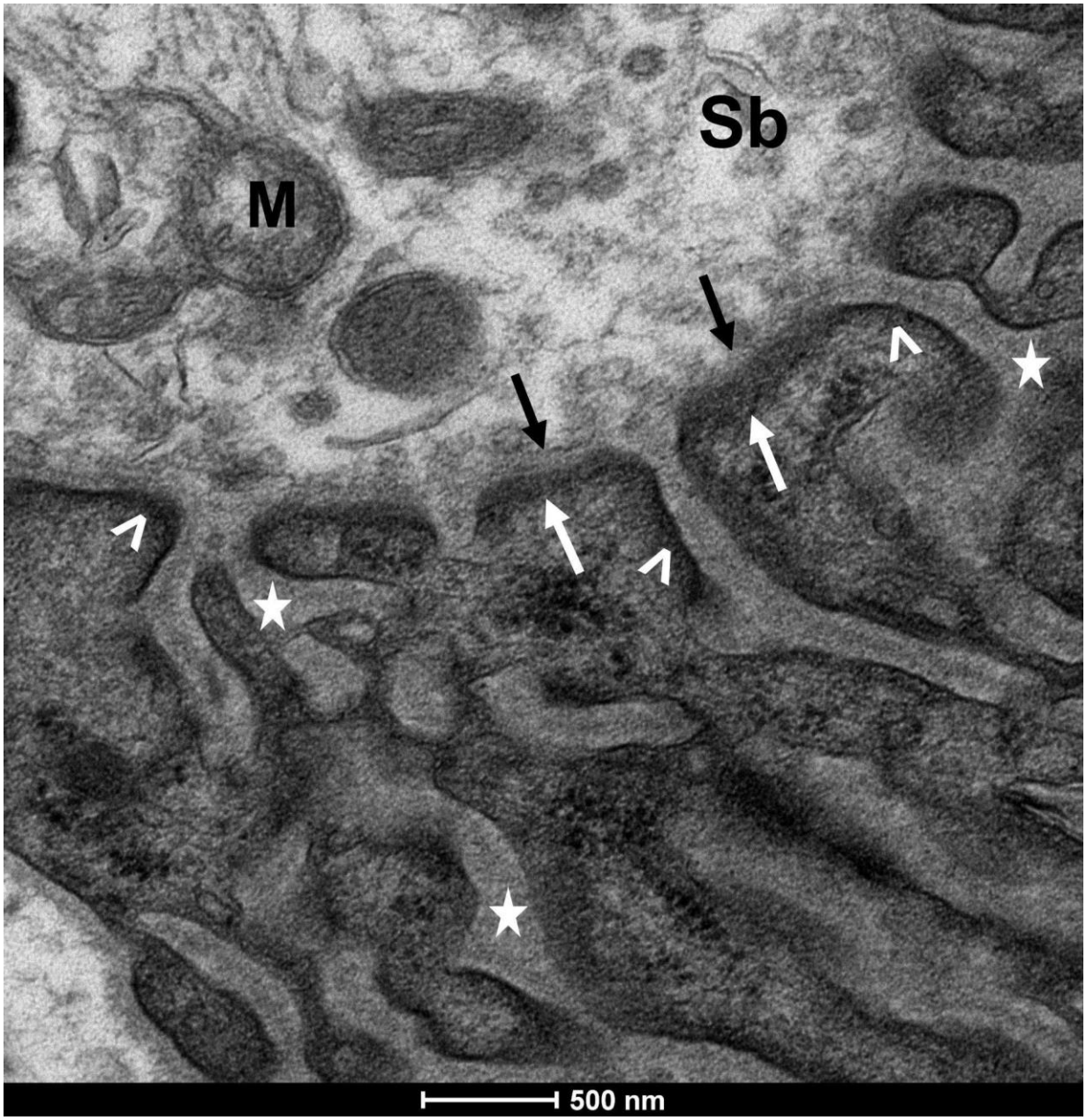

Figure 2. Components of the neuromuscular junction. Transmission electron microscopy image of a Wistar rat soleus muscle NMJ. Sb (Synaptic button); **(→)** ACh vesicle; **(*)** Junctional folds; **(>)** nAChRs cluster; **(+)** presynaptic membrane; **(-)** postsynaptic membrane.

I - Presynaptic membrane (nerve terminal)

The terminal branches of lower motor neuron axons form synaptic boutons, hosting synaptic vesicles carrying the neurotransmitter acetylcholine (ACh). This nerve terminal holds various cellular constituents, including mitochondria, endoplasmic reticulum, lysosomes, organic substances, and metal ions [31, 32]. Terminal or perisynaptic Schwann cells (tSCs) are found in this region [33-35], they are non-myelinating glial cells whose extensions cover the nerve terminals, protecting them from chemical and mechanical injuries [36]. Additionally, tSCs are the main cells

responsible for the structural plasticity of NMJs by perceiving possible alterations in synaptic transmission [37, 38]. One to three tSCs surround the nerve terminal, and actively participate in the development, maintenance, and repair of synaptic function [30], in addition to producing a basal lamina that maintains the structure of the NMJ [39].

II - Synaptic cleft

The synaptic cleft separates the presynaptic nerve terminal from the postsynaptic membrane by a narrow gap of 50 to 80 nm in width. It is filled with the synaptic basal lamina, composed of molecules secreted by both the nerve terminal and the associated muscle fiber [40]. This region houses crucial proteins for NMJ stability, function, and upkeep, including those responsible for the clustering of nicotinic acetylcholine receptors (nAChRs) on the sarcolemma, such as agrin, laminins-4, 9, and 11, matrix metalloproteinase-3 (MMP3), and collagen IV. Acetylcholinesterase (AChE), essential for degrading ACh post-muscle contraction, is also concentrated here [41, 42], culminating in the termination of neuromuscular transmission [43].

III - Postsynaptic membrane

The postsynaptic membrane compromises the plasma membrane of the muscle fiber with junctional folds, where the nAChRs and the sarcoplasm of the muscle fiber (cytoplasm) are located [34, 35]. These folds exhibit two distinct regions: the crest, enriched with nAChRs and additional proteins like rapsyn, utrophin, and α-dystrobrevin-1 to ensure stability; and the trough, hosting α-dystrobrevin-2, dystrophin, NCAMs for muscle integrity and axonal guidance. Alongside these, voltage-dependent sodium channels responsible for generating action potentials are also present [43-45]. The sarcolemma's invaginations amplify the postsynaptic membrane's surface area and facilitate the juxtaposition of nAChRs with the presynaptic zones, while sodium channels extend within the sarcoplasm. Basal lamina encompassing extracellular matrix components tightly enwraps the muscle fibers, connecting with the basal lamina of the synaptic cleft produced by tSCs at the NMJ's periphery [43].

At the NMJ, nAChRs are the primary receptors in the muscle to establish neuromuscular motor communication [46], thus maintaining and facilitating synaptic transmission. Structurally, they comprise five subunits arranged in a rosette pattern, which collectively form ion channels [47]. These receptors are distributed in two forms: immature extrajunctional, present in embryonic muscle fibers, composed of subunits two alpha (α), beta (β), delta (δ), and gamma (γ); and mature junctional, in which α (2), β, and δ subunits are maintained, and the γ subunit is replaced by epsilon (ε) [31].

Activation of nAChRs is initiated by the simultaneous binding of two ACh molecules or other agonists at the juncture of the αδ and αε subunits, thereby inducing a conformational alteration that opens the ion pore and triggers its active state [48, 49].

This active state's duration is modulated by the interaction between the receptor and ACh molecules, promptly broken down by AChE, returning nAChRs to their quiescent configuration [49]. In instances of injury or pathology, nAChRs often revert to an embryonic pattern, featuring the gamma subunit instead of epsilon [50]. This exchange of γ- for ε-subunits contributes to several changes in stability, kinetic, and transmission properties [28]. There are also positive and negative signals involved in the maintenance of the NMJ, and fundamentally, nAChRs clusters [30]. The main positive signal is the binding that occurs in the Agrin/LRP4/Musk/Rapsyn pathway [25].

3.2. Pathophysiology of nerve injury

Following nerve transection, a cascade of physiological and metabolic responses is triggered at the cellular level in the injury site and in the cell body of the affected neurons in an attempt to stabilize the damage resulting from the injury [28]. In neurotmesis, the nerve is divided into two stumps, distal and proximal to the site of injury, which are subject to relatively distinct processes [51]. Shortly after, the process of Wallerian degeneration (WD) begins in the distal stump, while the proximal stump changes its gene expression profile, adopting a repair profile, inducing degenerative changes followed by a regenerative process [30]. Shortly after axotomy, axons from the proximal stump undergo a process of swelling, characterized by a reorganization of the cytoskeletal structure to seal themselves through a fibrotic cascade to contain leakage of the axoplasm [3].

In the distal stump, where axons lose contact with neuronal bodies, Wallerian degeneration takes place, manifesting as myelin breakdown and axonal disintegration. This process initiates with a rapid influx of intracellular calcium, triggering protease activation and granulation within the axoplasm through the proteolysis of microtubules and neurofilaments. This succession of events further undermines the organizational integrity of the cellular structure [51, 52]. Within this milieu, damage-associated molecular patterns (DAMPs) and pro-inflammatory agents, including tumor necrosis factor (TNF-)α, interleukin (IL-) 1β, and CCL2, activate the initial immune response, mostly attributed to macrophages [53]. One of the primary functions of these macrophages is the clearance of tissue debris, a role reinforced by Schwann cells through myelin autophagy [54]. It is important to note that Schwann cells, fibroblasts, and resident macrophages also contribute to the inflammatory milieu by releasing proinflammatory mediators [55].

Furthermore, additional components of the immune system have been associated with effective Wallerian degeneration, often through their modulation of the macrophage-mediated response. Neutrophils are notably the first subset of cells to infiltrate the injured nerve, driving initial tissue clearance and recruiting monocytes from the peripheral circulation, which subsequently differentiate into macrophages [55]. Complement proteins and antibodies present in the serum enhance macrophage attraction and response by opsonizing cellular debris, thereby facilitating phagocytosis. The last cells to participate in the immune response within the damaged nerve are T

lymphocytes [55, 56]. While recognized for their role in the amplification and regulation of the inflammatory response, their specific function in nerve regeneration remains underexplored. It's worth mentioning that nerve regeneration has traditionally been correlated with distinct macrophage subsets: pro-inflammatory type 1 macrophages (M1) driving the degenerative phase, and anti-inflammatory type 2 macrophages (M2) guiding the regenerative phase [57]. These subtypes undergo polarization in response to cues from the degenerative or regenerative environment, yielding unique phenotypes, metabolic traits, and functions [57]. However, classifying macrophages solely into M1 and M2 categories oversimplifies the intricate cell landscape within the nerve, where an array of macrophages expressing various pro- and anti-inflammatory markers coexist.

Within tissue clearance, regeneration slowly begins at the proximal end of the injury site and proceeds toward the distal segment. In this context, Schwann cells close to the damaged region dedifferentiate, proliferate, and migrate to the lesion site. There, they align up within endoneurial tubes, forming longitudinal columns known as bands of Büngner, inside of which they release growth and trophic factors to stimulate axonal elongation up to the target [5]. Importantly, the correct orientation of Büngner's bands depends on a polarized vasculature, induced by macrophage-derived VEGF-A upon hypoxia stimulus. Those newly formed blood vessels are essential for regeneration as they serve as tracks, guiding Schwann cell migration across the wound and subsequent axonal elongation [58].

In the proximal stump, neurotmesis evokes a retrograde response in neuronal cell bodies [59]. Surviving neurons undergo a series of physiological and morphological changes called chromatolysis, which is characterized by swelling and rounding of the cell body, dissolution of Nissl granules, and eccentric displacement of the nucleus and endoplasmic reticulum [1, 60]. These structural modifications are paralleled by a shift in physiological cellular metabolism towards the synthesis of proteins involved in axon regeneration [59], such as those related to the cytoskeleton and growth factors [51]. With the elimination of myelin debris, regeneration slowly begins at the proximal end of the injury site and proceeds toward the distal segment. The severed axons produce a large number of sprouts, closely associated with Schwann cells, forming several growth cones in the distal direction.

On the other hand, the distance of the injury from the cell body implies a worsening of the regenerative condition, as observed in sensory neurons, where the closer proximity to the dorsal root ganglia is directly related to the number of dead nerve cells [61] and a greater effective distance for regeneration. Strikingly, although axons do regenerate, studies have demonstrated that the morphological recovery of the nerve and muscle is not definitive for functional recovery, as there may still be impaired synaptic functionality [62, 63].

Following the injury, nerve endings that formed NMJs are lost, and even with successful axonal sprouting, the failure of reinnervation limits muscle function recovery [64] (Figure 3A). Irregular nerve branching, poly-innervation [65], and collateral reinnervation of muscle fibers commonly occur. Denervated NMJs suffer severe

degeneration and subsequent disintegration [66] and disassembly of their nAChRs and anchoring proteins, which are fundamental for their function maintenance [67]. When axons are damaged, they release DAMPs that activate tSCs. These tSCs, in turn, release chemokines, which serve as guidance substrates, facilitating the formation of tSCs bridges and thus promoting NMJ reinnervation [28, 39]. The nAChR-ε subunit is replaced by nAChR-γ, altering the transmission of the electrical signal leading to muscle failure and atrophy [68], as ACh is also no longer available at the synapse.

Denervation also leads to significant changes in the Agrin/LRP4/Musk/Ra pathway, prejudicing the maintenance of nAChR clusters [69] and leading to alterations of the area and conformation of the NMJ [10]. Shortly after injury proteins of this pathway have increased synthesis but its complex disorganization leads to failure in proper function, inactivation of MMP3, and accumulation of Agrin in the synaptic cleft [28]. The NMJ microenvironment is also deprived of other retrograde and anterograde signals that maintain its stability [28], in which activated tSC extend their processes synthesizing nAChR in non-synaptic muscle regions.

In the regenerative process, the Agrin protein has a fundamental role in initiating the receptor clustering pathway, remodeling, and returning the NMJs to their conventional shape [30]. The LRP4 protein, dependent on Agrin for activation [69], also has a fundamental role in the regenerative process, contributing to the activation of tSCs after injury, which is responsible for guiding the reinnervation of NMJs in denervated fibers [10]. Notably, active tSCs also maintain NMJ organization by secreting substrates that regulate postsynaptic proteins, such as MMP3, which is involved in basal lamina and endplate integrity [66, 70]. In the maintenance of postsynaptic structures, other muscle-related proteins play a crucial role, as it has been demonstrated that the prevention of denervation is associated with the increased expression of MuSK, Dok7, and those involved in the ubiquitin-proteasome pathway, such as MURF-1 and atrogin-1 [10, 28]. The shift of gamma to the epsilon subunit in the nAChR serves as an indicator of regeneration, as it occurs only after reinnervation and differentiation of the myotube.

Altogether, major cellular and molecular events take place and deprive not only the associated nerve, Schwann cells, and muscle fibers but also the endplate, eliciting a series of retrograde and anterograde signals that, even with morphological regeneration of axons, can result in no definitive association with functional recovery. Understanding the therapeutic niche in the NMJ, as an end-gate player, is essential to provide positive outcomes after reinnervation, which includes not only reinnervation through the arrival of regenerating axons to denervated postsynaptic muscle domains but also its capability of synaptic activation (Figure 3B).

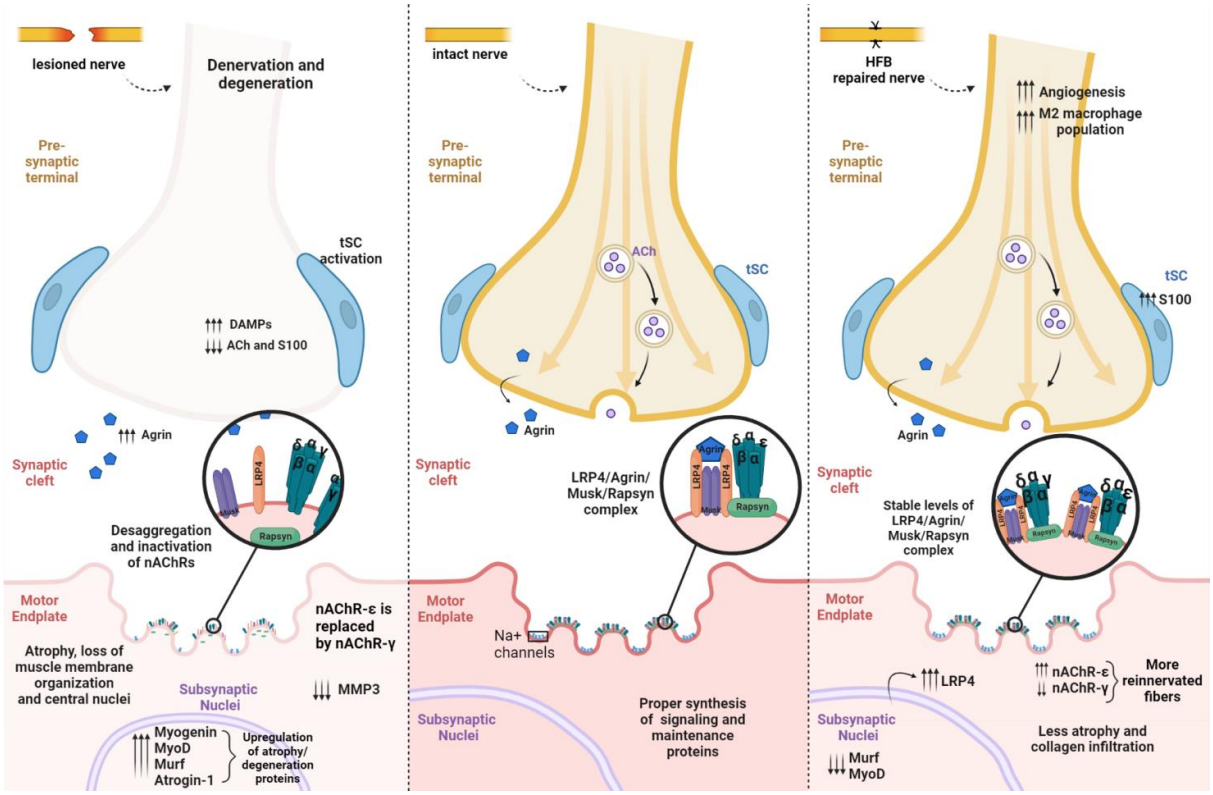

Figure 3. Cellular and molecular events associated with muscle denervation and repair at the neuromuscular junction level. Denervated **(A)**, healthy **(B),** and HFB repaired **(C)** neuromuscular junction. Following nerve injury, all components of the NMJ are hindered and the Agrin/LRP4/Musk/Rapsyn signaling pathway plays a significant role in the nAChRs cluster formation and NMJ maintenance.

4. Approaches to Peripheral Nerve Repair

In recent years, several approaches have been tested and used to restore functionality to the injured nerve [71, 72]. Most experimental models use rodents performing surgical lesions of the facial, ulnar, or sciatic nerves [73]. Treatments that result in complete morphologic and functional recovery are still a challenge for medical-surgical practice. The main difficulties are related to nerve reconnection and regeneration itself, in which regenerating axons fail to select their original endoneurial tubes [51], local revascularization, prolonged period of injury without medical intervention, progressive loss of regenerative character in Schwann cells, and atrophy of the innervated organs [51, 74-76].

Among the techniques for correcting nerve transection, end-to-end neurorrhaphy is the gold standard [46]. This type of neurorrhaphy is only possible when the nerve stumps are preserved, visible, and intact, without tissue loss, and there is no tension for re-approximation and reconnection of the stumps [11]. When such favorable characteristics for reconnection are not present, other techniques are used, including end-to-side neurorrhaphy [77], grafts and conduits [10, 22], and the use of tissue repair adjuvants such as fibrin sealants [78] and photobiomodulation [79].

Over the years, suture materials and techniques have presented problems and limitations, which motivated research on adhesive materials that can bond tissues. The first research on hemostatic and adhesive agents began around 1940, during World War II when fibrin glue was proposed. The fibrin glues or sealants, which can connect tissues more quickly, are important as they promote tissue adhesion and hemostasis [7]. At that time, a mixture of human fibrinogen and thrombin was mainly applied to areas of skin affected by war wounds. The structural characteristics of fibrin(ogen) can be encapsulated by the processes of fibrin polymerization and cross-linking. These processes facilitate a multitude of biological functions, which include, but are not limited to, thrombin binding, fibrinolysis, the control of coagulation protein activity, the binding of growth factors, and interactions with various cells [80].

In the 1970s, the concept of fibrin glue was re-evaluated, leading to the introduction of the first commercial sealant, *Tisseel* (Baxter International, Inc., Deerfield, IL), containing human fibrinogen and bovine thrombin. These sealants have been successfully marketed for years [72, 81, 82]. However, its commercialization was suspended and its use was prohibited in the USA by the Food and Drug Administration (FDA) agency in 1978, due to the risk of transmission of infectious diseases conveyed by human blood-derived products [7, 82]. In the early 1980s, the discovery of the human immunodeficiency virus added credibility to the FDA's position, which feared widespread viral transmission [8]. However, in May 1998, the FDA revoked the suspension and approved the clinical application of fibrin sealants in the USA, when they were once again marketed [8].

Fibrin sealants are adhesive substances that mimic the final stages of blood coagulation. They form a stable, physiological fibrin clot which aids in wound repair. In addition to this, they serve two other primary functions. Firstly, they provide physical support for the extracellular matrix. Secondly, they facilitate the delivery of treatment compounds. This is made possible by their capacity to maintain the biochemical factors and original properties of implants [80, 83-85]. Therefore, they reduce the risk of bleeding, allow for the use of fewer sutures, and protect the injured environment against infections by microorganisms [85, 86]. They also allow for a decrease in inflammatory reactions, a lower incidence of trauma due to sutures [1, 78], and faster surgery and recovery, due to easy and fast applications in emergency conditions, allowing for a non-experienced surgeon to perform the repair. Whitlock et al. [87] investigated experienced and novice surgeons regarding the speed and quality of nerve repair in rodents, and showed a shorter surgery time in both scenarios with sealant repair, instead of sutures, and still, equivalent quality in sealant repairs between surgeons, demonstrating a faster learning curve.

In general lines, fibrin sealants are produced in two ways: from autologous or homologous blood derivatives. Autologous sealants use the patient's blood. Although they are biocompatible and do not present a risk of transmission of infectious diseases, they are not viable in surgeries and emergency applications. As an alternative, homologous fibrin sealants, produced by a pool of human blood, have been used.

However, in these cases, there are risks of transmission of infectious diseases such as hepatitis, HIV, and human parvovirus [14]. In addition to having a high cost of raw materials, with a need for blood extraction of bovine or human thrombin and human fibrinogen. Due to their composition with human blood, another common problem is rapid fibrinolysis, which starts less than 24 hours after application and prematurely detaches the nerve stumps [14].

Even with its not-so-recent introduction in human clinics, there is still no consensus on the use and efficacy of fibrin sealants for nerve repair, with a predominance in the literature of studies with rodent models, and few evaluations in humans [9, 78]. The use of sealants is still not approved by regulatory agencies such as the FDA for nerve repair, but the interest in this therapy, not only for nerve reconstruction, is growing. In a study with American surgeons, Owosu et al. [88] showed that a portion of them already use or consider using fibrin sealants in repairs, although there is still a preference for suturing as the main repair technique. The lack of data on the results and knowledge of the treatments were identified as the main barriers to the use of adjuvant therapies. However, most surgeons are open to the possibility.

Regarding efficiency in nerve repair, several studies show beneficial effects associated with the application of sealants, alone or with sutures, at the site of the injury. A systematic review conducted by Sameem and collaborators [78] supports, with the majority of studies in rodents, an equal, if not superior, performance in repair with fibrin sealants compared to micro-sutures only, based on histopathological, biomechanical, and electrophysiological characteristics. However, in treatments with sealant only, cases with difficulties such as complete failure and gaps in neural reconnection were also observed. A recent systematic analysis [9] indicates that nerve regeneration may be similar in fibrin glue repairs and/or suture repairs, but the use of fibrin glue significantly reduced operation times, which may pose both clinical and economic benefits. However, fibrin glue alone was reported to result in lower strength and more dehiscence [9, 89].

Until today, commercially available fibrin sealants are produced from both bovine and human thrombin and fibrinogen (homologous), which present disadvantages and risks, so that in addition to being transmitters of infectious diseases, they can generate fibrosis, toxicity, and necrosis [1]. They can also lead to the development of antibodies against bovine thrombin, and anaphylactic reaction to bovine proteins, among other adverse reactions [7, 82].

5. HFB in nerve repair

Considering the disadvantages present in commercially available fibrin sealants, a group of researchers from the Center for the Study of Venoms and Venomous Animals (CEVAP) at São Paulo State University, Botucatu, São Paulo, Brazil, began to standardize a new fibrin sealant in the 1990s. The HFB is a unique

heterologous fibrin worldwide, as it does not use human blood, and does not transmit infectious diseases. In addition, it is a natural, biodegradable, bioabsorbable, and non-toxic biopharmaceutical with excellent adhesive capacity, and can be used in several surgical procedures.

Compared to other clinically used commercial fibrin sealants, it has a low production cost, high availability of raw materials for its manufacture, and the possibility of adapting its formulation according to the type of procedure [82]. Its formulation allows its use in clinical medicine and various surgical procedures, such as skin grafts and surgical reconstructions, aiding in hemostasis, colostomy, and suture reinforcement [11, 14]. Furthermore, its healing power was tested in 40 patients of a phase I/II clinical trial for the treatment of chronic venous ulcers. Clinical results showed it as a safe, non-immunogenic product with promising efficacy. This is because there was an improvement in the quality of the ulcer bed, a significant reduction in the ulcer area, and healing in several patients [90, 91].

In the last years, HFB has been used in association with sutures (Figure 4) and other therapeutic factors to enhance or face difficulties in the current gold-standard treatment for nerve injury. Generally, in the face of a nerve transection, the application of HFB demonstrated positive results in reducing mechanical trauma to the nerve (points of suture) [23], obtained better or similar morphological and/or molecular performance when adjunct to traditional suture [7, 13, 23, 25], demonstrated easy usability with good adhesive capacity [17], and good biocompatibility with other materials [26, 92] (Figure 3C). Its healing power has been gaining attention and demonstrated valuable potential as an adjunct to enhance regeneration and motor function (Table 2).

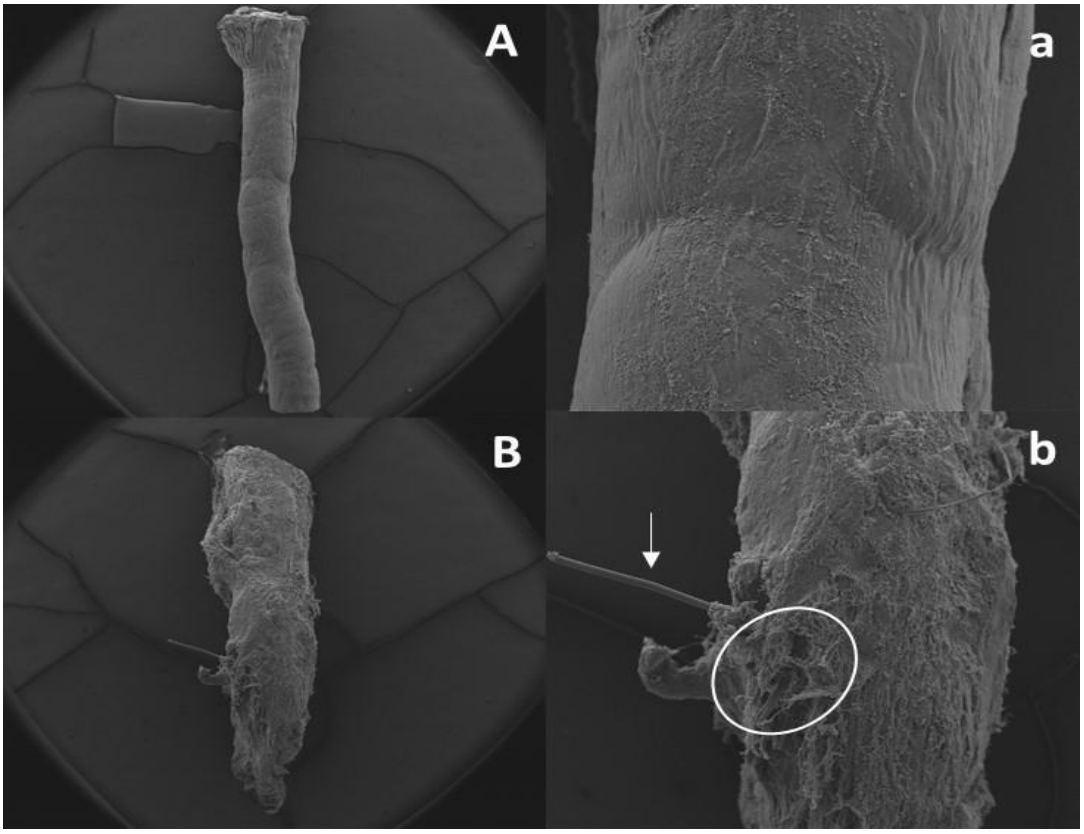

Figure 4. Nerve integrity of healthy and HFB-repaired nerves. Scanning electron microscopy of healthy **(A)** and HFB-repaired **(B)** nerves. Surface detail of epineurium can be seen in **a** and **b**. **(white arrow)** nylon suture thread; **(white ball)** HFB-associated connective tissue.

Table 2. Current strategies and potential therapeutic strategies aligned to HFB use for traumatic peripheral nerve injury.

Strategies (neurorrhaphy)	Intervention	Comments
Alone [13, 17, 19, 20, 23, 25, 93]	HFB as an adjunct to 1 to 3 stitches	HFB demonstrated angiogenic, neuroprotective, and immunomodulatory properties, which can enhance tissue regeneration, motor function, and wound healing, but satisfactory outcomes have not yet been achieved. The use of HFB also reduces trauma and the number of stitches.
Nerve conduit [10, 18, 26]	HFB embedded tubulization with suture	This association suggests a trophic action of the treatment, potentially accelerating regeneration through an increase in regeneration-associated factors, such as those related to Schwann cell reactivity (S100) and Agrin/Rapsyn/LRP4/Musk signaling pathway for the NMJ maintenance. Polycaprolactone has demonstrated good

		biocompatibility with HFB, surpassing other fibrin sealants.
Cell-based Therapy [16, 18, 22, 26, 94-96]	HFB as a scaffold for Embryonic Stem Cells, Mesenchymal Stem Cells, and Mononuclear Cells	HFB improves the effects of cell therapy by promoting an environment that enhances each particular scenario, such as growth factors release, and increased cell survivability resulting in neuroprotection.
Photobiomodulation [17, 19, 20, 93]	HFB as an adjunct to Low-level laser therapy with and without suture	HFB in association with LLLT has demonstrated a strong capability to accelerate myelination and functional recovery of innervated muscles. HFB allows nerve manipulation without trauma and enhances the nerve regeneration process.

Adjunct to suture alone

For short nerve injury gaps (< 1 cm), neurorrhaphy is commonly employed, repairing both proximal and distal ends, but the use of sutures can lead to inflammatory reactions such as granuloma and neuroma formation. In the last years, our group has been studying the effects of combining HFB with neurorrhaphy, also shading light to the NMJ recovery (Figure 5). HFB plays a crucial role in the healing process as the combination of fibrin with proteins enhances angiogenesis, wound contraction, collagen synthesis, and re-epithelialization. Further, it was able to reduce trauma in reconstruction to minimize the damage and inflammatory responses.

In a recent study, we demonstrated the early beneficial effects of the use of HFB in conjunction with two sutures for the repair of transected sciatic nerves in rats [13]. HFB application in comparison to suture alone improved overall nerve regeneration, with increased axonal growth and tissue vascularization (angiogenesis), proper restoration of neuromuscular junctions, reduced severe muscle degeneration (collagen infiltration), and enhanced relative area of M2 markers, 7 and 30 days after reconstruction. Remarkably, macrophages play a significant role in phagocytosis and cytokines releasement in the denervated NMJ immune response, and its balance between pro- and anti-inflammatory effectors at different phases of NMJ reinnervation appears to be crucial [64].

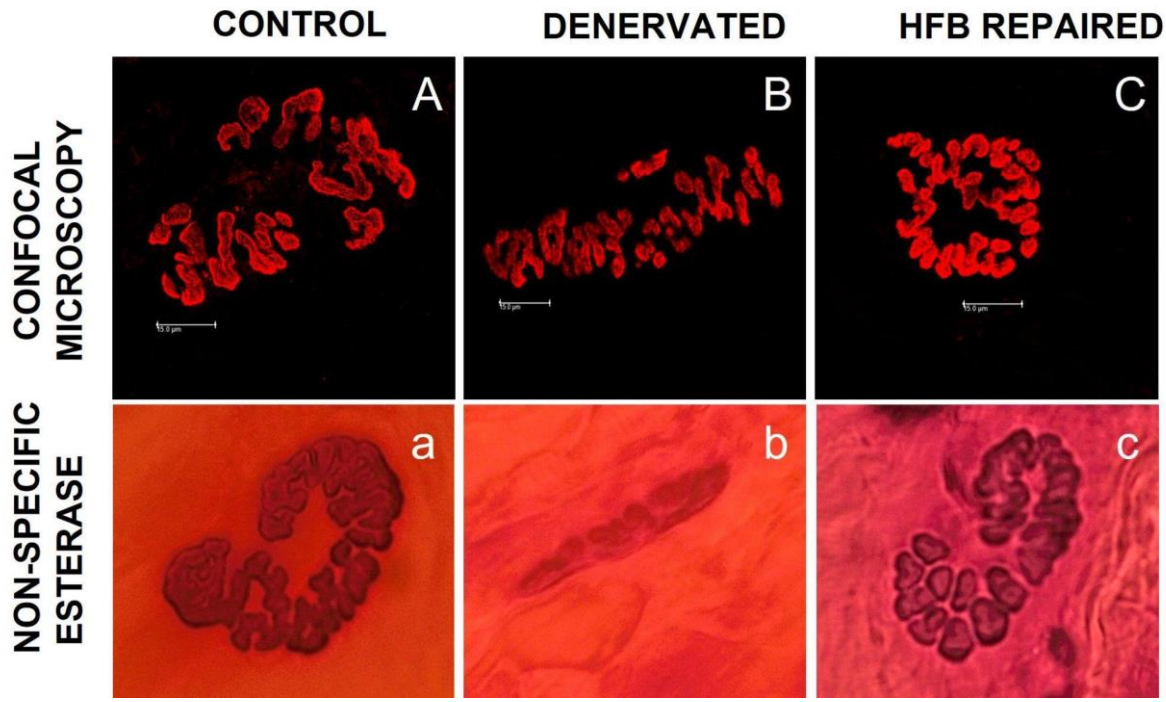

Figure 5. Neuromuscular junction morphology. Healthy **(A, a)**, denervated **(B, b)**, and HFB **(C, c)** repaired states, through nAChRs staining (confocal microscopy) with alpha-bungarotoxin and by non-specific esterase staining, which is based on the marking of positive esterase sites that contain AChE, leading to visualization of the entire NMJ morphology [97].

Sixty days after nerve reconstruction [23], with a 7-day interval between sciatic nerve injury and neurorrhaphy after 60 days of reconstruction, the association of HFB with one suture point showed restoration of nerve impulse and better axonal regeneration than suture alone. Ultra-structurally, the NMJs and associated muscle fibers of the HFB-treated groups showed proper regeneration. In this same study design [25], the use of HFB associated with a single suture point, compared to two suture points, reduced surgical time and showed potential to restore the microstructure of NMJs, as less degeneration was present and nAChRs/proteins associated with the mature pattern were observed to return. In addition, immature receptor values (γ) in the HFB group were lower than those in the suture-only group.

Multimodal approaches (cell-based therapies and nerve conduits)

Another therapeutic option for nerve injury is the use of nerve conduits, which serve as a bridge between the proximal and distal stumps, providing a scaffold for axonal regeneration [1]. This approach prevents intrusion of nearby tissues, guides the regeneration, and makes the repair site less prone to infiltration by fibroblasts and adverse inflammation, which may decrease fibrosis and improve overall nerve mobility [3]. HFB has already been associated with nerve conduit strategies and has demonstrated good biocompatibility with the polycaprolactone (PCL) grafts, which has been a challenge for other commercially available fibrin sealants [26], improving general regeneration (Table 2).

Our group used a PCL graft in addition to one suture point associated with HFB [10], and after 90 days of nerve reconstruction, although not fully regenerated, as

indicated by the nAChR cluster area, the compactness and endplate area of NMJs in the treated group were the only similar the Control, suggesting a better morphological approximation between the groups. Notably, it also demonstrated an increase in the expression of LRP-4, S100, and nAChR-ε proteins, and a decrease in MyoD, suggesting a positive influence on the neurodegenerative process, where the LRP-4 activates tSC, thus maintaining higher reinnervation of nAChRs and reducing muscle atrophy. The treatment favored a faster recovery in motor function assessment by improving print area when compared to suture alone. Indeed, the nerve guidance with HFB also enabled an approximation to the control group in terms of protein expression of Agrin, LRP-4, Musk, and Rapsyn.

Another promising augmentation method is cell-based therapy, which is a way of enhancement that can speed up the self-healing process and is currently under extensive research for stimulating regeneration after nerve injury [98]. The therapy employs stem cells due to their inherent ability to self-replicate and differentiate into specific cell types [1], which culminates in the release of neurotrophic growth factors and the myelination of axons. Schwann cells, the primary functional cells of the peripheral nervous system that promote myelination and regeneration, are the preferred initial seed cells, but other cell types have also been used and have achieved remarkable results [99]. For successful cell transplantation and adhesion at the injury site, an appropriate scaffold is necessary. HFB has demonstrated good biocompatibility, while further enhancing the power of regeneration-associated factors of the cell lineage and also improving the survival of the cells (Table 2).

The first study utilizing this association was conducted by Mozafari et al. [22], who observed axonal regeneration and sensory function improved using HFB with embryonic stem cells in a rodent model 60 days after sciatic nerve injury, where the combined effect was successful in supporting Schwann cells at the injury site and HFB facilitated the application and stabilization of the stem cells. In another study, Rodrigues-Sanchez et al. [26] used HFB as a base for PCL graft and canine adipose mesenchymal stem cells, observing that this multimodal approach supports the trophic microenvironment, resulting in a pro-regenerative state after critical sciatic nerve injury in rats. The treatment incorporated in HFB demonstrated enhanced motor function and electrophysiological recovery compared to the PCL group after 12 weeks. These results were linked to a change in the regeneration process favoring the development of myelinated fibers. HFB is demonstrated to be very permissive for use in conjunction with stem cells, allowing for an even more efficient regenerative process [92]. Further, Cartarozzi et al. [18] observed similar results engrafting HFB with mesenchymal stem cells in PCL conduits, where this association resulted in better reactivity of the glial cells leading to better regeneration and compacting of myelinated axons, as well as functional improvement in gait recovery. It was also observed that HFB enabled the survival of the cells seeded in the tubular prosthesis.

Photobiomodulation

Also known as LLLT, photobiomodulation is an emerging therapy that is increasingly being used for rehabilitation and functional restoration following injuries. The therapeutic effects of LLLT are linked to tissue biostimulation. This therapy triggers photoenergetic and photochemical reactions, leading to an increase in DNA and RNA synthesis within the cell nucleus [100]. In turn, this promotes cell proliferation and protein synthesis, including alterations in the action potential of nerve cells. For the

treatment of nerve injuries, it has been reported that this therapy stimulates myelination and axon regrowth by promoting Schwann cell proliferation [101]. In recent years, this technique has been studied in association with HFB, which has shown promising results, as HFB minimizes trauma and together exhibits strong regenerative power.

The initial study investigating this association was carried out by Buchaim et al. [17]. This study, which also involved a nerve graft, noted the collateral regeneration of axons from the vagus nerve into the autologous graft in all groups, but HFB+LLLT had enhanced myelination. In a subsequent study, Buchaim et al. [19] reported a comparable improvement in axonal recovery of the facial nerve post-suturing with the HFB-repaired group, which showed the closest results to the control in all nerve measurements. Additionally, the use of HFB facilitated the coaptation of the stumps without causing trauma to the nerve fibers. Further, Rosso et al. [20], also in a facial nerve model, observed better morphofunctional results in sutures or coaptation with HFB associated with LLLT, with an advantage in reducing trauma in the HFB group. In another recent study, this approach improved axonal growth in the stump distal to the lesion and minimized the atrophy on innervated muscles after experimental facial nerve transection [93]. HFB+LLLT had positive effects on the morphological and functional stimulation of the nerve, with the greatest regeneration for axon area and diameter.

Photobiomodulation and HFB were also assessed in other regenerative approaches, such as in bone, tendon, and skin repair [102-104]. All these investigations have revealed positive outcomes, underscoring the potential enhancement achievable through the synergistic use of HFB with other therapies. Unfortunately, no data was obtained regarding the NMJ regeneration process.

HFB in spinal cord injuries

Due to the proximity between the CNS and PNS interface, learnings can be made for the treatment of nerve injuries based on the use of HFB in CNS lesions, which has also been a hot topic approach. Spinal cord injuries result in a significant loss of motor and sensory functions. Ventral root avulsion, an experimental model, involves the detachment of the ventral (motor) roots from the spinal cord's surface. This leads to numerous morphological alterations, including the degeneration of motoneurons and rearrangements in the local spinal cord circuitry. Further, it has several commonly observed pathologies for nerve injury, such as WD.

In a rat ventral root avulsion model, Barbizan et al. [12] demonstrated that the root replantation with HFB enhanced motor recovery preserved the synaptic covering of the motoneurons, and improved neuronal survival. Barbizan et al. [16] further demonstrated that ventral root avulsion repair with HFB as a scaffold for mononuclear cells enhanced motoneuron survival and neurotrophic factor expression levels. In the same model, Spejo et al. [21] reported a potential immunomodulatory effect with increased expression of M2 macrophage marker genes and pro- and anti-inflammatory cytokines, along with greater neuronal survival when combined with HFB reconstruction. Kempe et al. [24] demonstrated a 50% increase in motor function, neuronal and synaptic survival, and immunomodulatory effects with the use of HFB, compared to its absence when combined with dimethyl fumarate after ventral root avulsion. Kempe et al. [27] further demonstrated the preservation of alpha motor neuron synapses and survivability of its associated sciatic nerve with spouting and

restoration of proper myelination and axon diameters by the combined treatment through ultrastructural evidence. Paes et al. [105] used HFB as a scaffold for human dental pulp stem cells for reimplantation after ventral root avulsion and also observed higher neuronal survivability and downregulation of glial reactivity, while also enhancing motor function in catwalk analysis.

All those works, for both peripheral and CNS injuries, highlight the HFB potential as an excellent scaffold for adjunct stem cell therapy and drug delivery systems. Indeed, the treatment of motor neuron injuries with HFB demonstrated improvement in tissue regeneration and motor function, although, in a different environment, the axon regeneration process was also enhanced.

Limitations and difficulties

Based on these presented studies and current strategies, which investigate the HFB association with nerve regeneration, further combinations with other therapies, such as regeneration-associated factors (growth factors), may enhance positive benefits. HFB readily allows for the encapsulation of bioactive complexes in its formulation, including growth factors, cytokines, drugs, and nucleic acids, which may further improve the therapy effect. Further, although remarkable results have been achieved with cell therapy, no studies have been conducted using Schwann cells, which are the most studied therapeutic model for nerve injury.

In relation to HFB volume, there is no current consensus on when it is used in nerve repair. The values range from 100 µL (2 drops) to 500 µL (10 drops). Despite this variability, it is believed that the healing effect, or the support provided by the scaffold therapy may not be compromised.

Regarding NMJ regeneration, no data was found on its association with cell therapy and photobiomodulation. Studies of the NMJ are crucial to understanding the sequence that extends from the central stimulus to the nerve-muscle tissue targets; this is particularly important as most therapies, while offering certain morphologic benefits, also present limitations related to motor function. The neuromuscular plasticity observed following nerve injuries and the subsequent reinnervation of muscles is remarkable, however, this may not be sufficient to restore fine movements due to the considerable misdirection of regenerating nerve fibers and failures or insufficiencies in NMJ reinnervation following injuries.

Another challenge lies in the development of pharmaceuticals that adhere to good manufacturing practices and produce consolidated, reproducible batches. To address this, CEVAP is launching the first Brazilian Contract Development and Manufacturing Organization (CDMO) [106]. This organization will provide services to both the public and private sectors by producing validated samples for clinical trials and offering academic training in translational science research. Furthermore, CEVAP is currently seeking support to conduct a Phase III multicenter clinical trial to validate the HFB findings, register with the Brazilian Health Regulatory Agency, and distribute the product throughout Brazil via the Unified Health System network.

6. Conclusion

Peripheral nerves inherently possess the ability to heal after an injury. Fibrin sealants have proven to be valuable in regenerative and surgical applications, particularly in cases of nerve injury. However, there's a limited recovery window before tissue degeneration obstructs the regeneration process and reconnection to the target. Despite the high costs and use of human blood associated with commercial sealants, HFB presents as a viable alternative. The use of HFB, in conjunction with conventional sutures, has been shown to enhance this regenerative effect, also reducing the number of suture points and surgical time. Moreover, HFB has an enhancing potential as a scaffold for other adjunct therapies, such as cell-based therapies and drug delivery systems, further improving the regenerative process.

Heterologous fibrin biopolymer provides a more conducive regenerative environment for nerves, muscles, and associated NMJs compared to sutures alone and has several advantages in relation to other fibrin sealants. Indeed, it has demonstrated a good capability of maintaining a less degenerated NMJ microenvironment and promoting early onset regeneration after injury. While clinical trials are necessary to establish definitively the benefits of fibrin sealants in human nerve repair, HFB shows significant promise as a potent bioproduct ready for clinical trials and eventual integration into clinical settings. Further research is warranted to determine if its use over extended periods post-treatment could lead to improved functional outcomes. The CMDO initiative will facilitate the translation of biopharmaceuticals from bench to bedside and pave the way for the international expansion of HFB.

Reference

1. Hussain G, Wang J, Rasul A, Anwar H, Qasim M, Zafar S, Aziz N, Razzaq A, Hussain R, de Aguilar JLG, Sun, T. Current Status of Therapeutic Approaches against Peripheral Nerve Injuries: A Detailed Story from Injury to Recovery. Int J Biol Sci. 2020 Jan 1;16(1):116-34.
2. Jones S, Eisenberg HM, Jia X. Advances and Future Applications of Augmented Peripheral Nerve Regeneration. Int J Mol Sci. 2016 Sep 7;17(9):1494.
3. Wang ML, Rivlin M, Graham JG, Beredjiklian PK. Peripheral nerve injury, scarring, and recovery. Connect Tissue Res. 2019;60(1):3-9.
4. Fu SY, Gordon T. Contributing factors to poor functional recovery after delayed nerve repair: prolonged axotomy. J Neurosci. 1995;15(5 Pt 2):3876-85.
5. Chan KM, Gordon T, Zochodne DW, Power HA. Improving peripheral nerve regeneration: from molecular mechanisms to potential therapeutic targets. Exp Neurol. 2014 Nov;261:826-35.
6. Robinson PP, Loescher AR, Smith KG. A prospective, quantitative study on the clinical outcome of lingual nerve repair. Br J Oral Maxillofac Surg. 2000;38(4):255-63.
7. Barros LC, Ferreira RS, Barraviera SR, Stolf HO, Thomazini-Santos IA, Mendes-Giannini MJ, Toscano E, Barraviera B. A new fibrin sealant from *Crotalus durissus terrificus* venom: applications in medicine. J Toxicol Environ Health B Crit Rev. 2009;12(8):553-71.
8. Fattahi T, Mohan M, Caldwell GT. Clinical applications of fibrin sealants. J Oral Maxillofac Surg. 2004;62(2):218-24.
9. Koopman JE, Duraku LS, de Jong T, de Vries RBM, Michiel Zuidam J, Hundepool CA. A systematic review and meta-analysis on the use of fibrin glue in peripheral nerve repair: Can we just glue it? J Plast Reconstr Aesthet Surg. 2022;75(3):1018-33.

10. Leite APS, Pinto CG, Tibúrcio FC, Muller KS, Padovani CR, Barraviera B, Ferreira Jr RS, Leal CV, Matsumura CY, Matheus SMM. Acetylcholine receptors of the neuromuscular junctions present normal distribution after peripheral nerve injury and repair through nerve guidance associated with fibrin biopolymer. Injury. 2023 Feb;54(2):345-61.
11. Biscola NP, Cartarozzi LP, Ulian-Benitez S, Barbizan R, Castro MV, Spejo AB, Ferreira Jr RS, Barraviera B, Oliveira ALR. Multiple uses of fibrin sealant for nervous system treatment following injury and disease. J Venom Anim Toxins incl Trop Dis. 2017;23:13. Epub 20170314. doi: 10.1186/s40409-017-0103-1.
12. Barbizan R, Castro MV, Rodrigues AC, Barraviera B, Ferreira RS, Oliveira AL. Motor recovery and synaptic preservation after ventral root avulsion and repair with a fibrin sealant derived from snake venom. PLoS One. 2013;8(5):e63260.
13. Tibúrcio FC, Muller KS, Leite APS, de Oliveira IRA, Barraviera B, Ferreira Jr RS, Padovani CR, Pinto CG, Matheus SMM. Neuroregeneration and immune response after neurorrhaphy are improved with the use of heterologous fibrin biopolymer in addition to suture repair alone. Muscle Nerve. 2023 Jun;67(6):522-36.
14. Buchaim DV, Cassaro CV, Shindo JVTC, Coletta BBD, Pomini KT, Rosso MPO, Campos LMG, Ferreira Jr RS, Barraviera B, Buchaim RL. Unique heterologous fibrin biopolymer with hemostatic, adhesive, sealant, scaffold and drug delivery properties: a systematic review. J Venom Anim Toxins incl Trop Dis. 2019;25:e20190038.
15. Page MJ, McKenzie JE, Bossuyt PM, Boutron I, Hoffmann TC, Mulrow CD, Shamseer L, Tetzlaff JM, Akl EA, Brennan SE, Chou R, Glanville J, Grimshaw JM, Hróbjartsson A, Lalu MM, Li T, Loder EW, Mayo-Wilson E, McDonald S, McGuinness LA, Stewart LA, Thomas J, Tricco AC, Welch VA, Whiting P, Moher D. The PRISMA 2020 statement: an updated guideline for reporting systematic reviews. BMJ. 2021 Mar;372(71).
16. Barbizan R, Castro MV, Barraviera B, Ferreira Jr RS, Oliveira AL. Influence of delivery method on neuroprotection by bone marrow mononuclear cell therapy following ventral root reimplantation with fibrin sealant. PLoS One. 2014;9(8):e105712.
17. Buchaim RL, Andreo JC, Barraviera B, Ferreira Junior RS, Buchaim DV, Rosa Junior GM, Oliveira ALR, Rodrigues AC. Effect of low-level laser therapy (LLLT) on peripheral nerve regeneration using fibrin glue derived from snake venom. Injury. 2015 Apr;46(4):655-60.
18. Cartarozzi LP, Spejo AB, Ferreira RS, Barraviera B, Duek E, Carvalho JL, Góes AM, Oliveira ALR. Mesenchymal stem cells engrafted in a fibrin scaffold stimulate Schwann cell reactivity and axonal regeneration following sciatic nerve tubulization. Brain Res Bull. 2015 Mar;112:14-24.
19. Buchaim DV, Rodrigues AeC, Buchaim RL, Barraviera B, Ferreira Jr RS, Junior GMR, Bueno CRS, Roque DD, Dias DV, Dare LR, Andreo JC. The new heterologous fibrin sealant in combination with low-level laser therapy (LLLT) in the repair of the buccal branch of the facial nerve. Lasers Med Sci. 2016 Jul;31(5):965-72.
20. Rosso MPO, Rosa Júnior GM, Buchaim DV, German IJS, Pomini KT, de Souza RG, Pereira M, Favaretto Jr IA, Bueno CRS, Gonçalves JBO, Ferreira Jr RS, Barraviera B, Andreo JC, Buchaim RL. Stimulation of morphofunctional repair of the facial nerve with photobiomodulation, using the end-to-side technique or a new heterologous fibrin sealant. J Photochem Photobiol B. 2017 Oct;175:20-8.
21. Spejo AB, Chiarotto GB, Ferreira ADF, Gomes DA, Ferreira RS, Barraviera B, Oliveira ALR. Neuroprotection and immunomodulation following intraspinal axotomy of motoneurons by treatment with adult mesenchymal stem cells. J Neuroinflammation. 2018;15(230).
22. Mozafari R, Kyrylenko S, Castro MV, Ferreira RS, Barraviera B, Oliveira ALR. Combination of heterologous fibrin sealant and bioengineered human embryonic stem cells to improve regeneration following autogenous sciatic nerve grafting repair. J Venom Anim Toxins incl Trop Dis. 2018;24:11. Epub 20180412. doi: 10.1186/s40409-018-0147-x.
23. Leite APS, Pinto CG, Tibúrcio FC, Sartori AA, de Castro Rodrigues A, Barraviera B, Ferreira Jr RS, Filadelpho AL, Matheus SMM. Heterologous fibrin sealant potentiates axonal regeneration after peripheral nerve injury with reduction in the number of suture points. Injury. 2019 Apr;50(4):834-47.
24. Kempe PRG, Chiarotto GB, Barraviera B, Ferreira RS, de Oliveira ALR. Neuroprotection and immunomodulation by dimethyl fumarate and a heterologous fibrin biopolymer after ventral root avulsion and reimplantation. J Venom Anim Toxins incl Trop Dis. 2020;26:e20190093. Epub 20200520. doi: 10.1590/1678-9199-JVATITD-2019-0093.
25. Pinto CG, Leite APS, Sartori AA, Tibúrcio FC, Barraviera B, Ferreira Jr RS, Filadelpho AL, Carvalho SC, Matheus SMM. Heterologous fibrin biopolymer associated to a single suture stitch enables the return of neuromuscular junction to its mature pattern after peripheral nerve injury. Injury. 2021 Apr;52(4):731-7.

26. Rodríguez-Sánchez DN, Pinto GBA, Cartarozzi LP, de Oliveira ALR, Bovolato ALC, de Carvalho M, Silva JVL, Dernowsek JA, Golim M, Barraviera B, Ferreira Jr RS, Deffune E, Bertanha M, Amorim RM. 3D-printed nerve guidance conduits multi-functionalized with canine multipotent mesenchymal stromal cells promote neuroregeneration after sciatic nerve injury in rats. Stem Cell Res Ther. 2021 May 29;12(1):303.
27. Kempe PRG, de Castro MV, Khuriyeh VC, Barraviera B, Ferreira RS, de Oliveira ALR. Ultrastructural Evidence of Synapse Preservation and Axonal Regeneration Following Spinal Root Repair with Fibrin Biopolymer and Therapy with Dimethyl Fumarate. Polymers (Basel). 2023;15(15).
28. Zelada D, Bermedo-García F, Collao N, Henríquez JP. Motor function recovery: deciphering a regenerative niche at the neuromuscular synapse. Biol Rev Camb Philos Soc. 2021;96(2):752-66.
29. Jones RA, Harrison C, Eaton SL, Llavero Hurtado M, Graham LC, Alkhammash L, Oladiran OA, Gale A, Lamont DJ, Simpson H, Simmen MW, Soeller C, Wishart TM, Gillingwater TH. Cellular and Molecular Anatomy of the Human Neuromuscular Junction. Cell Rep. 2017 Nov 28;21(9):2348-56.
30. Rodríguez Cruz PM, Cossins J, Beeson D, Vincent A. The Neuromuscular Junction in Health and Disease: Molecular Mechanisms Governing Synaptic Formation and Homeostasis. Front Mol Neurosci. 2020;13:610964.
31. Sanes JR, Lichtman JW. Development of the vertebrate neuromuscular junction. Annu Rev Neurosci. 1999;22:389-442.
32. Hughes BW, Kusner LL, Kaminski HJ. Molecular architecture of the neuromuscular junction. Muscle Nerve. 2006;33(4):445-61.
33. Nishimune H, Shigemoto K. Practical Anatomy of the Neuromuscular Junction in Health and Disease. Neurol Clin. 2018;36(2):231-40.
34. Lepore E, Casola I, Dobrowolny G, Musarò A. Neuromuscular Junction as an Entity of Nerve-Muscle Communication. Cells. 2019;8(8).
35. Iyer SR, Shah SB, Lovering RM. The Neuromuscular Junction: Roles in Aging and Neuromuscular Disease. Int J Mol Sci. 2021;22(15).
36. Bloch-Gallego E. Mechanisms controlling neuromuscular junction stability. Cell Mol Life Sci. 2015;72(6):1029-43.
37. Sugiura Y, Lin W. Neuron-glia interactions: the roles of Schwann cells in neuromuscular synapse formation and function. Biosci Rep. 2011;31(5):295-302.
38. Ko CP, Robitaille R. Perisynaptic Schwann Cells at the Neuromuscular Synapse: Adaptable, Multitasking Glial Cells. Cold Spring Harb Perspect Biol. 2015;7(10):a020503.
39. Jablonka-Shariff A, Lu CY, Campbell K, Monk KR, Snyder-Warwick AK. Gpr126/Adgrg6 contributes to the terminal Schwann cell response at the neuromuscular junction following peripheral nerve injury. Glia. 2020;68(6):1182-200.
40. Patton BL, Miner JH, Chiu AY, Sanes JR. Distribution and function of laminins in the neuromuscular system of developing, adult, and mutant mice. J Cell Biol. 1997;139(6):1507-21.
41. Patton BL. Basal lamina and the organization of neuromuscular synapses. J Neurocytol. 2003;32(5-8):883-903.
42. Engel AG. The neuromuscular junction. Handb Clin Neurol. 2008;91:103-48.
43. Tintignac LA, Brenner HR, Rüegg MA. Mechanisms Regulating Neuromuscular Junction Development and Function and Causes of Muscle Wasting. Physiol Rev. 2015;95(3):809-52.
44. Ruff RL. Neurophysiology of the neuromuscular junction: overview. Ann N Y Acad Sci. 2003;998:1-10.
45. Conti-Fine BM, Milani M, Kaminski HJ. Myasthenia gravis: past, present, and future. J Clin Invest. 2006;116(11):2843-54.
46. Wu P, Chawla A, Spinner RJ, Yu C, Yaszemski MJ, Windebank AJ, Wang H. Key changes in denervated muscles and their impact on regeneration and reinnervation. Neural Regen Res. 2014 Oct 15;9(20):1796-809.
47. Ma J, Shen J, Garrett JP, Lee CA, Li Z, Elsaidi GA, Ritting A, Hick J, Tan KH, Smith TL, Smith BP, Koman LA. Gene expression of myogenic regulatory factors, nicotinic acetylcholine receptor subunits, and GAP-43 in skeletal muscle following denervation in a rat model. J Orthop Res. 2007 Nov;25(11):1498-505.
48. Grosman C, Auerbach A. Kinetic, mechanistic, and structural aspects of unliganded gating of acetylcholine receptor channels: a single-channel study of second transmembrane segment 12' mutants. J Gen Physiol. 2000;115(5):621-35.
49. Naguib M, Flood P, McArdle JJ, Brenner HR. Advances in neurobiology of the neuromuscular junction: implications for the anesthesiologist. Anesthesiology. 2002;96(1):202-31.
50. Unwin N. Nicotinic acetylcholine receptor and the structural basis of neuromuscular transmission: insights from Torpedo postsynaptic membranes. Q Rev Biophys. 2013;46(4):283-322.

51. Gordon T. Peripheral Nerve Regeneration and Muscle Reinnervation. Int J Mol Sci. 2020;21(22):8652.
52. Lubińska L. Patterns of Wallerian degeneration of myelinated fibres in short and long peripheral stumps and in isolated segments of rat phrenic nerve. Interpretation of the role of axoplasmic flow of the trophic factor. Brain Res. 1982;233(2):227-40.
53. Lindborg JA, Mack M, Zigmond RE. Neutrophils Are Critical for Myelin Removal in a Peripheral Nerve Injury Model of Wallerian Degeneration. J Neurosci. 2017;37(43):10258-77.
54. Gomez-Sanchez JA, Carty L, Iruarrizaga-Lejarreta M, Palomo-Irigoyen M, Varela-Rey M, Griffith M, Hantke J, Macias-Camara N, Azkargorta, Aurrekoetxea I, De Juan VG, Jefferies HBJ, Aspichueta P, Elortza F, Aransay AM, Martínez-Chantar M, Bass F, Mato JM, Mirsky R, Woodhoo A, Jessen KR. Schwann cell autophagy, myelinophagy, initiates myelin clearance from injured nerves. J Cell Biol. 2015;210(1):153-68.
55. Gaudet AD, Popovich PG, Ramer MS. Wallerian degeneration: gaining perspective on inflammatory events after peripheral nerve injury. J Neuroinflammation. 2011;8:110.
56. Moalem G, Xu K, Yu L. T lymphocytes play a role in neuropathic pain following peripheral nerve injury in rats. Neuroscience. 2004;129(3):767-77.
57. Zigmond RE, Echevarria FD. Macrophage biology in the peripheral nervous system after injury. Prog Neurobiol. 2019;173:102-21.
58. Cattin AL, Burden JJ, Van Emmenis L, Mackenzie FE, Hoving JJ, Garcia Calavia N, Guo Y, McLaughlin M, Rosenberg LH, Quereda V, Jamecna D, Napoli I, Parrinello S, Enver T, Ruhrberg C, Lloyd A. Macrophage-Induced Blood Vessels Guide Schwann Cell-Mediated Regeneration of Peripheral Nerves. Cell. 2015 Aug 27;162(5):1127-39.
59. Gordon T. Nerve Regeneration: Understanding Biology and Its Influence on Return of Function After Nerve Transfers. Hand Clin. 2016;32(2):103-17.
60. Rishal I, Fainzilber M. Axon-soma communication in neuronal injury. Nat Rev Neurosci. 2014;15(1):32-42.
61. Fu SY, Gordon T. The cellular and molecular basis of peripheral nerve regeneration. Mol Neurobiol. 1997;14(1-2):67-116.
62. Ma CH, Omura T, Cobos EJ, Latrémolière A, Ghasemlou N, Brenner GJ, van Veen E, Barret L, Sawada T, Gao F, Coppola G, Gertler F, Costigan M, Geschwind D, Woolf CJ. Accelerating axonal growth promotes motor recovery after peripheral nerve injury in mice. J Clin Invest. 2011 Nov;121(11):4332-47.
63. Sakuma M, Gorski G, Sheu SH, Lee S, Barrett LB, Singh B, Omura T, Latremoliere A, Woolf CJ. Lack of motor recovery after prolonged denervation of the neuromuscular junction is not due to regenerative failure. Eur J Neurosci. 2016 Feb;43(3):451-62.
64. Rios R, Jablonka-Shariff A, Broberg C, Snyder-Warwick AK. Macrophage roles in peripheral nervous system injury and pathology: Allies in neuromuscular junction recovery. Mol Cell Neurosci. 2021;111:103590.
65. Su HL, Chiang CY, Lu ZH, Cheng FC, Chen CJ, Sheu ML, Sheehan J, Pan HC. Late administration of high-frequency electrical stimulation increases nerve regeneration without aggravating neuropathic pain in a nerve crush injury. BMC Neurosci. 2018 Jun 25;19(1):37.
66. Chao T, Frump D, Lin M, Caiozzo VJ, Mozaffar T, Steward O, Gupta R. Matrix metalloproteinase 3 deletion preserves denervated motor endplates after traumatic nerve injury. Ann Neurol. 2013 Feb;73(2):210-23.
67. Palispis WA, Gupta R. Surgical repair in humans after traumatic nerve injury provides limited functional neural regeneration in adults. Exp Neurol. 2017;290:106-14.
68. Cisterna BA, Cardozo C, Sáez JC. Neuronal involvement in muscular atrophy. Front Cell Neurosci. 2014;8:405.
69. Guarino SR, Canciani A, Forneris F. Dissecting the Extracellular Complexity of Neuromuscular Junction Organizers. Front Mol Biosci. 2019;6:156.
70. VanSaun M, Humburg BC, Arnett MG, Pence M, Werle MJ. Activation of Matrix Metalloproteinase-3 is altered at the frog neuromuscular junction following changes in synaptic activity. Dev Neurobiol. 2007;67(11):1488-97.
71. Martins RS, Siqueira MG, Da Silva CF, Plese JP. Overall assessment of regeneration in peripheral nerve lesion repair using fibrin glue, suture, or a combination of the 2 techniques in a rat model. Which is the ideal choice? Surg Neurol. 2005;64(Suppl 1):S1:10-6.
72. Ray WZ, Mackinnon SE. Management of nerve gaps: autografts, allografts, nerve transfers, and end-to-side neurorrhaphy. Exp Neurol. 2010;223(1):77-85.

73. Wanner R, Gey M, Abaei A, Warnecke D, de Roy L, Dürselen L, Rasche V, Knoll B. Functional and Molecular Characterization of a Novel Traumatic Peripheral Nerve-Muscle Injury Model. Neuromolecular Med. 2017 Sep;19(2-3):357-74.
74. Sulaiman W, Gordon T. Neurobiology of peripheral nerve injury, regeneration, and functional recovery: from bench top research to bedside application. Ochsner J. 2013;13(1):100-8.
75. Jiang BG, Han N, Rao F, Wang YL, Kou YH, Zhang PX. Advance of Peripheral Nerve Injury Repair and Reconstruction. Chin Med J (Engl). 2017;130(24):2996-8.
76. Faroni A, Mobasseri SA, Kingham PJ, Reid AJ. Peripheral nerve regeneration: experimental strategies and future perspectives. Adv Drug Deliv Rev. 2015;82-83:160-7.
77. Viterbo F, Brock RS, Maciel F, Ayestaray B, Garbino JA, Rodrigues CP. End-to-side versus end-to-end neurorrhaphy at the peroneal nerve in rats. Acta Cir Bras. 2017;32(9):697-705.
78. Sameem M, Wood TJ, Bain JR. A systematic review on the use of fibrin glue for peripheral nerve repair. Plast Reconstr Surg. 2011;127(6):2381-90.
79. Rosso MPO, Buchaim DV, Kawano N, Furlanette G, Pomini KT, Buchaim RL. Photobiomodulation Therapy (PBMT) in Peripheral Nerve Regeneration: A Systematic Review. Bioengineering (Basel). 2018;5(2).
80. Bayer IS. Advances in Fibrin-Based Materials in Wound Repair: A Review. Molecules. 2022;27(14).
81. Isaacs JE, McDaniel CO, Owen JR, Wayne JS. Comparative analysis of biomechanical performance of available "nerve glues". J Hand Surg Am. 2008;33(6):893-9.
82. Ferreira RS, de Barros LC, Abbade LPF, Barraviera SRCS, Silvares MRC, de Pontes LG, dos Santos LD, Barraviera B. Heterologous fibrin sealant derived from snake venom: from bench to bedside - an overview. J Venom Anim Toxins incl Trop Dis. 2017;23:21. Epub 20170404. doi: 10.1186/s40409-017-0109-8.
83. Peretti GM, Randolph MA, Zaporojan V, Bonassar LJ, Xu JW, Fellers JC, Yaremchuk MJ. A biomechanical analysis of an engineered cell-scaffold implant for cartilage repair. Ann Plast Surg. 2001 May;46(5):533-7.
84. Ringe J, Kaps C, Burmester GR, Sittinger M. Stem cells for regenerative medicine: advances in the engineering of tissues and organs. Naturwissenschaften. 2002;89(8):338-51.
85. de Barros CN, Miluzzi Yamada AL, Junior RS, Barraviera B, Hussni CA, de Souza JB, Watanabe MJ, Rodrigues CA, Alves ALG. A new heterologous fibrin sealant as a scaffold to cartilage repair-Experimental study and preliminary results. Exp Biol Med (Maywood). 2016 Jul;241(13):1410-5.
86. Buchta C, Dettke M, Funovics PT, Höcker P, Knöbl P, Macher M, Quehenberger P, Treiti C, Worel N. Fibrin sealant produced by the CryoSeal FS System: product chemistry, material properties and possible preparation in the autologous preoperative setting. Vox Sang. 2004;86(4):257-62.
87. Whitlock EL, Kasukurthi R, Yan Y, Tung TH, Hunter DA, Mackinnon SE. Fibrin glue mitigates the learning curve of microneurosurgical repair. Microsurgery. 2010;30(3):218-22.
88. Owusu A, Mayeda B, Isaacs J. Surgeon perspectives on alternative nerve repair techniques. Hand (N Y). 2014;9(1):29-35.
89. Tse R, Ko JH. Nerve glue for upper extremity reconstruction. Hand Clin. 2012;28(4):529-40.
90. Abbade LPF, Barraviera SRCS, Silvares MRC, Lima ABBC, Haddad GR, Gatti MAN, Medolago NB, Carneiro MTR, dos Santos LD, Ferreira Jr RS, Barraviera B. Treatment of Chronic Venous Ulcers With Heterologous Fibrin Sealant: A Phase I/II Clinical Trial. Front Immunol. 2021 Feb 23;12:627541.
91. Abbade LPF, Ferreira RS, Dos Santos LD, Barraviera B. Chronic venous ulcers: a review on treatment with fibrin sealant and prognostic advances using proteomic strategies. J Venom Anim Toxins incl Trop Dis. 2020;26:e20190101. Epub 20200622. doi: 10.1590/1678-9199-JVATITD-2019-0101.
92. Ortiz AC, Fideles SOM, Pomini KT, Bellini MZ, Pereira ESBM, Reis CHB, Pilon JPG, de Marchi MA, Trazzi BFM, da Silva WS, da Cunha MR, Buchaim WS, Cunha MR, Buchaim DV, Buchaim RL. Potential of Fibrin Glue and Mesenchymal Stem Cells (MSCs) to Regenerate Nerve Injuries: A Systematic Review. Cells. 2022 Jan 10;11(2):221.
93. Bueno CRS, Tonin MCC, Buchaim DV, Barraviera B, Ferreira Junior RS, Santos PSDS, Reis CHB, Pastori CM, Pereira ESBM, Nogueira DMB, Cini MA, Rosa Jr GM, Buchaim RL. Morphofunctional Improvement of the Facial Nerve and Muscles with Repair Using Heterologous Fibrin Biopolymer and Photobiomodulation. Pharmaceuticals (Basel). 2023 Apr 27;16(5):653.
94. Cassaro CV, Justulin LA, de Lima PR, Golim MA, Biscola NP, de Castro MV, Oliveira ALR, Doiche DP, Pereira EJ, Ferreira Jr RS, Barraviera B. Fibrin biopolymer as scaffold candidate to treat bone defects in rats. J Venom Anim Toxins incl Trop Dis. 2019 Nov 4;25:e20190027. Epub 20191104. doi: 10.1590/1678-9199-JVATITD-2019-0027.

95. Gasparotto VP, Landim-Alvarenga FC, Oliveira AL, Simões GF, Lima-Neto JF, Barraviera B, Ferreira Jr RS. A new fibrin sealant as a three-dimensional scaffold candidate for mesenchymal stem cells. Stem Cell Res Ther. 2014;5(3):78. Epub 20140610. doi: 10.1186/scrt467.
96. Orsi PR, Landim-Alvarenga FC, Justulin LA, Kaneno R, de Assis Golim M, Dos Santos DC, Creste CFZ, Oba E, Maia L, Barraviera B, Ferreira Jr RS. A unique heterologous fibrin sealant (HFS) as a candidate biological scaffold for mesenchymal stem cells in osteoporotic rats. Stem Cell Res Ther. 2017 Sep 29;8(1):205.
97. Muller KS, Tibúrcio FC, de Barros JWF, Matsumura CY, Matheus SMM. Statin exposure during pregnancy promotes neuromuscular junction alterations in postpartum Wistar rats. Muscle Nerve. 2023;67(6):537-47.
98. Zhang RC, Du WQ, Zhang JY, Yu SX, Lu FZ, Ding HM, Cheng YB, Ren C, Geng DQ. Mesenchymal stem cell treatment for peripheral nerve injury: a narrative review. Neural Regen Res. 2021 Nov;16(11):2170-6.
99. Hsu YC, Chen SL, Wang DY, Chiu IM. Stem cell-based therapy in neural repair. Biomed J. 2013;36(3):98-105.
100. Modrak M, Talukder MAH, Gurgenashvili K, Noble M, Elfar JC. Peripheral nerve injury and myelination: Potential therapeutic strategies. J Neurosci Res. 2020;98(5):780-95.
101. Lopes B, Sousa P, Alvites R, Branquinho M, Sousa AC, Mendonça C, Atayde LM, Luís AL, Varejão ASP, Maurício AC. Peripheral Nerve Injury Treatments and Advances: One Health Perspective. Int J Mol Sci. 2022 Jan 14;23(2):918.
102. de Freitas Dutra Júnior E, Hidd SMCM, Amaral MM, Filho ALMM, Assis L, Ferreira RS, Barraviera B, Martignago CCS, Figueredo-Silva J, Oliveira RA, Tim CR. Treatment of partial injury of the calcaneus tendon with heterologous fibrin biopolymer and/or photobiomodulation in rats. Lasers Med Sci. 2022 Mar;37(2):971-81.
103. Reis CHB, Buchaim RL, Pomini KT, Hamzé AL, Zattiti IV, Duarte MAH, Alcade MP, Barraviera B, Ferreira Jr RS, Pontes FML, Grandini CR, Ortiz AC, Fideles SOM, Eugênio RMC, Rosa Jr GM, Teixeira DB, Pereira ESBM, Pilon JPG, Miglino MA, Buchaim DV. Effects of a Biocomplex Formed by Two Scaffold Biomaterials, Hydroxyapatite/Tricalcium Phosphate Ceramic and Fibrin Biopolymer, with Photobiomodulation, on Bone Repair. Polymers (Basel). 2022 May 19;14(10):2075.
104. Buchaim DV, Andreo JC, Pomini KT, Barraviera B, Ferreira RS, Duarte MAH, Alcade MP, Reis CHB, Teixeira DB, Bueno CRS, Detregiachi CRP, Araujo AC, Buchaim RL. A biocomplex to repair experimental critical size defects associated with photobiomodulation therapy. J Venom Anim Toxins incl Trop Dis. 2022 Feb 14;28:e20210056. Epub 20220214. doi: 10.1590/1678-9199-JVATITD-2021-0056.
105. Paes SM, Castro MV, Barbosa RM, Politti Cartarozzi L, Coser LO, Kempe PRG, Decarli MC, Moraes AM, Barraviera B, Ferreira Jr RS, Oliveira ALR. Human dental pulp stem cell monolayer and spheroid therapy after spinal motor root avulsion in adult rats. Brain Res. 2023 Mar 1;1802:148229.
106. Ferreira RS, Morales MM, Barretti P, Barraviera B. Launching a CDMO in Brazil aiming to develop biopharmaceuticals for clinical trials. J Venom Anim Toxins incl Trop Dis. 2022;28:e20220017. Epub 20220606. doi: 10.1590/1678-9199-JVATITD-2022-0017.

Capítulo 2

Artigo submetido para a revista: **Journal of the Peripheral Nervous System,** IF 3.9 (2023).

Nerve integrity is improved, preventing muscle atrophy and fibrosis, after experimental nerve repair associated with a heterologous fibrin biopolymer

Muller, KS[1,2]; Tibúrcio, FC[1,2]; Ferreira Junior, RS[3,4]; Barraviera, B[2,3,4]; Horta Júnior, JAC[1,2]; Matheus, SMM[1,2*]

[1]Department of Structural and Functional Biology, São Paulo State University (Unesp), Institute of Biosciences, Botucatu, SP, Brazil.
[2]Medical School, São Paulo State University (Unesp), Botucatu, SP, Brazil.
[3]Center for the Study of Venoms and Venomous Animals (Cevap), Sao Paulo State University (Unesp), Botucatu, SP, Brazil.
[4]Center for Translational Sciences and Biopharmaceuticals Development, Botucatu, SP, Brazil.

Abstract

Complete sectioning of the nerve (neurotmesis) results in the blockage of nerve conduction, leading to changes in the peripheral nervous system as a series of pathophysiological and metabolic responses occur to stabilize and repair the injured tissues. A critical concern arises from the disruption of connections and degeneration of neuromuscular junctions (NMJs), leading to profound atrophy and substantial loss of muscle function, impairing motor tasks and quality of life. The gold standard technique, neurorrhaphy, is insufficient for achieving significant motor recovery. A promising adjunct candidate is the heterologous fibrin biopolymer (HFB), a Brazilian sealant that is entirely biological and free from human blood, which has been demonstrated to overcome the limitations associated with traditional sealants while mitigating degeneration in nerves, muscles, and NMJs postinjury, thus promoting a more conducive environment for subsequent regeneration. However, questions about its late regenerative effects remain unexplored. In this regard, we investigated the effects of nerve reconstruction via neurorrhaphy associated with HFB 120 days after injury and repair of the sciatic nerve in Wistar rats, addressing aspects of the peripheral nervous system (nerve, NMJ, and muscle). Thirty-two adult male Wistar rats were randomly distributed into four experimental groups: Control (C), where the right sciatic nerve was visualized; Denervated (D), where neurotmesis was performed with removal of a 6 mm fragment of the sciatic nerve; Neurorrhaphy (N), after neurotmesis, where the stumps of the injured sciatic nerve were reconnected by neurorrhaphy; and Neurorrhaphy + HFB (NB), in which HFB was added after neurorrhaphy. At 120 days, the fibular nerves and cranial tibial muscles were collected. For nerve integrity, the

number of intact axons increased in the NB group, notably indicating an increase in the frequency of axons with a healthy G ratio/axon diameter ratio. With respect to NMJs, a closer approximation of the normal morphological parameters was observed in the NB group. Furthermore, NB increased the nAChR alpha-1 subunit and Rapsyn expression. This may have benefit muscle morphology, which demonstrated that groups NB and C exhibited healthy and proximal myofiber characteristics, group D exhibited degenerated fibers, and group N exhibited intermediate myofiber preservation. Overall, we suggest that the substantial increase in the number of regenerated axons in the NB provided further muscle reinnervation and prevented muscle degeneration. These findings highlight the beneficial effects of HFB in nerve repair, surpassing those achieved by neurorrhaphy alone.

1. Introduction

Nerve injuries are considered prominent health problems, with signs and symptoms varying according to the intensity of nerve damage (113). Despite the vast availability of information related to pathological mechanisms and recovery, treatments that ensure complete morphological and functional recovery in moderate to severe cases are not yet well established. The treatment options available for this type of injury depend on microsurgical repair interventions, and although neurorrhaphy is a well-established technique for treatment (113), it is insufficient for satisfactory motor restoration alone.

Faced with complete transection of the nerve, or neurotmesis, the main concern is to ensure nerve continuity, enabling axonal regeneration toward peripheral recovery from the injury. This occurs because the disconnection of the motor unit separating motor neurons from muscle fibers results in neuronal loss, nerve fiber degeneration, and functional loss of the target skeletal muscle (1, 25). Thus, a cascade of physiological and metabolic responses is triggered in an attempt to reverse the damage resulting from the injury (23). While the distal stump of the injured nerve undergoes Wallerian degeneration, manifesting as myelin breakdown and axonal disintegration, the striated skeletal tissue, deprived of its source of electrical stimuli, faces stimuli that trigger muscle atrophy and connective tissue infiltration. Additionally, the nerve endings where neuromuscular junctions (NMJs) are formed suffer fragmentation (80) and disaggregation of their nicotinic acetylcholine receptors (nAChRs) and anchored proteins, which are fundamental for maintaining their function and enabling muscle contraction (81).

The main difficulties related to achieving satisfactory motor recovery are related to the reconnection and nerve regeneration itself, where regenerated axons fail to reach their original endoneural tubes (54) or there is difficulty in local revascularization, progressive loss of the regenerative character in Schwann cells, atrophy of the innervated organs and the prolonged time between medical intervention after the injury, which are crucial factors that interfere with the positive outcome (9, 54, 60, 90). Given these difficulties, an emerging adjunct candidate is the heterologous fibrin biopolymer (HFB) (25).

This biopharmaceutical product, originating from Brazil, is composed of a thrombin-like enzyme derived from rattlesnake venom and fibrinogen obtained from buffalo blood (102). It stands out globally as a unique heterologous fibrin that does not contain human blood, thus eliminating the risk of transmitting infectious diseases. This biodegradable, bioabsorbable, and nontoxic product boasts superior adhesive properties and can be utilized in a variety of surgical procedures (91, 102). Compared to sutures, HFB creates a more favorable environment for regeneration while also offering numerous benefits over other commercial fibrin sealants (25).

Several studies have previously demonstrated positive outcomes for the association of HFB with nerve tissue reconstruction in the early to medium (7 to 90 days) regenerative period, in which it has immunomodulatory (107, 114, 115), angiogenic (107) and neuroprotective (44, 65, 77, 106, 107, 116-118) properties (for an in-depth review, please see (25)). Indeed, it has demonstrated a good ability to maintain a less degenerated nerve-muscle-NMJ microenvironment and promote early-onset regeneration after injury. Here, 120 days after repair, we further demonstrated that HFB consolidates the establishment of a more conducive regenerated environment than isolated sutures, providing greater nerve integrity, which consequently prevents severe cases of atrophy and muscle fibrosis.

2. Methods

2.1. Animal care

Thirty-two adult male Wistar rats aged between 90 and 95 days with an average body weight of 300 g were used from the Central Animal Facility of Unesp, Botucatu Campus. Throughout the experimental period, the animals were kept in the Rodent Animal Facility 5 of the Experimental Research Unit (Unipex) of Botucatu Medical School (FMB/Unesp) in polyethylene boxes (measuring 40 × 30 × 15 cm) with solid

bottoms lined with sawdust substrate under controlled conditions of luminosity (12 h light/12 h dark), temperature (22 ± 2 °C), filtered water and Presence® feed ad libitum. The animals were randomly distributed into 4 experimental groups: the control (C), denervated (D), neurorrhaphy (N), and neurorrhaphy + HFB (NB) groups. All mentioned procedures were approved by the local ethics committee and were registered under the number CEUA-FMB:1402/2021.

2.2. Surgeries

The animals were anesthetized through intraperitoneal injection of an anesthetic solution containing ketamine (Dopalen®, 70 mg/kg) and xylazine (Anasedan®, 30 mg/kg). After trichotomy of the right pelvic limb, the animals were positioned in the ventral decubitus position, and the front and hind legs were kept in abduction. Lidocaine (7 mg/kg) was applied at the incision site and subjected to antisepsis with iodized alcohol, followed by an incision on the lateral face of the thigh, from the height of the greater trochanter to the knee, with exposure of the right sciatic nerves.

In the animals in group C, only the location and visualization of the sciatic nerve were performed, and then the soft tissues and skin were repositioned and sutured (Mononylon 7-0 and 5-0, Polysuture) (Figure 1A). In the animals in groups D, N, and NB, in a standardized way, approximately 3 millimeters above the trifurcation, a nerve lesion was generated by transection of the sciatic nerve (neurotmesis). In the animals in group D, to avoid spontaneous regeneration, a 6 mm fragment of the nerve was removed, and the proximal and distal stumps were inverted 180° and fixed in the adjacent musculature, with simple points with nylon thread (Mononylon 10-0, Polysuture) (Figure 1B). In groups N and NB, immediately after neurotmesis, the nerve stumps were reconnected. In group N, the stumps were reconnected by end-to-end neurorrhaphy (epineural anastomosis) with 2 stitches and nylon thread (Mononylon 10-0, Polysuture) (Figure 1C). In group NB, nerve reconstruction was performed by neurorrhaphy with 2 stitches followed by the application of 250 µL of HFB (13) (Figure 1D), provided by CEVAP, Unesp Botucatu, SP, Brazil, whose components and application formula are contained in its patents (Registration numbers: BR1020140114327 and BR1020140114360)(102). At the time of use, the components were thawed and reconstituted. The application was made through the simultaneous placement of fraction 1 (125 µL) with fraction 2 (125 µL) - prepared immediately before

the application, through the homogenization of equal amounts of fibrinogen and diluent factor - at the site of the injury.

After nerve reconstruction was performed, the soft tissues and skin were sutured at simple points using nylon thread (Mononylon 7-0 and 5-0, Polysuture), and the animals were kept under surveillance and heating until recovery. Tramadol (5 mg/kg) was then administered for pain analgesia, and enrofloxacin (Baytril®, 10 mg/kg) was administered via subcutaneous injection to prevent opportunistic infections. For three consecutive days, the postsurgical protocol included the administration of the analgesic for 3 days every 24 hours and, if necessary, for up to 5 days, in addition to the application of iodopovidone during the healing period at the incision site. After the experimental period, 120 days after the surgery, the animals were anesthetized through intraperitoneal injection of an anesthetic solution of ketamine (Dopalen, 70 mg/kg) and xylazine (Anasedan, 30 mg/kg). For the analyses of the cranial tibial muscle, its associated NMJs and the fibular nerve, the tissues were collected fresh, stored and immediately kept in an appropriate fixative solution (Karnovsky, freshly made with 4% paraformaldehyde and 2.5% glutaraldehyde, or 4% paraformaldehyde) or frozen. After the collection of biological material, the animals were euthanized through intracardiac injection of thiopental sodium.

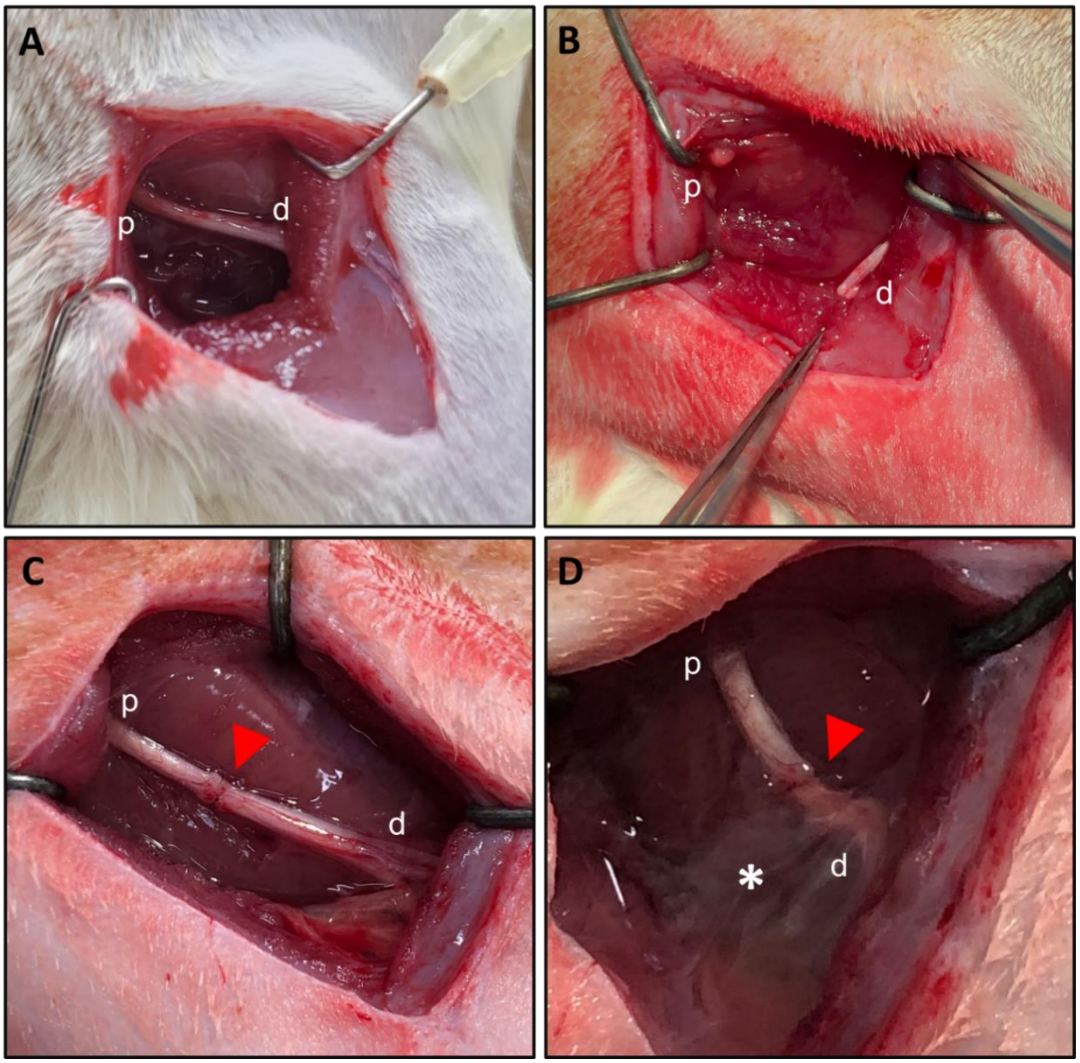

Figure 1. Images of the experimental surgical procedure showing nerve assessment in the control (A), denervated (B), neurorrhaphy (C) and neurorrhaphy + HFB (D) groups. (p): proximal stump; (d): distal stump; (red arrowhead): location/point of neurorrhaphy; (*): polymerized HFB.

2.3. Muscle integrity analysis (n=5)

The animals were weighed and anesthetized, and the cranial tibial muscles were removed, cleaned in saline solution, dissected, and weighed for subsequent calculation of the relative weight of the muscle (muscle weight/animal weight *100) for each animal.

For the ultrastructural analysis of muscle fibers, portions of the cranial tibial muscle were sectioned into rectangles and stored in Karnovsky solution for later processing, and longitudinal sections were obtained. The material was processed following the routine of the Electron Microscopy Center of the Institute of Biosciences (CME/IBB/UNESP) and was photodocumented using a transmission electron microscope (TECNAI Spirit, Fei).

The distal ends of the cranial tibial muscle were sectioned and fixed in 10% buffered formalin for 24 hours, washed in running water for 48 hours, submerged in Paraplast® and sectioned with a microtome (4 µm). Two histological slides were made for each animal from each experimental group. After staining, the slides were photographed at 200× magnification on an Olympus Bx41 microscope (SC30 camera).

The first slide was subjected to H.E. staining, and approximately 400 muscle fibers from 3 to 4 random fields were subjected to morphometric analysis of the area, perimeter, circularity, minimum and maximum diameter, Feret diameter, minimum Feret, angulation and Feret angle of the muscle fibers and counting the number of central nuclei. These measurements were analyzed using ImageJ software (v.1.53) (110).

The second slide was subjected to Picrosirius Red staining, in which the connective tissue was stained red and the muscle fibers were stained yellow. The quantification of the connective tissue was performed via percentage analysis of the total muscle sections through the threshold tool of ImageJ software (v.1.53).

2.4. Assessment of neuromuscular junctions (n=5)

For the characterization of the NMJs, entire longitudinal sections of 400 µm of the right cranial tibial muscle were made using a vibratome (Hyrax V50 Vibratome/Carl Zeiss). These sections were preserved in Karnovsky solution and then subjected to reactions with nonspecific esterase (119). Photomicrographs of the NMJs were obtained with an Olympus Bx41 microscope (SC30 camera). Measurements of the area, perimeter, minimum and maximum diameter, Feret diameter and minimum Feret were taken for 50 NMJs of each animal with ImageJ software.

2.5. Fibular nerve analysis (n=5)

After the right fibular nerves were exposed, a fragment of approximately 1 cm was removed and fixed in Karnovsky solution for at least 24 hours. Then, the fragments were placed in fresh osmium tetroxide solution for 24 hours, washed in phosphate buffer, stored in 70% alcohol and incubated with historesin. After this routine, the blocks containing the nerves were sectioned transversely (2 µm) on a Leica RM2265 ultramicrotome. The histological slides were counterstained with 1% toluidine blue in ultrapure water and photographed on an Olympus Bx41 microscope (SC30 camera). Images were obtained at magnifications of 100x, 400x and 1000x using immersion oil.

Due to marked atrophy and degeneration, it was not possible to collect the fibular nerves of the animals in the Denervated group. The nerves were analyzed through ImageJ software (v.1.53) to determine the total number of axons and the area and perimeter of the nerve fascicle using images at 100x and 400x, and the free software “AxonDepSeeg” (111), which uses machine learning and neural networks to perform morphometry of nerve fibers in an automated manner, was used to determine the area and perimeter of the axon, diameter of the axon, area and thickness of the myelin sheath, area and perimeter of the nerve fiber, and G ratio for all nerve fibers in 5 randomly chosen fields at 1000x magnification (totaling at least 50% of the fibers present in the fascicle). After measurement from the AxonDepSeeg software, an inclusion criterion was adopted to remove errors in which measurements with areas < 1 µm were removed.

2.6. Protein expression analysis by Western blotting (n=5)

The proximal portions of the cranial tibial muscle were thawed, weighed, sonicated, and homogenized in RIPA buffer supplemented with protease inhibitors (50 mg of tissue/100 µL of extraction buffer). The tissue extracts were extracted by centrifugation for 20 minutes at 14000 rpm at 4°C. For each animal, the protein content was determined using the Bradford method (Bio-Rad protein assay), and the corresponding 50 micrograms of protein were applied to a polyacrylamide gel. After electrophoresis, the proteins were transferred to nitrocellulose membranes and incubated with the following primary antibodies overnight: the nAChRs Alpha-1 (1:1000, Santa Cruz, #sc-136130), Gamma (1:1000, Santa Cruz, #sc-13998) and Epsilon (1:2000, Santa Cruz, #sc-376747); the proteins associated with cluster formation of nAChRs: Agrin (1:1000, Abcam, #ab12362), LRP4 (1:1000, Abcam, #ab174637), MuSK (1:1000, Bioss, #bs6473R), and Rapsyn (1:1000, Santa Cruz, #sc-58585). After washing, the membranes were incubated for 1 hour with the following secondary antibody: HRP-conjugated anti-rabbit IgG (1:10000, Santa Cruz, #sc-2005) or HRP-conjugated anti-mouse IgG (1:5000, Abcam, #ab6728). The proteins were visualized using a chemiluminescent substrate (AMERSHAM ECLTM PRIME, GE Healthcare). Semiquantitative densitometry analysis of the bands was performed by ImageJ software (v.1.53), and the data were normalized to the GAPDH expression values (1:5000, Cell Signaling, #14C10) of the same membrane and are reported in arbitrary units.

2.7. Statistical analysis

All data related to morphological and morphometric quantifications and statistical analyses were analyzed blindly by the principal researcher. The results of all quantitative variables were compared between the groups, and before any analysis, the normal distribution and homoscedasticity of the data were verified through the Shapiro–Wilk test. Comparisons between the groups with an adherence to the normal distribution of probabilities (all muscle, nerve, and NMJ morphometric analysis and western blotting quantification) were performed by parametric analysis of variance (ANOVA) for the model with one factor complemented with the Tukey multiple comparisons test or by the nonparametric procedure (Kruskal–Wallis) complemented by the Dunn test in the absence of adherence to the normal distribution (counting and percentage analysis of muscle fibers). All the data were considered significant at the 5% level ($p \leq 0.05$). The data were analyzed with GraphPad Prism 9 software, and all the graphs were generated with the same software.

3. Results

3.1. *HFB promoted improved NMJ morphological recovery*

According to the morphological analyses, in group C, NMJs with a regular and circular shape were observed, similar to a “pretzel”, consistent with a healthy shape (Figure 2A, 2a), while in group D, the NMJs were morphologically flattened and exhibited evident fragmentation, which are typical characteristics of degeneration (Figure 2B, 2b). In groups N and NB, an intermediate pattern was observed between groups C and D (Figure 2C, 2c and 2D, 2d). In group NB, more NMJs with circular shapes and continuous arms, tending toward the “pretzel” shape, were identified.

Morphometric analysis confirmed these findings, as group NB presented area (Figure 2E) and perimeter (Figure 2F) values that were statistically similar to those of group C. Furthermore, group NB exhibited superior values and differed from group N in terms of the minimum diameter (Figure 2I), minimum Feret (Figure 2J) and circularity (Figure 2K), being the only group similar to group C, except for circularity. The Feret diameter (Figure 2G) and maximum diameter (Figure 2H) of the NMJs in all the groups were similar.

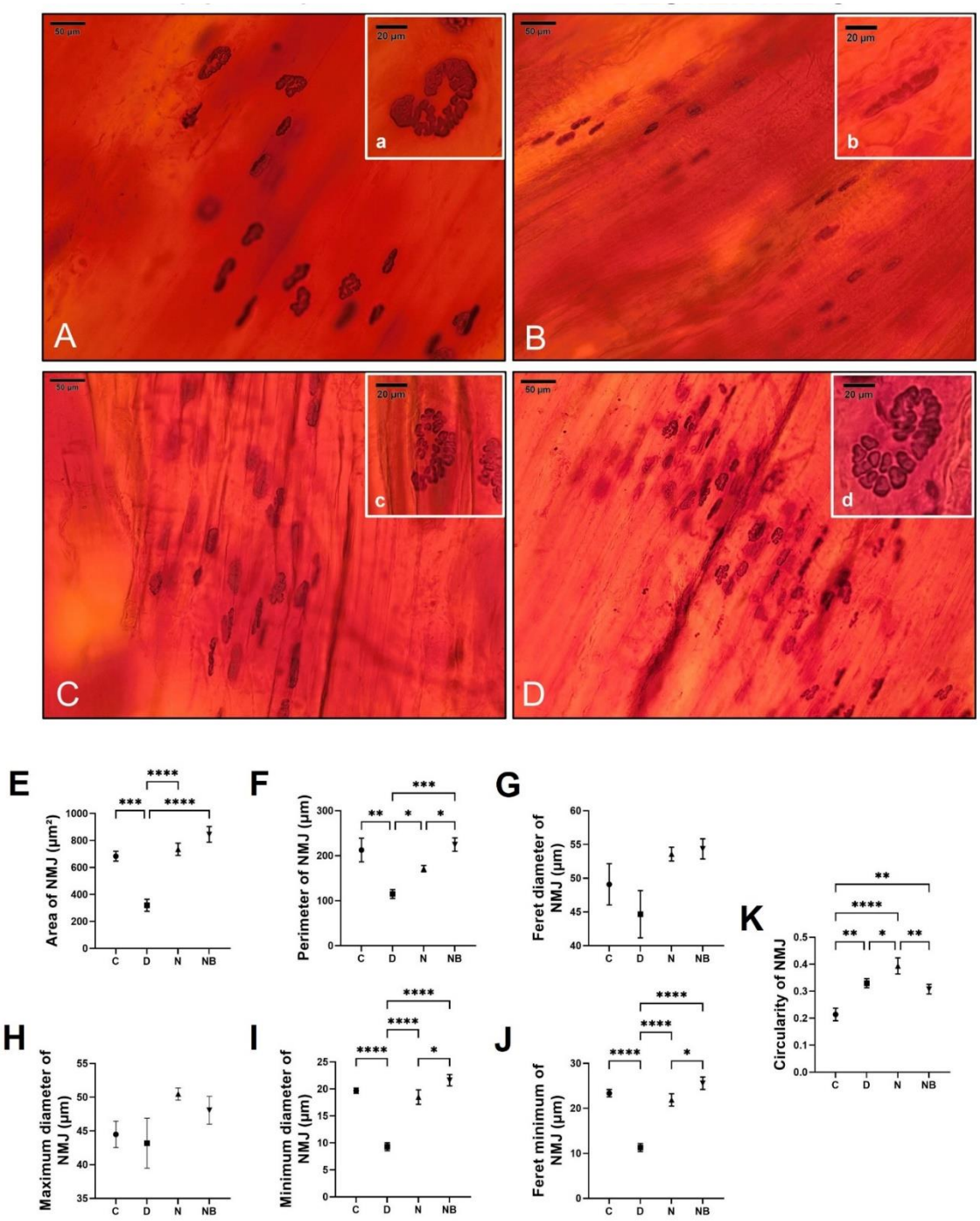

Figure 2. Photomicrographs of the cranial tibial muscle (total assembly) of the control group (A), denervated group (B), neurorrhaphy group (C), and neurorrhaphy + HFB group (D). The JNMs were marked through the reaction of nonspecific esterase and visualized by conventional optical microscopy with an increase of 200x (scale bar 50 µm). Details: JNM at 400x (scale bar 20 µm) (a, b, c and d). Graphs of the analyses of the area (E), perimeter (F), farthest diameter (G), maximum and minimum diameter (H and I), farthest minimum diameter (J), and circularity (K) of the NMJs of all the experimental groups. The values are expressed as the average and standard error of the mean and were analyzed by ANOVA followed by the Tukey test. Asterisks indicate statistically significant differences (*p<0.05; **p<0.001; ***p<0.0001; ****p<0.00001).

3.2. HFB prevented muscle atrophy and fibrosis

Analysis of the relative weights of the cranial tibial muscle (normalization of the muscle weight by the total body weight of the animal multiplied by 100) revealed that group C had the highest relative weight, followed by groups N, NB, and D (Figure 4A). Group C was different from the other groups, while groups NB and N presented similar values to each other, with all groups having higher values and differing from group D.

Regarding muscle fiber morphology, the NB and C groups exhibited normal patterns with similar myofiber characteristics, exhibiting fibers in polygonal shapes with peripheral nuclei and preserved endomysium and perimysium (Figure 3A-A' and 3D-D'). In group D, fibers were reduced in size, and there was a large infiltration of connective tissue in the perimysium (Figure 3B'), in addition to a large number of central nuclei (Figure 3B). Group N presented fibers within an intermediate pattern, exhibiting shapes varying from polygonal to rounded, with varied sizes, in addition to the presence of central nuclei and some infiltration of connective tissue (Figure 3C-C').

Ultrastructurally, in group C, the myofibrils were organized, forming intact sarcomeres with a straight Z line, intermyofibrillar mitochondria of variable sizes, and T tubules organized in triads, as well as peripheral nuclei (Figure 3A''). In group D, disorganization of the sarcomeres was observed in most of the myofibrils, with regions containing fragmented Z lines and focal areas of injury, showing myelin, a concentration of mitochondria, and abundant central nuclei (Figure 3B''). In groups N and NB, the ultrastructure revealed recovery of muscle tissue, with organized sarcomeres and few central nuclei, although focal areas of injury were still present (Figure 6C'' and 6D''). Qualitatively, a trend toward greater organization and approximation of the sarcomeres in groups NB to C was observed, in addition to fewer groupings of extracellular disorganization of the sarcomeres.

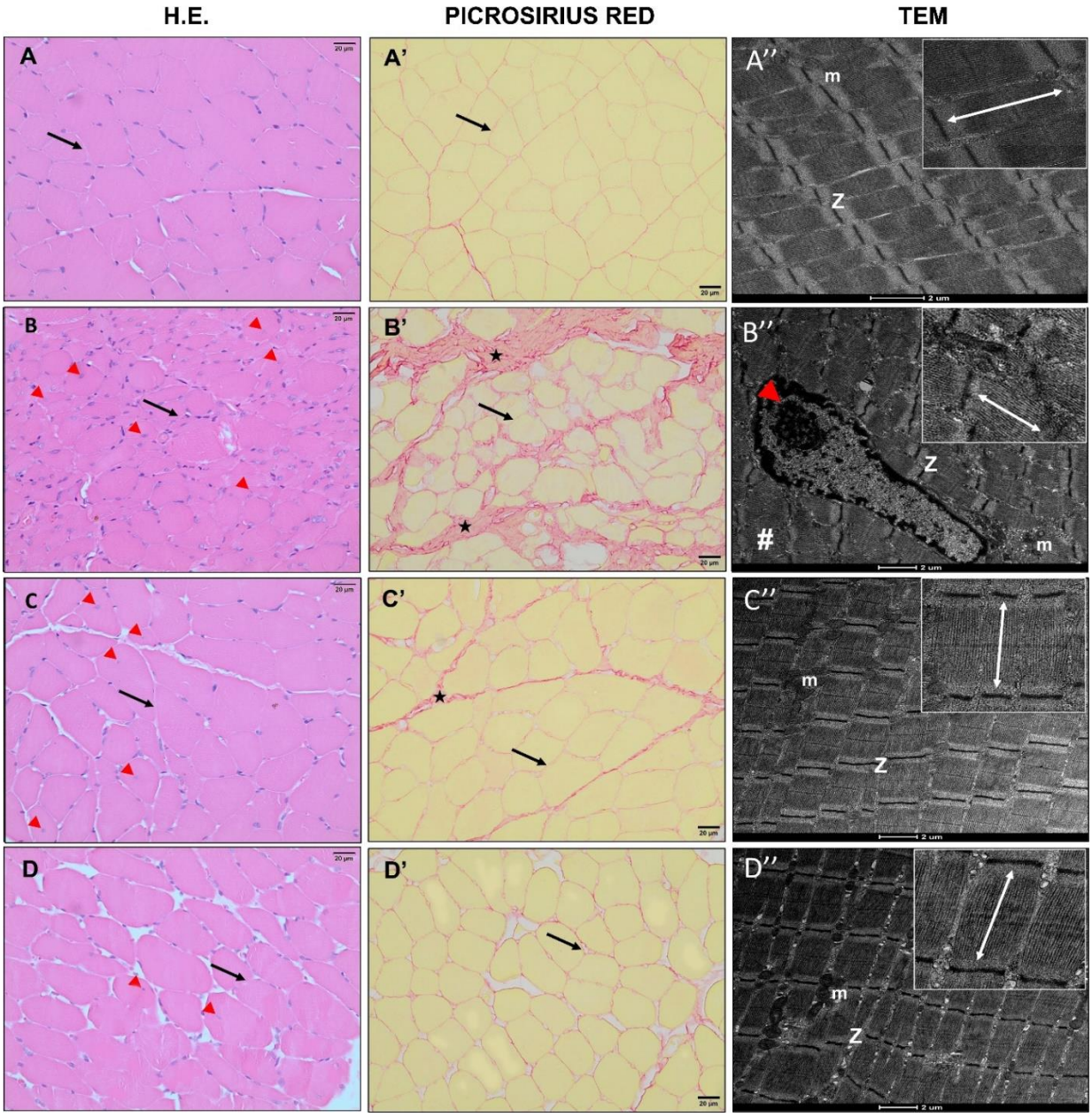

Figure 3. Photomicrographs of cross-sections of cranial tibial muscle sections from the control, denervated, neurorrhaphy and neurorrhaphy + HFB groups at 400x magnification (scale bar 20 µm) stained with hematoxylin and eosin (A-D) and Picrosirius Red (A'-D'). Photomicrograph of the ultrastructure of muscle fibers (A''-D'') in the control, denervated, neurorrhaphy and neurorrhaphy + HFB groups at 4800× magnification. In the upper right corner, the details of the sarcomeres are shown at 11000x. Endomysium (→), Perimysium (*), central nucleus (red arrowhead), Z line (Z), Mitochondria (M), Sarcomeres (←→), Disarray (#) and central nucleus (white star)

According to the morphometric analyses of muscle fibers in the NB group (Figure 4B), the perimeter (Figure 4C), maximum and minimum diameter (Figure 4D and 4E), Feret diameter and minimum Feret (Figure 4G and 4H) values were found to be significantly similar to those in group C and were also greater than those in group

N for all these parameters. Group D presented lower values than did the other experimental groups. In general, for all the mentioned analyses, group C presented the highest values, followed by group NB, with groups N and D being further away in values.

Furthermore, to assess compensatory hypertrophy in the regenerated fibers, a relative frequency analysis (Figure 4J) of the area of all muscle fibers for each experimental group was also performed, in which an approximation of group NB (Figure 4J - blue) to group C (Figure 4J - red) was observed among all area intervals of the fibers. Group N (Figure 4J - green) exhibited an increase in the number of regenerated fibers with smaller areas in the interval from 400 to 2400 μm. The same trend was observed in group D (Figure 8J - brown), with a much larger absolute number of fibers between the low-area intervals between 0 and 1200 μm.

In addition, regarding the number of central nuclei (Figure 4F), the quantification of intramuscular connective tissue (Figure 4I), and the number of central nuclei, group NB was also similar to group C and different from the other groups, presenting values slightly greater than those of group C, while the highest values were observed in group D, followed by group N.

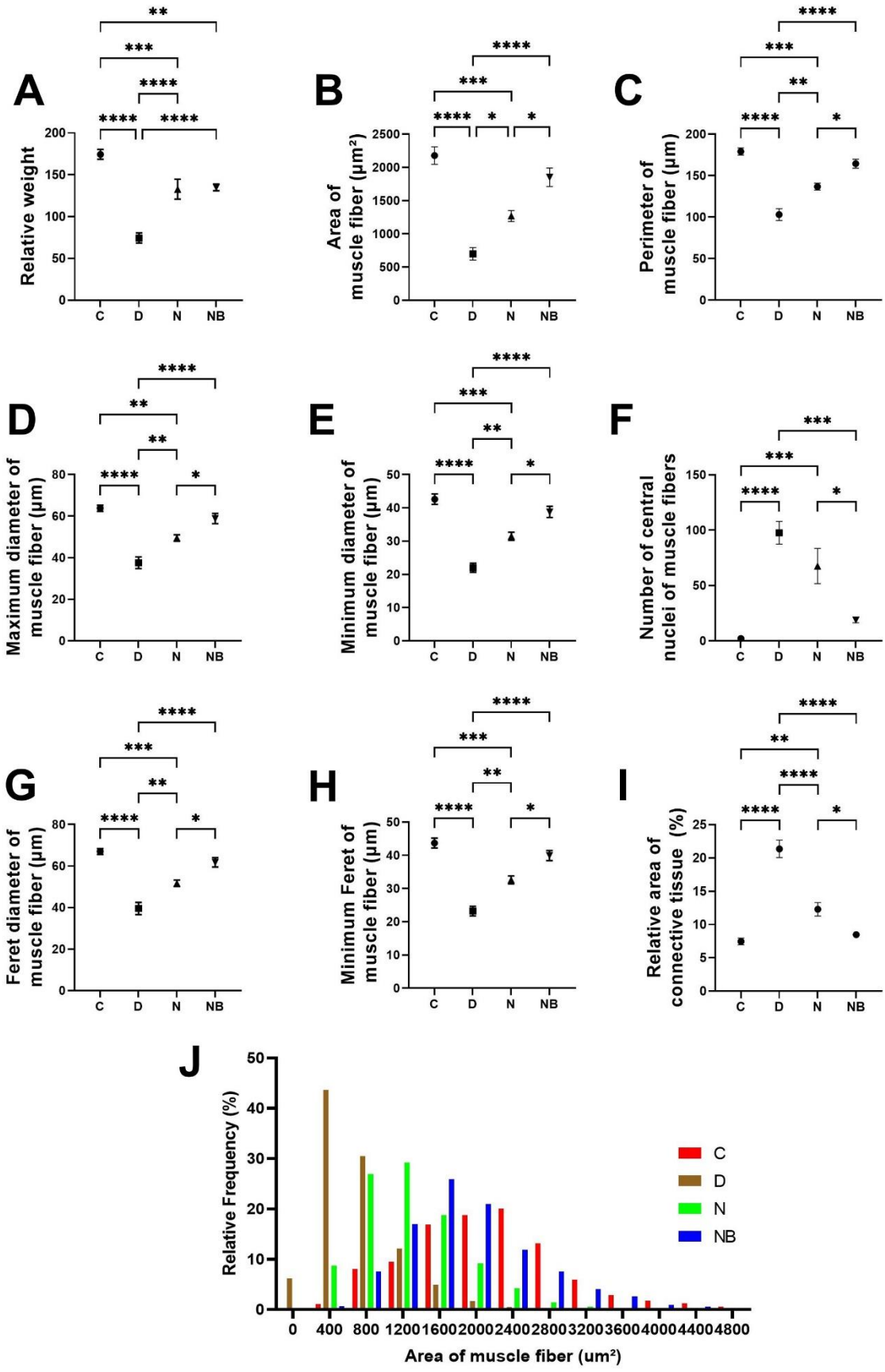
A
Relative weight
B
Area of muscle fiber (μm²)
C
Perimeter of muscle fiber (μm)
D
Maximum diameter of muscle fiber (μm)
E
Minimum diameter of muscle fiber (μm)
F
Number of central nuclei of muscle fibers
G
Feret diameter of muscle fiber (μm)
H
Minimum Feret of muscle fiber (μm)
I
Relative area of connective tissue (%)
C
D
N
NB
J
Relative Frequency (%)
Area of muscle fiber (um²)
0 400 800 1200 1600 2000 2400 2800 3200 3600 4000 4400 4800

Figure 4. Graphs of the relative weight (A), area (B), perimeter (C), maximum and minimum diameter (D and E), number of central nuclei (F), Feret diameter (G), minimum Feret (H), percentage of intramuscular collagen (I) and relative frequency of the area (J) of the muscle fibers of the cranial tibial muscle of all experimental groups (C-Control, red; D- Denervated, brown; N-Neurorrhaphy, green; NB-Neurorrhaphy + HFB, blue). The values are expressed as the average and standard error of the mean and were analyzed by one-way ANOVA followed by the Tukey test. Asterisks indicate statistically significant differences (*p<0.05; **p<0.001; ***p<0.0001; ****p<0.00001).

3.3. HFB enhanced nerve integrity

The morphology of nerve fibers was normal in group C, with intact axons and myelin sheaths (Figure 5A). In groups NB and N, intact nerve fibers of various sizes were observed (Figure 5B and 5C), some of which showed signs of irregularity compared to those in group C.

Regarding the morphometric values, the smallest values of the area and perimeter of the nerve bundles were observed in groups NB and N, both of which were similar to each other and different from those in group C (Figure 5D and 9E). Notably, although they were smaller in size, group NBs, in relation to groups C and N, showed an increase in the number of intact axons in the following order: NB > C > N (Figure 5F).

Concerning the parameters of area (Figure 5G), perimeter (Figure 5H), and axon diameter (Figure 5J), the highest values were found in group C, which was different from those of groups NB and N, which demonstrated similar values. Group C also presented the greatest increase in the thickness of the myelin sheath (Figure 5I), followed by groups N and NB, with group NB exhibiting significantly greater differences than groups C and N. For the G ratio (Figure 5K), although all groups showed values within the standards of normality, the NB group presented the highest values, which were significantly different from those of the N and C groups.

Considering the values found in the NB group against the number of nerve fibers, a frequency analysis was performed for parameters of the axon area (Figure 6A), G ratio (Figure 6B), and myelin sheath thickness (Figure 6C). A large increase in the quantity of small-caliber fibers was observed in the NB and N groups at intervals ranging from 1.5 to 2.5 µm. Additionally, in group NB, several intermediate-sized fibers (2.5 to 4 µm) were observed, which were closer and slightly smaller than those in group C, while group N presented a smaller number of these fibers. Regarding the thickness of the myelin sheath, both groups N and NB demonstrated an increase in the frequency of fibers with a smaller sheath thickness (interval of 0.6 to 1.2 µm) (Figure 6C). Already

in the interval of 1.4 to 2.4 µm (intermediate thickness), group C presented the highest number. These parameters were reflected in the frequency of the G ratio (Figure 6B), where group NB presented the highest values, followed by groups N and C, all within the values of normality (0.4 to 0.7).

Figure 6 D, E, and F show the correlations between the G ratio and axon diameter in the C, N, and NB groups. This analysis clearly revealed that the values of the NB/G ratio were related to the greater number of small nerve fibers, and the NB group was closer to the C group.

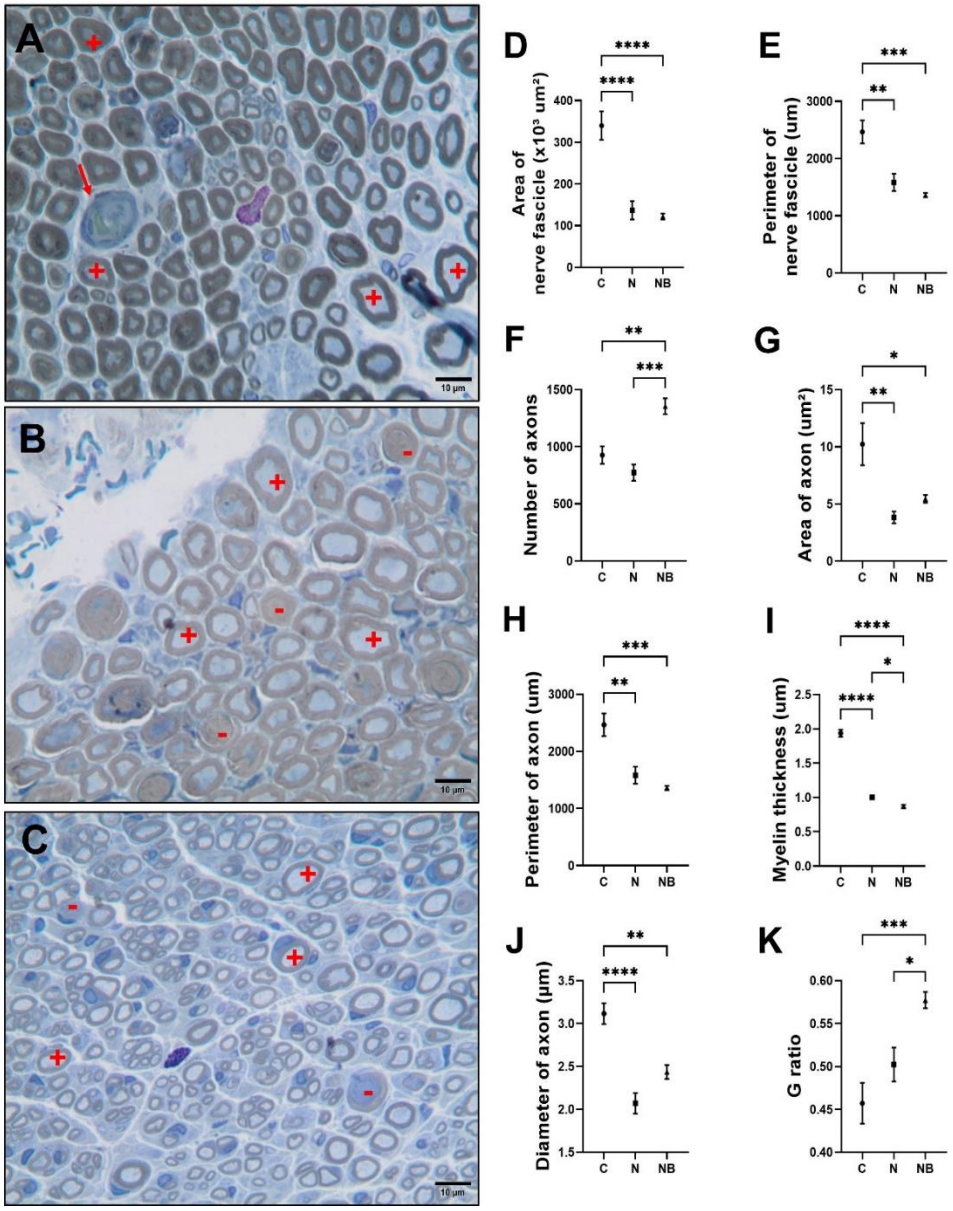

Figure 5. Photomicrographs of cross-sections of fibular nerves from the control (A), neurorrhaphy (B), and neurorrhaphy + HFB (C) experimental groups stained with osmium tetroxide and counterstained with toluidine blue (scale bar 10 µm). Intact nerve fibers (+), irregular nerve fibers (-), and blood vessels

(red arrowhead). Graphs of the area and perimeter of the nerve bundle (D and E), number of intact axons (F), area and perimeter of the axon (G and H), thickness of the myelin sheath (I), diameter of the axon (J) and G ratio (K) of the fibular nerves of the C-Control, N-Neurorrhaphy and NB-Neurorrhaphy + HFB experimental groups. The values are expressed as the average and standard error of the mean and were analyzed by one-way ANOVA followed by the Tukey test. Asterisks indicate statistically significant differences (*p<0.05; **p<0.001; ***p<0.0001; ****p<0.00001).

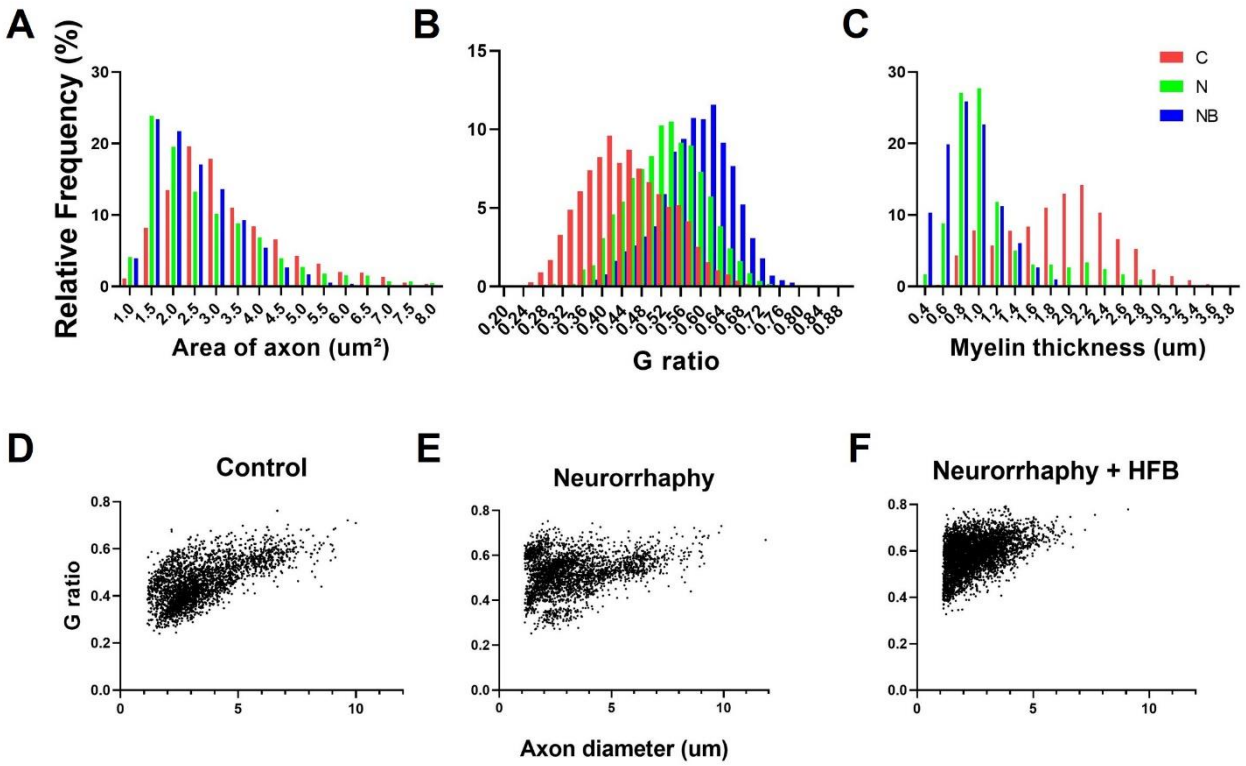

Figure 6. Graphs of the relative frequencies of the axon area (A), myelin sheath thickness (B), and G ratio (C) and the correlations (D, E, and F) between the G ratio and the respective axon diameter for the control experimental groups are shown in red (C), neurorrhaphy in green (N) and neurorrhaphy + HFB in blue (NB). For the analyses of each group, the same number of nerve fibers was used in a standardized manner, although this value changed according to the experimental treatment.

3.4. HFB potentiated nAChR alpha-1 protein expression

Regarding nAChR subunit protein expression, the NB group exhibited an increase in alpha-1 (Figure 7B) expression, which was significantly greater than that of all the other groups. However, no differences were observed in the expression of the epsilon (Figure 7A) or gamma (Figure 7C) subunit. The NB group presented a significant increase in Rapsyn compared to the other groups (Figure 7E). Conversely, the protein expression levels of MusK (Figure 7D), agrin (Figure 7F), and LRP4 (Figure 7G) remained consistent across the groups. All the data were normalized to the GAPDH

values on the same membranes used for protein analysis (Figure 3H and Supplementary Material 1).

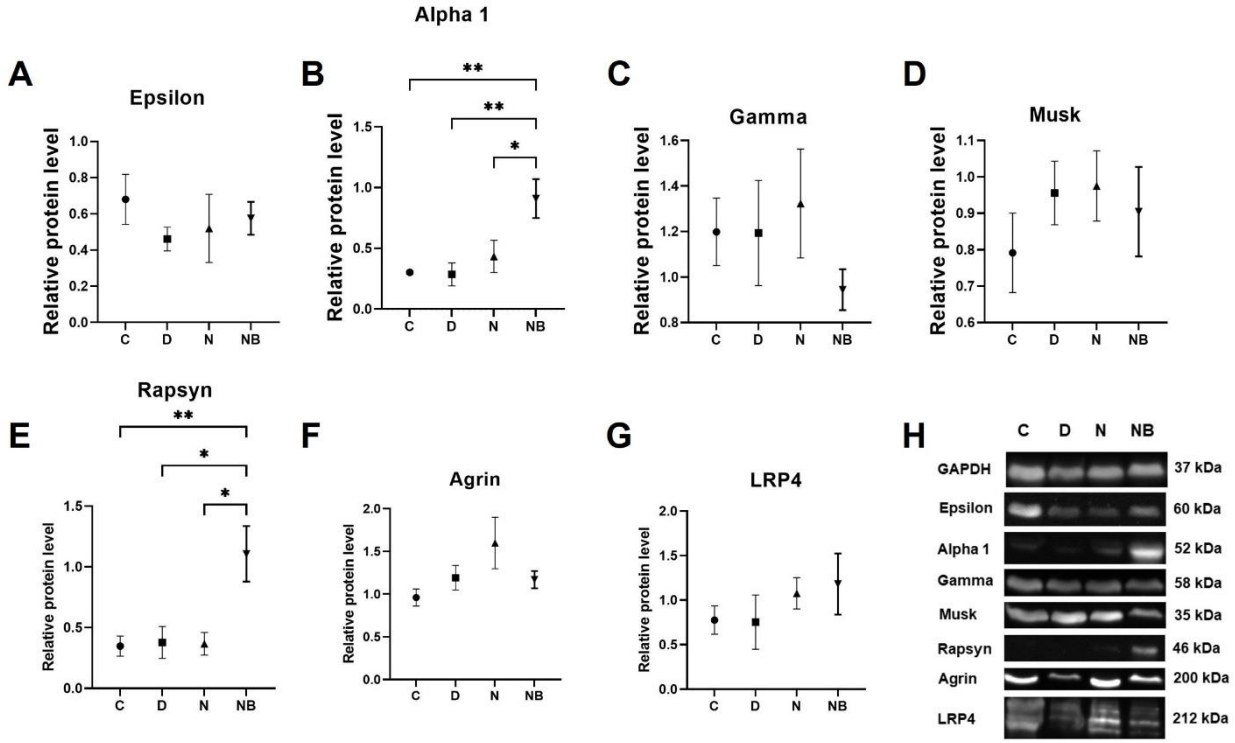

Figure 7. Protein quantification analysis (n = 5) of the epsilon (A), alpha1 (B), and gamma (C) subunits of nAChRs and of the muscokinase (Musk) (D), rapsyn (E), agrin (F), and LRP4 (G) subunits of the agrin/Rapsyn/Musk/LRP4 signaling pathway and labeling of proteins on membranes (H) in all experimental groups (C-Control; D- Denervated; N-Neurorrhaphy; NB-Neurorrhaphy+HFB). Values are expressed as the mean and standard error of the mean (SEM) and were evaluated by analysis of variance (one-way ANOVA) followed by the Tukey test. Asterisks indicate statistically significant differences (*p<0.05; **p<0.001).

4. Discussion

In recent years, our group and other researchers have investigated the regenerative effects of HFB combined with neurorrhaphy for repairing nerve injuries in rats (25). HFB has shown promising results in restoring NMJs and promoting axonal regeneration. Seven to 90 days after reconstruction, studies have demonstrated that HFB, when associated with sutures, enhances nerve impulse restoration (106), attenuates muscle degeneration (107), and improves molecular expression related to NMJ function (44, 77). Additionally, combining HFB with a biomaterial tube further enhances NMJ aggregation and accelerates motor function recovery (77).

Through the results of the analyses carried out here, it was possible to observe a preventive effect resulting from the association of HFB with neurorrhaphy after 120 days of reconstruction, mainly on axonal fibers, muscles, and the associated NMJs. These tissues were positively influenced by the association with HFB, where various morphometric parameters approached those of group C, with evident signs of fibrosis and muscle atrophy reduction and nerve connection and NMJ restoration compared to those of group N.

Here, concerning the morphology and morphometry of the NMJs, it was possible to observe a closer approximation of the “healthy” morphological parameters in the NB group. The larger area values found in the NB group may be related to the difference in circularity and perimeter between the NB group and the N group. Functionally healthy junctions present a continuous and longer pattern in their junctional folds. Conversely, in denervated and remodeling junctions, fragmentation occurs, which breaks its continuity and leads to a decrease in the perimeter. Taken together, these findings indicate a trend toward approximation with a “pretzel” shape (Figure 1 - details). Furthermore, for circularity, although the NB group did not match the C group, it was different from the N and D groups, corroborating the hypothesis that the NMJs of the other groups, which were less circular and more branched, demonstrated more irregular patterns.

Jones and collaborators demonstrated that the variables linked to the size of the NMJs are precise for determining changes, in which the area and general diameter of the NMJ and the degree of synaptic fragmentation, together with the diameter of the presynaptic axon, are critical in defining synaptic morphology (112). It is important to note that the technique used in this study to visualize the NMJs was the “nonspecific esterase” method, which is based on the marking of positive esterase sites, which contain ACh, leading to the general visualization of the NMJ morphology, including the synaptic cleft and the pre- and postsynaptic regions (120).

Regarding the muscle fiber data, the quantitative results related to the area, perimeter, maximum and minimum diameters, and Feret diameter were notable; the results for the NB group were similar to those for the C group but different from those for the N group. This pattern was repeated concerning the percentage of intramuscular collagen and the number of central nuclei. This similarity indicates the prevention of adverse scenarios and the approximation of the normal pattern of fibers, which was

not statistically significant in our studies in which shorter recovery periods were studied (7, 30, 60, and 90 days after injury).

Interestingly, the regeneration of skeletal muscle consists of two main phases that occur simultaneously and competitively, namely, the actual regeneration of the myofiber and the production of connective tissue (121). Given that the excessive production of connective tissue is capable of completely inhibiting muscle regeneration, reducing the infiltration of connective tissue in the initial periods of injury is essential for achieving better regenerative results. Over the years, we have demonstrated that HFB has the potential to reduce the infiltration of muscular connective tissue, being superior to isolated neurorrhaphy at 30 (107) and 90 (106) days, but still different from the control, both for fiber morphometry requirements and for collagen infiltration, until the moment when the scenario balances, at 120 days, and the NB group is similar to the C group and different from the N group.

Central nuclei generally appear in skeletal muscle fibers after damage induced by a variety of injuries; thus, regularly, myonuclei occupy the periphery of myofibrils, but under pathological conditions, the presence of central nuclei is observed (122). Therefore, nuclear positioning is also commonly used as a morphological marker of change; in contrast, central nuclei are also commonly found in regenerating muscle fibers (123). Given that morphometry, collagen infiltration, and the number of central nuclei in the NB group reached those in the control group, these results suggest that the combination of HFB had a significant impact on reducing atrophy and intramuscular collagen infiltration postinjury, preventing fibrosis and allowing effective regeneration and growth of muscle fibers.

For the correct maintenance of the regenerative process, a complex interplay between the Agrin/LRP4/Musk/Rapsyn pathway occurs (25). The Agrin and MusK proteins are crucial for initiating receptor clustering and remodeling and restoring NMJs to their normal form. The activation of LRP4 by agrin is key for regeneration, as it aids in terminal Schwann cell activation postinjury and guides the reinnervation of NMJs in denervated fibers. Further nAChR clustering and formation at the NMJ rely on Rapsyn, which binds to the cluster and recruits other synaptic components to that scaffold. Agrin triggers the phosphorylation of MusK and nAChR, facilitating the clustering and anchoring of nAChR-Rapsyn complexes to the cytoskeleton (23, 124).

As previously demonstrated at other time points (44, 77), the HFB association promoted the return of nAChR morphology and the maturation of nAChR-associated

proteins. The protein expression values for both the NB and N groups, in addition to our morphometric analysis, suggested NMJ regeneration and reinnervation, as both groups were close to the C group. However, at 120 days after injury, we observed an increase in the expression of the Alpha1 subunit and Rapsyn protein.

Following denervation, there is an alteration in nAChR density and distribution beyond synaptic sites, which is regulated, in part, by nAChR subunit profiles (40). Our results for the N- and NB-group nAChR subunits indicated that the regeneration process was complete, with the NB group further demonstrating lower values for the gama (immature subunit for NMJ) protein. However, the increase in the Alpha-1 subunit may indicate that restoration was incomplete, as nAChR activity beyond synaptic sites ceases after full nerve impulse restoration or that HFB promoted more nAChR aggregation (125). Despite not accounting for these clusters here, the overexpression of rapsyn suggested a multifaceted relationship. Rapsyn has been shown to directly influence the quantity of nAChR in the membrane (124), as its expression can attenuate progressive denervation, nAChR fragmentation and neuromuscular dysfunction (126, 127). Notably, Rapsyn is also thought to bind and anchor neurotransmitter receptors to the postsynaptic membrane (128), which may influence alpha-1 expression.

With the increased proximity of the striated skeletal tissue and its associated NMJs, changes in the association of nAChRs and the protein complexes of NMJs are directly associated with the basal lamina and cytoskeletal components of the target striated skeletal muscle and vice versa (76). Myonuclei play a fundamental role in the development and maintenance of NMJs, participating in the rearrangement of the cytoskeleton, protein synthesis and the formation of nAChR clusters (129). These proteins, which are found in the sarcolemma of muscle fibers and are produced in the synaptic nucleus of NMJs (130), directly impair muscle function, including recovery after injury. Although we observed mitigated atrophy and fibrosis in our muscle analysis, attention is drawn to the solely over-expression of Rapsyn.

Our nerve regeneration data revealed a large increase in the number of axons in the NB group. This increase was compatible with other studies that investigated the association of HFB with neurorrhaphy at different reconstruction times, both isolated (107) and associated with photobiomodulation, among others. Seven days after reconstruction, HFB has strong immunogenic potential, recruiting macrophages to the injury site, which accelerates the process of Wallerian degeneration and contributes to

the regenerative process and the beginning of the growth of new endoneurial tubes (107).

It is well described in the literature that after injury, regenerated and regenerating nerve fibers have a smaller axon diameter and myelin sheath thickness than intact nerve fibers (118, 131). Through frequency analysis of the area and thickness, a considerable increase in the number of low-caliber fibers was observed in the treatment groups; however, in the NB group, the number of intermediate-caliber fibers was similar to group C. An increase in the number of nerve fibers with a low to intermediate sheath thickness was also observed in groups N and NB, although neither of the two groups exhibited large caliber fibers, as in group C, a factor that is also rarely found in regenerated fibers after injury.

These values are reflected in the G ratio, which is the proportion between the axonal diameter and the fiber diameter and is widely used as an index of ideal myelination, where values between 0.4 and 0.7 indicate normality, with values of approximately 0.7 indicating degenerative or regenerative processes of the myelin sheath (132). All groups demonstrated values within normality and were already experimentally observed in other works using HFB (77, 108, 115, 116, 118, 133).

Notably, the individual analysis of each nerve fiber indicated that the NB group exhibited a large increase in the number of axons with a proportion of G ratio/axon diameter close to the ideal, with a G ratio ranging from 0.4 to 0.6 and a diameter ranging from 3 to 5 µm (Figure 6F). In contrast, the N group showed an increase in the number of small and hypomyelinated nerve fibers (Figure 6E). This correlation allows us to infer that although the various morphometric parameters of the NB group were significantly inferior to those of the C group, given the large increase in the number of small regenerated fibers, a large proportion of these fibers demonstrated a pattern of normality and possible functional repair, surpassing that of the N group. The positive results in relation to the tibial muscle and the NMJs corroborate the suggestion of this efficiency in regeneration in the NB group.

One limitation of the present study is the use of the nonspecific esterase technique for marking and visualizing NMJs. Other more “specific” techniques, which highlight the presynaptic portion (through VAChT) or the postsynaptic region (nAChRs, with α-bungarotoxin), would have allowed a better visualization and understanding of the possible structure and junctions. Furthermore, the lack of functional analyses, such as the “CatWalk XT” gait test, prevents the direct conclusion that HFB promotes an

improvement in functional recovery after injury, although morphological and morphometric progress is clear. It is also relevant to note that here, we investigated the tibialis cranial muscle, a predominantly glycolytic muscle, while in other studies, the soleus muscle, a predominantly oxidative muscle, was investigated. The biochemical and metabolic profile of each muscle type can lead to changes in responses in a more intimate investigation.

In recent years, the use of HFBs has been experimentally demonstrated to create a stable and protective microenvironment at the reconstruction site, resulting in positive outcomes across various medical applications. HFBs hold promise as excellent scaffolds for drug delivery systems and other adjunct therapies, such as photobiomodulation or stem cell therapy. Their good biocompatibility further enhances the regenerative potential of cell lineages and improves cell survival. Indeed, HFBs have emerged as strong candidates for regenerative medicine, and additional research is needed to assess their effectiveness in other therapeutic contexts. We highlight that it has already been tested and provided good results in a phase I/II nonrandomized, single-arm clinical trial for the treatment of chronic venous ulcers (105).

The potential of HFB seems to be associated with the ability to accelerate the degenerative phase, thus minimizing and preventing its deleterious effects and allowing for better tissue development during regeneration (25). After injury, the electrical impulse is initially altered by tSCs, followed by signaling to increase the synthesis of nAChR subunits in NMJs, accompanied by an increase in the myogenic regulatory factors MyoD and myogenin in the muscle (134). With the failure of electrical signal transmission and, therefore, muscle contraction, subsequent changes in the aggregation of nAChR clusters occur, mainly through changes in the Agrin/Rapsyn/Musk/LRP4 signaling pathway, increasing the fragmentation of the motor plate (40, 135). Long-term denervation leads to a reduction in the number of satellite cells and consequent protein degradation, with high expression of genes linked to the ubiquitin–proteasome pathway, such as atrogin-1, MafbX and MURF1 (136). In this way, faster regeneration provides a less degenerated microenvironment and a better chance of restoring healthy morphology and function.

5. Conclusion

After 120 days of reconstruction, HFB associated with neurorrhaphy prevented muscle fibrosis and atrophy, possibly because of the substantial increase in

regenerated axons in the NB group and its further reinnervation. Our findings highlight the late beneficial effects of HFB in nerve repair and further support its potential to surpass the regeneration effects achieved by neurorrhaphy alone. Indeed, over time, HFB has demonstrated a good ability to maintain a less degenerated neuromuscular junction microenvironment and promote better early regeneration after injury.

6. References

1. Lopes B, Sousa P, Alvites R, Branquinho M, Sousa AC, Mendonça C, et al. Peripheral Nerve Injury Treatments and Advances: One Health Perspective. Int J Mol Sci. 2022;23(2).
2. Hussain G, Wang J, Rasul A, Anwar H, Qasim M, Zafar S, et al. Current Status of Therapeutic Approaches against Peripheral Nerve Injuries: A Detailed Story from Injury to Recovery. Int J Biol Sci. 2020;16(1):116-34.
3. Muller KS, Tibúrcio FC, Ferreira RS, Barraviera B, Matheus SMM. Heterologous fibrin biopolymer as an emerging approach to peripheral nerve repair: a scoping review. J Venom Anim Toxins Incl Trop Dis. 2024;30:e20230060.
4. Rodríguez Cruz PM, Cossins J, Beeson D, Vincent A. The Neuromuscular Junction in Health and Disease: Molecular Mechanisms Governing Synaptic Formation and Homeostasis. Front Mol Neurosci. 2020;13:610964.
5. Chao T, Frump D, Lin M, Caiozzo VJ, Mozaffar T, Steward O, et al. Matrix metalloproteinase 3 deletion preserves denervated motor endplates after traumatic nerve injury. Ann Neurol. 2013;73(2):210-23.
6. Palispis WA, Gupta R. Surgical repair in humans after traumatic nerve injury provides limited functional neural regeneration in adults. Exp Neurol. 2017;290:106-14.
7. Gordon T. Peripheral Nerve Regeneration and Muscle Reinnervation. International Journal of Molecular Sciences. 2020;21(22):8652.
8. Jiang BG, Han N, Rao F, Wang YL, Kou YH, Zhang PX. Advance of Peripheral Nerve Injury Repair and Reconstruction. Chin Med J (Engl). 2017;130(24):2996-8.
9. Sulaiman W, Gordon T. Neurobiology of peripheral nerve injury, regeneration, and functional recovery: from bench top research to bedside application. Ochsner J. 2013;13(1):100-8.
10. Faroni A, Mobasseri SA, Kingham PJ, Reid AJ. Peripheral nerve regeneration: experimental strategies and future perspectives. Adv Drug Deliv Rev. 2015;82-83:160-7.
11. Ferreira RS, de Barros LC, Abbade LPF, Barraviera SRCS, Silvares MRC, de Pontes LG, et al. Heterologous fibrin sealant derived from snake venom: from bench to bedside - an overview. J Venom Anim Toxins Incl Trop Dis. 2017;23:21.
12. Biscola NP, Cartarozzi LP, Ulian-Benitez S, Barbizan R, Castro MV, Spejo AB, et al. Multiple uses of fibrin sealant for nervous system treatment following injury and disease. J Venom Anim Toxins Incl Trop Dis. 2017;23:13.
13. Tibúrcio FC, Muller KS, Leite APS, de Oliveira IRA, Barraviera B, Ferreira RS, et al. Neuroregeneration and immune response after neurorrhaphy are improved with the use of heterologous fibrin biopolymer in addition to suture repair alone. Muscle Nerve. 2023;67(6):522-36.
14. Spejo AB, Chiarotto GB, Ferreira ADF, Gomes DA, Ferreira RS, Barraviera B, et al. Neuroprotection and immunomodulation following intraspinal axotomy of motoneurons by treatment with adult mesenchymal stem cells. J Neuroinflammation. 2018;15(1):230.
15. Kempe PRG, Chiarotto GB, Barraviera B, Ferreira RS, de Oliveira ALR. Neuroprotection and immunomodulation by dimethyl fumarate and a heterologous fibrin biopolymer after ventral root avulsion and reimplantation. J Venom Anim Toxins Incl Trop Dis. 2020;26:e20190093.
16. Pinto CG, Leite APS, Sartori AA, Tibúrcio FC, Barraviera B, Junior RSF, et al. Heterologous fibrin biopolymer a single suture stitch enables the return of neuromuscular junction to its mature pattern after peripheral nerve injury. Injury. 2021;52(4):731-7.
17. Rodríguez-Sánchez DN, Pinto GBA, Cartarozzi LP, de Oliveira ALR, Bovolato ALC, de Carvalho M, et al. 3D-printed nerve guidance conduits multifunctionalized with canine multipotent mesenchymal stromal cells promote neuroregeneration after sciatic nerve injury in rats. Stem Cell Res Ther. 2021;12(1):303.

18. Bueno CRS, Tonin MCC, Buchaim DV, Barraviera B, Ferreira Junior RS, Santos PSDS, et al. Morphofunctional Improvement of the Facial Nerve and Muscles with Repair Using Heterologous Fibrin Biopolymer and Photobiomodulation. Pharmaceuticals (Basel). 2023;16(5).
19. Scorisa JM, Zanon RG, Freria CM, de Oliveira AL. Glatiramer acetate positively influences spinal motoneuron survival and synaptic plasticity after ventral root avulsion. Neurosci Lett. 2009;451(1):34-9.
20. Leite APS, Pinto CG, Tibúrcio FC, Sartori AA, de Castro Rodrigues A, Barraviera B, et al. Heterologous fibrin sealant potentiates axonal regeneration after peripheral nerve injury with reduction in the number of suture points. Injury. 2019;50(4):834-47.
21. Leite APS, Pinto CG, Tibúrcio FC, Muller KS, Padovani CR, Barraviera B, et al. Acetylcholine receptors of the neuromuscular junctions present normal distribution after peripheral nerve injury and repair through nerve guidance associated with fibrin biopolymer. Injury. 2023;54(2):345-61.
22. Kempe PRG, de Castro MV, Khuriyeh VC, Barraviera B, Ferreira RS, de Oliveira ALR. Ultrastructural Evidence of Synapse Preservation and Axonal Regeneration Following Spinal Root Repair with Fibrin Biopolymer and Therapy with Dimethyl Fumarate. Polymers (Basel). 2023;15(15).
23. Schneider CA, Rasband WS, Eliceiri KW. NIH Image to ImageJ: 25 years of image analysis. Nat Methods. 2012;9(7):671-5.
24. LEHRER GM, ORNSTEIN L. A diazo coupling method for the electron microscopic localization of cholinesterase. J Biophys Biochem Cytol. 1959;6:399-406.
25. Zaimi A, Wabartha M, Herman V, Antonsanti PL, Perone CS, Cohen-Adad J. AxonDeepSeg: automatic axon and myelin segmentation from microscopy data using convolutional neural networks. Sci Rep. 2018;8(1):3816.
26. Muller KS, Tibúrcio FC, de Barros JWF, Matsumura CY, Matheus SMM. Statin exposure during pregnancy promotes neuromuscular junction alterations in postpartum Wistar rats. Muscle Nerve. 2023;67(6):537-47.
27. Jones RA, Reich CD, Dissanayake KN, Kristmundsdottir F, Findlater GS, Ribchester RR, et al. NMJ-morph reveals principal components of synaptic morphology influencing structure-function relationships at the neuromuscular junction. Open Biol. 2016;6(12).
28. Lehto M, Järvinen M, Nelimarkka O. Scar formation after skeletal muscle injury. A histological and autoradiographical study in rats. Arch Orthop Trauma Surg (1978). 1986;104(6):366-70.
29. Folker ES, Baylies MK. Nuclear positioning in muscle development and disease. Front Physiol. 2013;4:363.
30. Ogawa Y, Yamamoto M, Sato M, Odaka K, Kasahara M, Hinata N, et al. Localization of T-cell factor 4 positive fibroblasts and CD206-positive macrophages during skeletal muscle regeneration in mice. Ann Anat. 2021;235:151694.
31. Martínez-Martínez P, Losen M, Duimel H, Frederik P, Spaans F, Molenaar P, et al. Overexpression of rapsyn in rat muscle increases acetylcholine receptor levels in chronic experimental autoimmune myasthenia gravis. Am J Pathol. 2007;170(2):644-57.
32. Ma J, Shen J, Garrett JP, Lee CA, Li Z, Elsaidi GA, et al. Gene expression of myogenic regulatory factors, nicotinic acetylcholine receptor subunits, and GAP-43 in skeletal muscle following denervation in a rat model. J Orthop Res. 2007;25(11):1498-505.
33. Moresi V, Williams AH, Meadows E, Flynn JM, Potthoff MJ, McAnally J, et al. Myogenin and class II HDACs control neurogenic muscle atrophy by inducing E3 ubiquitin ligases. Cell. 2010;143(1):35-45.
34. Gao N, Zhao K, Cao Y, Ren X, Jing H, Xing G, et al. A Role of Lamin A/C in Preventing Neuromuscular Junction Decline in Mice. J Neurosci. 2020;40(38):7203-15.
35. Liao X, Wang Y, Lai X, Wang S. The role of Rapsyn in neuromuscular junction and congenital myasthenic syndrome. Biomol Biomed. 2023;23(5):772-84.
36. Xing G, Xiong WC, Mei L. Rapsyn as a signaling and scaffolding molecule in neuromuscular junction formation and maintenance. Neurosci Lett. 2020;731:135013.
37. Moimas S, Novati F, Ronchi G, Zacchigna S, Fregnan F, Zentilin L, et al. Effect of vascular endothelial growth factor gene therapy on posttraumatic peripheral nerve regeneration and denervation-related muscle atrophy. Gene Ther. 2013;20(10):1014-21.
38. Yang X, Xue P, Chen H, Yuan M, Kang Y, Duscher D, et al. Denervation drives skeletal muscle atrophy and induces mitochondrial dysfunction, mitophagy and apoptosis via miR-142a-5p/MFN1 axis. Theranostics. 2020;10(3):1415-32.
39. Ge MH, Tian H, Mao L, Li DY, Lin JQ, Hu HS, et al. Zinc attenuates ferroptosis and promotes functional recovery in contusion spinal cord injury by activating Nrf2/GPX4 defense pathway. CNS Neurosci Ther. 2021;27(9):1023-40.
40. Schmalbruch H. Fiber composition of the rat sciatic nerve. Anat Rec. 1986;215(1):71-81.

41. Mendonça AC, Barbieri CH, Mazzer N. Directly applied low intensity direct electric current enhances peripheral nerve regeneration in rats. J Neurosci Methods. 2003;129(2):183-90.
42. Buchaim RL, Andreo JC, Barraviera B, Ferreira Junior RS, Buchaim DV, Rosa Junior GM, et al. Effect of low-level laser therapy (LLLT) on peripheral nerve regeneration using fibrin glue derived from snake venom. Injury. 2015;46(4):655-60.
43. Rosso MPO, Rosa Júnior GM, Buchaim DV, German IJS, Pomini KT, de Souza RG, et al. Stimulation of morphofunctional repair of the facial nerve with photobiomodulation, using the end-to-side technique or a new heterologous fibrin sealant. J Photochem Photobiol B. 2017;175:20-8.
44. Abbade LPF, Barraviera SRCS, Silvares MRC, Lima ABBC, Haddad GR, Gatti MAN, et al. Treatment of Chronic Venous Ulcers With Heterologous Fibrin Sealant: A Phase I/II Clinical Trial. Front Immunol. 2021;12:627541.
45. Furey MJ, Midha R, Xu QG, Belkas J, Gordon T. Prolonged target deprivation reduces the capacity of injured motoneurons to regenerate. Neurosurgery. 2007;60(4):723-32; discussion 32-3.
46. Tu H, Zhang D, Corrick RM, Muelleman RL, Wadman MC, Li YL. Morphological Regeneration and Functional Recovery of Neuromuscular Junctions after Tourniquet-Induced Injuries in Mouse Hindlimb. Front Physiol. 2017;8:207.
47. Wiberg R, Jonsson S, Novikova LN, Kingham PJ. Investigation of the Expression of Myogenic Transcription Factors, microRNAs and Muscle-Specific E3 Ubiquitin Ligases in the Medial Gastrocnemius and Soleus Muscles following Peripheral Nerve Injury. PLoS One. 2015;10(12):e0142699.

Capítulo 3

Artigo a ser submetido para a revista: **Polymers,** IF 4.9 (2023)

Motor neuron preservation is improved after experimental nerve repair associated with heterologous fibrin biopolymer

Kevin Silva Muller[1,2]; Felipe Cantore Tibúrcio[1,2]; Rui Seabra Ferreira Junior[3,4]; Benedito Barraviera[2,3,4]; Selma Maria Michelin Matheus[1,2]; José de Anchieta de Castro e Horta Júnior[1,2*]

[1]Department of Structural and Functional Biology, São Paulo State University (Unesp), Institute of Biosciences, Botucatu, SP, Brazil.
[2]Medical School, São Paulo State University (Unesp), Botucatu, SP, Brazil.
[3]Center for the Study of Venoms and Venomous Animals (Cevap), Sao Paulo State University (Unesp), Botucatu, SP, Brazil.
[4]Center for Translational Sciences and Biopharmaceuticals Development, Botucatu, SP, Brazil.

***Corresponding author:** José de Anchieta de Castro e Horta Júnior, PhD, Division of Anatomy, Department of Structural and Functional Biology, Institute of Biosciences, São Paulo State University (Unesp). Rua Professor Doutor Antonio Celso Wagner Zanin, 250, Unesp Campus de Botucatu, Botucatu, SP, Brazil. Zip code: 18618689. Telephone: +55 (14) 3880-0029. Email: anchieta.e@unesp.br

Abstract

Nerve injuries present significant challenges due to their frequent occurrence and substantial impact on quality of life. Although neurorrhaphy is a well-established treatment method, achieving meaningful morphofunctional recovery remains a challenge, as the first major challenge is to maintain the viability of injured neurons and then to address axon elongation and insufficient reinnervation. The Brazilian biopharmaceutical heterologous fibrin biopolymer (HFB), which is free of human components, shows potential as an adjunct when combined with neurorrhaphy for muscle nerve regeneration and for the treatment of spinal cord injuries. However, its late regenerative effects on nerves and the spinal cord after nerve injury remain unexplored. Therefore, we investigated the effects of neurorrhaphy combined with HFB 120 days after repairing the right sciatic nerve on the soma and axons of injured motor

neurons and the associated glia. For this purpose, thirty-six adult male Wistar rats (CEUA-FMB 1402/2021) were divided into four groups (n=9/group): Control (C), where the sciatic nerve was visualized; Denervated (D), where neurotmesis was performed; Neurorrhaphy (N) and Neurorrhaphy+HFB (NB), where after neurotmesis, the stumps were reconnected by neurorrhaphy (2 points); and in the NB group, where HFB was added. At 105 days postinjury, the neurotracer Fluorogold (FG) was applied to the right cranial tibial muscle for retrograde labeling of motor neurons in the anterior column of the lumbar portion (L2-L5) of the spinal cord. At 120 days, transcardiac perfusion was performed to obtain the spinal cord, sciatic nerve, and cranial tibial muscle. Immunofluorescence was performed for visualization of NF200 and S100 in the sciatic nerve, IBA-1+ cells and FG-labeled neurons and their 3D reconstruction (Neurolucida) in the spinal cord. Motor neuron and neuromuscular junctions (NMJs) were processed for visualization by transmission electron microscopy. Ultrastructurally, the NB and N neurons showed signs of preserving their organelles. Reinnervation and flow of FG from the muscle to the spinal cord were observed in the C, N, and NB groups, where the NB group had more labeled neurons than did the N group. NB motor neuron dispersion was lower and closer to that of the C group, although for both treated groups, FG+ neurons were disorganized through the anterior horn. NB further improved microglial cell counts and reconstructed sciatic nerve topography with myelination closer to C while maintaining the waving axonal structural pattern. Regarding NMJs, NB synaptic gutters were more occupied and closer to C than N. These findings highlight the beneficial effects of HFB on the preservation, maintenance, and further axonal regeneration of motor neurons, surpassing the regenerative outcome achieved by neurorrhaphy alone.

Keywords: neurorrhaphy; degeneration; regenerative medicine.

1. Introduction

Nerve injuries are common, with a high prevalence and global incidence, affecting approximately 18 individuals per 100,000 people each year (2) and surpassing the incidence of ovarian and stomach cancers (3). Many individuals affected by nerve injuries, both severe and moderate, have incomplete recovery, resulting in transient or permanent loss of motor and sensory functions, in addition to chronic pain, muscle atrophy and weakness. Approximately half of all nerve injuries show incomplete recovery with poor functional restoration.

After complete transection of the nerve, or neurotmesis, all structures of the neuromuscular apparatus are impaired, from muscle fibers to the cell body of the motor neuron in the spinal cord. The nerve is segmented into two stumps, distal and proximal to the site of the lesion, which are subject to relatively distinct processes (54). The proximal stump remains connected to the cell body in the marrow and adopts a regenerative profile, while the target organ and the distal stump are deprived of their source of electrical stimulus and undergo degenerative changes, namely, Wallerian degeneration, followed by a regeneration process after reinnervation.

In the proximal stump, neurotmesis evokes a retrograde response in neuronal cell bodies (10), with structural changes and alterations in their gene expression profile resulting in a regenerative function instead of synaptic/transmission (52). The surviving neurons undergo a series of physiological and morphological changes called chromatolysis (1, 67), while further retrograde synaptic changes known as synaptic stripping occur, a process by which resident glia selectively remove synapses from injured neurons (69). This stimulus quickly recruits astrocytes and microglia near the affected synaptic terminals that, in their regenerative mode, react through conformational and structural changes in their cytoplasmic projections communicating with the membrane of the injured motor neuron and the degenerated synaptic terminals (71).

One important challenge for reinnervation is the mismatched pairing of regenerating axons, which can connect with other nerve bundles, directing them to other muscles or other tissues (72). These errors alter the original connectivity of motor neurons, leading to motor functional deficiencies. Surprisingly, although the axons regenerate, studies have shown that the morphological recovery of the nerve and muscle is not sufficient to promote functional recovery, as there may still be impairment of synaptic functionality (74, 75).

Given the difficulties associated with regeneration, adjuvant therapies have been studied. One such promising candidate is the heterologous fibrin biopolymer (HFB) (25). This biopharmaceutical innovation, which is biodegradable, bioabsorbable, and nontoxic, is a unique blend of a thrombin-like enzyme extracted from rattlesnake venom and fibrinogen sourced from buffalo blood; thus, this sealant is not entirely dependent on human blood. Furthermore, it exhibits excellent adhesive qualities and is currently employed in a wide range of surgical procedures, including in clinical trials

(91, 102, 105). Compared to sutures alone, HFB provides a more conducive environment for regeneration and offers several advantages over other commercially available fibrin sealants (25).

Several studies have previously demonstrated positive outcomes for the association of HFB with nerve tissue repair, but its effects on motor neurons and the spinal cord parenchyma after peripheral nerve injury remain unexplored. Although in a relatively different scenario, after ventral root avulsion, the association with HFB improved axon regeneration, glial response and motor function (25). Thus, we hypothesize that this association, after a long regenerative approach, will enhance motor neuron survival while also attenuating the glial response, thus promoting a better scenario for a positive outcome regarding motor function and regeneration.

2. Methods

a. Animal care

This study utilized thirty-six adults male Wistar rats sourced from the Central Animal Facility at Unesp, Botucatu Campus. These rats were between 90 and 95 days old and had an average body weight of 300 g. During the entire experimental phase, the rats were housed in Rodent Animal Facility 5 of the Experimental Research Unit (Unipex) of the Faculty of Medicine of Botucatu (FMB/Unesp). The animals were kept in polyethylene boxes (dimensions 40 × 30 × 15 cm) with solid bottoms covered with sawdust substrate under regulated light (12 h light/12 h dark) and temperature (24 ± 2°C) conditions and were provided with filtered water and Presence® feed *ad libitum*. The rats were randomly assigned to four experimental groups: the control (C), denervated (D), neurorrhaphy (N) and neurorrhaphy + BHF (NB) groups. All procedures mentioned were sanctioned by the local ethics committee and registered under the number CEUA-FMB:1402/2021.

b. Surgeries

The animals were anesthetized via intraperitoneal injection of an anesthetic mixture comprising ketamine (Dopalen, 70 mg/kg) and xylazine (Anasedan, 30 mg/kg). Following the shaving of the right pelvic limb, the animals were placed in a prone position, with their front and rear legs spread apart. Lidocaine (7 mg/kg) was administered at the site of the incision, followed by antisepsis using iodized alcohol.

An incision was then made on the lateral aspect of the thigh, extending from the level of the greater trochanter to the knee, exposing the right sciatic nerves.

In the animals in group C, only the sciatic nerve was identified and visualized, after which the soft tissues and skin were repositioned and stitched (Mononylon 7-0 and 5-0, Polysuture) (Figure 1). In the animals in groups D, N, and NB, a nerve lesion was created by transecting the sciatic nerve (neurotmesis) in a standardized manner, approximately 3 mm above its trifurcation. In the animals in group D, to prevent spontaneous regeneration, a 6 mm segment of the nerve was excised, and the proximal and distal stumps were rotated 180° and anchored to the adjacent muscle tissue using simple stitches with nylon thread (Mononylon 10-0, Polysuture) (Figure 1). In groups N and NB, the nerve stumps were reconnected immediately after neurotmesis. In group N, the stumps were rejoined by end-to-end neurorrhaphy (epineural anastomosis) with 2 simple stitches using nylon thread (Mononylon 10-0, Polysuture) (Figure 1). In group NB, nerve reconstruction was carried out by neurorrhaphy with 2 simple stitches, followed by the application of 250 µL of BHF (13) (Figure 1), supplied by CEVAP, Unesp Botucatu, SP, Brazil, the components and application formula of which are detailed in its patents (Registration numbers: BR1020140114327 and BR1020140114360) (11). At the time of use, the components were thawed and reconstituted. The application was made through the simultaneous placement of fraction 1 (125 µL) with fraction 2 (125 µL) - prepared immediately before the application, through the homogenization of equal amounts of fibrinogen and diluent factor - at the site of the injury.

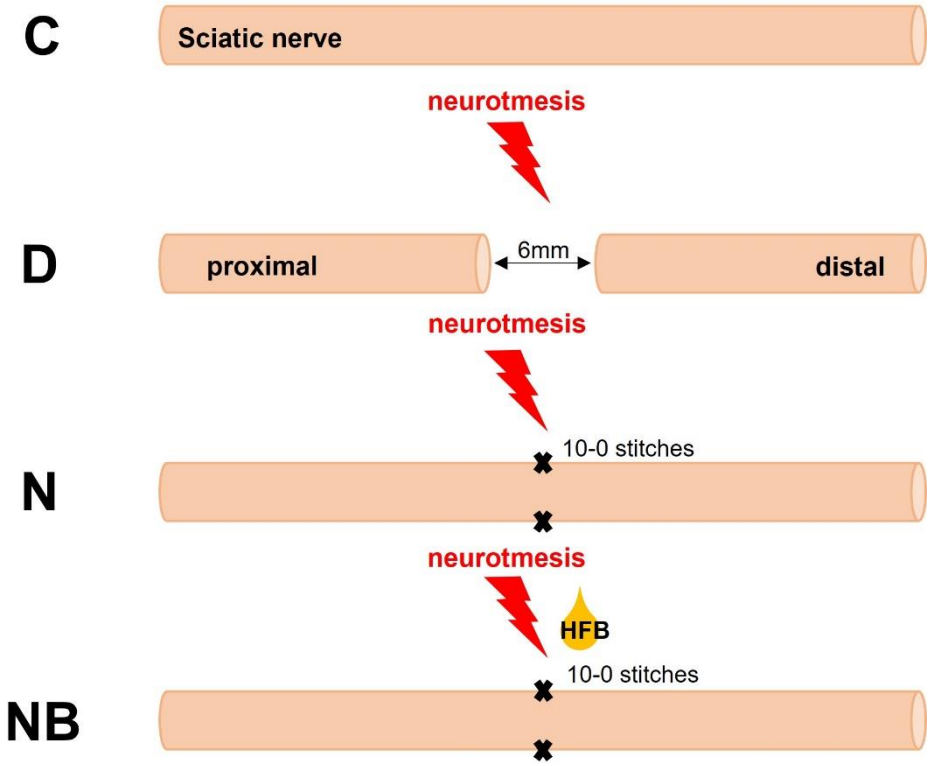

Figure 1. Surgical procedures performed in the control (C), denervated (D), neurorrhaphy (N), and neurorrhaphy + HFB (NB) groups.

Following nerve reconstruction, the soft tissues and skin were stitched using simple stitches with nylon thread (Mononylon 7-0 and 5-0, Polysuture), and the animals were monitored and kept warm until they recovered. Tramadol (5 mg/kg) was then administered for pain relief, and enrofloxacin (Baytril®, 10 mg/kg) was given via subcutaneous injection to prevent opportunistic infections. For three consecutive days, the postoperative protocol included the administration of the analgesic every 24 hours for 3 days and, if necessary, for up to 5 days, in addition to the application of Iodopovidone during the healing period at the incision site.

At 105 days after surgery, six animals from each group were again anesthetized through intraperitoneal injection of an anesthetic solution of ketamine (Dopalen, 70 mg/kg) and xylazine (Anasedan, 30 mg/kg). After the anesthetic, the animals were positioned in dorsal recumbency, and the right pelvic limb was shaved. Injections of the neurotracer FluoroGold (FG) at 4% in 0.9% NaCl were performed in a standardized manner at 3 points along the belly of the right cranial tibial muscle. At each point, 2 µL of the neurotracer was injected slowly over 5 minutes, with 6 mm of needle penetration from the skin. The first point was made 4 mm from the anterior portion of the animals'

tibial crest and 26 mm from the calcaneus. The following points were made 5 mm above and below the first point. After the injection, the needle was kept in position for 5 minutes to prevent tracer reflux and was slowly removed.

At 120 days after surgery (15 days after FG injection), the animals were anesthetized via intraperitoneal injection of an anesthetic solution of ketamine (Dopalen, 70 mg/kg) and xylazine (Anasedan, 30 mg/kg). For the collection of the spinal cord and the right sciatic nerve, transcardiac perfusion was performed on the 6 animals from each group in which the neurotracer injection was performed. The perfusion protocol consisted of the initial passage of 0.9% saline solution with heparin (30 ml/minute) for approximately 1 min until the vascular bed was emptied, as indicated by the whitening of the liver, followed by the passage of a 4% formaldehyde fixing solution freshly prepared from paraformaldehyde and sodium phosphate buffer (PBS) (0.1 M, pH 7.4) for 30 min (30 ml/minute). At least 30 minutes after the procedure was completed, the spinal cords and sciatic nerves were collected and stored in 4% formaldehyde for one day. The next day, the meninges and nerve roots were removed, and the spinal cords were removed and stored in a 30% sucrose solution made in 0.1 M PBS, pH 7.4.

c. Immunohistochemistry for FG and IBA-1 (n=5)

For each animal, the lumbar intumescence of the spinal cord was longitudinally sectioned into 40 µm thick slices using a sliding microtome (Leica SM2010R) equipped with a freezing stage (BFS-30MP, Physiotemp, Inc.). The sections were collected sequentially in a series of 4 vials filled with antifreeze solution so that the interval between consecutive sections in each vial was 160 µm. The series of sections were stored at -20°C until processing.

Histological sections from 1 vial were washed in 0.1 M PBS (pH 7.4), after which endogenous peroxidase activity in a solution of 3% hydrogen peroxide in PBS decreased. Subsequently, the sections were washed in PBS and 0.05 M Tris buffer supplemented with 0.25% Triton X-100 in saline, pH 7.6 (TBS-TX), and incubated in a 2% goat serum solution to block nonspecific labeling. After this, the primary antibodies were incubated in TBS-TX for 48 h at 4°C, and the sections were kept under constant agitation according to the following protocols: anti-FluoroGold (made in rabbit, #AB138870, Abcam, 1/10,000) and anti-IBA1 (made in rabbit, WAKO, 1/5,000). After incubation, the sections were washed in TBS-TX (0.05 M, pH 7.6) and incubated with

a biotinylated secondary antibody, namely, an anti-rabbit IgG (#BA-1000, Vector Laboratories, 1/200) produced in goat, for 2 hours at room temperature. Then, the sections were washed in TBS-TX, incubated in avidin-biotin peroxidase complex (Vectastain ABC Kit, PK-4000, 1/200), and diluted in TBS-TX for 1.5 hour at room temperature. Then, the sections were washed in 0.05 M Tris-HCl buffer (pH 8.0). Finally, the peroxidase bound to the ABC complex was detected by a hydrogen peroxide reaction using 3,3'-diaminobenzidine-tetrahydrochloride intensified with nickel ammonium sulfate (DAB-Ni) as a chromogen. After the immunohistochemistry process, the sections were transferred to a 0.4% gelatin solution in 0.05 M Tris-HCl buffer and mounted on slides. For fluorogold analysis, all FG+ neurons from 1 vial for each experimental case were counted.

d. 3D reconstruction (n=1)

For 3D reconstruction, the spinal cord of one animal from each group was longitudinally sectioned into 40 µm thick slices and immediately mounted on a slide with a 0.1% gelatin solution. Then, all the sections were photographed with fluorescence microscopy (Zeiss Scope. A1), and the images were reconstructed into a single panel for each section.

Subsequently, three-dimensional reconstruction was carried out with Neurolucida software (version 10, MBF Bioscience, MicroBrightfield, Inc.). The reconstructions of each cut of the spinal cord delimited the entire lumbar intumescence. The steps for creating the 3D models included calibrating the program, inserting information about the evaluation interval and the number of sections used in the reconstruction, defining the contours that limit the cytoarchitectonic reference structures, and individually aligning each new section with respect to its immediate predecessor. In each section, the external contour of the spinal cord, the columns of gray matter of the spinal cord, and the retrogradely labeled neurons were delineated. The cytoarchitectonic organization of the regions of interest was illustrated on boards with images of the three-dimensional models. Furthermore, the 3D reconstructed spinal cord was used to assess the spinal cord area for IBA-1+ cell analysis.

e. Microglia optic densitometry (n=5)

The optic densitometry protocol was used to analyze the microglia. An optical microscope (Axioplan2, Carl Zeiss) equipped with a digital camera (AxioCam HRc, Zeiss) was used to determine the optimal lighting conditions, and a 20X objective lens was used to capture all images. The light beam was centered on the CCD of the digital camera, and the illumination intensity was fixed by observing the RGB brightness histogram of the image to distribute it along the dynamic range of the digital camera. All field illumination parameters, diaphragm openings, filter sets, and camera exposure times were manually controlled to avoid variations in these parameters during the capture session. All images were captured in the same session, and 11 reference images were initially acquired for optical density calibration, representing densities between 0.04 and 1.0, using a stepped neutral density filter (Edmund Industrial Optics, #32-599). Next, for each animal, approximately 2500 µm (8 images) of each anterior spinal cord session (3~4) was captured according to the 3D reconstructed FG-labeled neurons.

Then, those images were combined in a mosaic to create panoramic images of the entire lumbar intumescence. In ImageJ, to exclude empty spaces generated by variations in section width from our analysis, an ROI frame (1900 × 600 microns) was adopted and used to perform comparative quantification of the optical density of the tissue sections among the various experimental groups, reflecting the amount of IBA-1+ cell immunoreactivity. For the analysis of each set of images captured in the same session, optical density calibration was initially performed using reference images captured from a filter of optic density. Furthermore, a standardized ⅓ of the same ROI and images were used for IBA-1+ cell counting across groups.

To ensure uniformity in IBA-1+ immunolabeling, all sections from the experimental cases were processed simultaneously using solutions with identical compositions, and immunohistochemical parameters such as antibody concentration, staining duration, and development time were kept consistent across all sections to achieve uniform staining intensity.

f. Transmission electron microscopy (n=3)

The lumbar portion of the spinal cord was collected and reduced. Subsequently, the spinal segments were reduced to a 2 mm segment. The right side, referring to the nerve lesion, was highlighted, and 2 segments from the anterior column region were stored for processing and ultrastructural analysis by transmission electron microscopy

at the Electron Microscopy Center of the Institute of Biosciences of Botucatu. Furthermore, for one animal from each group, the remainder of the lumbar portion immediately above the reduced portion was sectioned transversely for visualization of the motor neurons through Nissl staining.

Due to the variation in the cutting plane height for viewing the cellular ultrastructure of α-motoneurons, an inclusion criterion was established in which only neurons with large cell bodies in the nuclear plane in the presence of a condensed and evident nucleolus were photographed and analyzed.

Furthermore, neuromuscular junctions were also assessed. For that, portions of the cranial tibial muscle were sectioned into longitudinal sections, processed following the routine of the Electron Microscopy Center of the Institute of Biosciences (CME/IBB/UNESP) and photodocumented using a transmission electron microscope (TECNAI Spirit, Fei).

g. Immunofluorescence for NF-200 and S100 (n=5)

Fragments of the sciatic nerve related to the reconstruction area were collected and subsequently stored in 4% paraformaldehyde for 24 hours, cryoprotected in 10%, 20% and 30% sucrose (diluted in 0.1 M PBS) for 24 hours each, embedded in freezing medium (Tissue Plus® O.C.T. Compound, Fisher Healthcare), frozen in N-hexane cooled in liquid nitrogen and stored in a biofreezer at -80°C for later sectioning, mounting on slides and performing immunostaining.

Then, the slides were thawed at room temperature for 1 hour, washed in PBS, and incubated in blocking solution (3% BSA (w/v) in PBS for 1 hour, followed by incubation with a primary antibody (NF200, rabbit; #N5389, Sigma, 1/1,000; S-100, rabbit; #ab4066, Abcam; 1/1,000, diluted in PBS, 1% BSA (w/v), 0.2% Triton-X (v/v)) for 18 hours in a dark humid box at 4°C. The next day, the slides were again washed in PB buffer and incubated for 1 hour in secondary antibody (IgG Mouse Alexa Fluor 488, made in rabbit; #ab15007, Abcam; 1/1,000, diluted in PBS, 1% BSA (w/v); 0.2% Triton-X (v/v)). Then, they were again washed in PBS and mounted with coverslips and mounting medium (VectaShield).

The slides were photographed by a Leica TCS SP5 confocal microscope, 2 fields per animal were randomly chosen, and the images were analyzed using ImageJ software (version 1.45 s, National Institute of Health, USA). To exclude empty spaces

generated by variations in section width from our analysis, a frame (500 × 500 microns) covering only the sample areas was used. The average fluorescence intensity values were obtained through the quantification of the fluorescent area for each animal through the threshold tool.

h. Statistical analysis

All data related to morphological and morphometric quantifications and statistical analyses were analyzed blindly by the principal researcher. The results of all quantitative variables were compared between groups, and before any analysis, the normal distribution and homoscedasticity of the data were verified through the Shapiro–Wilk test or appropriate normality test. Comparisons between the groups with an adherence to the normal distribution of probabilities were carried out using the parametric analysis of variance (ANOVA) technique for the model with one factor, complemented with the Tukey multiple comparisons test, or by the nonparametric procedure (Kruskal–Wallis) complemented by the Dunn test in the absence of an adherence to the normal distribution. All data were. The data were analyzed with GraphPad Prism 9 software using a 5% significance level ($p \leq 0.05$), and all graphs were made using the same software.

3. Results

a. Motor neuron ultrastructure analysis (n=3)

In group C, organelles (mitochondria, Golgi complex, lysosomes, Nissl bodies) were uniformly distributed and within healthy standards (Figure 2A). In group D, the motor neurons exhibited morphological changes indicative of neurodegeneration and cell death, such as disorganization and increased mitochondrial electrolucency, chromatolysis and invasion by astrocytes. Furthermore, these motor neurons had interruptions in the cell membrane and were close to astrocytes and microglia, suggesting invasion and phagocytosis of cellular debris (Figure 2B). In the motor neurons of groups N and NB, signs of preservation of a large part of their organelles, such as the Golgi apparatus, mitochondria and Nissl bodies, were observed, although some signs indicative of injury and proximity to glial cells were also observed (Figure 2C and 2D).

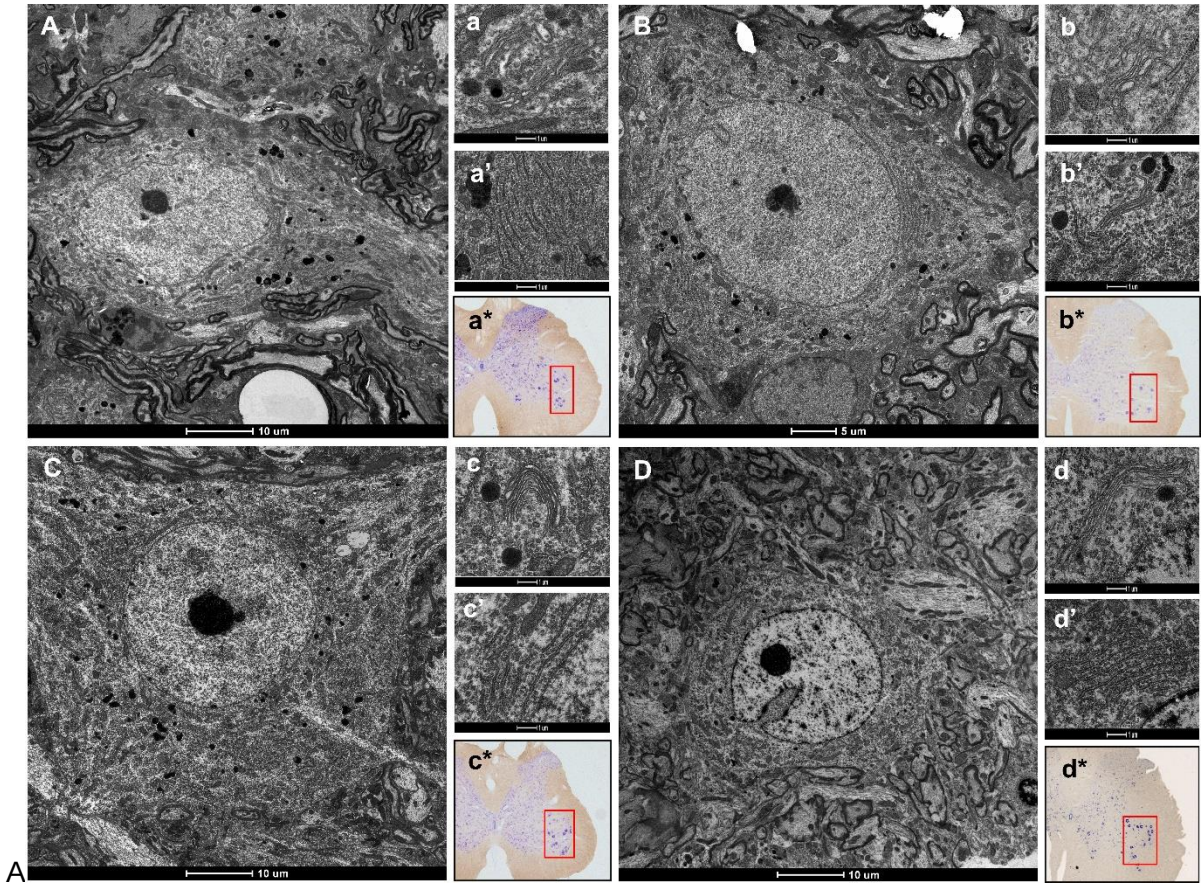

Figure 2. Photomicrograph of the ultrastructure of motor neurons from the anterior column of the control (A), denervated (B), neurorrhaphy (C) and neurorrhaphy + BHF (D) groups viewed by transmission electron microscopy at a magnification of 3200×. The first image shows a general overview of the motor neuron, while the subsequent images highlight the Golgi complex (a-d) and Nissl bodies (a'-d').

b. Quantification of FG-labeled neurons (n=5)

The presence of retrogradely labeled neurons was observed in the animals in groups C, N, and NB (Figure 3A, 3C, and 3D), and there was no labeling in the animals in group D (Figure 3B).

In terms of the number of retrogradely labeled neurons, the greatest number of neurons was observed in group C, followed by groups NB, N, and D (Figure 3E). Groups NB and N showed no statistical differences to group C but NB had more neurons than group N. Group D was significantly different from all the other groups.

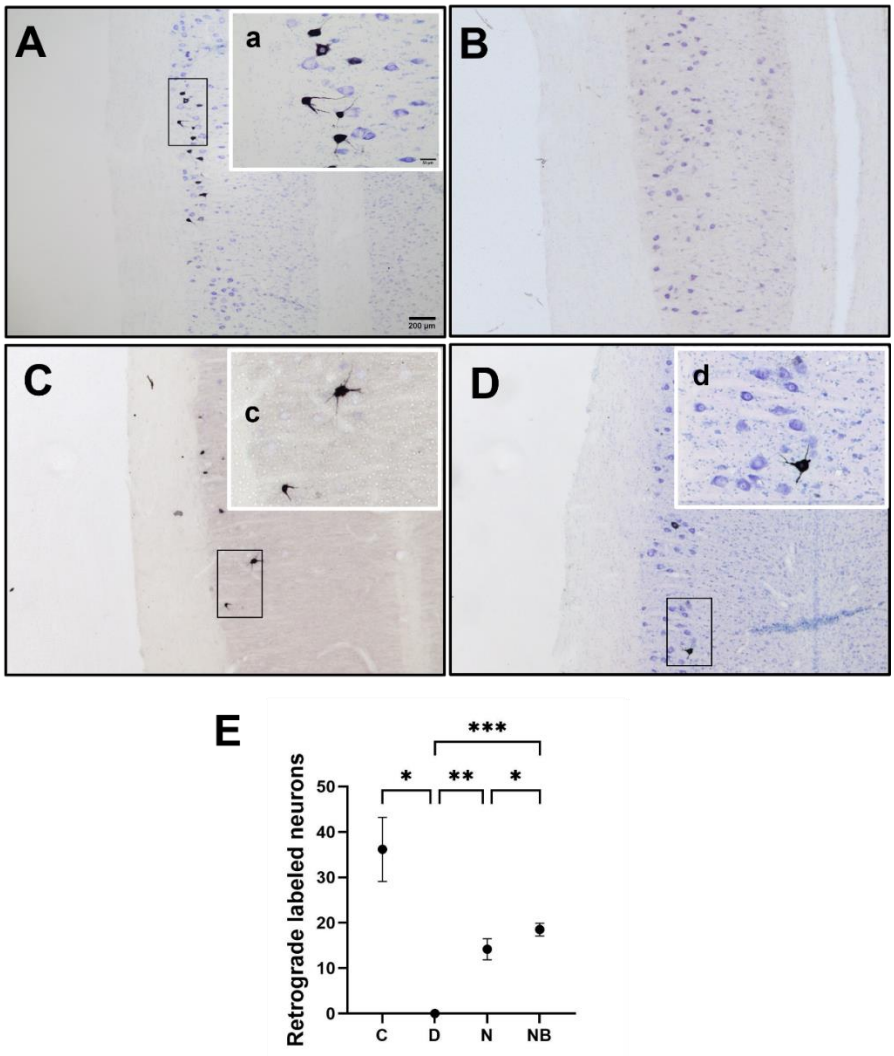

Figure 3. Representative photomicrographs of the retrograde labeling of motor neurons by fluorogold and anti-fluoro-gold immunoreactivity assays for the control group (A), denervated group (B), neurorrhaphy group (C) and neurorrhaphy + BHF group (D). In detail, the neurons can be seen in greater enlargement. Graph of the number of motor neurons retrogradely labeled by fluorogold injection (E) in the cranial tibial muscle of all the experimental groups: C (control), D (denervated), N (neurorrhaphy) and NB (neurorrhaphy + HFB). The values are expressed as the mean and standard error of the mean and were analyzed by ANOVA followed by the Tukey test. Asterisks indicate statistically significant differences (*p<0.05; **p<0.001; ***p<0.0001).

c. Qualitative motor neuron dispersion data from 3D reconstruction (n=1)

FG-labeled neurons were identified along the anterior column of the spinal cord in the C, N, and NB groups, and this pool was subsequently 3D reconstructed (Figure 4).

The neuron pool in the C group spanned a length of 5465 µm, compared to 5530 µm in the N group and 5000 µm in the NB group. The average global distance between

neurons was 1336.6 µm in the C group, 1624.8 µm in the N group, and 2039.6 µm in the NB group. The average distance between neighboring neurons was 81.3 µm in the C group, 481.6 µm in the N group, and 166.3 µm in the NB group. The closest and farthest distances between neurons in the C group were 33.6 µm and 346 µm, respectively, compared to 98.6 µm and 2283.4 µm in the N group and 57.5 µm and 336.4 µm in the NB group. Regarding the depth of the neuron pool across the ventral dorsal section, the neurons of the C group were labeled across 600 µm (480 to 1080), the neurons of the N group were labeled across 320 µm (840 to 1160), and the neurons of the NB group were labeled across 400 µm (760 to 1160).

Taken together, these data suggest that neurons from the treated groups were more dispersed through the anterior column in both length and depth than were those from the C group, with the neurons in the NB group being less spread, with more neurons closer to each other than to those in the N group.

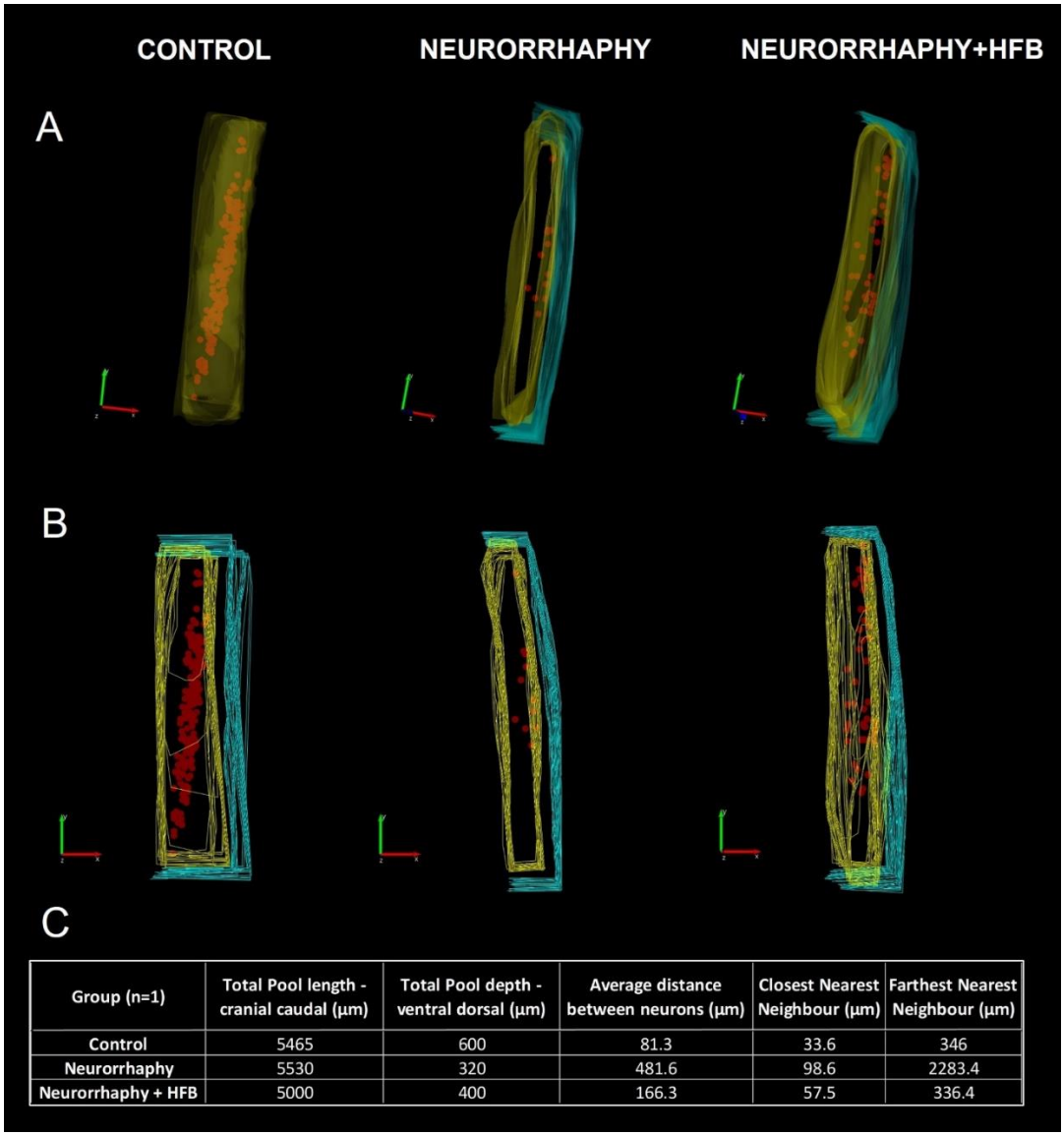

Group (n=1)	Total Pool length - cranial caudal (µm)	Total Pool depth - ventral dorsal (µm)	Average distance between neurons (µm)	Closest Nearest Neighbour (µm)	Farthest Nearest Neighbour (µm)
Control	5465	600	81.3	33.6	346
Neurorrhaphy	5530	320	481.6	98.6	2283.4
Neurorrhaphy + HFB	5000	400	166.3	57.5	336.4

Figure 4. 3D reconstruction of the anterior column of the spinal cord and retrograde labeled motor neurons after FG injection into the tibialis cranial muscle for one animal in the control group (A), Neurorrhaphy (B) and Neurorrhaphy + HFB (C).

d. Microglial reactivity response (N=5)

Microglia were assessed through IBA-1 (Ionized calcium binding adaptor molecule – a microglia/macrophage calcium-binding marker). In the control group (Fig. 5A), the optic density of IBA-1+ cells were greater than that in the other experimental groups (Fig. 5E). Furthermore, NB (Figure 5C) and N (Figure 5D) demonstrated similar values and both were greater, but equal, to D (Figure 5B). In terms of the number of IBA-1+ cells, the NB and C groups had greater numbers of cells, which were similar to each

other, while the N group was lower and differed among all the groups. D showed the lowest values among the groups and differed from all the other groups.

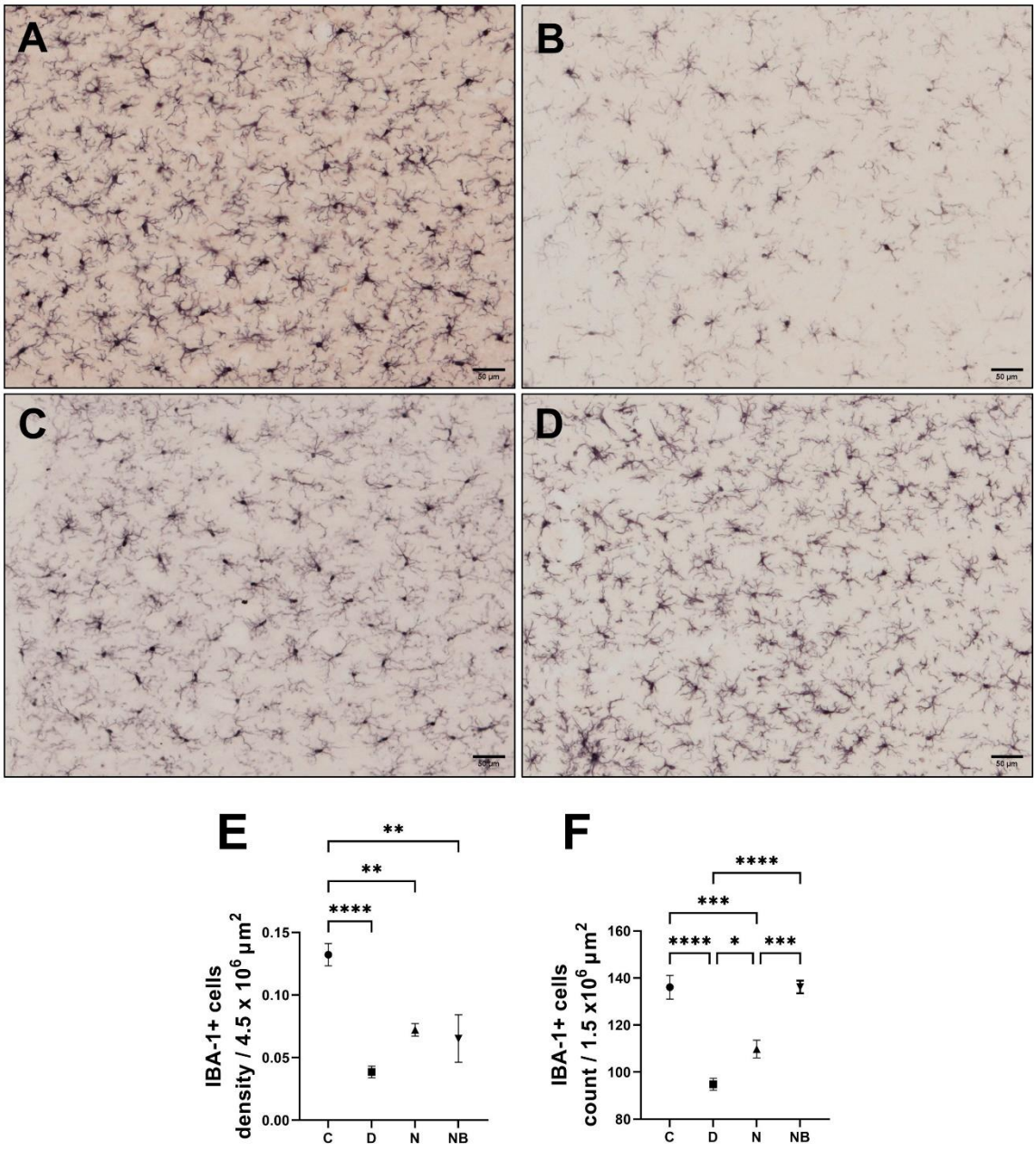

Figure 5. Representative photomicrographs of microglia labeled with anti-IBA1 antibody for all experimental groups and graphs of the optic densitometry analysis of IBA-1+ cells (E) and IBA-1+ cells count (F) from the control group (A), denervated group (B), neurorrhaphy group (C) and neurorrhaphy + HFB group (D). The values are expressed as the mean and standard error of the mean and were analyzed by ANOVA followed by the Tukey test. Asterisks indicate statistically significant differences (*p<0.05; **p<0.001; ***p<0.0001; ****p<0.00001).

e. Sciatic nerve integrity (n=5)

For NF-200 quantification, which analyzes the organization of the intermediary filaments that comprise the axons of regenerated nerves, in both the N and NB groups, the axons established a wave pattern of arrangement to the nerve axis (Figure 6A-D), which is compatible with healthy standards, although the NB group demonstrated a more continuous pattern, similar to that of the C group. Regarding the quantitative analysis, the NB group was equal to the N and C groups, while only the C and NB groups differed from the D group (Figure 6E).

For the quantification of S-100, which is a characteristic marker of Schwann cells, C, N and NB demonstrated intense labeling with wave patterns (Figure 6A'-D'). The mean intensity area quantification revealed similarity between the NB and C groups, while N differed from C and was solely equal to D. Furthermore, the N group differed from C (Figure 6E').

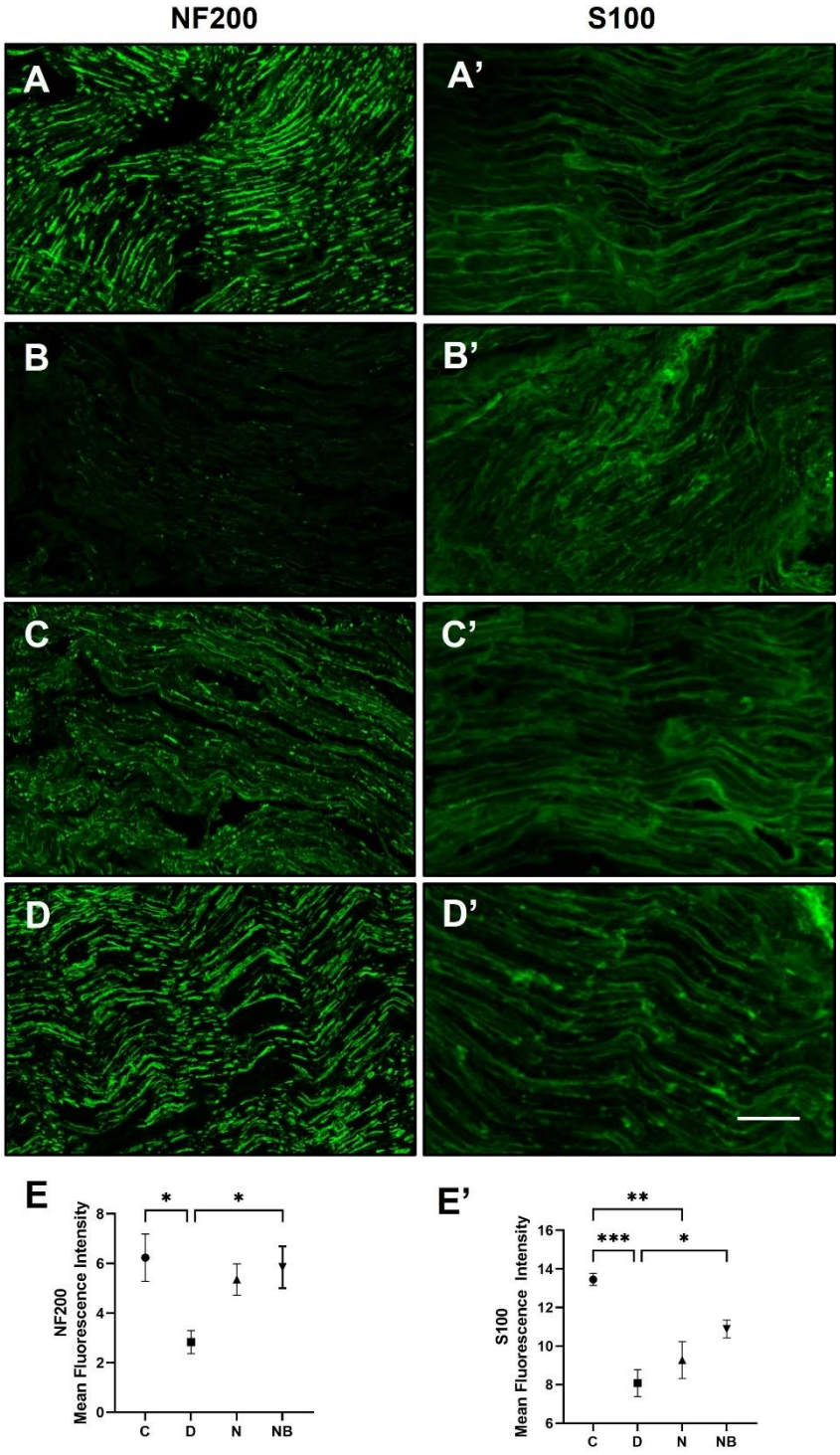

Figure 6. Immunolabeling of anti-neurofilament (A-D) and anti-S100 (A'-D') for the control group (A), denervated group (B), neurorrhaphy group (C) and neurorrhaphy + HFB group (D) and graphs of the mean fluorescence intensity area (E and E') of all experimental groups: C (control), D (denervated), N (neurorrhaphy) and NB (neurorrhaphy + HFB). The values are expressed as the mean and standard error of the mean and were analyzed by ANOVA followed by the Tukey test. Asterisks indicate statistically significant differences (*p<0.05; **p<0.001; ***p<0.0001). Scale bar = 20 μm

f. Neuromuscular Junctions ultrastructure (n=3)

Ultrastructurally in group C (Figure 7A), several synaptic buttons were observed, arranged in synaptic gutters with varied shapes and depths. In the synaptic buttons, synaptic vesicles, mitochondria, and multivesicular bodies were present. Characteristically, the presynaptic membrane had denser regions that correspond to the active zones, opposed to the apex of the junctional folds of the postsynaptic membrane. The postsynaptic membrane was intact and contained numerous and long junctional folds, with a denser apex corresponding to the location of acetylcholine receptors.

In group D (Figure 7B), the degeneration of the presynaptic region was notable, with the absence of synaptic buttons and gutters. In the postsynaptic region, junctional folds were noticed, disorganized and with their apex presenting reduced electron density.

In group N (Figure 7C), some synaptic buttons presented variable morphology, but the majority of the ultrastructurally observed synaptic gutters were unoccupied. The junctional folds were organized and with a very dense apex (nAChR concentration).

In group NB (Figure 7D), most of the synaptic gutters were occupied with synaptic buttons containing synaptic vesicles, mitochondria, and other characteristic organelles. The presence of the active zone was detected opposed to the apex of the junctional folds of high electron density (nAChR concentration).

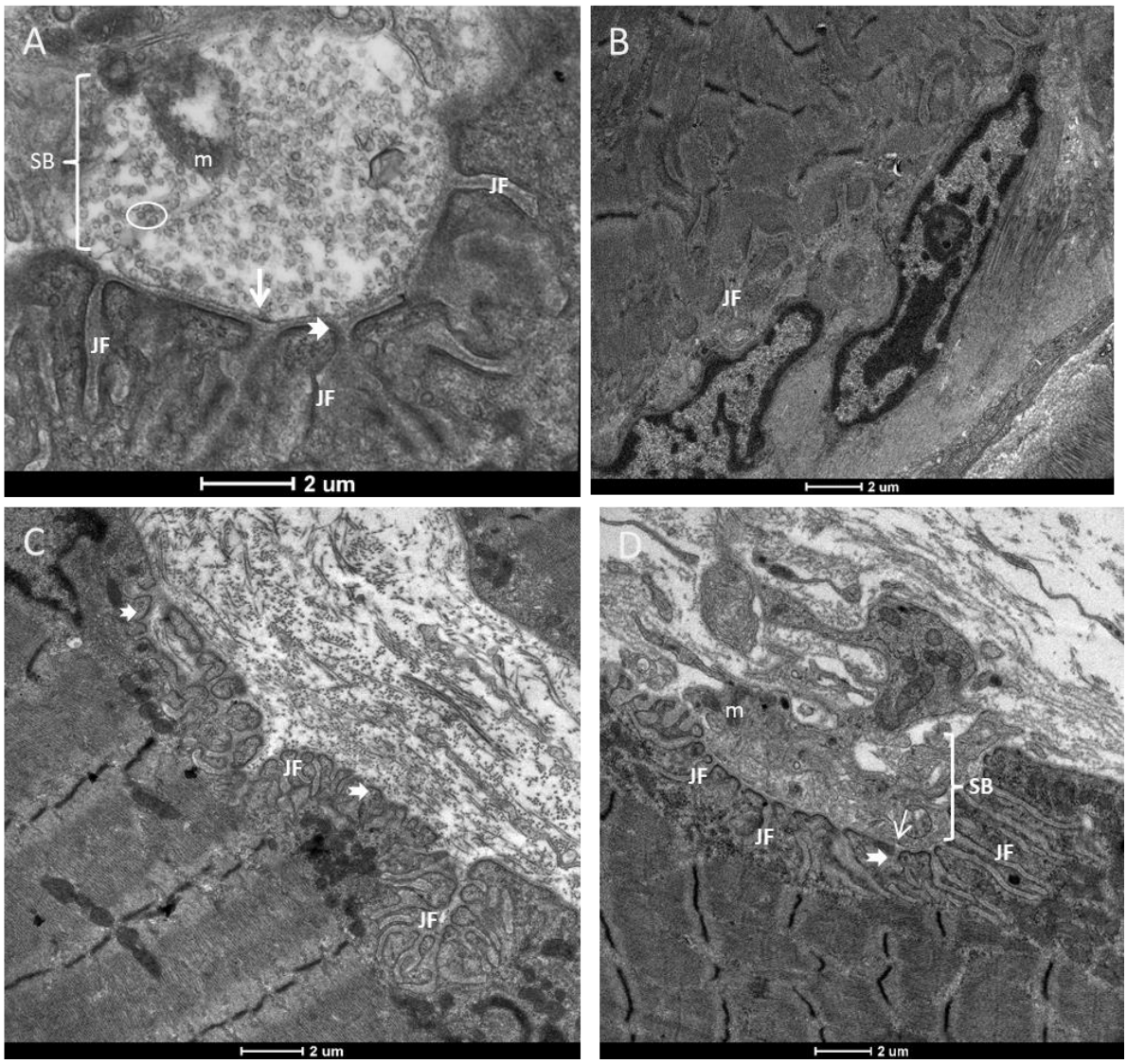

Figure 7. Photomicrograph of the ultrastructure of neuromuscular junctions from the tibial cranialis muscle of the control (A), denervated (B), neurorrhaphy (C) and neurorrhaphy + BHF (D) groups viewed by transmission electron microscopy at a magnification of 6400x. SB: synaptic button; JF: junctional fold; m: mitochondria; white ball: synaptic vesicles containing ACh; narrow white arrow: presynaptic membrane; thick white arrow: postsynaptic membrane.

4. Discussion

The peripheral nerves inherently have the ability to heal after an injury. Sealants based on fibrin have been instrumental in both regenerative medicine and surgical procedures, particularly for nerve damage. Nevertheless, the window for recovery is narrow before degeneration of tissue hinders the processes of regeneration and reconnection. Given the expensive nature and the requirement of human blood for the production of commercial sealants, HFB has emerged as a cost-effective substitute.

When used alongside neurorrhaphy, HFB has been observed to amplify regenerative outcomes and outperform other sealants available on the market in various respects.

Here, we evaluated the potential of HFB combined with neurorrhaphy to improve the spinal cord response to neurotmesis in a rat model. We demonstrated that this association is beneficial for the injured motor neuron, enhancing its survival in opposition to neurorrhaphy alone and its further dispersion and reinnervation through the anterior horn, although both treated groups had greater dispersion than C. This may have influenced sciatic nerve topography, improving axon elongation and myelination, as, although not statistically significant for all parameters, both trends of proximity between NB and C and between D and N were observed.

The connections between neurons and their compartments in the nervous system play a crucial role in regulating neuronal characteristics. These connections affect aspects such as dendritic and axonal morphology, the electrical properties of membranes, the production of neurotransmitters, interactions with other parenchyma cells and molecular metabolism (137). After nerve transection, the success of proximal stump regeneration is dictated by the arrangement of an appropriate substrate of extracellular matrix components and trophic factors at the injury site (1), in addition to motor neuron survival. This process involves a series of molecular events that influence the final outcome, and the development of a stable and pro-regenerative framework in the early stages is favorable for good morphological recovery (66). Indeed, HFB plays a crucial role in the healing/repair process, as the combination of fibrin and other coagulation factors with proteins increases angiogenesis, wound stabilization, collagen synthesis, and regeneration of the cell type characteristic of the tissue (102). Furthermore, with a focus on nerve reconstruction, it is possible to reduce trauma (number of points) in the reconstruction, minimizing damage and inflammatory responses (25).

We observed good reinnervation and flow of FG from the muscle to the spinal cord in groups C, N, and NB, with the exception of group D, as expected. Although lower than that in the C group, the number of labeled motor neurons in the NB group was greater than that in the N group, suggesting that there was greater neuronal reinnervation or survival in the cranial tibial muscle. In unspecific neuron pool counting, increased neuronal survival has also been previously reported in several studies of ventral root avulsion in association with HFB (114, 115, 138-141).

Our qualitative analysis of the ultrastructures of the neurons corroborated our hypothesis of good reinnervation and survival of motor neurons. Although signs of injury were identified in groups N and NB, the approximation of the morphological parameters of these cellular organelles in relation to group C is clear. In contrast, group D showed clear signs of degeneration and neuronal death.

Another major problem in neuron survival is further growth and reinnervation of the target muscles. Although performed in only one animal, the 3D reconstruction of the dispersion of neurons in the anterior column may indicate disorganization in relation to the control group, which maintains a certain compaction of its motor neuron pool. In the treated groups, where reinnervation occurred, the neuron pool underwent a decompaction and greater dispersion along the anterior column, since the nerve was disconnected and reconnected, so that there may have been a reinnervation by neurons that previously did not innervate the cranial tibial muscle. This implies a reorganization of the descending pathways and motor coordination since a surviving neuron begins to connect another motor unit, requiring a mechanism of plasticity and new motor learning. In this way, although there has been a repair with greater survival of neurons, there is still a disorganization and decompaction of the previously innervated motor units and consequently the activation of these muscles by the descending pathways. Indeed, maintaining a better survival rate of motor neurons in addiction to motor plasticity and rehabilitation may be advantageous for achieving a better outcome, but target reinnervation is still a significant challenge to address and surpass for gold-standard rehabilitation.

Another significant challenge in achieving proper function after injury is managing gliosis and its harmful effects (14). Glial cells directly impact neuronal survival, synapse stability and functionality by retracting synaptic boutons (14, 18), while they further secrete neuroprotective factors that promote the survival of damaged neurons and guide axonal growth toward the periphery (115). Several studies in a ventral root avulsion model have reported the potential of HFB for attenuation of the glial response in the early periods after injury (115, 142), but its prolonged effects in a late regenerative scenario remain to be clarified.

At first glance, in our nerve injury model, after 120 days, we surprisingly observed a superior microglial cell density in the C group, while all the microglial cell density in the injured groups was equal and greater. Although a higher IBA-1+ cell density may suggest increased microgliosis, it is known that microglia and neurons

maintain an intimate relationship, which is more likely to be a response directly associated with neuron survival (13, 14, 32), as an injured spinal cord parenchyma with fewer neurons maintains fewer associated glial cells. Furthermore, in rats, microgliosis tends to increase and peak 3 to 15 days after injury, slowly decreases up to the first month and then stabilizes (143). Four months after injury, this response may have ceased, and the role of microglia may have shifted to sustain neuronal function rather than the injury response. Furthermore, in our microglial cell counts, we observed an increase in the NB group compared to the N group, which may be directly associated with the greater number of surviving neurons, which was previously demonstrated in a specific manner with the tibialis cranial motor neuron pool. Notably, the C group demonstrated greater IBA-1+ cell density with equal cell numbers, which can be associated with more glial cell extensions and cellular interactions, probably resulting in a more stable association between neurons and glia (144).

In the early periods after injury, diminishing astrogliosis and the microglial response also play a role in maintaining synapse stability and function, which can be associated with improvements in motor and sensory recovery (139). We did not perform any analysis regarding synaptic preservation, but as a takeaway from the literature, by reducing the glial reaction, the neuronal circuitry can be protected and improved, and a reduction in gliosis can be related to a better preservation of glutamatergic and GABAergic synapses (14, 68, 71, 115, 145). This interaction has been previously reported for ventral root avulsion repair with HFB (118, 138) but is associated with increased neuron survival, which can be attributed to the increase in neuronal survival observed in the NB group. However, if glia remains chronically activated, those cells can induce proinflammatory response resulting in further synaptic uptake, tissue damage and even neurodegeneration.

The process of axon growth and remyelination is dictated by Schwann cells, which envelop the axons, creating a myelin sheath from multiple concentric layers of the cytoplasmic membrane (146). In our treated groups, immunolabeling of axons and Schwann cells revealed structural changes, as NB exhibited greater values and was closer to group C, while only NB differed from group D. These findings suggest an improvement in overall nerve integrity recovery and myelination.

In addition to S100 proteins, brain-derived neurotrophic factor (BDNF) is another fundamental endogenous regulator of the attenuation of motor neuron degeneration, further axon myelination and reinnervation through the establishment of

neuromuscular junctions during development and after peripheral nerve injury (147, 148). Studies have already demonstrated a positive association between HFB and the expression of BDNF in nerves and muscles (62, 64, 66); moreover, this protein can be secreted by macrophages recruited to the injury site (66), which are boosted after nerve injury due to the immunogenic properties of HFB (107). Furthermore, both proteins also contribute positively to the increase in the expression of intermediate neurofilaments, the main proteins related to the control of axonal caliber and volume, allowing the elongation of growing nerve fibers (61, 62, 64, 149).

We further emphasize in relation to NMJ ultrastructure that due to the presence and organization of synaptic buttons and gutters, as well as the characteristics of the presynaptic and postsynaptic membranes, group NB appears to be more similar to C in opposition to N, which presented several unoccupied synaptic gutters with dense junctional folds. This can suggest that HFB endorsed reinnervation and helped reassembling healthier neuromuscular junctions. But, the lack of a more reliable and quantifiable source of analysis for NMJs morphology and morphometry here represents a limitation of this work.

Indeed, the treatment of spinal cord injuries with HFB has improved tissue regeneration and motor function, although in different environments, the process of axon regeneration and reinnervation has also been enhanced. Taken together, the results observed here, in addition to the studies and experience of HFB for other nervous tissue injuries, we suggest that HFB in peripheral nerve repair, a part of its muscle-nerve benefits, exhibits further potential for preserving the spinal cord microenvironment. This preservation increases neuronal survival, which may contribute to better reinnervation and the maintenance of muscle and neuromuscular junctions.

5. References

1. Hussain G, Wang J, Rasul A, Anwar H, Qasim M, Zafar S, et al. Current Status of Therapeutic Approaches against Peripheral Nerve Injuries: A Detailed Story from Injury to Recovery. Int J Biol Sci. 2020;16(1):116-34. Epub 20200101. doi: 10.7150/ijbs.35653. PubMed PMID: 31892850; PubMed Central PMCID: PMC6930373.

2. Jones S, Eisenberg HM, Jia X. Advances and Future Applications of Augmented Peripheral Nerve Regeneration. Int J Mol Sci. 2016;17(9). Epub 20160907. doi: 10.3390/ijms17091494. PubMed PMID: 27618010; PubMed Central PMCID: PMC5037771.

3. Murphy RNA, de Schoulepnikoff C, Chen JHC, Columb MO, Bedford J, Wong JK, et al. The incidence and management of peripheral nerve injury in England (2005-2020). J Plast Reconstr Aesthet Surg. 2023;80:75-85. Epub 20230216. doi: 10.1016/j.bjps.2023.02.017. PubMed PMID: 36996504.
4. Kouyoumdjian JA, Graça CR, Ferreira VFM. Peripheral nerve injuries: A retrospective survey of 1124 cases. Neurol India. 2017;65(3):551-5. doi: 10.4103/neuroindia.NI_987_16. PubMed PMID: 28488619.
5. Asplund M, Nilsson M, Jacobsson A, von Holst H. Incidence of traumatic peripheral nerve injuries and amputations in Sweden between 1998 and 2006. Neuroepidemiology. 2009;32(3):217-28. Epub 20090128. doi: 10.1159/000197900. PubMed PMID: 19174611.
6. Kim SJ, Kwon YM, Ahn SM, Lee JH, Lee CH. Epidemiology of upper extremity peripheral nerve injury in South Korea, 2008 to 2018. Medicine (Baltimore). 2022;101(48):e31655. doi: 10.1097/MD.0000000000031655. PubMed PMID: 36482555; PubMed Central PMCID: PMC9726405.
7. Wang ML, Rivlin M, Graham JG, Beredjiklian PK. Peripheral nerve injury, scarring, and recovery. Connect Tissue Res. 2019;60(1):3-9. Epub 20180906. doi: 10.1080/03008207.2018.1489381. PubMed PMID: 30187777.
8. Carlstedt T. An overture to basic science aspects of nerve injuries. J Hand Surg Eur Vol. 2011;36(9):726-9. Epub 20110913. doi: 10.1177/1753193411422329. PubMed PMID: 21914690.
9. Faroni A, Mobasseri SA, Kingham PJ, Reid AJ. Peripheral nerve regeneration: experimental strategies and future perspectives. Adv Drug Deliv Rev. 2015;82-83:160-7. Epub 20141114. doi: 10.1016/j.addr.2014.11.010. PubMed PMID: 25446133.
10. Gordon T. Nerve Regeneration: Understanding Biology and Its Influence on Return of Function After Nerve Transfers. Hand Clin. 2016;32(2):103-17. Epub 20160310. doi: 10.1016/j.hcl.2015.12.001. PubMed PMID: 27094884.
11. Zelada D, Bermedo-García F, Collao N, Henríquez JP. Motor function recovery: deciphering a regenerative niche at the neuromuscular synapse. Biol Rev Camb Philos Soc. 2021;96(2):752-66. Epub 20201217. doi: 10.1111/brv.12675. PubMed PMID: 33336525; PubMed Central PMCID: PMC7986695.
12. Jones RA, Harrison C, Eaton SL, Llavero Hurtado M, Graham LC, Alkhammash L, et al. Cellular and Molecular Anatomy of the Human Neuromuscular Junction. Cell Rep. 2017;21(9):2348-56. doi: 10.1016/j.celrep.2017.11.008. PubMed PMID: 29186674; PubMed Central PMCID: PMC5723673.
13. Jessen KR. Glial cells. Int J Biochem Cell Biol. 2004;36(10):1861-7. doi: 10.1016/j.biocel.2004.02.023. PubMed PMID: 15203098.
14. Ceprian M, Fulton D. Glial Cell AMPA Receptors in Nervous System Health, Injury and Disease. Int J Mol Sci. 2019;20(10). Epub 20190517. doi: 10.3390/ijms20102450. PubMed PMID: 31108947; PubMed Central PMCID: PMC6566241.
15. Pekny M, Pekna M, Messing A, Steinhäuser C, Lee JM, Parpura V, et al. Astrocytes: a central element in neurological diseases. Acta Neuropathol. 2016;131(3):323-45. Epub 20151215. doi: 10.1007/s00401-015-1513-1. PubMed PMID: 26671410.
16. Sofroniew MV, Vinters HV. Astrocytes: biology and pathology. Acta Neuropathol. 2010;119(1):7-35. Epub 20091210. doi: 10.1007/s00401-009-0619-8. PubMed PMID: 20012068; PubMed Central PMCID: PMC2799634.
17. Feng Z, Ko CP. The role of glial cells in the formation and maintenance of the neuromuscular junction. Ann N Y Acad Sci. 2008;1132:19-28. doi: 10.1196/annals.1405.016. PubMed PMID: 18567850.
18. Escartin C, Galea E, Lakatos A, O'Callaghan JP, Petzold GC, Serrano-Pozo A, et al. Reactive astrocyte nomenclature, definitions, and future directions. Nat Neurosci. 2021;24(3):312-25. Epub 20210215. doi: 10.1038/s41593-020-00783-4. PubMed PMID: 33589835; PubMed Central PMCID: PMC8007081.
19. Salter MW, Stevens B. Microglia emerge as central players in brain disease. Nat Med. 2017;23(9):1018-27. doi: 10.1038/nm.4397. PubMed PMID: 28886007.
20. Brandenburg S, Müller A, Turkowski K, Radev YT, Rot S, Schmidt C, et al. Resident microglia rather than peripheral macrophages promote vascularization in brain tumors and are source of alternative pro-angiogenic factors. Acta Neuropathol. 2016;131(3):365-78. Epub 20151230. doi: 10.1007/s00401-015-1529-6. PubMed PMID: 26718201.

21. Savage JC, Carrier M, Tremblay M. Morphology of Microglia Across Contexts of Health and Disease. Methods Mol Biol. 2019;2034:13-26. doi: 10.1007/978-1-4939-9658-2_2. PubMed PMID: 31392674.
22. Green TRF, Murphy SM, Rowe RK. Comparisons of quantitative approaches for assessing microglial morphology reveal inconsistencies, ecological fallacy, and a need for standardization. Sci Rep. 2022;12(1):18196. Epub 20221028. doi: 10.1038/s41598-022-23091-2. PubMed PMID: 36307475; PubMed Central PMCID: PMC9616881.
23. Rodríguez Cruz PM, Cossins J, Beeson D, Vincent A. The Neuromuscular Junction in Health and Disease: Molecular Mechanisms Governing Synaptic Formation and Homeostasis. Front Mol Neurosci. 2020;13:610964. Epub 20201203. doi: 10.3389/fnmol.2020.610964. PubMed PMID: 33343299; PubMed Central PMCID: PMC7744297.
24. Tintignac LA, Brenner HR, Rüegg MA. Mechanisms Regulating Neuromuscular Junction Development and Function and Causes of Muscle Wasting. Physiol Rev. 2015;95(3):809-52. doi: 10.1152/physrev.00033.2014. PubMed PMID: 26109340.
25. Muller KS, Tibúrcio FC, Ferreira RS, Barraviera B, Matheus SMM. Heterologous fibrin biopolymer as an emerging approach to peripheral nerve repair: a scoping review. J Venom Anim Toxins Incl Trop Dis. 2024;30:e20230060. Epub 20240415. doi: 10.1590/1678-9199-JVATITD-2023-0060. PubMed PMID: 38628622; PubMed Central PMCID: PMC11019597.
26. Hughes BW, Kusner LL, Kaminski HJ. Molecular architecture of the neuromuscular junction. Muscle Nerve. 2006;33(4):445-61. doi: 10.1002/mus.20440. PubMed PMID: 16228970.
27. Sanes JR, Lichtman JW. Development of the vertebrate neuromuscular junction. Annu Rev Neurosci. 1999;22:389-442. doi: 10.1146/annurev.neuro.22.1.389. PubMed PMID: 10202544.
28. Nishimune H, Shigemoto K. Practical Anatomy of the Neuromuscular Junction in Health and Disease. Neurol Clin. 2018;36(2):231-40. doi: 10.1016/j.ncl.2018.01.009. PubMed PMID: 29655446; PubMed Central PMCID: PMC5903580.
29. Lepore E, Casola I, Dobrowolny G, Musarò A. Neuromuscular Junction as an Entity of Nerve-Muscle Communication. Cells. 2019;8(8). Epub 20190816. doi: 10.3390/cells8080906. PubMed PMID: 31426366; PubMed Central PMCID: PMC6721719.
30. Iyer SR, Shah SB, Lovering RM. The Neuromuscular Junction: Roles in Aging and Neuromuscular Disease. Int J Mol Sci. 2021;22(15). Epub 20210728. doi: 10.3390/ijms22158058. PubMed PMID: 34360831; PubMed Central PMCID: PMC8347593.
31. Bloch-Gallego E. Mechanisms controlling neuromuscular junction stability. Cell Mol Life Sci. 2015;72(6):1029-43. Epub 20141031. doi: 10.1007/s00018-014-1768-z. PubMed PMID: 25359233.
32. Sugiura Y, Lin W. Neuron-glia interactions: the roles of Schwann cells in neuromuscular synapse formation and function. Biosci Rep. 2011;31(5):295-302. doi: 10.1042/BSR20100107. PubMed PMID: 21517783; PubMed Central PMCID: PMC4573580.
33. Ko CP, Robitaille R. Perisynaptic Schwann Cells at the Neuromuscular Synapse: Adaptable, Multitasking Glial Cells. Cold Spring Harb Perspect Biol. 2015;7(10):a020503. Epub 20150820. doi: 10.1101/cshperspect.a020503. PubMed PMID: 26430218; PubMed Central PMCID: PMC4588062.
34. Patton BL, Miner JH, Chiu AY, Sanes JR. Distribution and function of laminins in the neuromuscular system of developing, adult, and mutant mice. J Cell Biol. 1997;139(6):1507-21. doi: 10.1083/jcb.139.6.1507. PubMed PMID: 9396756; PubMed Central PMCID: PMC2132624.
35. Patton BL. Basal lamina and the organization of neuromuscular synapses. J Neurocytol. 2003;32(5-8):883-903. doi: 10.1023/B:NEUR.0000020630.74955.19. PubMed PMID: 15034274.
36. Engel AG. The neuromuscular junction. Handb Clin Neurol. 2008;91:103-48. doi: 10.1016/S0072-9752(07)01503-5. PubMed PMID: 18631841.
37. Ruff RL. Neurophysiology of the neuromuscular junction: overview. Ann N Y Acad Sci. 2003;998:1-10. PubMed PMID: 14592857.
38. Conti-Fine BM, Milani M, Kaminski HJ. Myasthenia gravis: past, present, and future. J Clin Invest. 2006;116(11):2843-54. doi: 10.1172/JCI29894. PubMed PMID: 17080188; PubMed Central PMCID: PMC1626141.

39. Wu P, Chawla A, Spinner RJ, Yu C, Yaszemski MJ, Windebank AJ, et al. Key changes in denervated muscles and their impact on regeneration and reinnervation. Neural Regen Res. 2014;9(20):1796-809. doi: 10.4103/1673-5374.143424. PubMed PMID: 25422641; PubMed Central PMCID: PMC4239769.
40. Ma J, Shen J, Garrett JP, Lee CA, Li Z, Elsaidi GA, et al. Gene expression of myogenic regulatory factors, nicotinic acetylcholine receptor subunits, and GAP-43 in skeletal muscle following denervation in a rat model. J Orthop Res. 2007;25(11):1498-505. doi: 10.1002/jor.20414. PubMed PMID: 17568415.
41. Grosman C, Auerbach A. Kinetic, mechanistic, and structural aspects of unliganded gating of acetylcholine receptor channels: a single-channel study of second transmembrane segment 12' mutants. J Gen Physiol. 2000;115(5):621-35. doi: 10.1085/jgp.115.5.621. PubMed PMID: 10779319; PubMed Central PMCID: PMC2217228.
42. Naguib M, Flood P, McArdle JJ, Brenner HR. Advances in neurobiology of the neuromuscular junction: implications for the anesthesiologist. Anesthesiology. 2002;96(1):202-31. doi: 10.1097/00000542-200201000-00035. PubMed PMID: 11753022.
43. Unwin N. Nicotinic acetylcholine receptor and the structural basis of neuromuscular transmission: insights from Torpedo postsynaptic membranes. Q Rev Biophys. 2013;46(4):283-322. Epub 20130920. doi: 10.1017/S0033583513000061. PubMed PMID: 24050525; PubMed Central PMCID: PMC3820380.
44. Pinto CG, Leite APS, Sartori AA, Tibúrcio FC, Barraviera B, Junior RSF, et al. Heterologous fibrin biopolymer associated to a single suture stitch enables the return of neuromuscular junction to its mature pattern after peripheral nerve injury. Injury. 2021;52(4):731-7. Epub 20201017. doi: 10.1016/j.injury.2020.10.070. PubMed PMID: 33902866.
45. Lacomis D. What's in the Neuromuscular Junction Literature? J Clin Neuromuscul Dis. 2020;21(4):195-204. doi: 10.1097/CND.0000000000000285. PubMed PMID: 32453095.
46. Krivoi II, Petrov AM. Cholesterol and the Safety Factor for Neuromuscular Transmission. Int J Mol Sci. 2019;20(5). Epub 20190228. doi: 10.3390/ijms20051046. PubMed PMID: 30823359; PubMed Central PMCID: PMC6429197.
47. Seddon HJ. A Classification of Nerve Injuries. Br Med J. 1942;2(4260):237-9. doi: 10.1136/bmj.2.4260.237. PubMed PMID: 20784403; PubMed Central PMCID: PMC2164137.
48. SUNDERLAND S. A classification of peripheral nerve injuries producing loss of function. Brain. 1951;74(4):491-516. doi: 10.1093/brain/74.4.491. PubMed PMID: 14895767.
49. Colli BO. General aspects of acute peripheral nerve injuries. Arquivos Brasileiros de Neurocirurgia1993. p. 29.
50. Modrak M, Talukder MAH, Gurgenashvili K, Noble M, Elfar JC. Peripheral nerve injury and myelination: Potential therapeutic strategies. J Neurosci Res. 2020;98(5):780-95. Epub 20191013. doi: 10.1002/jnr.24538. PubMed PMID: 31608497; PubMed Central PMCID: PMC7072007.
51. Fu SY, Gordon T. Contributing factors to poor functional recovery after delayed nerve repair: prolonged axotomy. J Neurosci. 1995;15(5 Pt 2):3876-85. PubMed PMID: 7751952; PubMed Central PMCID: PMC6578210.
52. Chan KM, Gordon T, Zochodne DW, Power HA. Improving peripheral nerve regeneration: from molecular mechanisms to potential therapeutic targets. Exp Neurol. 2014;261:826-35. Epub 20140916. doi: 10.1016/j.expneurol.2014.09.006. PubMed PMID: 25220611.
53. Yi S, Tang X, Yu J, Liu J, Ding F, Gu X. Microarray and qPCR Analyses of Wallerian Degeneration in Rat Sciatic Nerves. Front Cell Neurosci. 2017;11:22. Epub 20170210. doi: 10.3389/fncel.2017.00022. PubMed PMID: 28239339; PubMed Central PMCID: PMC5301003.
54. Gordon T. Peripheral Nerve Regeneration and Muscle Reinnervation. International Journal of Molecular Sciences. 2020;21(22):8652. doi: 10.3390/ijms21228652.
55. Lubińska L. Patterns of Wallerian degeneration of myelinated fibres in short and long peripheral stumps and in isolated segments of rat phrenic nerve. Interpretation of the role of axoplasmic flow of the trophic factor. Brain Res. 1982;233(2):227-40. doi: 10.1016/0006-8993(82)91199-4. PubMed PMID: 6174177.

56. Lindborg JA, Mack M, Zigmond RE. Neutrophils Are Critical for Myelin Removal in a Peripheral Nerve Injury Model of Wallerian Degeneration. J Neurosci. 2017;37(43):10258-77. Epub 20170914. doi: 10.1523/JNEUROSCI.2085-17.2017. PubMed PMID: 28912156; PubMed Central PMCID: PMC5656991.
57. Gomez-Sanchez JA, Carty L, Iruarrizaga-Lejarreta M, Palomo-Irigoyen M, Varela-Rey M, Griffith M, et al. Schwann cell autophagy, myelinophagy, initiates myelin clearance from injured nerves. J Cell Biol. 2015;210(1):153-68. doi: 10.1083/jcb.201503019. PubMed PMID: 26150392; PubMed Central PMCID: PMC4494002.
58. Gaudet AD, Popovich PG, Ramer MS. Wallerian degeneration: gaining perspective on inflammatory events after peripheral nerve injury. J Neuroinflammation. 2011;8:110. Epub 20110830. doi: 10.1186/1742-2094-8-110. PubMed PMID: 21878126; PubMed Central PMCID: PMC3180276.
59. Cattin AL, Burden JJ, Van Emmenis L, Mackenzie FE, Hoving JJ, Garcia Calavia N, et al. Macrophage-Induced Blood Vessels Guide Schwann Cell-Mediated Regeneration of Peripheral Nerves. Cell. 2015;162(5):1127-39. Epub 20150813. doi: 10.1016/j.cell.2015.07.021. PubMed PMID: 26279190; PubMed Central PMCID: PMC4553238.
60. Jiang BG, Han N, Rao F, Wang YL, Kou YH, Zhang PX. Advance of Peripheral Nerve Injury Repair and Reconstruction. Chin Med J (Engl). 2017;130(24):2996-8. doi: 10.4103/0366-6999.220299. PubMed PMID: 29237933; PubMed Central PMCID: PMC5742928.
61. Bombeiro AL, Thomé R, Oliveira Nunes SL, Monteiro Moreira B, Verinaud L, Oliveira AL. MHC-I and PirB Upregulation in the Central and Peripheral Nervous System following Sciatic Nerve Injury. PLoS One. 2016;11(8):e0161463. Epub 20160823. doi: 10.1371/journal.pone.0161463. PubMed PMID: 27551751; PubMed Central PMCID: PMC4995013.
62. Bombeiro AL, Pereira BTN, de Oliveira ALR. Granulocyte-macrophage colony-stimulating factor improves mouse peripheral nerve regeneration following sciatic nerve crush. Eur J Neurosci. 2018;48(5):2152-64. Epub 20180829. doi: 10.1111/ejn.14106. PubMed PMID: 30099786.
63. Bombeiro AL, Pereira BTN, Bonfanti AP, Oliveira ALR. Immunomodulation by dimethyl fumarate treatment improves mouse sciatic nerve regeneration. Brain Res Bull. 2020;160:24-32. Epub 20200417. doi: 10.1016/j.brainresbull.2020.04.005. PubMed PMID: 32305403.
64. Bombeiro AL, Lima BHM, Bonfanti AP, Oliveira ALR. Improved mouse sciatic nerve regeneration following lymphocyte cell therapy. Mol Immunol. 2020;121:81-91. Epub 20200313. doi: 10.1016/j.molimm.2020.03.003. PubMed PMID: 32172028.
65. Rodríguez-Sánchez DN, Pinto GBA, Cartarozzi LP, de Oliveira ALR, Bovolato ALC, de Carvalho M, et al. 3D-printed nerve guidance conduits multi-functionalized with canine multipotent mesenchymal stromal cells promote neuroregeneration after sciatic nerve injury in rats. Stem Cell Res Ther. 2021;12(1):303. Epub 20210529. doi: 10.1186/s13287-021-02315-8. PubMed PMID: 34051869; PubMed Central PMCID: PMC8164252.
66. Cartarozzi LP, Spejo AB, Ferreira RS, Barraviera B, Duek E, Carvalho JL, et al. Mesenchymal stem cells engrafted in a fibrin scaffold stimulate Schwann cell reactivity and axonal regeneration following sciatic nerve tubulization. Brain Res Bull. 2015;112:14-24. Epub 20150117. doi: 10.1016/j.brainresbull.2015.01.005. PubMed PMID: 25602253.
67. Rishal I, Fainzilber M. Axon-soma communication in neuronal injury. Nat Rev Neurosci. 2014;15(1):32-42. Epub 20131211. doi: 10.1038/nrn3609. PubMed PMID: 24326686.
68. Cullheim S, Thams S. The microglial networks of the brain and their role in neuronal network plasticity after lesion. Brain Res Rev. 2007;55(1):89-96. Epub 20070419. doi: 10.1016/j.brainresrev.2007.03.012. PubMed PMID: 17509690.
69. Blinzinger K, Kreutzberg G. Displacement of synaptic terminals from regenerating motoneurons by microglial cells. Z Zellforsch Mikrosk Anat. 1968;85(2):145-57. doi: 10.1007/BF00325030. PubMed PMID: 5706753.
70. Alvarez FJ, Titus-Mitchell HE, Bullinger KL, Kraszpulski M, Nardelli P, Cope TC. Permanent central synaptic disconnection of proprioceptors after nerve injury and regeneration. I. Loss of VGLUT1/IA synapses on motoneurons. J Neurophysiol. 2011;106(5):2450-70. Epub 20110810. doi: 10.1152/jn.01095.2010. PubMed PMID: 21832035; PubMed Central PMCID: PMC3214094.

71. Rotterman TM, Akhter ET, Lane AR, MacPherson KP, García VV, Tansey MG, et al. Spinal Motor Circuit Synaptic Plasticity after Peripheral Nerve Injury Depends on Microglia Activation and a CCR2 Mechanism. J Neurosci. 2019;39(18):3412-33. Epub 20190304. doi: 10.1523/JNEUROSCI.2945-17.2019. PubMed PMID: 30833511; PubMed Central PMCID: PMC6495126.
72. Alvarez FJ, Rotterman TM, Akhter ET, Lane AR, English AW, Cope TC. Synaptic Plasticity on Motoneurons After Axotomy: A Necessary Change in Paradigm. Front Mol Neurosci. 2020;13:68. Epub 20200430. doi: 10.3389/fnmol.2020.00068. PubMed PMID: 32425754; PubMed Central PMCID: PMC7203341.
73. Fu SY, Gordon T. The cellular and molecular basis of peripheral nerve regeneration. Mol Neurobiol. 1997;14(1-2):67-116. doi: 10.1007/BF02740621. PubMed PMID: 9170101.
74. Ma CH, Omura T, Cobos EJ, Latrémolière A, Ghasemlou N, Brenner GJ, et al. Accelerating axonal growth promotes motor recovery after peripheral nerve injury in mice. J Clin Invest. 2011;121(11):4332-47. Epub 20111003. doi: 10.1172/JCI58675. PubMed PMID: 21965333; PubMed Central PMCID: PMC3223863.
75. Sakuma M, Gorski G, Sheu SH, Lee S, Barrett LB, Singh B, et al. Lack of motor recovery after prolonged denervation of the neuromuscular junction is not due to regenerative failure. Eur J Neurosci. 2016;43(3):451-62. Epub 20150928. doi: 10.1111/ejn.13059. PubMed PMID: 26332731; PubMed Central PMCID: PMC4738060.
76. Moimas S, Novati F, Ronchi G, Zacchigna S, Fregnan F, Zentilin L, et al. Effect of vascular endothelial growth factor gene therapy on post-traumatic peripheral nerve regeneration and denervation-related muscle atrophy. Gene Ther. 2013;20(10):1014-21. Epub 20130530. doi: 10.1038/gt.2013.26. PubMed PMID: 23719064; PubMed Central PMCID: PMC3795473.
77. Leite APS, Pinto CG, Tibúrcio FC, Muller KS, Padovani CR, Barraviera B, et al. Acetylcholine receptors of the neuromuscular junctions present normal distribution after peripheral nerve injury and repair through nerve guidance associated with fibrin biopolymer. Injury. 2023;54(2):345-61. Epub 20221123. doi: 10.1016/j.injury.2022.11.047. PubMed PMID: 36446670.
78. Rios R, Jablonka-Shariff A, Broberg C, Snyder-Warwick AK. Macrophage roles in peripheral nervous system injury and pathology: Allies in neuromuscular junction recovery. Mol Cell Neurosci. 2021;111:103590. Epub 20210108. doi: 10.1016/j.mcn.2021.103590. PubMed PMID: 33422671; PubMed Central PMCID: PMC8235592.
79. Su HL, Chiang CY, Lu ZH, Cheng FC, Chen CJ, Sheu ML, et al. Late administration of high-frequency electrical stimulation increases nerve regeneration without aggravating neuropathic pain in a nerve crush injury. BMC Neurosci. 2018;19(1):37. Epub 20180625. doi: 10.1186/s12868-018-0437-9. PubMed PMID: 29940857; PubMed Central PMCID: PMC6020201.
80. Chao T, Frump D, Lin M, Caiozzo VJ, Mozaffar T, Steward O, et al. Matrix metalloproteinase 3 deletion preserves denervated motor endplates after traumatic nerve injury. Ann Neurol. 2013;73(2):210-23. Epub 20121231. doi: 10.1002/ana.23781. PubMed PMID: 23281061.
81. Palispis WA, Gupta R. Surgical repair in humans after traumatic nerve injury provides limited functional neural regeneration in adults. Exp Neurol. 2017;290:106-14. Epub 20170119. doi: 10.1016/j.expneurol.2017.01.009. PubMed PMID: 28111229.
82. Jablonka-Shariff A, Lu CY, Campbell K, Monk KR, Snyder-Warwick AK. Gpr126/Adgrg6 contributes to the terminal Schwann cell response at the neuromuscular junction following peripheral nerve injury. Glia. 2020;68(6):1182-200. Epub 20191224. doi: 10.1002/glia.23769. PubMed PMID: 31873966; PubMed Central PMCID: PMC7148175.
83. Cisterna BA, Cardozo C, Sáez JC. Neuronal involvement in muscular atrophy. Front Cell Neurosci. 2014;8:405. Epub 20141210. doi: 10.3389/fncel.2014.00405. PubMed PMID: 25540609; PubMed Central PMCID: PMC4261799.
84. Guarino SR, Canciani A, Forneris F. Dissecting the Extracellular Complexity of Neuromuscular Junction Organizers. Front Mol Biosci. 2019;6:156. Epub 20200110. doi: 10.3389/fmolb.2019.00156. PubMed PMID: 31998752; PubMed Central PMCID: PMC6966886.

85. VanSaun M, Humburg BC, Arnett MG, Pence M, Werle MJ. Activation of Matrix Metalloproteinase-3 is altered at the frog neuromuscular junction following changes in synaptic activity. Dev Neurobiol. 2007;67(11):1488-97. doi: 10.1002/dneu.20523. PubMed PMID: 17525979.
86. Campbell WW. Evaluation and management of peripheral nerve injury. Clin Neurophysiol. 2008;119(9):1951-65. Epub 20080514. doi: 10.1016/j.clinph.2008.03.018. PubMed PMID: 18482862.
87. Martins RS, Siqueira MG, Da Silva CF, Plese JP. Overall assessment of regeneration in peripheral nerve lesion repair using fibrin glue, suture, or a combination of the 2 techniques in a rat model. Which is the ideal choice? Surg Neurol. 2005;64 Suppl 1:S1:10-6; discussion S1:6. doi: 10.1016/j.surneu.2005.04.022. PubMed PMID: 15967220.
88. Ray WZ, Mackinnon SE. Management of nerve gaps: autografts, allografts, nerve transfers, and end-to-side neurorrhaphy. Exp Neurol. 2010;223(1):77-85. Epub 20090405. doi: 10.1016/j.expneurol.2009.03.031. PubMed PMID: 19348799; PubMed Central PMCID: PMC2849924.
89. Wanner R, Gey M, Abaei A, Warnecke D, de Roy L, Dürselen L, et al. Functional and Molecular Characterization of a Novel Traumatic Peripheral Nerve-Muscle Injury Model. Neuromolecular Med. 2017;19(2-3):357-74. Epub 20170708. doi: 10.1007/s12017-017-8450-1. PubMed PMID: 28689354.
90. Sulaiman W, Gordon T. Neurobiology of peripheral nerve injury, regeneration, and functional recovery: from bench top research to bedside application. Ochsner J. 2013;13(1):100-8. PubMed PMID: 23531634; PubMed Central PMCID: PMC3603172.
91. Biscola NP, Cartarozzi LP, Ulian-Benitez S, Barbizan R, Castro MV, Spejo AB, et al. Multiple uses of fibrin sealant for nervous system treatment following injury and disease. J Venom Anim Toxins Incl Trop Dis. 2017;23:13. Epub 20170314. doi: 10.1186/s40409-017-0103-1. PubMed PMID: 28293254; PubMed Central PMCID: PMC5348778.
92. Robinson PP, Loescher AR, Smith KG. A prospective, quantitative study on the clinical outcome of lingual nerve repair. Br J Oral Maxillofac Surg. 2000;38(4):255-63. doi: 10.1054/bjom.2000.0463. PubMed PMID: 10922146.
93. Peretti GM, Randolph MA, Zaporojan V, Bonassar LJ, Xu JW, Fellers JC, et al. A biomechanical analysis of an engineered cell-scaffold implant for cartilage repair. Ann Plast Surg. 2001;46(5):533-7. doi: 10.1097/00000637-200105000-00013. PubMed PMID: 11352428.
94. Ringe J, Kaps C, Burmester GR, Sittinger M. Stem cells for regenerative medicine: advances in the engineering of tissues and organs. Naturwissenschaften. 2002;89(8):338-51. Epub 20020723. doi: 10.1007/s00114-002-0344-9. PubMed PMID: 12435034.
95. de Barros CN, Miluzzi Yamada AL, Junior RS, Barraviera B, Hussni CA, de Souza JB, et al. A new heterologous fibrin sealant as a scaffold to cartilage repair-Experimental study and preliminary results. Exp Biol Med (Maywood). 2016;241(13):1410-5. Epub 20150810. doi: 10.1177/1535370215597192. PubMed PMID: 26264444; PubMed Central PMCID: PMC4994917.
96. Bayer IS. Advances in Fibrin-Based Materials in Wound Repair: A Review. Molecules. 2022;27(14). Epub 20220714. doi: 10.3390/molecules27144504. PubMed PMID: 35889381; PubMed Central PMCID: PMC9322155.
97. Buchta C, Dettke M, Funovics PT, Höcker P, Knöbl P, Macher M, et al. Fibrin sealant produced by the CryoSeal FS System: product chemistry, material properties and possible preparation in the autologous preoperative setting. Vox Sang. 2004;86(4):257-62. doi: 10.1111/j.0042-9007.2004.00516.x. PubMed PMID: 15144531.
98. Sameem M, Wood TJ, Bain JR. A systematic review on the use of fibrin glue for peripheral nerve repair. Plast Reconstr Surg. 2011;127(6):2381-90. doi: 10.1097/PRS.0b013e3182131cf5. PubMed PMID: 21311390.
99. Buchaim DV, Cassaro CV, Shindo JVTC, Coletta BBD, Pomini KT, Rosso MPO, et al. Unique heterologous fibrin biopolymer with hemostatic, adhesive, sealant, scaffold and drug delivery properties: a systematic review. J Venom Anim Toxins Incl Trop Dis. 2019;25:e20190038. Epub 20191111. doi: 10.1590/1678-9199-JVATITD-2019-0038. PubMed PMID: 31839802; PubMed Central PMCID: PMC6894437.
100. Koopman JE, Duraku LS, de Jong T, de Vries RBM, Michiel Zuidam J, Hundepool CA. A systematic review and meta-analysis on the use of fibrin glue in peripheral nerve repair: Can we just

glue it? J Plast Reconstr Aesthet Surg. 2022;75(3):1018-33. Epub 20220119. doi: 10.1016/j.bjps.2022.01.007. PubMed PMID: 35125308.
101. Barros LC, Ferreira RS, Barraviera SR, Stolf HO, Thomazini-Santos IA, Mendes-Giannini MJ, et al. A new fibrin sealant from Crotalus durissus terrificus venom: applications in medicine. J Toxicol Environ Health B Crit Rev. 2009;12(8):553-71. doi: 10.1080/10937400903442514. PubMed PMID: 20183534.
102. Ferreira RS, de Barros LC, Abbade LPF, Barraviera SRCS, Silvares MRC, de Pontes LG, et al. Heterologous fibrin sealant derived from snake venom: from bench to bedside - an overview. J Venom Anim Toxins Incl Trop Dis. 2017;23:21. Epub 20170404. doi: 10.1186/s40409-017-0109-8. PubMed PMID: 28396682; PubMed Central PMCID: PMC5379742.
103. Fattahi T, Mohan M, Caldwell GT. Clinical applications of fibrin sealants. J Oral Maxillofac Surg. 2004;62(2):218-24. doi: 10.1016/j.joms.2003.01.005. PubMed PMID: 14762755.
104. Abbade LPF, Ferreira RS, Dos Santos LD, Barraviera B. Chronic venous ulcers: a review on treatment with fibrin sealant and prognostic advances using proteomic strategies. J Venom Anim Toxins Incl Trop Dis. 2020;26:e20190101. Epub 20200622. doi: 10.1590/1678-9199-JVATITD-2019-0101. PubMed PMID: 32636876; PubMed Central PMCID: PMC7315627.
105. Abbade LPF, Barraviera SRCS, Silvares MRC, Lima ABBC, Haddad GR, Gatti MAN, et al. Treatment of Chronic Venous Ulcers With Heterologous Fibrin Sealant: A Phase I/II Clinical Trial. Front Immunol. 2021;12:627541. Epub 20210223. doi: 10.3389/fimmu.2021.627541. PubMed PMID: 33708219; PubMed Central PMCID: PMC7940668.
106. Leite APS, Pinto CG, Tibúrcio FC, Sartori AA, de Castro Rodrigues A, Barraviera B, et al. Heterologous fibrin sealant potentiates axonal regeneration after peripheral nerve injury with reduction in the number of suture points. Injury. 2019;50(4):834-47. Epub 20190319. doi: 10.1016/j.injury.2019.03.027. PubMed PMID: 30922661.
107. Tibúrcio FC, Muller KS, Leite APS, de Oliveira IRA, Barraviera B, Ferreira RS, et al. Neuroregeneration and immune response after neurorrhaphy are improved with the use of heterologous fibrin biopolymer in addition to suture repair alone. Muscle Nerve. 2023;67(6):522-36. Epub 20230325. doi: 10.1002/mus.27815. PubMed PMID: 36905197.
108. Buchaim RL, Andreo JC, Barraviera B, Ferreira Junior RS, Buchaim DV, Rosa Junior GM, et al. Effect of low-level laser therapy (LLLT) on peripheral nerve regeneration using fibrin glue derived from snake venom. Injury. 2015;46(4):655-60. Epub 20150124. doi: 10.1016/j.injury.2015.01.031. PubMed PMID: 25669962.
109. Ortiz AC, Fideles SOM, Pomini KT, Bellini MZ, Pereira ESBM, Reis CHB, et al. Potential of Fibrin Glue and Mesenchymal Stem Cells (MSCs) to Regenerate Nerve Injuries: A Systematic Review. Cells. 2022;11(2). Epub 20220110. doi: 10.3390/cells11020221. PubMed PMID: 35053336; PubMed Central PMCID: PMC8773549.
110. Schneider CA, Rasband WS, Eliceiri KW. NIH Image to ImageJ: 25 years of image analysis. Nat Methods. 2012;9(7):671-5. doi: 10.1038/nmeth.2089. PubMed PMID: 22930834; PubMed Central PMCID: PMC5554542.
111. Zaimi A, Wabartha M, Herman V, Antonsanti PL, Perone CS, Cohen-Adad J. AxonDeepSeg: automatic axon and myelin segmentation from microscopy data using convolutional neural networks. Sci Rep. 2018;8(1):3816. Epub 20180228. doi: 10.1038/s41598-018-22181-4. PubMed PMID: 29491478; PubMed Central PMCID: PMC5830647.
112. Muller KS, Tibúrcio FC, de Barros JWF, Matsumura CY, Matheus SMM. Statin exposure during pregnancy promotes neuromuscular junction alterations in postpartum Wistar rats. Muscle Nerve. 2023;67(6):537-47. Epub 20230411. doi: 10.1002/mus.27825. PubMed PMID: 36975763.
113. Lopes B, Sousa P, Alvites R, Branquinho M, Sousa AC, Mendonça C, et al. Peripheral Nerve Injury Treatments and Advances: One Health Perspective. Int J Mol Sci. 2022;23(2). Epub 20220114. doi: 10.3390/ijms23020918. PubMed PMID: 35055104; PubMed Central PMCID: PMC8779751.
114. Spejo AB, Chiarotto GB, Ferreira ADF, Gomes DA, Ferreira RS, Barraviera B, et al. Neuroprotection and immunomodulation following intraspinal axotomy of motoneurons by treatment

with adult mesenchymal stem cells. J Neuroinflammation. 2018;15(1):230. Epub 20180814. doi: 10.1186/s12974-018-1268-4. PubMed PMID: 30107848; PubMed Central PMCID: PMC6092804.
115. Kempe PRG, Chiarotto GB, Barraviera B, Ferreira RS, de Oliveira ALR. Neuroprotection and immunomodulation by dimethyl fumarate and a heterologous fibrin biopolymer after ventral root avulsion and reimplantation. J Venom Anim Toxins Incl Trop Dis. 2020;26:e20190093. Epub 20200520. doi: 10.1590/1678-9199-JVATITD-2019-0093. PubMed PMID: 32518556; PubMed Central PMCID: PMC7250131.
116. Bueno CRS, Tonin MCC, Buchaim DV, Barraviera B, Ferreira Junior RS, Santos PSDS, et al. Morphofunctional Improvement of the Facial Nerve and Muscles with Repair Using Heterologous Fibrin Biopolymer and Photobiomodulation. Pharmaceuticals (Basel). 2023;16(5). Epub 20230427. doi: 10.3390/ph16050653. PubMed PMID: 37242436; PubMed Central PMCID: PMC10223113.
117. Scorisa JM, Zanon RG, Freria CM, de Oliveira AL. Glatiramer acetate positively influences spinal motoneuron survival and synaptic plasticity after ventral root avulsion. Neurosci Lett. 2009;451(1):34-9. Epub 20081216. doi: 10.1016/j.neulet.2008.12.017. PubMed PMID: 19103252.
118. Kempe PRG, de Castro MV, Khuriyeh VC, Barraviera B, Ferreira RS, de Oliveira ALR. Ultrastructural Evidence of Synapse Preservation and Axonal Regeneration Following Spinal Root Repair with Fibrin Biopolymer and Therapy with Dimethyl Fumarate. Polymers (Basel). 2023;15(15). Epub 20230726. doi: 10.3390/polym15153171. PubMed PMID: 37571065.
119. LEHRER GM, ORNSTEIN L. A diazo coupling method for the electron microscopic localization of cholinesterase. J Biophys Biochem Cytol. 1959;6:399-406. doi: 10.1083/jcb.6.3.399. PubMed PMID: 14415404; PubMed Central PMCID: PMC2224705.
120. Jones RA, Reich CD, Dissanayake KN, Kristmundsdottir F, Findlater GS, Ribchester RR, et al. NMJ-morph reveals principal components of synaptic morphology influencing structure-function relationships at the neuromuscular junction. Open Biol. 2016;6(12). doi: 10.1098/rsob.160240. PubMed PMID: 27927794; PubMed Central PMCID: PMC5204123.
121. Lehto M, Järvinen M, Nelimarkka O. Scar formation after skeletal muscle injury. A histological and autoradiographical study in rats. Arch Orthop Trauma Surg (1978). 1986;104(6):366-70. doi: 10.1007/BF00454432. PubMed PMID: 3964044.
122. Folker ES, Baylies MK. Nuclear positioning in muscle development and disease. Front Physiol. 2013;4:363. Epub 20131212. doi: 10.3389/fphys.2013.00363. PubMed PMID: 24376424; PubMed Central PMCID: PMC3859928.
123. Ogawa Y, Yamamoto M, Sato M, Odaka K, Kasahara M, Hinata N, et al. Localization of T-cell factor 4 positive fibroblasts and CD206-positive macrophages during skeletal muscle regeneration in mice. Ann Anat. 2021;235:151694. Epub 20210208. doi: 10.1016/j.aanat.2021.151694. PubMed PMID: 33571646.
124. Martínez-Martínez P, Losen M, Duimel H, Frederik P, Spaans F, Molenaar P, et al. Overexpression of rapsyn in rat muscle increases acetylcholine receptor levels in chronic experimental autoimmune myasthenia gravis. Am J Pathol. 2007;170(2):644-57. doi: 10.2353/ajpath.2007.060676. PubMed PMID: 17255332; PubMed Central PMCID: PMC1851878.
125. Moresi V, Williams AH, Meadows E, Flynn JM, Potthoff MJ, McAnally J, et al. Myogenin and class II HDACs control neurogenic muscle atrophy by inducing E3 ubiquitin ligases. Cell. 2010;143(1):35-45. doi: 10.1016/j.cell.2010.09.004. PubMed PMID: 20887891; PubMed Central PMCID: PMC2982779.
126. Gao N, Zhao K, Cao Y, Ren X, Jing H, Xing G, et al. A Role of Lamin A/C in Preventing Neuromuscular Junction Decline in Mice. J Neurosci. 2020;40(38):7203-15. Epub 20200817. doi: 10.1523/JNEUROSCI.0443-20.2020. PubMed PMID: 32817327; PubMed Central PMCID: PMC7534915.
127. Liao X, Wang Y, Lai X, Wang S. The role of Rapsyn in neuromuscular junction and congenital myasthenic syndrome. Biomol Biomed. 2023;23(5):772-84. Epub 20230904. doi: 10.17305/bb.2022.8641. PubMed PMID: 36815443; PubMed Central PMCID: PMC10494853.
128. Xing G, Xiong WC, Mei L. Rapsyn as a signaling and scaffolding molecule in neuromuscular junction formation and maintenance. Neurosci Lett. 2020;731:135013. Epub 20200426. doi: 10.1016/j.neulet.2020.135013. PubMed PMID: 32344108.

129. Yang X, Xue P, Chen H, Yuan M, Kang Y, Duscher D, et al. Denervation drives skeletal muscle atrophy and induces mitochondrial dysfunction, mitophagy and apoptosis via miR-142a-5p/MFN1 axis. Theranostics. 2020;10(3):1415-32. Epub 20200101. doi: 10.7150/thno.40857. PubMed PMID: 31938072; PubMed Central PMCID: PMC6956801.
130. Ge MH, Tian H, Mao L, Li DY, Lin JQ, Hu HS, et al. Zinc attenuates ferroptosis and promotes functional recovery in contusion spinal cord injury by activating Nrf2/GPX4 defense pathway. CNS Neurosci Ther. 2021;27(9):1023-40. Epub 20210505. doi: 10.1111/cns.13657. PubMed PMID: 33951302; PubMed Central PMCID: PMC8339532.
131. Schmalbruch H. Fiber composition of the rat sciatic nerve. Anat Rec. 1986;215(1):71-81. doi: 10.1002/ar.1092150111. PubMed PMID: 3706794.
132. Mendonça AC, Barbieri CH, Mazzer N. Directly applied low intensity direct electric current enhances peripheral nerve regeneration in rats. J Neurosci Methods. 2003;129(2):183-90. doi: 10.1016/s0165-0270(03)00207-3. PubMed PMID: 14511820.
133. Rosso MPO, Rosa Júnior GM, Buchaim DV, German IJS, Pomini KT, de Souza RG, et al. Stimulation of morphofunctional repair of the facial nerve with photobiomodulation, using the end-to-side technique or a new heterologous fibrin sealant. J Photochem Photobiol B. 2017;175:20-8. Epub 20170818. doi: 10.1016/j.jphotobiol.2017.08.023. PubMed PMID: 28846931.
134. Furey MJ, Midha R, Xu QG, Belkas J, Gordon T. Prolonged target deprivation reduces the capacity of injured motoneurons to regenerate. Neurosurgery. 2007;60(4):723-32; discussion 32-3. doi: 10.1227/01.NEU.0000255412.63184.CC. PubMed PMID: 17415210.
135. Tu H, Zhang D, Corrick RM, Muelleman RL, Wadman MC, Li YL. Morphological Regeneration and Functional Recovery of Neuromuscular Junctions after Tourniquet-Induced Injuries in Mouse Hindlimb. Front Physiol. 2017;8:207. Epub 20170406. doi: 10.3389/fphys.2017.00207. PubMed PMID: 28428759; PubMed Central PMCID: PMC5382216.
136. Wiberg R, Jonsson S, Novikova LN, Kingham PJ. Investigation of the Expression of Myogenic Transcription Factors, microRNAs and Muscle-Specific E3 Ubiquitin Ligases in the Medial Gastrocnemius and Soleus Muscles following Peripheral Nerve Injury. PLoS One. 2015;10(12):e0142699. Epub 20151221. doi: 10.1371/journal.pone.0142699. PubMed PMID: 26691660; PubMed Central PMCID: PMC4686181.
137. Navarro X, Vivó M, Valero-Cabré A. Neural plasticity after peripheral nerve injury and regeneration. Prog Neurobiol. 2007;82(4):163-201. Epub 20070622. doi: 10.1016/j.pneurobio.2007.06.005. PubMed PMID: 17643733.
138. Barbizan R, Castro MV, Rodrigues AC, Barraviera B, Ferreira RS, Oliveira AL. Motor recovery and synaptic preservation after ventral root avulsion and repair with a fibrin sealant derived from snake venom. PLoS One. 2013;8(5):e63260. Epub 20130507. doi: 10.1371/journal.pone.0063260. PubMed PMID: 23667596; PubMed Central PMCID: PMC3646764.
139. Perussi Biscola N, Politti Cartarozzi L, Ferreira Junior RS, Barraviera B, Leite Rodrigues de Oliveira A. Long-Standing Motor and Sensory Recovery following Acute Fibrin Sealant Based Neonatal Sciatic Nerve Repair. Neural Plast. 2016;2016:9028126. Epub 20160629. doi: 10.1155/2016/9028126. PubMed PMID: 27446617; PubMed Central PMCID: PMC4942656.
140. Cartarozzi LP, Perez M, Fernandes GG, Chiarotto GB, Luzo Â, Campos AC, et al. Neuroprotection and gliosis attenuation by intravenous application of human mesenchymal stem cells (hMSC) following ventral root crush in mice. Mol Cell Neurosci. 2022;118:103694. Epub 20211224. doi: 10.1016/j.mcn.2021.103694. PubMed PMID: 34954382.
141. Paes SM, Castro MV, Barbosa RM, Politti Cartarozzi L, Coser LO, Kempe PRG, et al. Human dental pulp stem cell monolayer and spheroid therapy after spinal motor root avulsion in adult rats. Brain Res. 2023;1802:148229. Epub 20221230. doi: 10.1016/j.brainres.2022.148229. PubMed PMID: 36592804.
142. Barbizan R, Castro MV, Barraviera B, Ferreira RS, Oliveira AL. Influence of delivery method on neuroprotection by bone marrow mononuclear cell therapy following ventral root reimplantation with fibrin sealant. PLoS One. 2014;9(8):e105712. Epub 20140826. doi: 10.1371/journal.pone.0105712. PubMed PMID: 25157845; PubMed Central PMCID: PMC4144952.

143. Perez JC, Gerber YN, Perrin FE. Dynamic Diversity of Glial Response Among Species in Spinal Cord Injury. Front Aging Neurosci. 2021;13:769548. Epub 20211126. doi: 10.3389/fnagi.2021.769548. PubMed PMID: 34899275; PubMed Central PMCID: PMC8662749.
144. Mason CA, Edmondson JC, Hatten ME. The extending astroglial process: development of glial cell shape, the growing tip, and interactions with neurons. J Neurosci. 1988;8(9):3124-34. doi: 10.1523/JNEUROSCI.08-09-03124.1988. PubMed PMID: 3171670; PubMed Central PMCID: PMC6569428.
145. Yang I, Han SJ, Kaur G, Crane C, Parsa AT. The role of microglia in central nervous system immunity and glioma immunology. J Clin Neurosci. 2010;17(1):6-10. Epub 20091118. doi: 10.1016/j.jocn.2009.05.006. PubMed PMID: 19926287; PubMed Central PMCID: PMC3786731.
146. Zochodne DW, Cheng C. Neurotrophins and other growth factors in the regenerative milieu of proximal nerve stump tips. J Anat. 2000;196 (Pt 2)(Pt 2):279-83. doi: 10.1046/j.1469-7580.2000.19620279.x. PubMed PMID: 10739024; PubMed Central PMCID: PMC1468061.
147. Rentería I, García-Suárez PC, Fry AC, Moncada-Jiménez J, Machado-Parra JP, Antunes BM, et al. The Molecular Effects of BDNF Synthesis on Skeletal Muscle: A Mini-Review. Front Physiol. 2022;13:934714. Epub 20220706. doi: 10.3389/fphys.2022.934714. PubMed PMID: 35874524; PubMed Central PMCID: PMC9306488.
148. Oliveira AL, Risling M, Negro A, Langone F, Cullheim S. Apoptosis of spinal interneurons induced by sciatic nerve axotomy in the neonatal rat is counteracted by nerve growth factor and ciliary neurotrophic factor. J Comp Neurol. 2002;447(4):381-93. doi: 10.1002/cne.10248. PubMed PMID: 11992523.
149. Hoffman PN, Cleveland DW, Griffin JW, Landes PW, Cowan NJ, Price DL. Neurofilament gene expression: a major determinant of axonal caliber. Proc Natl Acad Sci U S A. 1987;84(10):3472-6. doi: 10.1073/pnas.84.10.3472. PubMed PMID: 3472217; PubMed Central PMCID: PMC304893.

Conclusão

Nossos resultados destacam os efeitos benéficos tardios do BHF na reparação da lesão e asseguram seu potencial para superar os efeitos de regeneração alcançados pela neurorrafia sozinha, endossando o BHF como um bioproduto promissor para ensaios clínicos.

De fato, aos 120 dias, o BHF demonstrou uma boa capacidade para prevenir e manter um microambiente menos degenerado e impactado em todo o eixo da interação neuromuscular em comparação a neurorrafia.

Em relação ao ambiente do sistema nervoso central, sugerimos que o BHF apresenta potencial para melhorar a preservação dos neurônios motores e sua subsequente regeneração. Aos 120 dias, há redução da morte neuronal e microgliose crônica, além da atenuação da desorganização neuronal e uma integridade nervosa mais próxima do grupo controle, em comparação a neurorrafia isolada. A associação ao BHF beneficia o microambiente medular.

Em relação ao ambiente do sistema nervoso periférico, após 120 dias de reconstrução, o BHF associado à neurorrafia preveniu a fibrose e a atrofia muscular. Isso possivelmente aconteceu devido ao aumento substancial nos axônios regenerados no grupo NB e sua posterior reinervação.

Tomados em conjuntos, esses resultados contribuem para uma melhor preservação e restauração nervosa, manutenção da função e saúde muscular como um todo.

UNIVERSIDADE ESTADUAL PAULISTA
"JÚLIO DE MESQUITA FILHO"

Comissão de Ética no Uso de Animais

Criada pela da Portaria DFM nº 611 de 13/12/2012

CERTIFICADO Nº 1402/2021 – CEUA

Certificamos que o projeto intitulado: "**Biopolímero heterólogo de fibrina associado à secretoma de células-tronco mesenquimais na reconstrução nervosa experimental: Aspectos morfofuncionais e moleculares da interação neuromuscular" -** conduzido pelo Pesquisador: **Felipe Cantore Tibúrcio – Orientador**: Profa. Assoc. Selma Maria Michelin Matheus, coorientador: Profa. Dra. Cintia Yuri Matsumura – Colaboradores: Kevin Silva Muller e Rui Seabra Ferreira Júnior, registrado com o **nº 1402/2021**, que envolve a produção, manutenção ou utilização de animais pertencentes ao filo Chordata, subfilo Vertebrata (exceto humanos), para fins de pesquisa científica, encontra-se de acordo com os preceitos da Lei n. 11.794, de 08 de outubro de 2008, do Decreto n. 6.899, de 15 de julho de 2009, com as normas editadas pelo Conselho Nacional de Controle de Experimentação Animal (CONCEA), e foi APROVADO pela Comissão de Ética no Uso de Animais da Faculdade de Medicina de Botucatu, em reunião ordinária de 22 de fevereiro de 2022.

Finalidade	( ) Ensino (**X**) Pesquisa Científica
Finalidade	01/12/2025
Espécie/Linhagem/Raça	Ratos Wistar
Nº Total de animais	ZERO ANIMAIS - Animais já adquiridos com certificado do IB
Idade/Peso	90 dias – 300 gramas
Sexo	Machos

Profa. Associada Bertha Furlan Polegato
Presidente da Comissão de Ética no Uso de Animais
Faculdade de Medicina de Botucatu/UNESP

Sara Rosa Stanley Sampaio
Secretária da Comissão de Ética no Uso de Animais
Faculdade de Medicina de Botucatu/UNESP

The research project registered by the number 1402/2021 is in agreement with the Ethical Principles for Animal Research established by the National Council for Control of Animal Experimentation (CONCEA) and was approved by the Committee on Ethics in the Use of Animals of Botucatu Medical School - Sao Paulo State University (UNESP) on 22/february/2022.

Distrito Rubião Júnior, s/nº – Botucatu – SP. CEP: 18618-970 Fones: (14) 3880.1880 – Email Secretaria: ceua@fmb.unesp.br

UNIVERSIDADE ESTADUAL PAULISTA
"JÚLIO DE MESQUITA FILHO"
Campus de Botucatu

Comissão de Ética no Uso de Animais
Criada pela da Portaria FMB Nº611 de13/12/2012.

Ofício nº 026/2022 – CEUA – FMB/UNESP

Botucatu, 27 de setembro de 2022.

Prezada Senhora,

Em atendimento ao documento enviado em 28 de julho de 2022, solicitando a inclusão do Subprojeto referentes ao Projeto de Pesquisa **"Biopolímero heterólogo de fibrina associado à secretoma de células-tronco mesenquimais na reconstrução nervosa experimental: Aspectos morfofuncionais e moleculares da interação neuromuscular" (Protocolo CEUA 1402/2021)**, essa comissão considera a solicitação **APROVADA**. Reiteramos que a aprovação da solicitação pela CEUA não prevê a inclusão de nenhum animal adicional aos já solicitados no projeto de pesquisa **1402/2021**.

Subprojeto
"Implicações da reconstrução nervosa experimental associada ao biopolímero heterólogo de fibrina no sistema nervoso central e periférico".

Aluno
Kevin Silva Muller

Atenciosamente,

Profa. Associada. Bertha Furlan Polegato
Presidente da Comissão de Ética no Uso de Animais
Faculdade de Medicina de Botucatu – UNESP

Ilustríssima Senhora
Profa. Associada Selma Maria Michelin Matheus
Instituto de Biociências – Unesp Botucatu

ANEXO 2

Tabela 1. Relação dos anticorpos utilizados para o desenvolvimento deste trabalho frente a todas as técnicas de imunomarcação. IHC – Imunohistoquimica; IF – Imunofluorescência e WB – Western Blotting.

Proteína	Anticorpo	Fabricante e Código	Concentração
FluoroGold	Anti-Fluorogold	Chemicon / #MAB153	1:10000 (IHC)
NF-200	Anti-NF200	Sigma / #N5389	1:1000 (IF)
S100	Anti-S100	Abcam / #ab4066	1:1000 (IF)
Vglut-1	Vglut1	Chemicon / #MAB5502	1:4000 (IF)
nAChRα-1	AChRα1	Santa Cruz / #sc-136130	1:1000 (WB)
nAChRγ	AChRγ	Santa Cruz / #sc-13998	1:1000 (WB)
nAChRε	AChRε	Santa Cruz / #sc-13999	1:1000 (WB)
Musk	Musk	Biosscience / #bs-6473R	1:1000 (WB)
Rapsina	Rapsyn	Abcam / #ab-156002	1:1000 (WB)
Agrina	Anti-Agrin	Abcam / #ab233515	1:1000 (WB)
LRP4	Anti-LRP4	Abcam / #ab174637	1:1000 (WB)
Rabbit IgG HRP	Anti-Rabbit IgG HRP	Santa Cruz / #sc-2005	1:200 (IHC) / 1:5000 (WB)
Mouse IgG HRP	Anti-Mouse IgG HRP	Abcam / #ab6728	1: 10000 (WB)
Mouse IgG	Anti-Mouse IgG AlexaFluor488	Abcam / #ab150113	1:1000 (IF)
GAPDH	GAPDH (14C10)	Cell Signaling / #2118	1:10000 (WB)